UNIVERSITY OF
BIRMINGHAM

PHYSICAL PROPERTIES OF PARTICLES AND THEIR IMPLICATIONS FOR THE CALCULATION OF THE HUMAN REGIONAL LUNG DOSE

By

VAN TUAN VU

A thesis submitted to the University of Birmingham for the degree of

DOCTOR OF PHILOSPHY

Division of Environmental Health and Risk Management

School of Geography, Earth and Environmental Sciences

University of Birmingham

ABSTRACT

Ambient particles are of high concern due to their effects on both human health and climate change. This study aims to investigate the physical properties of particles and their implications for source apportionment and health human exposure studies. A wide range of particle number size distribution (PNSD) measurements was conducted in selected environments using state-of-the-art high time resolution instruments. It is found that PNSD varied in different environments, depending on emission sources and atmospheric processes.

A mass balance model was used to predict the penetration, infiltration factors, deposition and loss rates of indoor particles. The loss rates of indoor particles, which are mainly subject to deposition, coagulation and evaporation, were found to be a function of particle size and time. This study successfully predicted the concentration of indoor particles from outdoor datasets based on an enhanced mass balance model with consideration of the change in loss rate by time.

Moreover, HTDMA measurements were performed to study the hygroscopic properties of particles in outdoor and indoor environments, and from five major indoor sources. The particles emitted from indoor sources were mostly hydrophobic. An enhanced lung deposition model based on the ICRP and MPPD models was developed to predict the deposition fraction of particles in the human respiratory tract, with consideration of their hygroscopicity.

Furthermore, this work utilizes PNSD datasets to apportion the sources of particles by number, surface area and volume using a Positive Matrix Factorization (PMF) model. A combination of lung deposition models and the PMF technique was applied to identify which sources are mostly responsible for deposited particles in the different regions of lung.

To my beloved wife, Anh L.M Tran,

who accompanies me wholeheartedly in this journey.

To my beloved parents, Tuoi T. Nguyen and Tuan D. Vu,

who always encourage me to pursue my passion.

ACKNOWLEDGEMENTS

First and foremost, I would like to express my deepest gratitude to my first supervisor, Professor Roy M. Harrison, who has helped my childhood dream to be true by giving me a fascinating opportunity to work and learn in a very professional environment. I am particularly indebted to him for his intellectual guidance, kindness, and solicitude over the last three years. His invaluable advices have greatly impacted the quality of this thesis.

I am also very grateful to Dr Juana Mari Delgado-Saborit, my second supervisor, for her guidance and encouragement. She has been very kind and always willing to spend her precious time in providing me not only with scientific assistance but also mental support. Special thanks go to Dr Ždímal Vladimír, Dr Jakub Ondráček and other colleagues for their great support at the Institute of Chemical Process Fundamentals (ICPF), Czech Republic, where I spent a wonderful summer during my secondment.

I would like to acknowledge the wonderful financial support provided by the European Union through Human Exposure to Aerosol Contaminants in Modern Microenvironments (HEXACOMM) Marie Curie -ITN project.

I also appreciate other colleagues at the Norwegian Institute for Air Research (NILU) and the Spanish National Research Council (CSIC) for their support during my short research visits there. Thanks to my friends in the HEXACOMM team, we had a lot of fun during the training and conference.

I would like to thank Dr. David Beddows, Dr. Mauro Masiol, Dr. Stefano Zauli Sajani and Dr.Irina Nikolova, who provided me with useful material and academic advice. My warmest thanks to Mrs. Mary Harding, who has been very kind and help me to deal with the massive paperwork. To Carmela, Pallavi, Eunhwa, Paul, Suad and my friends in PH and GEES, thank you all for your invaluable help.

TABLE OF CONTENTS

LIST OF FIGURES

Chapter 1

Chapter 2

Chapter 3

Chapter 4

Chapter 5

Chapter 6

Chapter 7

Chapter 8

LIST OF TABLES

Chapter 1

Chapter 2

Chapter 3

Chapter 4

Chapter 5

Chapter 6

Chapter 7

LIST OF ABBREVIATIONS

ACC	Accumulation mode particles
AIT	Aitken mode particles
AL	Alveolar (region)
APS	Aerodynamic Particle Sizer
CFD	Computational fluid dynamics
CMD	Count median diameter
COPD	Chronic obstructive pulmonary disease
COWD	Wood smoke indicator
CPC	Condensation Particle Counter
DF	Deposition Fraction
DMA	Differential Mobility Analyser
EEPS	Engine Exhaust Particle Sizer
ET	Extrathoracic (region)
FMPS	Fast Mobility Particle Sizer
GF	(Hygroscopic) Growth factor
GSD	Geometric standard deviation
HTDMA	Hygroscopic Tandem Differential Mobility Analyzer
I/O	Indoor/outdoor
ICRP	International Commission on Radiological Protection model
MMD	Mass median diameter
MPPD	Multiple Path Particle Dosimetry
NU	Nucleation mode particles
PMF	Positive matrix factorization
PNSD	Particle number size distributions

RMSE	Root Mean Square Error
SMD	Surface area median diameter
SMPS	Scanning Mobility Particle Size Spectrometer
TB	Tracheo-bronchial region (region)
V_E	Minute Ventilation or Ventilation rate
VMD	Volume median diameter

Chapter 1: INTRODUCTION

This chapter first aims to give the background of ambient aerosols and then discusses their health effects. The main part of this chapter is a literature review of respiratory exposure dose analysis for inhaled aerosols. In this review, lung dose, or the dose rate of particles and their calculation methods, are defined. In addition, it briefly presents the main factors that control the dose of particles in the human respiratory tract, such as particle properties, minute ventilation or subject characterization. Finally, the main goals and outline of the PhD study are introduced in this chapter.

The Chapter 1, 2 and 3 contain some sections of verbatim text adapted from Vu et al. (2015b) published as part of this PhD. The author's contribution: contribution of ideas and writing.

1.1. Background of ambient aerosols

Ambient aerosols are a mixture of organic and inorganic substances suspended as liquid droplets or solid particles in the air, with diameters ranging between ~ 2 nm and ~ 100 µm. Atmospheric aerosols can scatter light efficiently, changing the balance of solar radiation reaching the earth's surface, thus resulting in climate change; they also have indirect impacts on the climate due to their effects on clouds formation by acting as cloud condensation nuclei. In addition, some of them may contain potentially toxic chemicals such as polycyclic aromatic hydrocarbons (PAHs), causing a series of health problems due to inhalation. As a result, there has been a rapid rise in research on ambient aerosols in recent decades.

Ambient particles may be either directly derived in the ambient air from both anthropogenic or natural sources, such as traffic emissions, biomass burning or volcanoes (primary

aerosols), or formed by chemical reactions such as atmospheric nucleation (secondary aerosols). Each source has a different contribution to different particle metrics (number, surface area and mass). In urban areas, traffic related emissions are well known as a major source of both particle number and mass.

Different types of sources generate particles with different physical and chemical properties, including their (number, surface area and mass) concentration, size, chemical composition, and aerodynamic, hygroscopic, optical and other properties. Of these particle properties, particle number size distribution is the most important parameter because it not only provides us information about sources and atmospheric processing of particles, but it also plays a vital role in determining regional lung deposition. In addition, particle size has marked effects upon atmospheric visibility and climate.

1.2. Health effects of ambient particles

Exposure to ambient aerosols has been found to be associated with an increase in mortality, such as exacerbation of asthma and cardiovascular problems in both epidemiological and toxicological studies (Donaldson et al., 2001; Kumar et al., 2010). A recent study published in Nature found that ambient air pollution, mostly by $PM_{2.5}$ may cause more than 3 million premature deaths on global scale every year (Lelieveld et al., 2015).

Aerosol properties in terms of physical and chemical characteristics play an important role in exposed route and thus have a consequent direct health effect. Many previous studies have found that particle mass and its chemical properties, such as PM_{10}, black carbon and heavy metals contained in PM are directly linked to the health effects; fine particles can also penetrate deeper into the lungs. However, some recent evidence suggests that the ultrafine particles that are most commonly measured in terms of their number concentrations could have a higher toxicity compared to corresponding masses of fine particles due to their large

surface area, oxidative capacity and radical species formation, which can lead to cellular DNA damage or induce inflammatory effects (Peters et al., 1997). Furthermore, the ultrafine particle is widely known to penetrate into the lung more easily. Therefore, the determination of the respiratory tract deposition of aerosol particles which depends much upon their size distribution is becoming crucial in addressing the question of what the most important metric linked to health outcome is (Harrison et al., 2010; Kumar et al., 2013).

1.3. Literature review of respiratory exposure-dose analysis for inhaled submicron aerosols

1.3.1. Introduction

Exposure to ambient aerosols is consistently associated with adverse health effects in numerous scientific studies (Pope and Dockery, 2006). In particular, smaller particles are able to penetrate into the deeper regions of the respiratory tract including the pulmonary epithelium, causing serious health problems such as lung morbidity and mortality (Donaldson et al., 1998). Estimation of the respiratory deposition dose plays a vital role not only in the determination of the particle-induced biological response in toxicological studies, but also in risk assessment of air pollution in epidemiological studies. Harrison et al. (2010) indicate that relating health outcomes to measured particle mass concentrations most likely underestimates the public health impacts and emphasize that the regional dose, not pollutant exposure, probably drives health outcomes.

The regional lung dose is defined as the proportion of inhaled particles deposited in the respiratory tract during an exposure time period. The lung dose of particles by number in different lung regions (i) with a specific particle size range (Dp_1-Dp_2) was calculated based on the following equation (Hussein et al., 2013):

$$\mathrm{Dose_{i,}} = \int_{Dp1}^{Dp2} V_E . DF_i . n_N^0 . \Delta t . d\log D_p \qquad (1.1)$$

where, DF_i is the deposited fraction of a specific particle in the human respiratory tract; n_N^0=dN/dlogD_p is the lognormal particle number size distributions; Δt is the exposure time period (minute) and D_p is the particle diameter (μm); V_E is defined as the minute ventilation or ventilation rate is the volume of gas inhaled or exhaled from the lungs during a time period (m^3 $minute^{-1}$). Equation (1.1) can be transformed into equation (1.2):

$$Dose_{i,} = C_{TN} * V_E * DF_i * \Delta t \quad (1.2)$$

where, DF_i is the total deposition fraction of aerosol population in the different regional lungs. C_{TN} is the total number concentration (particle cm^{-3}).

Therefore, the daily regional dose of particles can be calculated as the following equation:

$$\text{Daily Dose}_i = \sum_{j=1}^{n} C_j * VE_j * DF_{i,j} * t_j \quad (1.3)$$

where, C_j, VE_j, $DF_{i,j}$, t_j is the total concentration (particle cm^{-3}), minute ventilation (m^3 $minute^{-1}$) , deposition fraction and exposure time (minutes) of particles in the different exposure scenario j (such as in the working place, home or outdoor) and $\sum_{j=1}^{n} t_j = 1440$ minutes.

In a given exposure scenario, the respiratory tract deposited particle dose rate, which is defined as the total amount of particles deposited in the respiratory tract during a period of time, can be calculated as:

$$\text{Dose Rate} = DF * C * V_E \quad (1.4)$$

The dose not only depends upon the measured particle concentrations in each environment, but is also influenced by complex parameters including particle properties, breathing patterns, flow dynamics and lung structure. Although ambient aerosols and their deposition in the respiratory tract have been of much concern in recent years, there are few studies on the regional lung dose of ambient aerosols (Kristensson et al., 2013).

This work first discusses the factors governing the lung dose of particles. It then briefly reviews and compares the current mathematical models of regional lung deposition. The third part of this chapter will summarize the lung dose results from previous studies and finally discuss the current challenges and future solutions.

1.3.2. Factors controlling the lung dose of particles

From equation (1.3), it is obvious that the lung dose of particles is controlled by four important factors including concentration, minute ventilation, deposition fraction and exposure time. This section will discuss these four factors and identify which is the most important in lung dose monitoring.

1.3.2.1. Particle number concentration in different scenarios

a. Outdoor environments

Atmospheric aerosols are a mixture of primary particles emitted from anthropogenic activities (transportation, power generation, industries or cooking), and natural sources (volcanos, forest fires), and secondary particles formed by gas-to-particle conversion mechanisms. Aerosol concentration is found to be quite variable between environments, and even within in an environment types due to its strong dependence on the atmospheric process or local sources. Table 1.1 shows the range of particle number concentration of atmospheric aerosols in different environments. For example, the number concentrations of particles with diameters from 3 nm to 10 µm vary in urban areas, ranging from ~10^3 to ~10^6 particle cm^{-3} (Stanier et al., 2004; Wang et al., 2011b; Weijers et al., 2004), while the concentrations of particles with diameters in the range of 10 nm–20 µm at urban background sites are normally around 10^3-10^4 cm^{-3}. These values are lower than those in other urban sampling sites, such as downtown and traffic or and suburban areas, but they are much higher than those in rural and

clean background areas. Investigating the characteristics of particle number size distribution in four European cities, Von Bismarck-Osten et al. (2013) report that the average total urban particle number concentrations were 1.6-2 times higher than those in rural areas, but 2.4-3.4 times lower compared with those at the road side. Similar results were found in Munich, Germany (Held et al., 2008), and Guangzhou, China (Yue et al., 2013). A detailed information of particles in cities can be found in excellent reviews by Kumar et al. (2014) and Vu et al. (2015b).

Table 1.1: Particle number concentration of atmospheric aerosols (Seinfeld and Pandis, 2012).

Environments	**Number concentration (particles cm^{-3})**
Urban background	10^3 - 10^4
Urban polluted	10^4 - 4 x 10^6
Rural	10^3 – 10^4
Marine	10^2 – 4 x 10^2
Remote continental	50 – 10^4

b. Indoor environments

Indoor aerosols are a mixture of outdoor particles that infiltrate into indoor environments, particles released by indoor activities, and new particles formed by gas-to-particle conversion. Hence, their concentrations are strongly affected by the outdoor/indoor penetration process, which depends on building characteristics, the removal process from indoor air such as deposition or air exchange, and the emission rate of indoor sources (Bhangar et al., 2011). The penetration and deposition rates of particles are found to greatly depend upon particle size. In the absence of an indoor source, the indoor concentration level is normally found to be lower than the outdoor level. In recent decades, many studies on

particle characterization have been conducted in different indoor environments, such as homes, schools, offices, and other working places.

1.3.2.2. Variation in deposition fraction

As dissed below, the total and regional deposition fraction (or deposition fraction) vary between nearly zero and almost one, depending upon the inhalation conditions (breath rate, route and volume), subject category (lung morphology, age, gender, and disease), and particle properties (size, shape, density and chemical composition) (Löndahl et al., 2014).

a. Particle properties

Particle size

Particle size is the most important parameter in determining the regional lung deposition of particles because of its direct effects upon the main lung deposition mechanisms including diffusion, impaction and sedimentation (ICRP, 1994; Martonen et al., 2005).

Hygroscopicity, particle density and shape

When an inhaled particle penetrates into the human respiratory tract, its size and density may be changed due to its hygroscopic properties, altering its deposition efficiency. The hygroscopic growth factors of particles depend on their initial size and chemical composition, the regional lung's temperature and relative humidity, and its travelling time in the lung (Ruzer and Harley, 2012).

If the particle is spherical, the relationship between the growth factor and particle density is given by the following equation (Martonen et al., 2005):

$$\rho_i = \frac{\rho_0 - \rho_{H_2O}}{Gf_i^3} + \rho_{H_2O} \quad (1.10)$$

where, ρ_0 and ρ_i are the initial particle density and the particle density in the airway generation i (g cm^{-3}); Gf_i is the growth factor of the particle in the airway generation i; and ρ_{H_2O} is the particle density of water (g cm^{-3}).

Ferron et al. (1988) measured the growth and deposition of dry NaCl, $CoCl_2.6H_2O$ and $ZnSO_4.7H_2O$ particles in the human regional lung due to inhalation. Their study reported that small pure salt particles (D_p <1 μm) can grow and reach their final size during inhalation while the larger particles ((D_p >7 μm) grow by less than 20% during inhalation. The deposition of hydrophobic particles was found to be higher than those of hygroscopic particles with an equivalent diameter for submicron particles, but lower for micron-sized particles. Winkler-Heil et al. (2014) explain that diffusion has less effect on the submicron particles, whereas there are more efficient impaction and sedimentation effects on super-micron particles due to their hygroscopicity.

There are few studies on the effect of particle density and shape on regional lung deposition. Figure 1.1 shows the effect of particle density on the deposition fraction of particles. Particles with a higher density have a higher total deposition fraction than others with the same diameter but lower density. Note that the particle density we used in the ICRP model is "effective density".

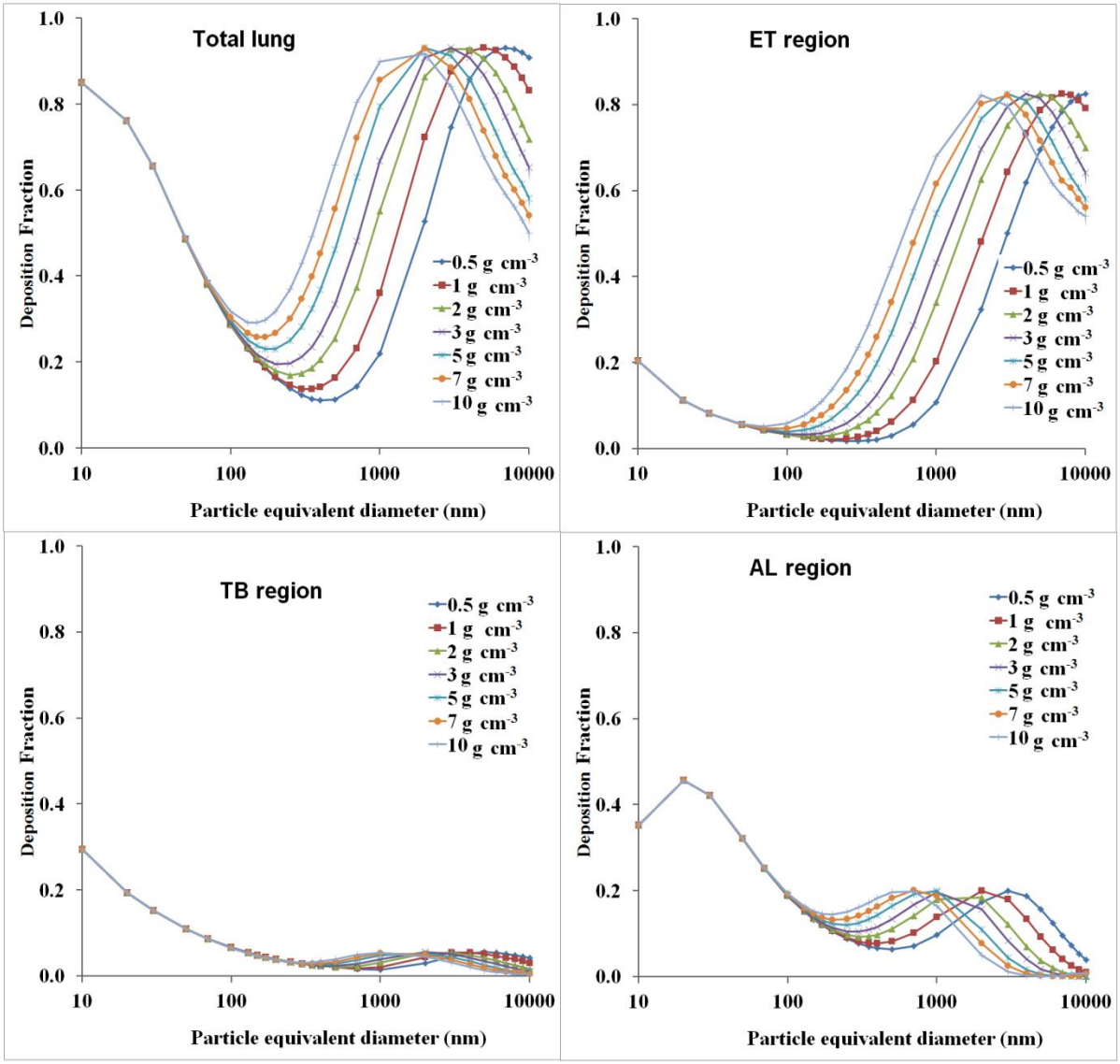

Figure 1.1: Regional lung deposition fraction of hydrophobic particles with different densities calculated for a man sitting, using an ICRP model. *The particle diameter is the equivalent diameter. For spherical particles, the equivalent diameter equals to the mobility diameter.*

b. Subject factors

The variation in subjects not only has a strong effect on the lung deposition fraction of a particle due to the differences between lung structures and breathing patterns, but has also an influence on the total lung dose because of varying minute ventilation. Kim and Kang (1997) compared the regional deposition of inhaled particles between men and women and found that there was a slight increase in women for ultrafine and coarse particles at the same

controlled breathing pattern. However, the total deposition fraction was slightly lower in women than men with a spontaneous breathing pattern. This is consistent with predictions of the ICRP model (ICRP, 1994).

There is no significant variation in the lung deposition fraction of fine particles found in adult and elderly groups (Bennett et al., 1996). There are both experimental and modelling studies for total lung deposition in children (Hofmann et al., 1989; Schiller-Scotland et al., 1994; Xu and Yu, 1986; Zeman, 1998). There are possibly higher deposition fractions in infants and young children compared to adults. However, these results are found to be variable and inconsistent due to the difficulty in monitoring breathing patterns in experimental studies and in modelling for the development of lung morphology. There is a lack of experimental data to validate the models.

The total deposition fraction has shown an increase in the total lung deposition of ultrafine and fine particles for patients with obstructive airway diseases such as asthma and chronic obstructive pulmonary disease (COPD) (Löndahl et al., 2014). In one of the earliest researches, Anderson et al. (1990) compared the total efficient respiratory tract deposition of non-hygroscopic ultrafine particles (di-2-ethylhexyl sebacate- DEHS, size range: 0.02-0.24 μm) in five subjects with obstructive lung disease- three subjects with restrictive lung disease and ten healthy subjects. The results showed that the total lung deposition fraction of ultrafine particles in patients with restrictive lung disease was similar to that in healthy subjects, but there is a significant increase in patients with obstructive lung disease.

Kim and Kang (1997) measured the total lung deposition fraction of monodisperse aerosols of DEHS with 1.0 μm mass median aerodynamic diameter (GSD ~1.2) and found the lung deposition fractions were double higher in COPD patients, around 50% higher in smokers with small airways disease and asthmatics, and 16% higher in smokers. This result was

consistent with Chalupa et al. (2004), who found the efficient lung deposition of ultrafine particles with a CMD of 23 nm and GSD of 1.6 was approximately 17% higher in asthmatic subjects during breathing at rest, but that there was no significant difference during breathing at exercise. Furthermore, Brown et al. (2002) compared the lung deposition fraction of technetium-99m-labeled ultrafine carbon aerosols with a CMD of 33 nm and geometric standard deviation (GSD, or ϭ) of 1.7 between 9 healthy subjects and 10 COPD patients, who were subdivided into a bronchitis (7 patients) and an emphysemic (3 patients) group. The data demonstrated that DFs in heathy subjects (DF ~0.62) was found to be slightly lower than those of bronchitic patients (0.67), but much higher than those of emphysemic patients (0.48). A lower lung deposition fraction of ultrafine particles in emphysemic patients was also found by Londahl et al. (2012).

Human physical activity and minute ventilation

Exercise increases the human respiratory tract dose of particles in a constant microenvironment due to the increase in both deposition fraction and minute ventilation. Daigle et al. (2003) measured the lung deposition of a polydisperse carbonaceous ultrafine particle (CMD ~26 nm, GSD ~1.6) in 17 healthy subjects during rest and exercise. The deposition fraction during rest was 0.66 ± 0.11, which increased to 0.83 ± 0.04 during moderate exercise, while the minute ventilation increased from 9.0 ± 1.3 L min^{-1} during rest to 38.1 ± 9.5 L min^{-1} during exercise. As a result, the total number of deposited particles was more than 4.5 times higher during exercise than at rest.

Similarly, Löndahl et al. (2007) compared the lung deposition of ultrafine hydrophobic and hygroscopic particles during rest and exercise. The deposition fraction showed a small increase in hydrophobic particles with diameter lower than 30 nm during exercise, but the minute ventilation increased fourfold; therefore, the dose increased more than four times at

the exercise level. Moreover, there was no significant difference in the average deposition fraction due to gender, but the minute ventilation for male subjects was four times higher than female subjects during exercise.

As discussed above, minute ventilation is a main factor in the increase in dose rate when doing exercise. Minute ventilation depends upon exercise level and subject characterization, such as age, gender and disease. Brown et al. (2002) measured the minute ventilation in COPD patients. The results showed that was 6.93 ± 1.63 and 10.9 ± 6.2 L min^{-1} in bronchitic and emphysemic patients, which was found to be higher than that for healthy subjects (5.83 ± 1.36 L min^{-1}). Likewise, Londahl et al. (2012) found the minute ventilation in COPD patients was 10.6 ± 2.9 L min^{-1}, while for healthy subjects it was 8.4 ± 1.5 L min^{-1}. Higher minute ventilation was found in patients with asthma than healthy subjects (Chalupa et al., 2004). Table 1.2 and Table 1.3 show the minute ventilation for healthy people.

Table 1.2: Minute ventilation (L min^{-1}) for Caucasian people by ICRP (1994).

Activity	**Ages**							
	3 months	1 year	5 years	10 years	15 years		30 years	
					Female	Male	Female	Male
Resting (sleeping)	1.5	2.5	4.0	5.2	5.8	7.0	5.3	7.5
Sitting	-	3.7	5.3	6.3	6.7	8.0	6.5	9.0
Light exercise	3.2	5.8	9.5	18.7	21.7	23.0	20.8	25.0
Heavy exercise	-	-	-	39.7	42.8	48.7	45.0	50.0

Table 1.3: Minute ventilation (L min^{-1}) for people in US by EPA (2009).

Ages category	Sleep or Nap		Light activities		Moderated Activities		Heavy activities	
	Male	Female	Male	Female	Male	Female	Male	Female
<1 year	3.1	2.9	7.9	7.3	14.5	14.0	27.5	24.2
1 year	4.5	4.6	11.6	11.6	21.4	21.0	40.3	36.5
2 years	4.6	4.6	11.7	12.0	21.5	21.3	40.5	37.6
3 to <6 years	4.4	4.2	11.4	10.9	21.0	20.0	39.0	34.5
6 to <11 years	4.6	4.4	11.6	11.1	22.3	21.0	43.6	39.4
11 to <16 years	5.3	4.8	13.2	12.0	26.4	23.6	50.8	46.6
16 to <21 years	5.3	4.4	13.4	11.1	29.0	23.2	53.2	44.1
21 to <31 years	4.7	3.9	13.0	10.6	29.2	22.9	53.9	45.7
31 to <41 years	5.2	4.0	13.6	11.1	30.3	22.7	54.3	44.4
41 to <51 years	5.7	4.4	14.4	11.8	31.6	24.5	57.3	47.0
51 to <61 years	3.8	4.6	14.6	12.0	32.7	25.2	58.4	47.4
61 to <71 years	6.0	4.5	14.1	10.8	29.8	21.4	54.1	40.0
71 to <81 years	6.1	4.5	13.9	10.8	29.3	21.1	52.5	40.6
>81 years	6.0	4.5	13.8	10.4	28.5	20.9	53.3	41.9

1.4. Lung deposition models

Many models have been developed in recent years to predict the lung deposition of particles. Martonen et al. (2005) classified these approaches into four categories; namely, empirical, deterministic, and stochastic models and computational fluid dynamics (CFD). Empirical models are developed by fitting algebraic relationships to experimental data to derive the lung deposition of particle equations, while deterministic models describe the particle trajectories by particle momentum equations based on the simulation of air and particle motion, with simple assumptions of airway structures and airflow conditions. The stochastic models are designed to account for lung morphological variability, in which the morphometric parameters are given randomly by statistical distribution based on experimental measurements. The last type of model is the CFD models, version of which have been more developed in recent years since computers have become more powerful. In the CFD models, particle motions and deposition are determined by computational fluid

dynamic simulations, which can describe the influence of complicated flow air patterns on the particle motion and deposition in the respiratory airway system. One of the great strengths of CFPD models is that they can predict the particle deposition fraction and localized patterns in a specific selected geometric unit of the human respiratory tract.

From other modelling perspective, Hofmann (2011) divided current particle models into four categories: the whole lung approach (i.e. deposition in the whole or regional lung); the local lung approach (i.e. deposition in the localized lung region such as the airway bifurcations); the Lagrangian approach; and the Eulerian approach. The Lagrangian approach considers the transport and deposition of individual particles, while the Eulerian approach focuses on the fate of a population of particles in the human respiratory tract. For more detail, the readers can refer to the reviews of lung deposition models by Hofmann (2011) and Martonen et al. (2005). The International Commission on Radiological Protection (ICRP) and Multiple-Path Particle Dosimetry Model (MPPD) models are two of the most popular models for predicting particle deposition in the whole and regional lung.

1.5. Summary of lung dose studies

On the microenvironment scale, Wang et al. (2010) predicted the regional lung deposition of nanoparticles for workers in a carbon black manufacturing factory. The exposure concentration was 25.7×10^3, 42.1×10^3, and 13.7×10^3 particle cm^{-3} (based on the assumption of minute ventilation for workers being 1.5 m^3 h^{-1}, the estimated lung dose rate was 38.4×10^9, 63.2×10^9, and 20.6×10^9 particles $hour^{-1}$) in the packaging, warehouse and pelletizing areas, respectively. More than 64% of the total particle number was found in the alveolar region. In a later research, Wang et al. (2011a) reported that the estimated lung dose rate was 138.0×10^9, 92.2×10^9, and 227.0×10^9 particles $hour^{-1}$ in three working areas, the forming, threading and heat treating areas in a fastener manufacturing plant.

Similarly, Elihn et al. (2011) investigated the regional lung deposition of ultrafine particles in seven industrial plants and at the different sites of 24 work activities and found the deposited particle number varied between different working places. Löndahl et al. (2009) experimentally compared the human lung deposition of particles from the kerbside of a busy street, from traffic exhaust and biomass combustion. The results showed that the deposition doses (if inhaled total particle mass concentration of 100 μg m^{-3}) of particle numbers from these above sources were 80.0×10^9, 103×10^9, and 6.5×10^9 particles $hour^{-1}$.

For the daily lung dose calculation, Buonanno et al. (2011) developed a numerical methodology based on the Monte Carlo method to estimate the tracheobronchial and alveolar dose of submicron particles for different population age groups in Italy, using a combined data set of particle number size distribution collected in major microenvironments and Italian human activity data. The daily tracheobronchial and alveolar number dose for all of the age groups was 65×10^9 and 150×10^9 particles day^{-1}, and the major sources of doses were found to be indoor cooking (females), working time (males) and transportation (children).

Hussein et al. (2013) modelled the regional deposited dose of submicron aerosol particles for males and females in the absence of indoor sources. The results demonstrated that the daily dose of submicron particles in the respiratory tract for adult males was $40 \times 10^9$and 57×10^9 (particles day^{-1}) on weekends and workdays. In terms of regional lung dose, most of the inhaled particles by number (62.8%) deposited in the alveolar region, followed by the tracheobronchial region (22.7%) and the extra-thoracic region (14.5%). Furthermore, Hussein et al. (2015) indicated that the daily lung dose of particles by number could increase four folds due to exposure for 5 minutes of aerosols emitted during printing job.

1.6. Goals of this PhD study

The regional dose, not pollutant exposure, probably drives health outcomes in the epidemiology studies (Harrison et al., 2011). Therefore, the aim of this study is to develop an approach for the calculation of the human regional lung dose based on ICRP/MPPD models. In addition, this study also aims to comprehensively investigate the physical properties of particles which play important roles in the lung deposition calculation. Moreover, the identification of the most relevant sources of atmospheric particles and the association between a particle source and lung deposition could play a vital role not only for risk assessment of air pollution in epidemiological studies, but also for policymakers to introduce optimal legislation for air quality control for the protection of public health. Hence, the last purpose of this study is to apportion the sources of particles deposition in the human respiratory tract. To address these issues, the study focuses on:

(1) Measurement of particle size distribution for particle number from both indoor and outdoor environments.

(2) Indoor/outdoor modelling for particle size using a mass balance model.

(3) The hygroscopic growth of particles and its implication for lung deposition calculation.

(4) Source apportionment of the lung dose of ambient submicron particles.

(5) Lung dose of particles emitted from different major indoor sources and the modelling of daily human lung dose of particles.

1.7. Thesis outline

This thesis consists of eight chapters, as shown in Figure 1.2. Chapter 1 gives the background of ambient aerosols and their health effects, a literature review of the existing knowledge of

the dose of particles in the human respiratory system. It then presents the main goals of this PhD study.

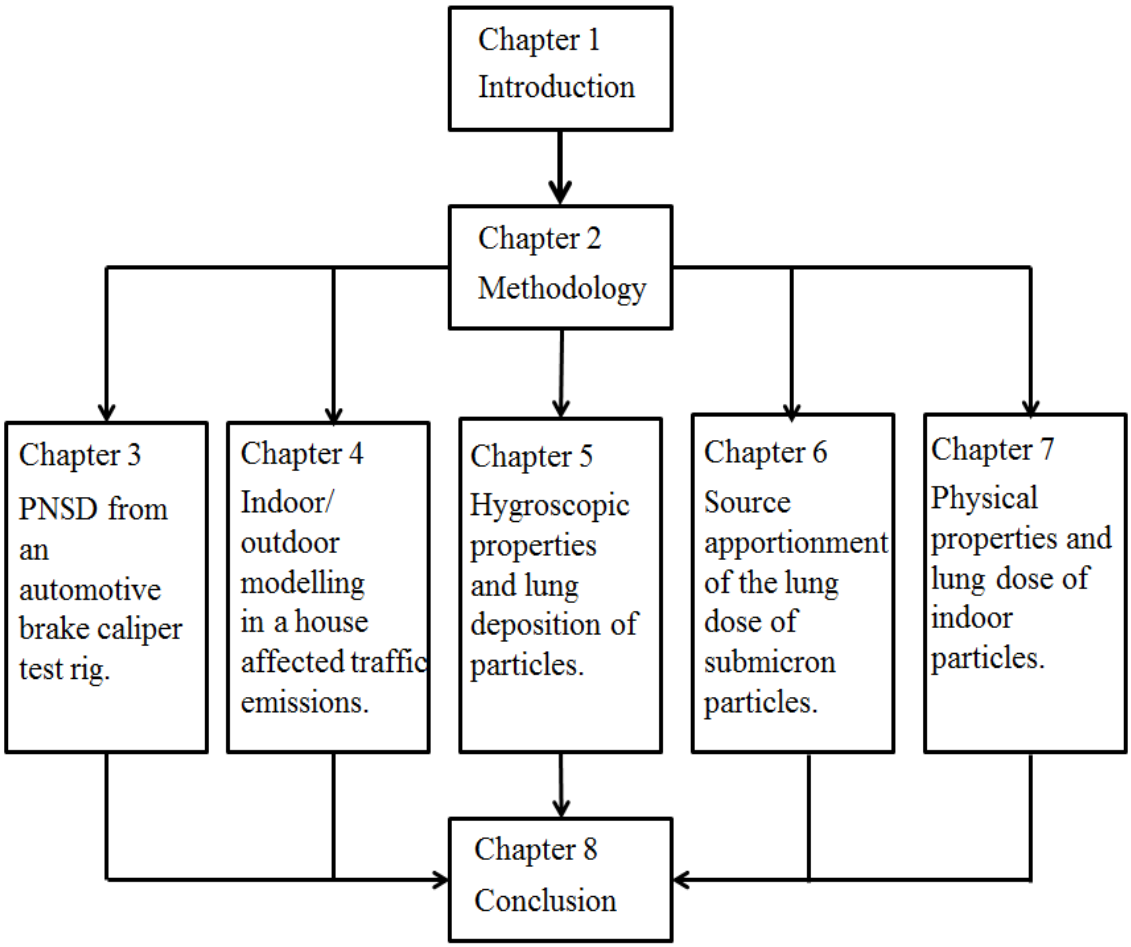

Figure 1.2: The structure of this PhD thesis.

Chapter 2 provides the descriptions of the instruments used for measuring the concentration, size and hygroscopic properties of particles, as well as the information on lung deposition (ICRP, MPPD) and source apportionment models (PMF).

Chapter 3 presents the concentrations and wide range of size distributions of brake wear particles which were measured from a laboratory test rig.

Chapter 4 evaluates the use of a dynamic mass balance model for predicting the penetration factor, infiltration factor and deposition rate of submicron particles in a house located at a site

of busy traffic in Bologna (Italy). This chapter also discusses the roles of coagulation and evaporation processes in estimating the loss of indoor particles.

Chapter 5 reviews the existing knowledge on the hygroscopic properties of particles and their influence on the lung deposition fraction calculation. In addition, it applies the modified ICRP model to estimate the regional lung deposition fraction of particles collected from a street canyon and an urban background site in London and a rural site in the west of London, UK.

Chapter 6 presents the results of source apportionment of submicron particles at an urban background area in London, UK. This chapter also identities which source is most responsible for particles deposited in the human respiratory system.

Chapter 7 presents the results of physical properties of particles gained from the indoor/outdoor experiments in Prague, Czech Republic from HEXACOMM sampling campaigns. This chapter also discusses the lung deposition of particles emitted from five major indoor sources.

Chapter 8 gives a summary of the thesis, followed by an overall conclusion derived from this research. It also discusses the implications, limitation and future directions for this study.

Chapter 2: METHODOLOGY

This chapter outlines the general methodology used in the study. It first lists the real time instruments used to characterize the concentration, size and hygroscopic properties of particles, including a Scanning Mobility Particle Size Spectrometer (SMPS), Engine Exhaust Particle Sizer (EEPS), Fast Mobility Particle Sizer (FMPS), Aerodynamic Particle Sizer (APS), and Hygroscopic Tandem Differential Mobility Analyser (HTDMA). It then provides information on the two human respiratory tract deposition models: a semi-experimental model supplied by the International Commission on Radiological Protection (ICRP model) and a Multiple-Path Particle Dosimetry Model developed by Applied Research Associates, Inc. (MPPD model version 2.11). In addition, the chapter describes a positive matrix factorization (PMF) model and its application on particle number size distribution in the source apportionment study of particles. Finally, it summarizes the software and programing language used for the data analysis.

2.1. Real time measurement instruments

2.1.1. Scanning Mobility Particle Size Spectrometer (SMPS)

An SMPS spectrometer is a high resolution nanoparticle sizer that is widely used to measure aerosol size distributions in the size range from few to 1000 nm. The principal operation of this spectrometer is based on the electrical mobility properties of particles. An SMPS system mainly consists of an electrostatic classifier (EC) combined with a Differential Mobility Analyser (DMA) to classify particle sizes based on their mobility, and a Condensation

Particle Counter (CPC) to count the particle number concentration. In our study, we used an SMPS model 3696 from TSI (TSI, 2010).

An aerosol impactor on the inlet should be mounted outside the electrostatic classifier to remove large particles which may carry many more than a single charge. There are three impactors, with nozzle diameters of 0.0475, 0.0508 and 0.0871 cm. The impactor is selected, depending upon the type of DMA, CPC, aerosol sample flowrate and the collected size range. In our study, we used an impactor with a nozzle diameter of 0.0508 cm that can remove particles with a diameter larger than 1 μm. Before entering the DMA, sample aerosols are neutralized by an aerosol neutralizer based on either radioactive or soft x-ray sources (TSI, 2010).

Differential Mobility Analyzer (DMA)

A DMA column consists of a high voltage centre rod and an outer grounded tube, generating an electric field inside. As the aerosol sample flow come from the top to the bottom of the column, the neutralized aerosols are forced to the outer tube or drawn to the inner rod due to the effect of the electrical field on the charged particles; they are then separated according to size based on their electric mobility. For example, particles with a higher electrical mobility move towards the inner rod faster than those with a lower electrical mobility, and they make contact with the central rod sooner (TSI, 2010).

The electrical mobility of an aerosol depends on its size, charge (which is controlled by a neutralizer before entering the DMA), sample and sheath flows, the voltage of the central rod, and the DMA geometry. At a given voltage and flow rate, only particles with a certain size can pass through an output slit which is located at the bottom of the rod, and continue to the CPC for concentration measurement. In our study, we used a long DMA from TSI in the SMPS system.

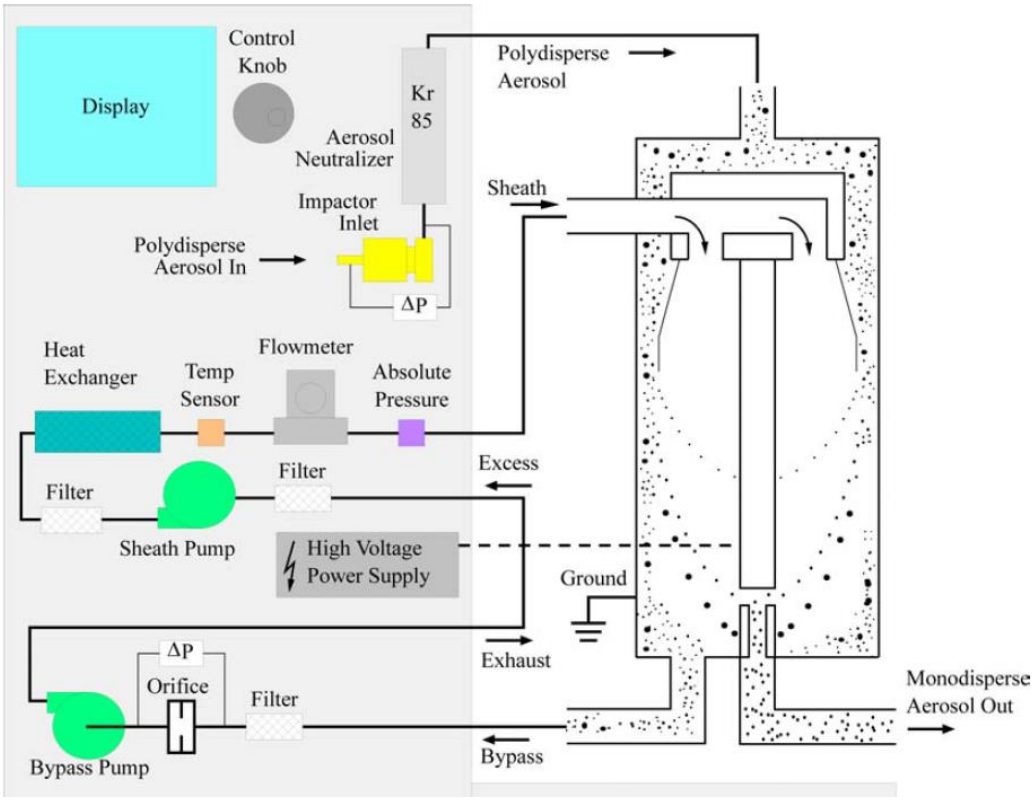

Figure 2.1: Flow schematic of an electric classifier with a long DMA (TSI, 2010).

Condensation Particle Counter (CPC)

CPCs are used to detect the monodisperse aerosol once it passes through the DMA. The principal operation of a CPC is that it uses heterogeneous condensation to grow the particle; these grown particles will be detected by an optical detector. In our study, we employ the CPCs from TSI using n-butanol as a supersaturated vapour. In these CPCs, the aerosol sample stream passes through a heated saturator, where butanol is vaporized and contaminated by diffused butanol vapours. Then, the aerosol and butanol vapour will pass into a cooled condenser where butanol vapour is supersaturated and condensed. Particles in the sample stream will be act as condensation nuclei and start to grow into larger droplets due to condensation. The large droplets will enter into an optical detector and be easily counted by number (TSI, 2007).

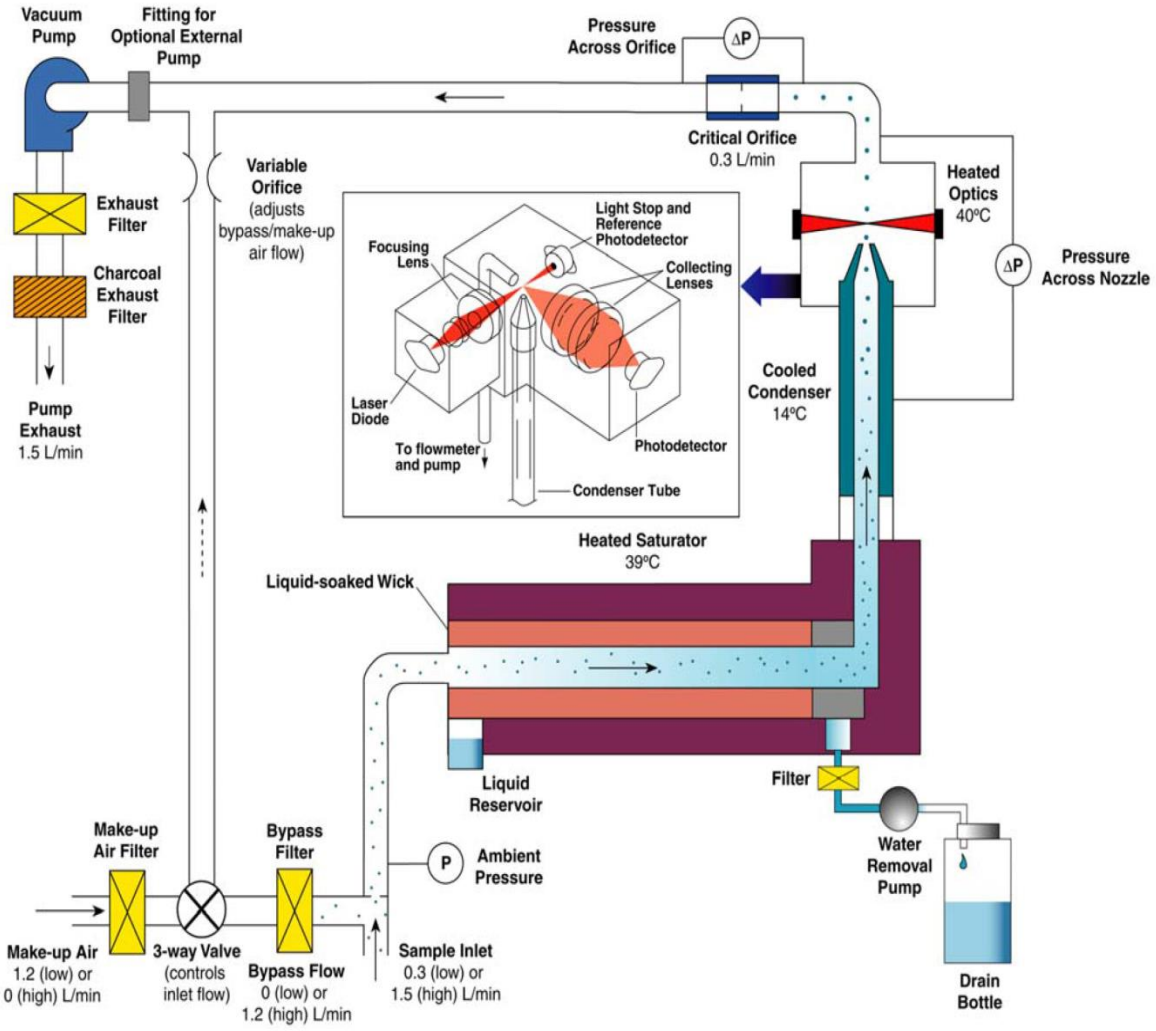

Figure 2.2: Schematic of CPC model 3775 (TSI, 2007).

2.1.2. Fast Mobility Sizers (EEPS and FMPS)

Two commercial TSI fast mobility spectrometers, the Engine Exhaust Particle Sizer (EEPS) and the Fast Mobility Particle Sizer (FMPS), were deployed in our measurements of traffic-related emissions. The EEPS/FMSP instruments and a SMPS system are similar in their principal classification of particle based on particle electric mobility, but differ in their charger, flow and detector schematic.

In an EEPS/FMPS system, particles are positively charged using a unipolar corona charger. They are expelled forward in the electric field generated by a high-voltage electrode column,

and classified according to their electrical mobility. A charged particle strikes its respective electrometer in a series of electrometers in the stack. Due to its different electric mobility for different charges, a particle with a higher charge strikes an electrometer near the top while those with lower charges strike an electrometer lower in the stack. The charge transferred from a particle to an electrometer after its strike will inverse to its concentration and size (TSI, 2005).

The EEPS and FMPS are similar in their operation and design, but differ in their time resolution measurement. The EEPS/FMPS instruments can measure a particle size range of 5.6-560 nm with the fastest time resolution (for one size distribution measurement) at 0.1 s from EEPS and 1s from FMPS.

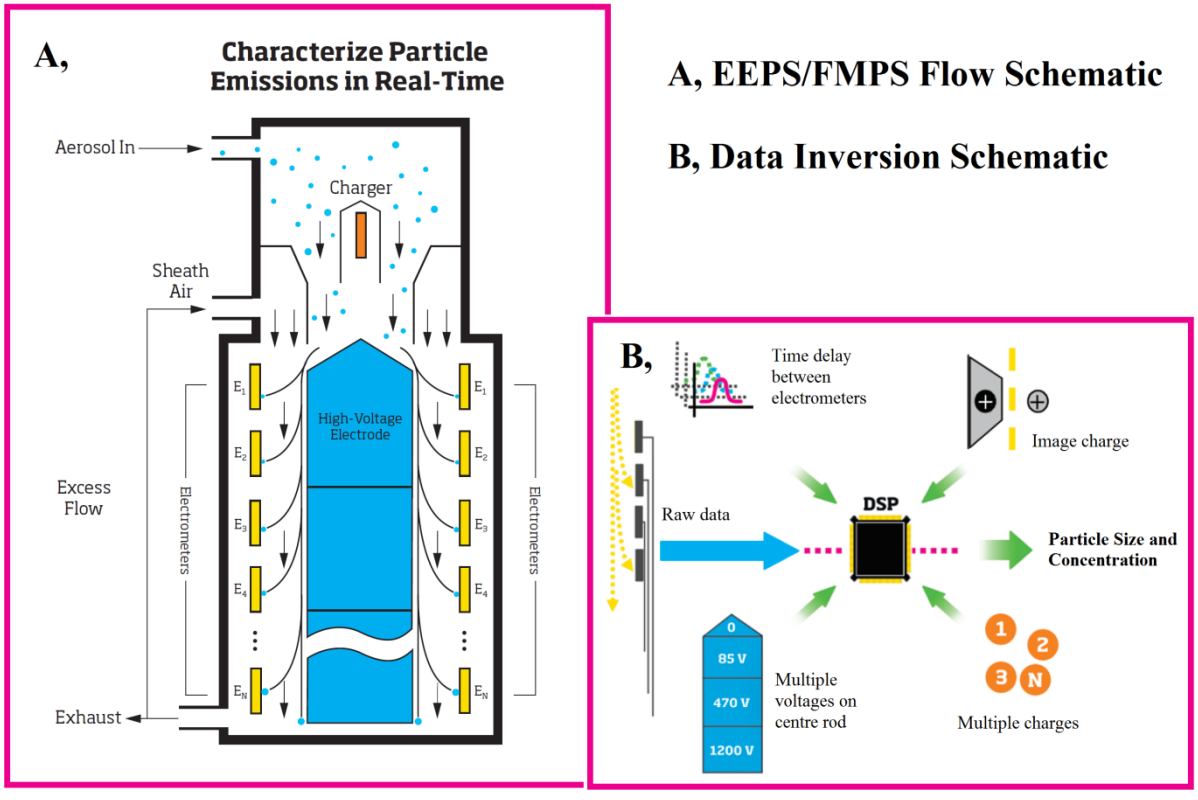

Figure 2.3: Flow and Data Inversion Schematic of EEPS/FMPS (TSI, 2005).

2.1.3. Aerodynamic Particle Sizer (APS)

The APS sizes a particle in according to aerodynamic diameter in the range of 0.5-200 μm based on a time-of-flight technique and detects particles using a light-scattering technique (Hinds, 1999; TSI, 2006). In an APS, there are two partially overlapping laser beams to detect particles. Once particles enter into the sample inlet, they are accelerated by the airflow through an accelerating orifice. Small particles of less than 0.3 μm, with approximately the same velocity as the air, will continue with the accelerating flow and exit. Larger particles accelerate more slowly due to the increased inertia; their velocities depend on their sizes.

Light is scattered as a particle passes through the laser beam, and it is detected by an avalanche photodetector (APD). The pulse of scattered light from the APD will be converted into an electrical pulse. The particle velocity can be determined from the time interval between the two electrical pulses created by that particle when it passes through two laser beams, resulting in a determination of its size (TSI, 2006).

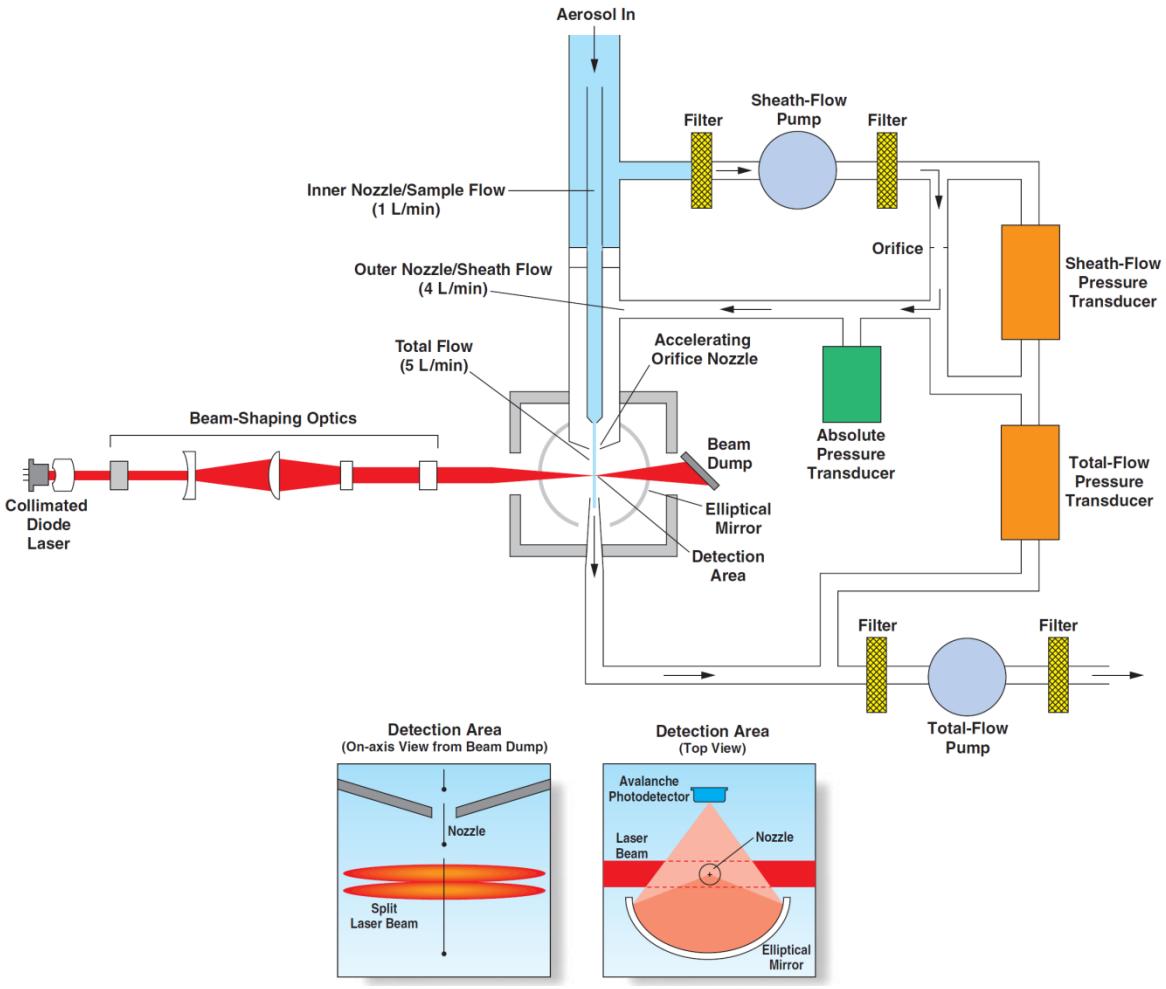

Figure 2.4: Operation of APS 3221 (TSI, 2006).

In our study, we used the APS model 3211 from TSI, which can measure the particle size distribution in the size range of 0.5-20 µm. One of this instrument's limitations is that an error known as coincidence can occur when a second particle arrives in the timing zone; the space between the two laser beams (12 µm) before the first has finished its time of flight, leads to the instrument under-estimating the particle concentration. This type of error occurs when we measure in an extremely polluted environment (the default setting for the maximum level of aerosols to avoid coincidence is 1000 particle/cm^3). For ambient air, the number of coarse particle is small, therefore the coincidence is negligible. However, when we measure the particles emitted from a brake rig text, the coarse particle level exceeds 1000 particle/cm^3. To prevent coincidence error, we used an aerosol diluter (TSI, model 3302A) to dilute the

aerosols in sample flow before they enter into the APS inlet. The dilution ratios of this diluter were set up in the range from 20 to 100 times.

2.1.4. Hygroscopic Tandem Differential Mobility Analyser (HTDMA)

The Hygroscopic Tandem Differential Mobility Analyzer (HTDMA) used in this study was developed by the Laboratory of Aerosol Chemistry and Physics, Institute of Chemical Process Fundamentals of the ASCR, (ICPF, Czech Republic). This system consists of two DMAs (Vienna type), an aerosol bipolar charger, an aerosol drier, an aerosol humidifier, and a CPC 3772 (TSI).

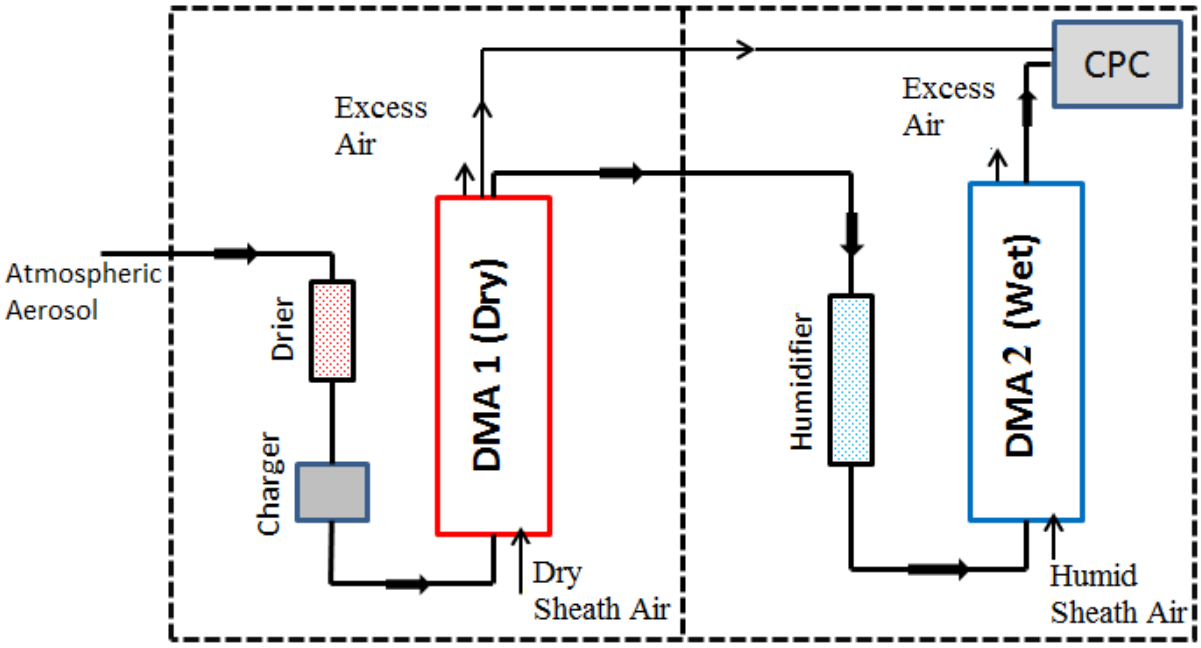

Figure 2.5: HTDMA schematic.

In this system, the atmospheric aerosol sample flow is first dehydrated though an aerosol drier, and neutralized by an aerosol charger before passing through the first DMA. The sample flow and sheath air should be kept at low relative humidity (RH <20%) to make ensure the aerosols are dry. Dry aerosols were selected by the first DMA in a narrow quasi-monodisperse size interval, and then they undergo at a high relative humidity environment

(approximately at 90% RH) by an aerosol humidifier, and continued to pass through the second DMA. The size of wet monodisperse aerosols are classified by the second DMA and the number concentration is measured by a CPC. The growth factor of a particle is determined by a ratio of a wet particle diameter measured by the second DMA and a dry particle diameter measured by the first DMA.

2.2. Lung deposition models

2.2.1. International Commission on Radiological Protection (ICRP) model

The ICRP model is a semi-empirical model which determines the deposition fraction of particles in five regions of the airway system (the nose and mouth, throat and larynx, upper airways, lower airways, and alveolar) based on numerical fitting experimental data and theory calculation. The deposition of particles is controlled by different transport processes, which strongly depend on particle size. In the empirical modelling of the deposition data, the deposition fraction of particles is calculated by two kinds of deposition processes known as aerodynamic and thermodynamic transport.

In terms of aerodynamic deposition, particles with an aerodynamic diameter greater than 0.5 μm are mainly deposited in the regions of the respiratory tract due to inertial motion (impaction), and gravitational settling (sedimentation). For very large particles or fiber, their deposition is determined more by interception with the surfaces in the extra-thoracic region.

The aerodynamic deposition efficiency is given by the following equation:

$$\eta_{ae} = 1 - (1-\eta_I)(1-\eta_S) \quad (2.1)$$

Where, η_{ae}, η_I, η_S is deposition by aerodynamic transport, impaction and sedimentation.

In terms of thermodynamic deposition, particles with an equivalent physical diameter of less than several hundred nano-meters are mainly deposited by the transport process of Brownian

diffusion. This thermodynamic transport is determined by the thermodynamic diameter of the particle, which is considered to be equal to the particle volume equivalent diameter.

ICRP (1994) recommended that simultaneous thermodynamic and aerodynamic transport is only significant for particles in a transit regime size range of 0.1 μm thermodynamic diameter to 1 μm aerodynamic diameter. Thermodynamic transport predominantly accounts for the deposition of small particles, while aerodynamic transport is mainly responsible for large particles. For particles in a transit regime size range, their deposition efficiencies will be combined by the following equation:

$$\eta = (\eta_{th}^{2} + \eta_{ae}^{2})^{1/2} \quad (2.2)$$

Where, η is the total deposition and η_{th}, η_{ae} is the deposition efficiencies determined by thermodynamic and aerodynamic transport.

General equations of deposition efficiency of particles from the ICRP model

In the ICRP model, each regions of the respiratory tract is represented by an equivalent particle filter, as shown in Figure 2.6. In the empirical filtration model, each anatomical region can be represented by one or more filters in series, in which each filter can be characterized by two parameters: its volume and its overall efficiency in removing airborne particles.

The deposition efficiency (DE_j) of particles that are deposited in the j^{th} filter is given by equation (2.3):

$$DE_j = \eta_j \emptyset_j \prod_{jj=0}^{j-1} (1 - \eta_j) \quad (2.3)$$

where, η_j is the filtration efficiency of the j^{th} filter and $\emptyset_j$ is the fraction of tidal air that reaches the j^{th} filter on inhalation.

In terms of regional lung deposition, its efficiency (η_j) is expressed in terms of three parameters: *a*, *R* and *p* which are combined in the general form $a^* R^p$ (Rudolf et al., 1990). These three parameters depend upon the particle size, components of the total volumetric flow rate, anatomical dead space, scaling parameters for different subjects, and the time constant for conduction (residence of air) in the different airways. The values of *a*, *R* and *p* recommended by ICRP (1994) are given in Table 2.1.

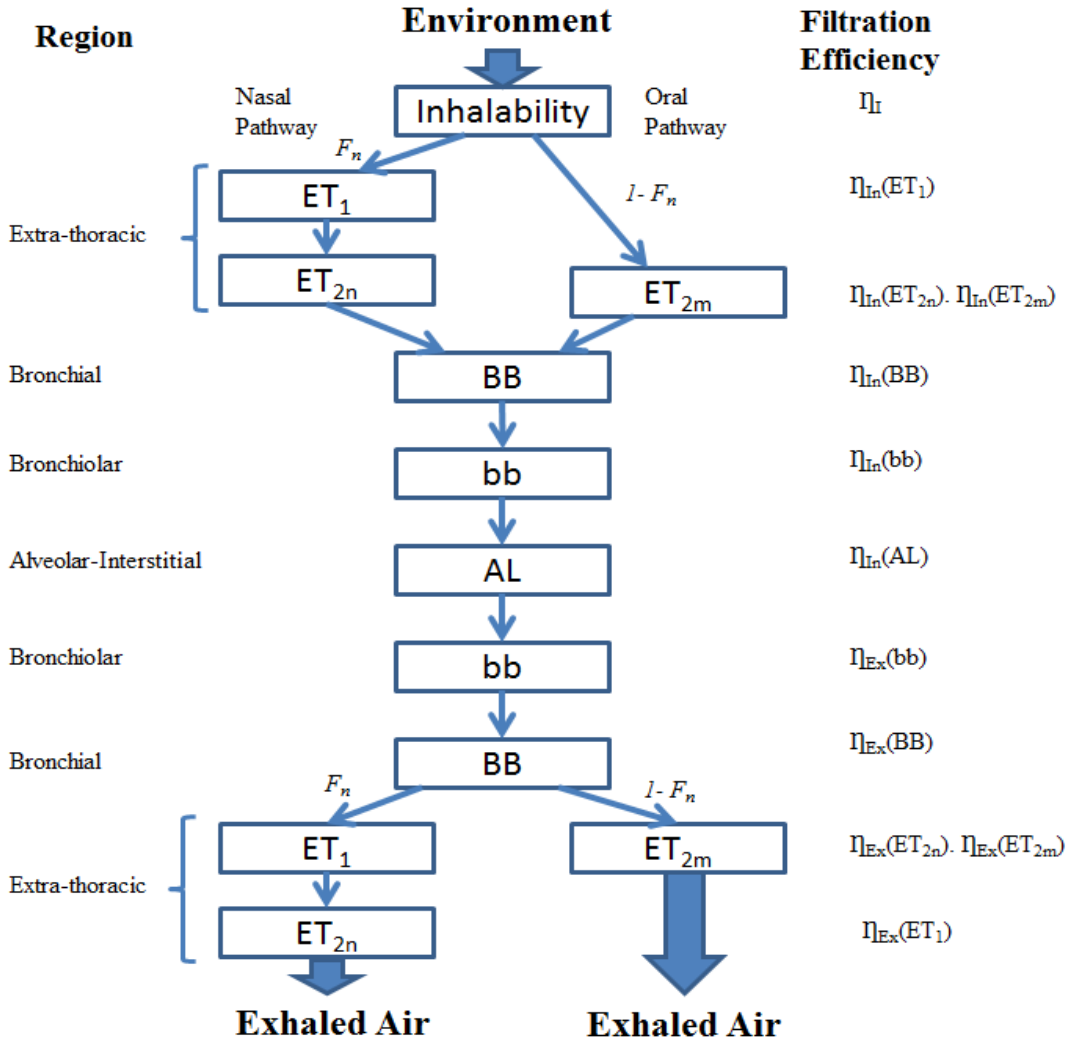

Figure 2.6: Empirical representation of the inhalability of particles and their deposition in the extrathoracic (ET), bronchial (BB), bronchiolar (bb), and alveolar regions (AL) of the respiratory tract during continuous cyclic breathing by transport through a series of filters (ICRP, 1994).

Table 2.1: Recommended parameters for substitution in the ICRP model of regional deposition due to inhalation (ICRP, 1994).

Phase	Filter j	Region	Regional deposition efficiency, η_j						Volumetric Fraction $\emptyset_j$
			Aerodynamic			Thermodynamic			
			$\eta_{ae} = 1 - \exp(-aPR^p)$			$\eta_{th} = 1 - \exp(-aPR^p)$			
			a	*R*	*p*	*a*	*R*	*p*	
Inhalation	1	$ET_1^{(*)}$	3.0×10^{-4}	$d_{ae}^2 V_n SF_t^3$	1	18	$D(V_n SF_t)^{-1/4}$	1/2	1
	2	$ET_2^{(**)}$	5.5×10^{-5}	$d_{ae}^2 V_n SF_t^3$	1.17	15.1	$D(V_n SF_t)^{-1/4}$	0.538	1
	3	BB	4.08×10^{-6}	$d_{ae}^2 V_n SF_t^{2.3}$	1.152	$22.02 d_t^{1.24} \Psi_{th}$	Dt_B	0.6391	$1 - \frac{V_D(ET)}{V_T}$
	4	bb	0.1147	$(0.056 + t_b^{1.5}) d_{ae}^{t_b^{-0.25}}$	1.173	$-76.8 + 167 SF_b^{0.65}$	Dt_b	0.5676	$1 - \frac{[V_D(ET) + V_D(BB)]}{V_T}$
	5	AL	$0.146 SF_A^{0.98}$	$d_{ae}^2 t_A$	0.6495	$170 + 103 SF_A^{2.13}$	Dt_A	0.6101	$1 - \frac{[V_D(ET) + V_D(BB) + V_D(bb)]}{V_T}$
Exhalation	6	bb	0.1147	$(0.056 + t_b^{1.5}) d_{ae}^{t_b^{-0.25}}$	1.173	$-76.8 + 167 SF_b^{0.65}$	Dt_b	0.5676	$1 - \frac{[V_D(ET) + V_D(BB)]}{V_T}$
	7	BB	4.08×10^{-6}	$d_{ae}^2 V_n SF_t^{2.3}$	1.152	$22.02 d_t^{1.24} \Psi_{th}$	Dt_B	0.6391	$1 - \frac{V_D(ET)}{V_T}$
	8	$ET_2^{(**)}$	5.5×10^{-5}	$d_{ae}^2 V_n SF_t^3$	1.17	15	$D(V_n SF_t)^{-1/4}$	0.538	1
	9	$ET_1^{(*)}$	3.0×10^{-4}	$d_{ae}^2 V_n SF_t^3$	1	18	$D(V_n SF_t)^{-1/4}$	1/2	1

Note: $(*)\eta_{ae} = 0.5[1 - 1/exp(-aPR^p)]$ *and* $\eta_{th} = 0.5[1 - exp(-aPR^p)]$; $(**)\eta_{ae} = 1 - 1/exp(-aPR^p)$ *and* $\eta_{th} = 1 - exp(-aPR^p)$; d_{ae}, d_{th} *are the aerodynamic and thermodynamic diameter of a particle (μm).* V_n*is the total volumetric flow rate (mL/s).* $V_D(ET)$, $V_D(BB)$, $V_D(bb)$ *are the anatomical dead spaces of ET, BB and bb (L).* SF_t, SF_b, SF_A*are scaling parameters for different subjects; D: diffusion coefficient;* t_B, t_b, t_A *are the time constants for conduction of air though BB, bb and AL;* Ψ_{th} *is an empirical correction factor for enhancement of thermodynamic deposition.*

2.2.2. Multiple Path Particle Dosimetry (MPPD) model

The MPPD model of the human lung is a mathematical lung deposition model developed by Asgharian et al. (2001). The MPPD model is most realistic deposition model, which considers the branching asymmetry of airways and related air flows based on detailed information on measured lung geometries.

There are four options of human lung structure provided in the software model: symmetric, multiple-path, stochastic geometry and age-specific model. The symmetric and multiple path models use a symmetric tree for the whole lung and the lobar data, as provided by Yeh and Schum (1980). These models should be used to predict the regional lung (ET, TB, AL) or total lung deposition of particles or average lobar-specific deposition. The stochastic model uses data provided by Koblinger and Hofmann (1990). In this model, the asymmetric structures of the tracheo-bronchial (TB) region are generated stochastically based on the morphometric measurements of Yeh and Schum (1980).

This model mode can be used to accurately predict particle deposition in the specific lung airways, as well as the regional lung; however it requires a powerful computer because of the large datasets of generated lung structure. The age-specific model is built based on the measurement data of Mortensen et al. (1989) and Mortensen et al. (1983). There are two options in this model: (1) the age-specific symmetric model uses a dichotomous, branching, symmetric tree single path model, and (2) the age-specific 5-lobe model uses 5-lobe symmetric geometries which are similar to the Yeh-Schum 5-lobe lobar-specific model, but different in the lung structure. These models are recommended for calculation of the particle deposition in children and young adults in the age range from 3 months to 21 years.

Like the ICRP model, the mechanisms for particle deposition are considered by the diffusion and sedimentation within an airway and impaction at the airway bifurcations. Therefore,

deposition efficiency of particles in each airway branch is the function of the air velocity, airway dimensions, bifurcation angle, gravity angle and particle density (Ingham, 1975; Wang, 1975; Zhang et al., 1997). This model assumes that airway branching is dichotomous and that each airway branch is cylindrical and straight. However, it neglects the interception because this is only used for spherical particles with a size range from 0.01 to 20 μm.

2.2.3. Comparison of the ICRP and MPPD models

This section compares the lung deposition models. The ICRP and MPPD models are two popular models that have been used in recent years to calculate deposition fraction (DF) of particles in the different regions of the respiratory tract. A computational program on was written on R-programming based on the ICRP's equations (as shown in Table 2.1) to generate the ICRP deposition fraction curves. (The code was written by the author- Tuan V. Vu).

In the comparison, we calculated the regional lung deposition of spherical particles with unit density for a man under nasal sitting breathing conditions. The parameters were input in the model based on the ICRP's recommendations (FRC=3301 mL; V_T =750 mL; V_n = 300 mL). The input parameters in the MPPD model were the set up in Table 2.2. The information on the functional residual capacity, upper respiratory tract volume, breathing frequency, and tidal volume is also provided by ICRP (1994). The inspiratory and pause fractions of the residence time of particles in the lung are referred to Ferron et al. (1988).

Table 2.2: MPPD model input for a man in resting (sitting) and light exercise states.

Airway Morphometry	Species	Sitting	Light exercise
	Model	Yeh/ Schum 5-Lobe	
	FRC (mL)	3301	
	URT Volume (mL)	50	
Particle Properties	Nanoparticle Model	YES	
	Inhalability Adjustment	YES	
Exposure Scenario	Acceleration of gravity (cm^2 s^{-1})	981	
	Body orientation	Upright	
	Breathing Frequency (min^{-1})	12	20
	Tidal Volume (mL)	750	1250
	Inspiratory Fraction	0.435	0.435
	Pause Fraction	0.05	0.05
	Breathing Scenario	Nasal	Nasal

Note: FRC: functional residual capacity; URT: Upper Respiratory Tract

As a result, figure 2.7 shows the comparison between the ICRP/MPPD models for a man in resting (sitting) and light exercise states. For particles with diameters lower than 10 nm, MPPD model likely underestimate both total and regional lung deposition of particles. For particles larger than 10 nm, the results between two models are found to be consistent, although the deposition fraction of fine particles (0.01 μm < Dp <1μm) from ICRP model was found to be slightly lower than those from the MPPD model. The variation between these deposition efficiencies was lower than 10%, but these errors could be acceptable when compared to those from subject variability. Hofmann (2011), who also compared the ICRP and MPPD models for mono-disperse aerosols, noted that these differences probably derived from the application of different morphometric lung models, analytical deposition equations and modelling techniques.

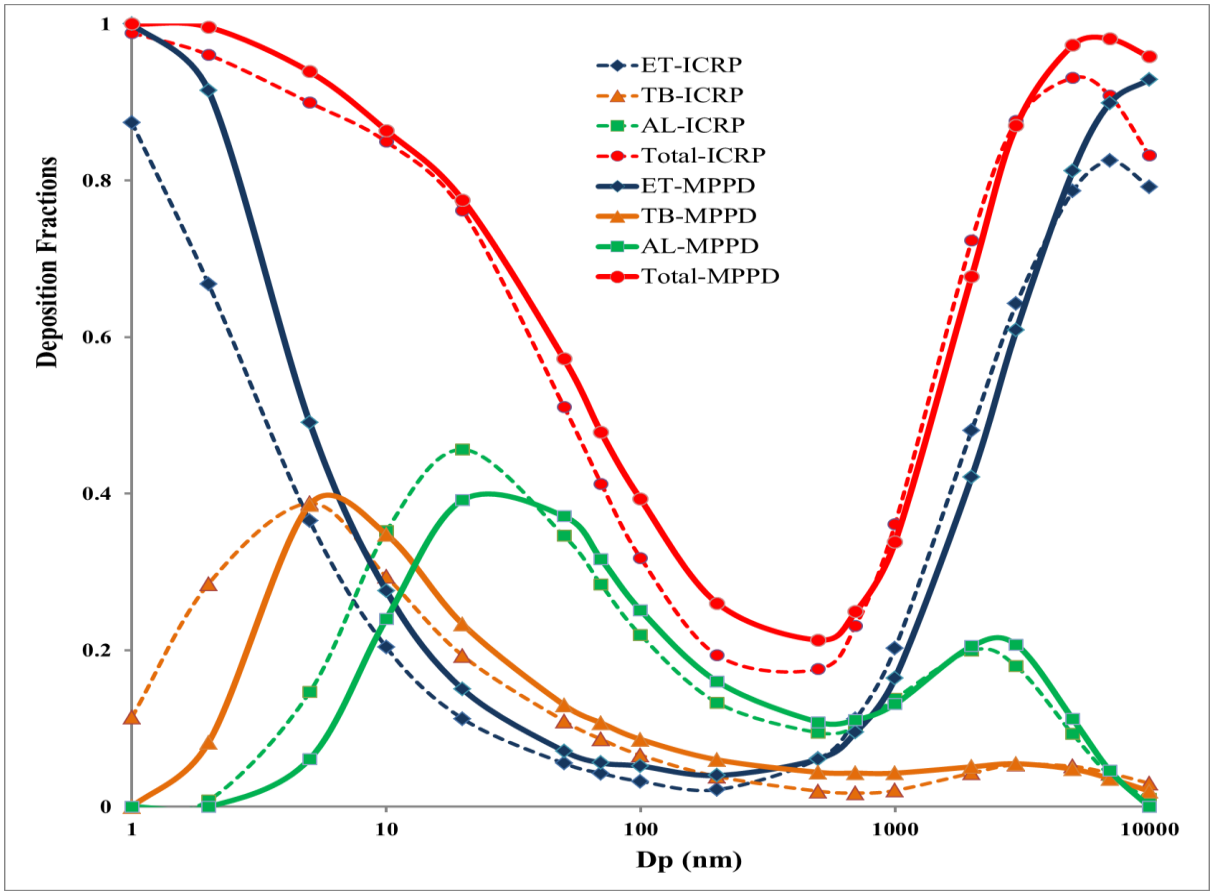

Figure 2.7: Regional lung deposition fraction of spherical particles with unit density for a man under nasal sitting breathing conditions based on ICRP and MPPD models.

Current problems and application of the ICRP/MPPD models

In general, the mathematical lung deposition models have great advantages. For examples, they can predict lung deposition in a variety of inhalation conditions, give a detailed dose analysis, and complete the experimental gaps. However, they still have some disadvantages because of their assumptions in simple geometry and ideal flow conditions. Hofmann (2011) indicates two major problems in the application of analytical whole lung models: (1) the inter-subject variability of morphological and physiological parameters and (2) the assumption of flow conditions to airway bifurcations for realistic inspiratory and expiratory flow patterns.

Although ICRP used some experimental data sets to fit their empirical equation, very limited data from experiments were used in that model. There should be more experimental data for the validation and empirical adjustments for the models. Some software products have been developed such as the MPPD model or the ExDoM model (Aleksandropoulou and Lazaridis, 2013), which allow users to easily estimate the lung deposition of aerosols. However, these products do not fully consider the effects of particle shape or hygroscopicity.

2.3. Source apportionment model (PMF model)

Positive Matrix Factorization (PMF) has been a widely used tool in recent years to identify and apportion the sources of particles by number (Vu et al., 2015b). In the source apportionment of particles in terms of number, each size bin in the dataset is considered as an input variable. The goal of PMF is to identify the number of factors (p), the size profile (f) of each source, and the amount of number (g) contributed by each factor to each individual measurement using the following equation:

$$x_{ij} = \sum_{k=1}^{p} g_{ik} f_{kj} + e_{ij} \quad (2.4)$$

where, x_{ij} is the particle number concentration of size bin j on the i^{th} sample, and e_{ij} is the residual for each measurement/ size bin.

The number of PMF factors is determined by the minimum of the object Q, which is based on these uncertainties (u) in a combination with the environmental meaning of each factor.

$$Q = \sum_{i=1}^{n} \sum_{j=1}^{m} \left[\frac{x_{ij} - \sum_{k=1}^{p} g_{ik} f_{kj}}{u_{ij}} \right]^2 \quad (2.5)$$

PMF solutions are interpreted based on (1) modal characteristics of number (volume) size distribution, (2) diurnal patterns of contribution, (3) source contributions to total number or volume concentration, (4) the correlation of the G-matrix with the measured gaseous or

composition species and (5) source directionality by the local wind trajectories and conditional probability functions (Ogulei et al., 2007).

The number of variables has ranged from 16 to 158, depending on the numbers of measurements, the quality of variables and the goals of the study. To smooth the size distribution data and reduce uncertainty in the number concentration, some studies have tried to reduce the original number of size bins by summing sets of consecutive size bins (Thimmaiah et al., 2009; Zhou et al., 2005). In addition, Zhou et al. (2004) suggest that data from days with intense nucleation events, which considerably affect the stability of particle size distribution data should be excluded. In some instances the last size interval has not been included because of a drop in collection efficiency or low data capture (Gu et al., 2011; Kim et al., 2003). In some studies, auxiliary data such as ion species, heavy metals, gaseous pollutants, meteorological parameters and traffic data have been added to help separate and identify the sources of particulate matter (Harrison et al., 2011; Ogulei et al., 2006b; Thimmaiah et al., 2009). In this study, we ran a PMF (US EPA model version 3) on a profile of 6,098 hourly particle number sizer distribution comprising 51 size bins ranging from 16.6 to 604 nm.

Calculation of measurement errors and uncertainties

Since the error matrix for particle counts is not provided by the experimental instruments, several methods to assign measurement errors (σ) have been reported. The most popular formula to calculate measurement errors was introduced by (Ogulei et al., 2006a) as the following empirical equation:

$$\sigma_{i,j} = \begin{cases} \alpha(N_{i,j} + \bar{N}_j) & \text{if } N_{i,j} > 0 \\ 2\,\bar{N}_j & \text{if } N_{i,j} = 0 \end{cases} \quad (2.6)$$

where, $\sigma_{i,j}$ is the calculated measurement error for size bin j and measurement i^{th}. $N_{i,j}$ is the measured number concentration for size bin j and measurement i^{th}, and $\overline{N}_j$ is the arithmetic mean of the reported values for size bin j. $\alpha = 0.01$ is an arbitrary constant and was determined by a trial and error method. The missing data are replaced by $\overline{N}j$, the mean value for the size bin, and the uncertainty is assumed to be three times $\overline{N}j$.

There are several approaches to estimate uncertainty. This study calculated the uncertainty (u_{ij}) of a size bin j and sample i in the following equation (Ogulei et al., 2006b):

$$u_{ij} = \sigma_{i,j} + C_3(N_{i,j}) \quad (2.7)$$

where, $\sigma_{i,j}$ is the calculated measurement error for size bin j and measurement i^{th}. $N_{i,j}$ is the measured number concentration for size bin j and measurement i^{th}. C_3 is a dimensionless constant value and should be chosen when the scaled residuals are approximately randomly distributed between -2 to +2.

2.4. Data handling

Data statistical analysis, polar plots and concentration weighted trajectories were performed in the CRAN R program (Version 3.1.5) using the "Open-air" package developed by Carslaw and Ropkins (2012). This study used an enhanced algorithm which was developed in CRAN R by Beddows et al. (2010) to merge two types of data sets (aerodynamic and mobility) collected from APS and SMPS instruments into one particle size spectrum matrix. A mass balance model and a coagulation model were coded and performed in CRAN R by the author. To analyse the growth factors from the HTDMA, this study used a TDMAinv conversion approach provided by the Laboratory of Atmospheric Chemistry, Paul Scherrer Institute (PSI, Switzerland) (Gysel et al., 2009) which was run on the Igor Wave Metric software, version 6.1. This study also used Microsoft Excel 2010 for some simple plots, and SigmaPlot version 13.0 for contour plots.

Chapter 3: AN INVESTIGATION INTO THE PARTICLE SIZE DISTRIBUTION COLLECTED FROM AN AUTOMOTIVE BRAKE CALIPER TEST RIG

This chapter investigates brake wear particle size distribution which is known as an essential parameter in source identification and human respiratory deposition determination. Concentrations and size distributions of brake wear particles were measured from a laboratory test rig using an Aerodynamic Particle Sizer Spectrometer (APS 3321 operated in series with an Aerosol Diluter 3302A), a Condensation Particle Counter (CPC 3775) and a high time resolution Engine Exhaust Particle Sizer Spectrometer (EEPS). The number of both ultrafine and coarse particles increased during braking. Particle nucleation was observed at an appropriate high brake pad temperature. As a result, the braking processes released particles with a wide range of size distributions, ranging from few nanometers to micrometers. They showed a bi-modal size distribution with a major mode around 120-140 nm in the submicron size range, and a peak mode around 1.1-1.58 µm in the coarse size range. The count median diameter (CMD) depends upon brake load. The particle volume size distribution showed a bimodal size distribution including a major coarse mode (accounting for around 95% of total volume) with a volume median diameter (VMD) of 1.6-2.4 µm, and a minor accumulation mode.

The author's contribution: writing, contribution of ideas, experimental design and measurements, and numerical calculations.

3.1. Introduction

Non-exhaust particles which typically arise from road-tyre interaction, brake wear, and re-suspension contribute significantly to urban airborne concentrations. Previous studies show that brake wear can contribute 11-21% by mass to total traffic-related PM10 emissions (Grigoratos and Martini, 2015). It is therefore closely associated with human health problems. Despite its significant contributions to ambient PM emissions, knowledge of its particle size distribution, particularly its nucleation mode (D_p, particle diameter, is lower than 30 nm) is limited.

In previous studies, the particles generated from the mechanical processes of brake wear are well-known to have a wide range of diameters, from a few hundred nanometres to a few tens of micrometres (Thorpe and Harrison, 2008). Several studies have reported that brake aerosol size distributions have a primary peak at approximately 1 μm (Iijima et al., 2007; Wahlström et al., 2010b) for the coarse mode particles. In addition, some recent studies have applied a Scanning Mobility Particle Sizer (SMPS) system to measure particle sizes from 10 nm to 600 nm and have found showed a dominant peak at a particle size of about 100 nm (Kukutschová et al., 2011; Wahlström et al., 2010a).

Nanoparticles (Dp <30 nm) formed from brake emissions were suggested by Garg et al. (2000). However, the evidence of the occurrence of nucleation particles is limited. The first evidence was reported by Mathissen et al. (2011), who set up a sampling tube close to the brake disc of a diesel car and measured the particle sizes under different driving situations using an Engine Exhaust Particle Sizer Spectrometer (EEPS). The experiment found that full braking presented a unimodal particle number size distribution with a peak at approximately 11 nm. Recently, Kwak et al. (2014) have presented the second evidence after observing

nanoparticles particles emitted from brake emissions using a proving ground and road simulator.

However, test rig evidence of brake nanoparticles has been unclear until now. Therefore, this chapter aims at investigating brake wear particle size distribution in a wide size range, from few nanometers to 20 μm, in order to address a concern the whatever the formation of brake wear particles occurs by nucleation process. In addition, it studies the effects of different brake pressures, in the range from 30 psi to 60 psi, which correspond to light, medium and heavy braking, on the evolution of particle size.

3.2. Experimental design and instruments

The concentrations and size distributions of brake wear particles were measured from a laboratory test rig as shown in Figure 3.1. In this test system, an electric motor drove a disc (rotor) at a constant 1500 rpm and airborne wear particles were generated from the contact between the rotor and pads in a closed metal chamber. The pad and cast iron disc were bought from a commercial company. The chamber size was 40 cm × 50 cm × 36 cm. This pad and disc was simulated as a typical brake system from a car. Different braking loads were applied to the calipers using pneumatic pressures (30, 40 and 60 psi). The rotor speed and these pressure loadings also represent for the typical vehicle speed and braking loading of a car driving in cities.

The temperature rise at the back of the pad was measured using a K-type thermocouple. Before each brake loading, the discs and pads heated by braking were cooled by the air flow from a fan. The brakes were applied for 5-10 minutes, then released when these pad's temperature reached a maximum level or nucleation occurred. This study conducted 3, 3 and 2 times of PNSD measurements at 30, 40, and 60 psi, respectively.

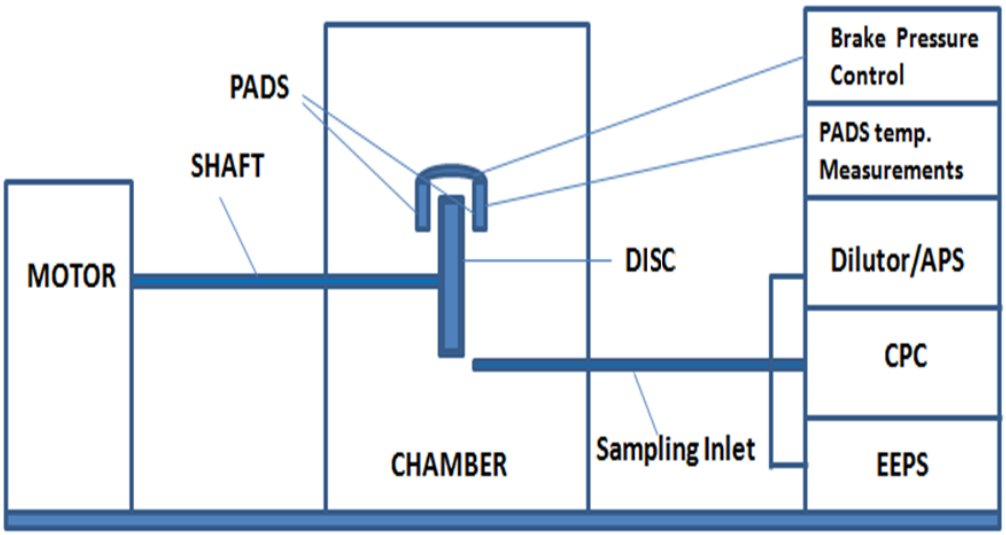

Figure 3.1: Schematic diagram of the test system.

The brake caliper- disc assembly was concealed within a simple metal enclosure. A sampling inlet was connected to a suite of aerosol instruments which measured the size distribution of the particles generated across the size range of 0.06–18 µm. The instruments included an Aerodynamic Particle Sizer Spectrometer (TSI APS model 3321 operated in series with a TSI Aerosol diluter model 3302A), a Condensation Particle Counter (TSI CPC model 3775) and a high time resolution Engine Exhaust Particle Sizer Spectrometer (TSI EEPS model 3090). The list of instruments and their operation details are given in Table 3.1.

Table 3.1: List of instruments used in the brake rig test.

Instruments	**Size range**	**Resolution**	**Measurement parameter/symbol**
Aerosol Diluter 3302A	dilution ratio 100:1	Continuous working	For diluting aerosol from the brake emission
Aerodynamic Particle Sizer Spectrometer (APS 3321)	0.53-20 µm	60 s	Particle number size distribution (aerodynamic diameter)
Condensation Particle Counter (CPC 3775)	>4 nm	0.1 s	Total number concentration
Engine Exhaust Particle Sizer Spectrometer (EEPS 3090)	5.6 - 560 nm	0.1 s	Particle number size distribution (mobility diameter)
Digital Thermometer (RS 206-3722)	-	1 s	Pad temperature measurement

3.3. Results

3.3.1. Particle number, surface and mass concentrations

Number concentration

The submicron particle number concentrations were measured by the CPC 3775 and EEPS, while super-micron and coarse particles were measured by an APS sampler. When the braking pressure was applied, the particle number concentrations suddenly increased and reached their maximum values in the first minute of braking. For example, the total concentrations in the first minute of braking at a 45 psi load were 2.2×10^4 and 1.1×10^4 particle cm^{-3} for submicron particles and super-micron particles ($0.6\ \mu m < D_a < 18\ \mu m$) measured by CPC and APS while these values were 7.5×10^3 and 157 particles cm^{-3}, respectively in the background air.

In the next minute of braking, these numbers dropped dramatically to stable values around 1.1×10^4 and 7.1×10^3 particles cm^{-3}. When the braking continued, the pad temperature increased, therefore generating more concentrations of volatile organic compounds. When the temperature increased to a critical level and the concentrations of volatile organic compounds were high enough to be saturated, nucleation occurred, as seen in Figure 3.2. Nucleation events were found at 45 psi (around 118.7-144.3 ^oC) and at 60 psi braking loads (at 155.6 ^oC). There was no nucleation event at 30 psi braking.

A decrease in the total number concentration of larger particles was found during nucleation. When braking stopped, nucleation was immediately suppressed. As shown in Table 3.2, the total number concentration of particles increased with higher braking loads.

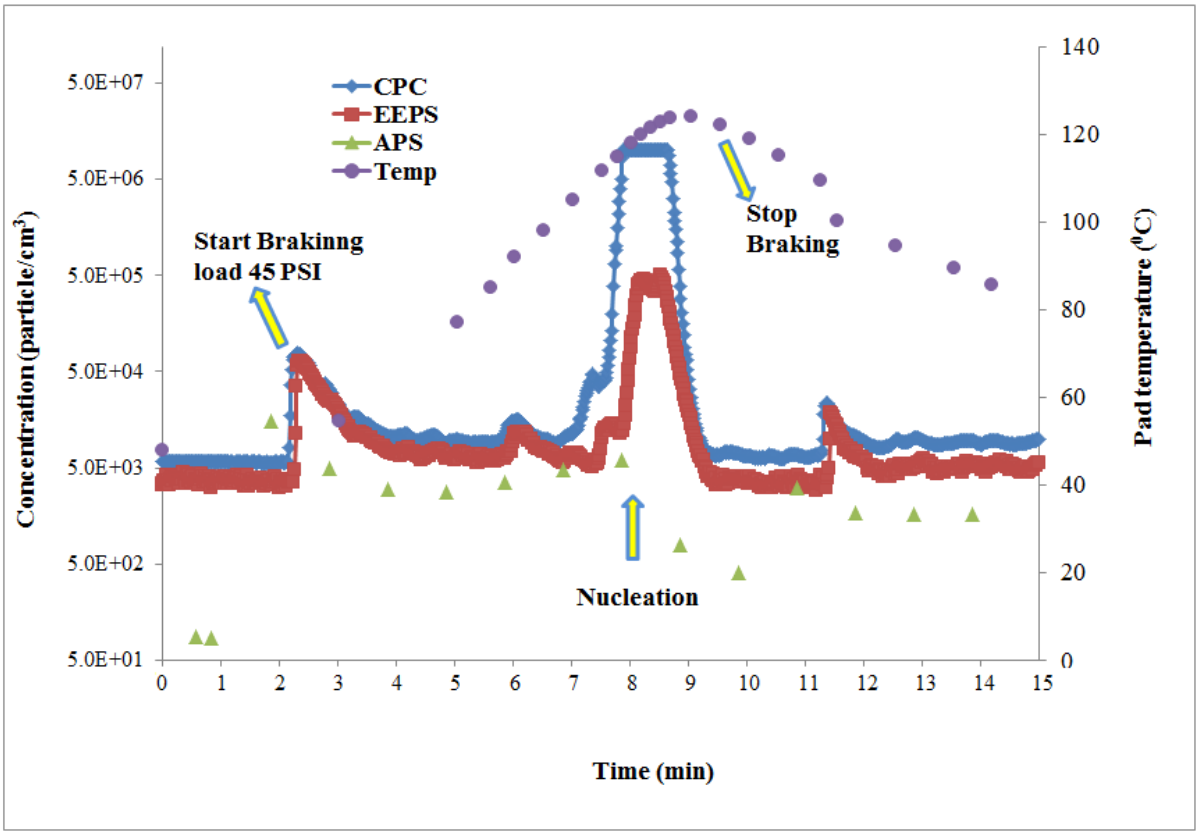

Figure 3.2: Total particle number concentrations from EEPS, CPC and APS during 15 minutes braking period at 45 psi load.

Surface area and mass concentration

The total surface concentrations of submicron particles were extracted from the EEPS and APS measurements. Note is that particles measured by the EEPS are assumed as spheres, and their diameter is the mobility diameter, while the diameter of larger particles measured by the APS is aerodynamic. To estimate the mass from the EEPS measurements, we assumed the effective density of brake wear particles to be 5 g cm^{-3} (Sanders et al., 2003; Wahlström et al., 2010a).

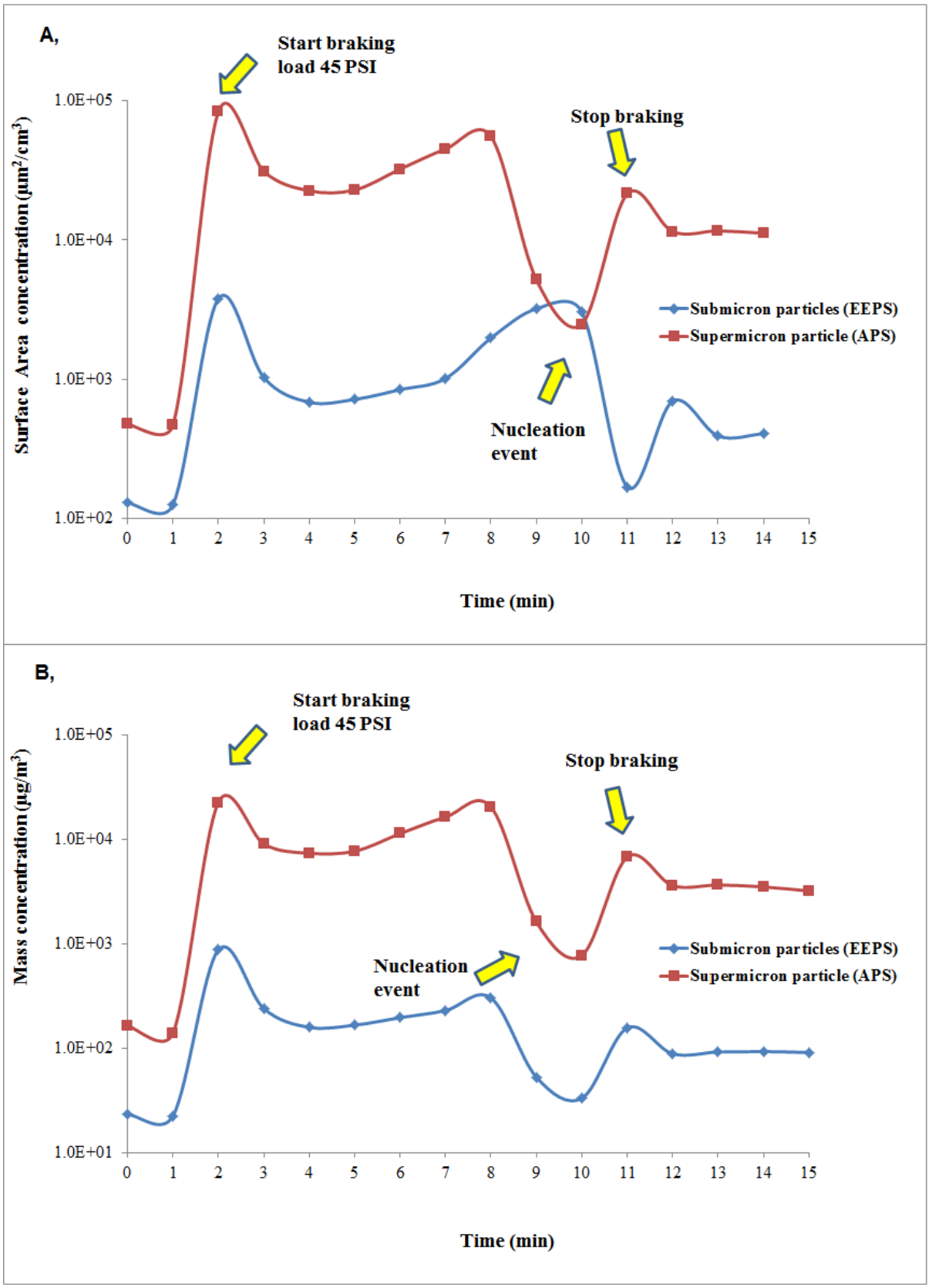

Figure 3.3: Total particle surface area (A) and mass (B) concentrations from EEPS and APS during a 15 minute braking period at 45 psi load.

Figure 3.3 shows the particle surface area and mass concentration during braking at 45 psi. In the first minute of braking, both surface area and mass concentration measured from the APS and EEPS were found to have increased. The total surface area and mass concentrations increased from 590.4 $\mu m^2\ cm^{-3}$ and 161.0 $\mu g\ m^{-3}$ before braking to $8.7 \times 10^4\ \mu m^2\ cm^{-3}$ and $2.3 \times 10^4\ \mu g\ m^{-3}$, respectively.

In the following two minutes of braking, the surface area and mass concentrations decreased to $2.3 \times 10^4\ \mu m^2\ cm^{-3}$ and to $7.9 \times 10^3\ \mu g\ m^{-3}$, then increased again to $5.7 \times 10^4\ \mu m^2\ cm^{-3}$ and $2.1 \times 10^4\ \mu g\ m^{-3}$ before the nucleation occurred. In the nucleation event, the surface area concentration of larger particles measured by the APS decreased from $5.4 \times 10^4\ \mu m^2\ cm^{-3}$ to $2.5 \times 10^3\ \mu m^2\ cm^{-3}$. In contrast, that of the submicron particles measured by the EEPS increased from $1.9 \times 10^3\ \mu m^2\ cm^{-3}$ to $3.2 \times 10^3\ \mu m^2\ cm^{-3}$, probably due to the nanoparticle formation. Total mass concentration of both submicron and super-micron particles decreased from $2.1 \times 10^4\ \mu g\ m^{-3}$ to $8.0 \times 10^2\ \mu g\ m^{-3}$.

A decrease of particle mass is maybe due to the change of the properties of brake pad because of high temperature during nucleation event. The total surface area and mass concentration increased again to $2.2 \times 10^4\ \mu m^2\ cm^{-3}$ and $6.9 \times 10^3\ \mu g\ m^{-3}$ after the nucleation event. Number, surface area and mass concentrations at different brake loadings (30, 45 and 60 psi) are given in Tables 3.2 and 3.3.

Table 3.2: Particle number concentration and size during experiments at different brake loads (30, 45 and 60 psi).

Press.	Instru-ments	Before braking		Braking start point		Braking		Nucleation			After braking stops	
		TN (10^3)	CMD	TN (10^3)	CMD	TN (10^3)	CMD	Temp.	TN (10^3)	CMD	TN (10^3)	CMD
30 PSI	CPC	9.3±2.5	-	22.5±0.7	-	12.3±1.8	-	Max 100	No Nucleation event		7.0±1.1	-
	EEPS	6.1±1.4	60±7	16.1±1.1	130±18	11.2±3.3	108±12				5.2±2.2	73±28
	APS	0.24±0.12	1.0±0.1	7.9±4.3	1.1±0.1	2.8±0.2	1.3±0.1				0.4±0.1	1.0±0.1
45 PSI	CPC	11.0±4.5	-	37.9±14.9	-	17.5±7.8	-	118.7-144.3	-	15.7±6.0	15.7±6.0	-
	EEPS	5.9±1.9	59±15	25.5±10.3	140±14	10.3±4.3	122±18		-	7.9±2.2	7.9±2.2	49±29
	APS	0.9±0.4	1.1±0.1	11.6±4.8	1.1±0.1	4.0±0.2	1.4±0.1		1.9±1.1	2.2±0.2	2.2±0.2	1.2±0.1
60 PSI	CPC	26.4±4.5	-	66.0±9.3	-	32.0±7.7	-	155.6	-	28.7±8.1	28.7±8.1	-
	EEPS	21.0±4.3	59±2	45.8±6.3	139±8	23.3±4.9	132±11		-	13.3±2.1	13.3±2.1	46±8
	APS	2.9±2.4	1.1±0.1	11.2±2.9	1.2±0.1	8.3±2.6	1.5±0.1		1.1±0.6	1.7±0.2	1.7±0.2	1.2±0.1

Note: TN: Total number of particles (particles cm^{-3}); CMD: Count Median Diameter for EEPS (nm) and APS (µm).

Table 3.3: Particle surface area and mass concentration and size during experiments at different brake loads (30, 45 and 60 psi).

Surface area(10^3 µm^3 cm^{-3})											
Pressure	Instruments	Before braking		Braking start point		Braking		Nucleation		After braking stops	
		TS	SMD	TS	SMD	TS	SMD	TS	SMD	TS	SMD
30 PSI	EEPS	0.17±0.01	125±21	1.2±0.4	200±17	0.65±0.14	207±15	No Nucleation		0.44±0.21	210±15
	APS	0.62±0.23	1.4±0.1	33.5±15.4	1.5±0.1	18.2±2.5	1.7±0.1			3.1±1.5	1.6±0.1
45 PSI	EEPS	0.27±0.04	133±11	2.9±1.6	223±7	1.37±0.64	219±13	10.4±3.2	-	0.45±0.13	216±2
	APS	0.61±0.32	1.5±0.1	69.6±15.4	1.5±0.1	32.4±2.9	1.9±0.2	2.4±1.3	-	1.3±0.4	1.8±0.1
60 PSI	EEPS	0.75±0.06	140±5	2.4±1.1	216±3	2.46±0.26	235±19	44.7±18.8	-	0.44±0.08	227±16
	APS	6.5±0.3	1.3±0.1	50.1±30.1	1.4±0.1	75.6±14.7	2.0±0.2	20.4±11.2	-	10.1±2.3	1.7±0.1
Mass (mg m^{-3})											
Pressure	Instruments	Before braking		Braking start point		Braking		Nucleation		After braking stops	
		TM	MMD	TM	MMD	TM	MMD	TM	MMD	TM	MMD
30 PSI	EEPS	0.02±0.01	389±11	0.36±0.03	332±2.8	0.12±0.01	330±4.8	No Nucleation		0.03±0.01	313±9.9
	APS	0.21±0.08	2.1±0.2	9.90±3.63	1.7±0.1	6.20±1.80	1.9±0.1			0.53±0.04	2.9±0.3
45 PSI	EEPS	0.07±0.04	328±22	0.62±0.31	334±4.5	0.20±0.04	337±2.4	0.27±0.12	254±107	0.09±0.01	334±7
	APS	0.61±0.32	1.8±0.4	16.5±5.8	1.8±0.2	11.8±0.9	2.3±0.2	4.9±3.4	2.3±0.2	4.1±0.4	2.1±0.1
60 PSI	EEPS	0.1±0.01	296±22	0.37±0.01	330±3.7	0.31±0.08	332±6.1	2.15±1.38	119±9	0.06±0.01	319±8
	APS	1.77±0.05	1.7±0.5	24.5±4.4	1.9±0.2	23.9±8.2	2.2±0.3	2.2±0.9	2.2±0.2	2.2±0.4	2.1±0.2

Note: TS: Total surface area concentration (10^3 µm^3 cm^{-3}); SMD: Surface area Median Diameter for EEPS (nm) and APS (µm).
TM: Total mass concentration (mg/m^3); MMD: Mass Median Diameter for EEPS (nm) and APS (µm).

Table 3.4: Comparison of PNSD of brake wear particles between this study and previous studies

Brake testing	Vehicle type	Brake Type	Pad/shoes	Instruments	Size range (μm)	Diameter	CMD (μm)	References
Test rig (braking)	Car	Disc	-	EEPS	0.06-0.56	Mob.	0.98-0.15	This study
				APS	0.5-20	Aero.	1.4-1.5	
Field	Car	Disc	LM	GRIMM	0.25-32	Opt.	0.35-0.40	Wahlström and Olofsson (2014)
Field	Train	Disc	-	GRIMM	0.25-32	Opt.	0.28; 0.35	Abbasi et al.(2012b)
Field	Car	Disc	-	EEPS	0.06-0.56	Mob.	0.01	Mathissen et al. (2011)
Field/Road simulation	Car	Disc	NAO	FMPS	0.05-0.52	Mob.	0.01	Kwak et al. (2014)
Dynamometer	-	Disc/drum	SM	MOUDI/ELPI	0.1-18	Aero.	< 0.03	Garg et al. (2003)
Dynamometer	Care	Disc	LM/SM/NAO	MOUDI/ELPI	0.1-18	Aero.	1-2	Sander et al. (2003)
Dynamometer	Car	Disc	LM	SMPS	0.01-0.45	Mob.	0.1	Kukutschová et al. (2011)
				APS	0.5-20	Aero.	1.5-2	
Pin-on-dics	Truck	Disc	SM	LA700	0.04-262	Opt.	0.35	Mosleh et al. (2004)
Pin-on-dics	Car	Cast iron	LM/NAO	GRIMM	0.25-32	Opt.	0.35	Wahlström et al. (2010a)
				SMPS	0.01-0.52	Mob.	0.1	
Pin-on-dics	Train	Railway wheel	cast iron	GRIMM	0.25-32	Opt.	~ 0.3	Olofsson (2011)
				SMPS	0.01-0.52	Mob.	0.07	
Pin-on-dics	Train	Railway wheel	Organic	GRIMM	0.25-32	Opt.	0.3-0.4	Abbasi et al. (2012a)
				SMPS	0.01-0.52	Mob.	0.07-0.12	
Test rig	-	Disc	LM / NAO	GRIMM	0.25-32	Opt.	0.35	Wahlström et al. (2009)
Test rig	-	Disc	LM / NAO	APS	0.5-20	Aero.	1-2	Iijima et al. (2007)

Note: LM: Low metallic; SM: Semi-metallic; NAO: Non-asbestos organic; Mob: mobility; Opt: Optical; Aero: Aerodyamic.

3.3.2. Evolution of number submicron particle size distribution

Figure 3.4 shows the evolution of submicron particles at a 45 psi brake load. Before starting braking, the particle number size distribution displays an approximately uni-modal lognormal structure with a count median diameter (CMD) ranging from 60 to 68.2 nm.

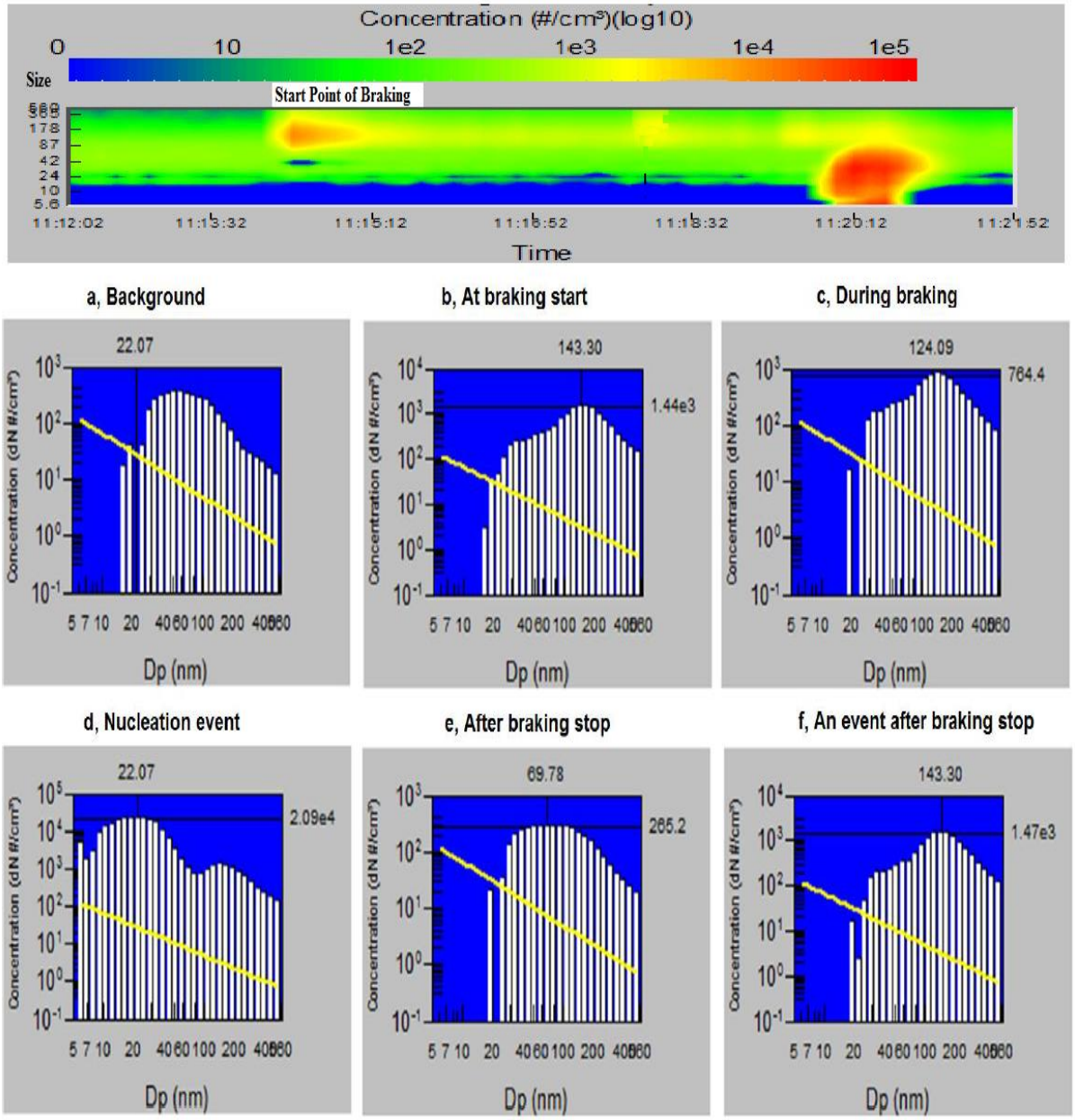

Figure 3.4: Submicron particle size distribution during the experiment period at 45 psi brake load. *The yellow line shows the detection limit level of the instrument.*

In the first minute of braking: A bi-modal lognormal distribution of submicron particles was found with the first mode at 29.43 nm and the second major mode at 154.4 nm. The majority of particles was found in the accumulation mode with an average CMD ranging from 144 to 158.9 nm. In terms of super-micron particles, the CMD increased from 1.01 μm before braking to 1.12 μm. In this period, the majority of accumulation and coarse particles were generated from the friction processes between the disc and pad. Nano particles were also found, which grew rapidly probably due to coagulation process.

During braking period: After the first minute of braking, the CMD of submicron particles decreased to 124.1 - 130.5 nm, while the CMD of super-micron particles increased to 1.26 μm. A bi-modal size distribution of submicron particles was found, with the first mode at 34.0 nm and the second major mode at 143.3 nm. The first mode was maybe due to the growth of nano-particles, while a decrease in accumulation mode particles compared to the braking start point shifted the CMD of accumulation mode from 154.4 nm to 143.3 nm. During this period, there were few the Aitken mode particles (20 nm< Da <80 nm) than those compared to in the background air. More large particles (Da >80 nm) were found than those in the background air, but much fewer than those in the first minute of braking.

Nucleation event: After 5 minutes of braking, nucleation occurred when the temperature reached 118.7^{o}C. Because of nucleation, many new particles were formed, leading to a decrease in CMD of both EEPS and APS size distributions. The CMD of submicron particles was found in the nucleation mode with an average of 20.4 nm, while that of super-micron particles decreased to 1.16 μm.

The formation of new particles probably due to the condensation of organic compounds emitted from organic binder in the brake pad. When the pad temperature increased, lead to breakdown and oxidation of organic binders in the brake pad. The products of breakdown are

semi-volatile and hence vaporise, subsequently condensing as they cool. This could be either by homogeneous nucleation or heterogeneous nucleation, but heterogeneous nucleation would require an involatile core particle (possibly metallic).

In the last experiment, we controlled the temperature of the brake pads and found that the organic vapour became totally super-saturated at approximately 172^{o}C, as seen in Figure 3.5. In the field measurements, the brake pad temperature can reach 400 ^{o}C (Mathissen et al., 2011). Thus, nucleation probably occurs.

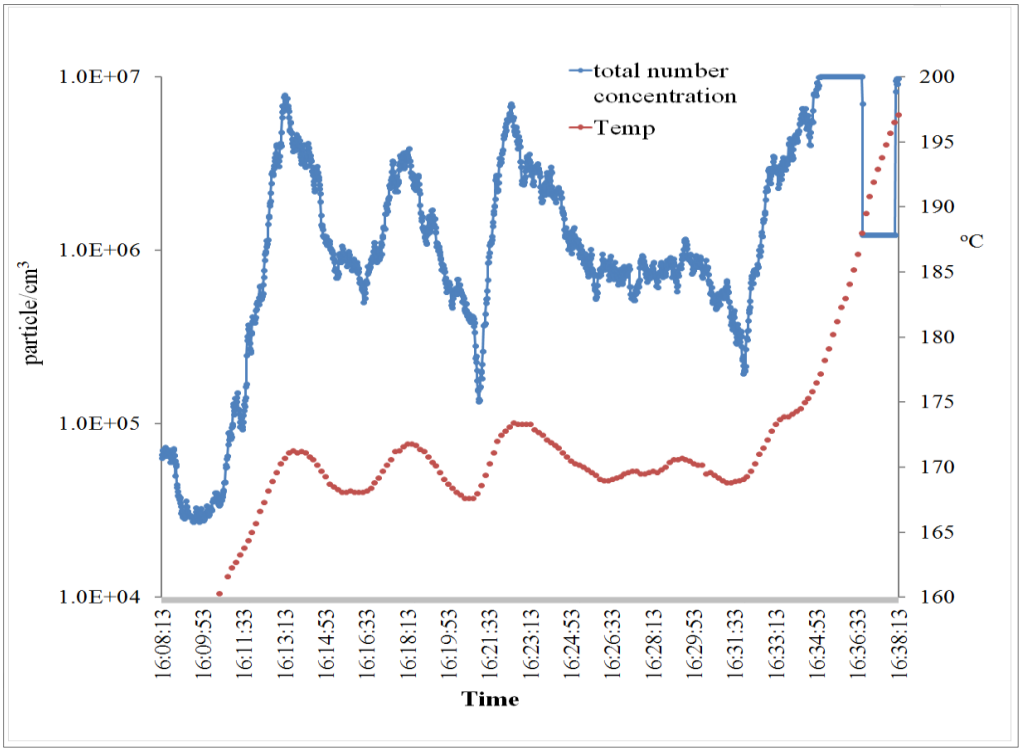

Figure 3.5: Effect of temperature on the nucleation event.

After braking stops: The nucleation immediately ended when braking stopped. The CMD of submicron particle size distributions ranged from 72.5 to 84.4 nm due to the quick growth of small particles formed during nucleation. Due to the high temperature, a small burning event of the brake linings sometimes occurs and thus generates more brake dust in the size range of accumulation and coarse mode, as seen in Figure 3.4 (f). The CMD of coarse particles was

around 1.26 μm, suggesting that coarse particles were still abundant in the chamber environment after braking.

The size distributions of coarse particles measured by APS are shown in Figure 3.6. Table 3.4 show a comparison of PNSD obtained in this study and previous studies.

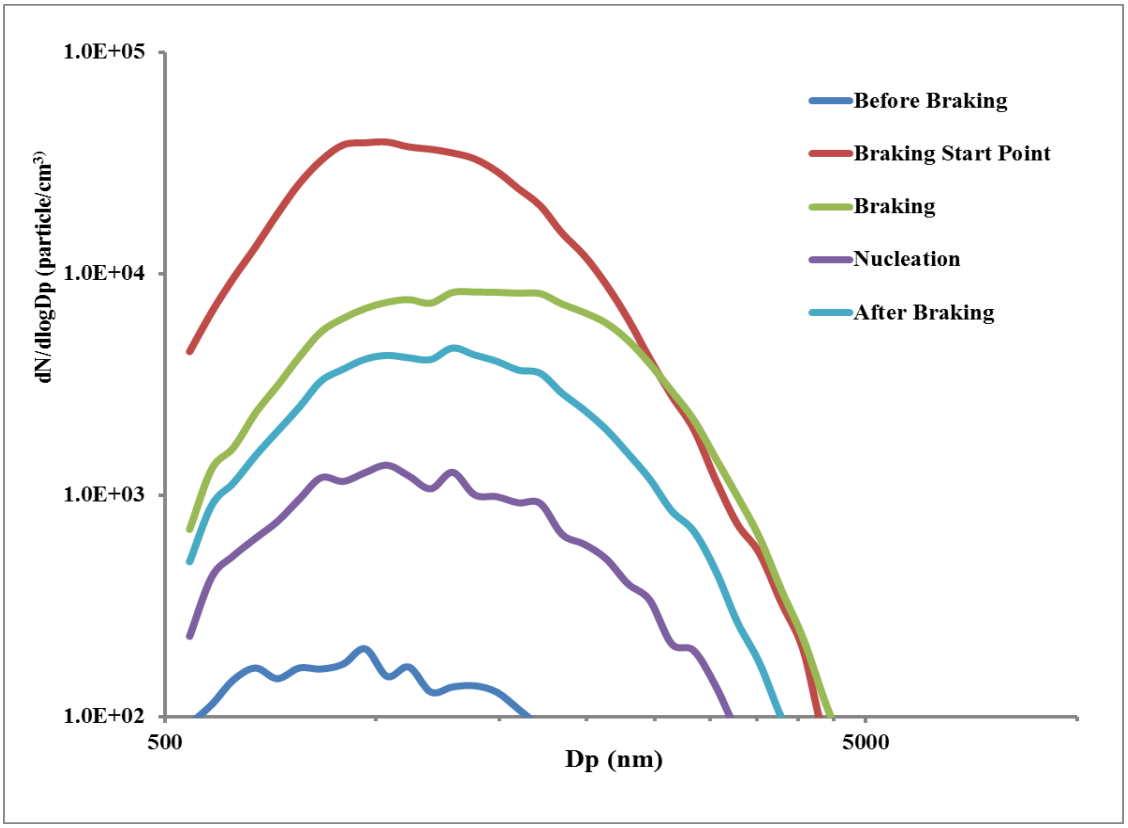

Figure 3.6: Number size distribution of coarse particles at 45 psi braking load.

3.3.3. Particle volume (mass) size distribution

Particle volume

As shown in Figure 3.7, volume size distributions of brake wear particles displayed a bi-modal lognormal structure with a major coarse mode at around 1.6 to 2.4 μm (aerodynamic diameter) and a minor accumulation mode at around 323.3-327.3 nm (mobility diameter). When nucleation occurred, the volume median diameter (VMD) of the accumulation mode

decreased to 100 nm. The VMD of coarse particles increased from 1.9 to 2.4 µm when the pressure load increased from 30 psi to 60 psi during braking.

Coarse mode particles were found as the majority of total particle volume (86.2-95.7%), followed by accumulation mode particles (4.0-11.7%).

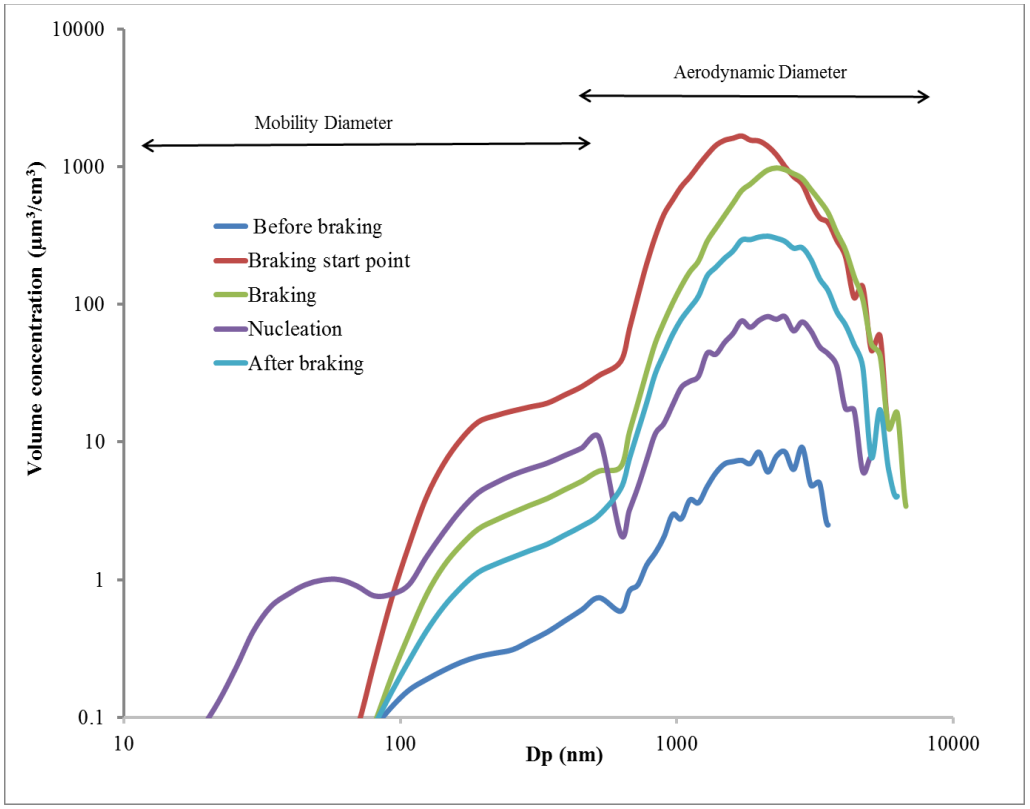

Figure 3.7: Brake wear particle volume size distribution at 45 psi brake load.

Particle mass

In the calculation of mass, the effective density of brake wear particles was assumed to be 5 g cm^{-3} as discussed above. By this assumption, the particle size distribution measured by EEPS in mobility diameter was converted to those in aerodynamic diameter. The mass size distribution is shown in Figure 3.8.

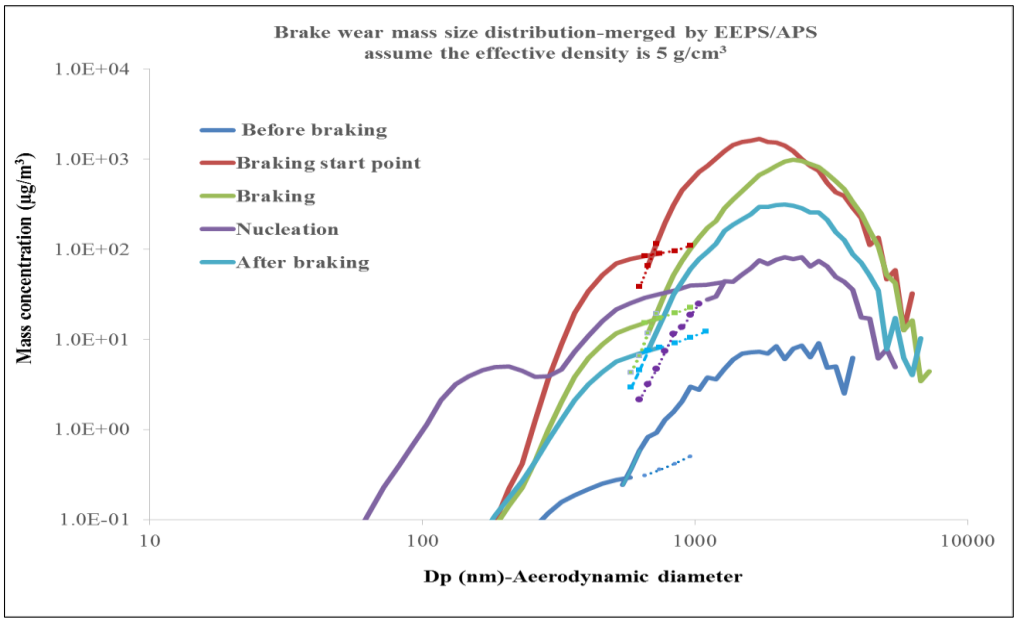

Figure 3.8: Brake wear particle mass size distribution at 45 psi brake load. *The dot lines show the common EEPS/APS spectra size range which does not match well.*

3.4. Conclusion

The evolution of particle size distribution was investigated. Particle size changed quickly from the first minute of braking to the nucleation event. Brake particles display a wide range of number size distribution, from few nanometers to 20 µm. Accumulation and coarse particles were found to be dominant during braking, while nano/ultrafine particles were mainly found during nucleation events. In submicron size range, the brake particles showed a bi-modal size distribution with a major mode around 140 nm and a minor mode around 35 nm. In the accumulation and coarse size range, the brake particles mainly distributed around 1.1 to 1.58 µm. The CMD of coarse particles increased from 1.26 to 1.49 µm when the brake load increased from 30 psi to 60 psi. The particle mass size distribution showed bi-modal size distribution, with a major coarse mode (accounting for around 95% of total volume) and a minor accumulation mode. The mass median diameter (MMD) of coarse mode particles ranged from 1.6 to 2.4 µm.

Chapter 4: INDOOR/OUTDOOR MODELLING OF SUBMICRON PARTICLES IN A HOUSE HEAVILY AFFECTED BY ROAD TRAFFIC EMISSIONS

This chapter evaluates the use of a dynamic mass balance model for predicting the penetration factor, infiltration factor and deposition rate of submicron particles in a house located in an area with busy traffic. Particle number size distributions (PNSD) were measured by a Fast Mobility Particle Sizer system (FMPS model 3091, 5.6-560 nm) in both indoor and outdoor environments at a house located at a site of busy traffic in Bologna (Italy) in the period February-April 2012. The results show that the mass balance model could not determine the unknown penetration factor and deposition rate separately because of their inverse relationship, but it could predict successfully the infiltration rate. When the penetration rate was controlled to be approximately unity in our experiment design, the deposition rate and loss rate of particles at different times was calculated. The loss rate of small particles (nucleation and Aitken mode) in the indoor environment was found to be much higher than those of larger particles (accumulation mode). The study also found the important roles of coagulation and evaporation processes in estimating the loss of indoor particles.

The author's contribution: writing, contribution of ideas and numerical calculations.

4.1. Introduction

Numerous studies have shown that people spend approximately 90% of their time indoors (Harrison et al., 2009). Whilst indoors, people are probably exposed to either indoor particles generated from indoor activities (i.e cooking or cleaning) or outdoor particles penetrating from outdoor environments. Ogulei et al. (2006a) found that particles of outdoor origin (traffic emissions and wood burning) could contribute approximately 3.5% of the total indoor particle number by running a PMF model on the particle number size distribution, measured in a townhouse in the northwest of Washington DC in the US. Therefore, determination of the transport mechanisms as well as the fraction of outdoor aerosols that penetrate into indoor environments is needed in order to apportion the sources of particles to their total lung dose in human exposure studies.

The infiltration rate (F) of aerosols, which is defined as the equilibrium fraction of outdoor particles that penetrate indoors and remains suspended, is controlled by three main factors, the penetration factor (P), the deposition rate (k_d) and the air exchange rate (a_{ex}). The penetration factor, or efficiency of particles at a specific diameter, is defined as the fraction of particles that pass through the building envelope. Thus, penetration efficiency and the infiltration factor must be less than unity. These penetration and deposition processes of particles not only greatly depend upon the building characteristics, such as building envelope and surface area, but also on the characteristics of the particles, especially particle size. Furthermore, other processes such as evaporation and coagulation could have significant effects on the particle losses in a house in an area with busy traffic because of high number concentration and volatile components.

However, there are limited studies of modelling indoor particles from outdoor particles from a traffic site. Therefore, the objective of this study is to evaluate the use of a dynamic mass

balance model for predicting the penetration factor, infiltration factor and deposition rate of submicron particles. The contribution of coagulation to the loss of indoor particles is also investigated.

4.2. Methodology

4.2.1. Instruments and sampling site

Particle number size distributions (PNSD) were measured by a Fast Mobility Particle Sizer (FMPS) system (model 3091, 5.6-560 nm) in both the indoor and outdoor environments of a house located at a busy traffic site in Bologna (Italy) during period February-April 2012, in two sampling campaigns. The first sampling campaign was conducted from 22nd February to 7th March and the second from 16th to 30th April. Indoor sampling monitoring was conducted in an unoccupied apartment located on the ground floor of a two-storey building as shown in Figure 4.1. This building is close to a busy street (31,000 vehicles per day) and near a two-way street canyon.

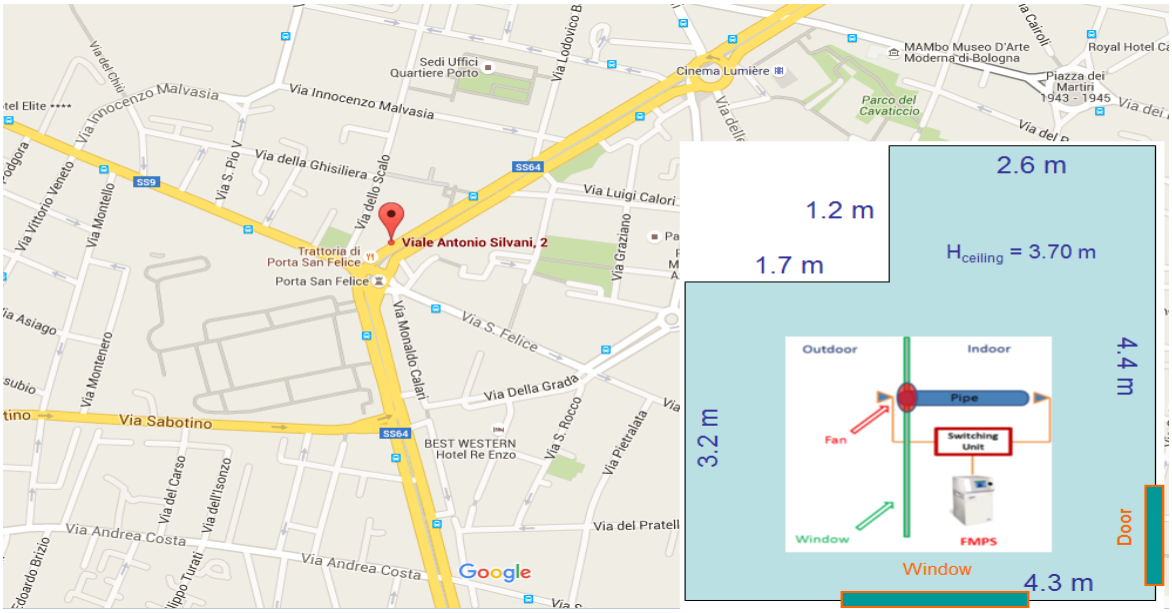

Figure 4.1: Sampling site and experimental conditions.

The FMPS spectrometer measured the size and number concentration of particles every second. This FMPS was connected to a switching valve (Mod 11sc 200, Pneumoidraulica Engineering S.rl., Vicenza, Italy) to measure both indoor and outdoor size distribution every 10 minutes. The length of sampling inlet is approximately 2.1 m. The FMPS data set was corrected for particles loss (as shown in Figure 4.10) before data analysis. Air exchange rate (a_{ex}) was controlled by a novel mechanical system which consisted of an external fan connected to an air pipe to force the air into the centre of the room. The fan was set at a suitable speed to obtain a stable a_{ex} of 0.5 h^{-1}. We also measured the air exchange rate via CO_2 decay data and from this system obtained a similar value of a_{ex} to our estimation. Table 4.1 summaries more information of sampling site.

Table 4.1: Input parameters for mass balance models, deposition and coagulation models.

Parameters	**Values**
Room volume	62.5 m^3
Upward surface area	16.9 m^2
Downward surface area	16.9 m^2
Vertical surface area	64.4 m^2
Air temperature	297 K
Relative humidity	33.2 %
Air exchange rate	0.5 (h^{-1})
Particle size bins	27 (14.3 -523 nm)
Mass balance model time step	20 minutes
Coagulation model time step	1 second

4.2.2. Data preparation

The FMPS system can measure particle size ranging from 5.6 to 560 nm; however, we did not include the size bins below 13 nm in our calculation because a high uncertainty in measurements of particles in these size bins was reported from previous studies (Jeong and Evans, 2009; Kaminski et al., 2013). There were many cases of zero data in several of the last size bins for unknown reasons in the second sampling campaign, thus we also did not include

the size bins over 300 nm for this campaign. The switching valve allowed the FMPS to measure outdoor and indoor size distributions every 10 minutes; this study therefore averaged the data from each 10 minute period, apart from the 2 minute samples at the beginning of each period, to avoid any mixing of outdoor and indoor air streams. The data was analysed using R programing. This study used the "open-air" package developed by Carslaw and Ropkins (2012) for polar plots and time average. Contour plots were performed using the Sigma Plot software, version 13.0. An indoor mass balance model and coagulation model were written on R by the author (Tuan V. Vu).

4.2.3. Indoor mass balance model

The indoor particle concentration can be described using a mass balance model (Chen and Zhao, 2011):

$$\frac{\partial C_{in}}{\partial t} = a_{ER} * P * C_{out} - a_{ER} * C_{in} - k_d * C_{in} + \frac{S}{V} + J_{Other} \quad (4.1)$$

Where C_{in} is the indoor particle concentration (particles cm^{-3}),

C_{out} is the outdoor particle concentration (particles cm^{-3}),

P is the penetration factor,

a_{ER} is the air exchange rate (h^{-1}),

k_d is the deposition rate (h^{-1}),

S is the emission rate of particles (particles h^{-1}),

V is volume of the room (cm^3), and t is the time (h).

J_{Other}: particle production or loss rate due to other indoor processes such as coagulation, nucleation, condensation or evaporation (particles h^{-1}).

For each time step of the specified period (Δt), the indoor concentration is modelled using a numerical backward difference (Chen and Zhao, 2011):

$$C_{in\,(t+\Delta t)} = \frac{a_{ER}*P*C_{out\,(t+\Delta t)}}{a_{ER}+k_d}\left(1 - e^{-(a_{ER}+k_d)*\Delta t}\right) + C_{in\,(t)}e^{-(a_{ER}+k_d)*\Delta t} + \frac{S*\Delta t}{V} + J_{other} * \Delta t \quad (4.2)$$

There was no indoor source during the sampling campaign (S=0) and the air exchange rate (a_{ex}) was controlled by 0.5 (h^{-1}), therefore the indoor concentration can be estimated following the equation:

$$C_{in\,(t+\Delta t)} = \frac{0.5*P*C_{out\,(t+\Delta t)}}{0.5+k_d}\left(1 - e^{-(0.5+k_d)*\Delta t}\right) + C_{in\,(t)}e^{-(0.5+k_d)*\Delta t} + J_{other} * \Delta t \quad (4.3)$$

Based on the outdoor concentration (C_{out}), and the initial indoor concentration (C_{in} at a specific time, such as t=0), we can estimate the indoor concentration C_{in} based on equation (4.3). The outdoor and indoor switching valve time was 10 minutes, thus the time step between two outdoor measurements (Δt) is 20 minutes (1/3 hour).

To determine the penetration factor and deposition rate (P, k_p), the p and k values (with $0< P \leq 1$ and $k_P> 0$) were changed with an interval of 0.01 until modelled C_{in} best fitted with observed C_{in}. To evaluate goodness-of-fit in the comparison of the model to the observed data set, we used two criteria:

1. The Root Mean Square Error (RMSE) between the model and observed indoor concentrations:

$$\text{RMSE} = \sqrt{\frac{\sum_{i=1}^{N}(C_{in\ by\ mass\ balance\ model} - C_{in\ by\ measurement})^2}{N}}$$

where, N: total number of samples

2. The Pearson Correlation Coefficient of determination (r) between two indoor data sets estimated by a mass balance model and observed by real measurements.

4.2.4. Coagulation Model

The coagulation equation was introduced by the following equation (Müller, 1928; Seinfeld and Pandis, 2012):

$$\frac{\partial N_v}{\partial t} = \frac{1}{2}\int_0^v \beta_{v-\tilde{v},\tilde{v}}\, N_{v-\tilde{v}} N_{\tilde{v}} \mathrm{d}\tilde{v} - N_v \int_0^\infty \beta_{v,\tilde{v}} N_{\tilde{v}} \mathrm{d}\tilde{v} \quad (4.4)$$

where v-ṽ and ṽ are the volumes of two coagulating particles, v is the volume of the new particle due to coagulation, and N is the time-dependent number concentration (particles cm^{-3}) of particles with a volume of v, v-ṽ or ṽ. $\beta_{v-\tilde{v},\tilde{v}}$ is the coagulation rate coefficient (coagulation kernel) of the two colliding particles (cm^3 $particle^{-1}s^{-1}$).

For a monomer size distribution, equation (4.4) is discretized and written in fully implicit finite-difference form as (Jacobson, 2005; Seinfeld and Pandis, 2012):

$$\frac{N_{k,t} - N_{k,t-\Delta t}}{\Delta t} = \frac{1}{2}\int_{j=1}^{k-1} \beta_{k-j.j}\, N_{k-j,t} N_{j,t} - \int_{j=1}^{\infty} \beta_{k,j} N_{k,t}\, N_{j,t} \quad (4.5)$$

where, k is the size bin which is produced when particles in bin k-j coagulate with particles in size bin j. Δt (s) is the time step and t and t - Δt are the final and initial times respectively. A size distribution is defined as a monomer size distribution when "the volume of each particle in size bin k equals the volume of particles in the smallest size bin multiplied by k" (Jacobson et al., 2005).

To solve equation (4.5), several techniques can be used, one of which is the semi-implicit coagulation model discussed by Jacobson (1994). In this model, $N_{j,t}$ is replaced by $N_{j,t-\Delta t}$. Therefore, equation (4.5) is re-written as:

$$N_{k,t} = \frac{N_{k,t-\Delta t} + \frac{1}{2}\Delta t \sum_{j=1}^{k-1} \beta_{k-j.j} N_{k-j,t} N_{j,t}}{1 + \Delta t \sum_{j=1}^{\infty} \beta_{k.j} N_{j,t} N_{j,t-\Delta t}} \quad (4.6)$$

Equation (4.6) is responsible for the loss of particles by number when two particles coagulate, but does not conserve volume. In order to conserve volume concentration, equation (4.6) is reformed as:

$$v_{k,t} = \frac{v_{k,t-\Delta t} + \Delta t \sum_{j=1}^{k-1} \beta_{k-j.j} v_{k-j,t} N_{j,t-\Delta t}}{1 + \Delta t \sum_{j=1}^{\infty} \beta_{k.j} N_{j,t-\Delta t}} \tag{4.7}$$

where, $v_{k,t} = v_k N_{k,t}$.

For an arbitrary size distribution, equation (4.7) becomes:

$$v_{k,t} = \frac{v_{k,t-\Delta t} + \Delta t \sum_{j=1}^{k} (\sum_{i=1}^{k-1} f_{i,j,k} \beta_{k-j.j} v_{i,t} N_{j,t-\Delta t})}{1 + \Delta t \sum_{j=1}^{N_B} (1 - f_{i,j,k}) \beta_{k.j} N_{j,t-\Delta t}} \tag{4.8}$$

where, $f_{i,j,k}$is the volume fraction and N_B is the last size bin.

$$f_{i,j,k} = \begin{cases} \left(\frac{v_{k-1} - V_{i,j}}{v_{k+1} - V_k}\right)\frac{v_k}{V_{i,j}} & v_k \le V_{i,j} < v_{k+1} \quad with\ k < N_B \\ 1 - f_{i,j,k-1} & v_{k-1} \le V_{i,j} < v_k \quad with\ k > 1 \\ 1 & V_{i,j} < v_k \quad with\ k = N_B \\ 0 & all\ other\ cases \end{cases} \tag{4.9}$$

The final number concentration of particles due to coagulation is:

$$N_{k,t} = \frac{v_{k,t}}{v_k} \tag{4.10}$$

Coagulation rate coefficient (kernel)

The coagulation rate coefficient is calculated by:

$$\beta_{i,j} = K_{i,j} CE_{i,j} \tag{4.11}$$

where, $\beta_{i,j}$ is the coagulation rate coefficient of particles (cm^3 $particle^{-1}$ s^{-1}); $K_{i,j}$ is the collision kernel (cm^3 $particle^{-1}$ s^{-1}) and $CE_{i,j}$ is a coalescence efficiency between particle size i and size j.

Collision kernel

The collision kernel is calculated in this research with consideration of the following physical processes:

- Brownian motion

- Convective Brownian motion enhancement
- Van der Waals and viscous force
- Gravitational collection
- Turbulent inertial motion and shear

All the collision kernel calculations were calculated in R program, based on the equations in previous work by (Alam, 1987; Jacobson, 1994; Sceats, 1989). As a result, the fine particles (D_p <1 μm) are mainly subject to the Brownian motion, Convective Brownian motion enhancement and Van der Waals/viscous force. The coagulation efficiencies of two particles were calculated and are shown in Figure 4.2.

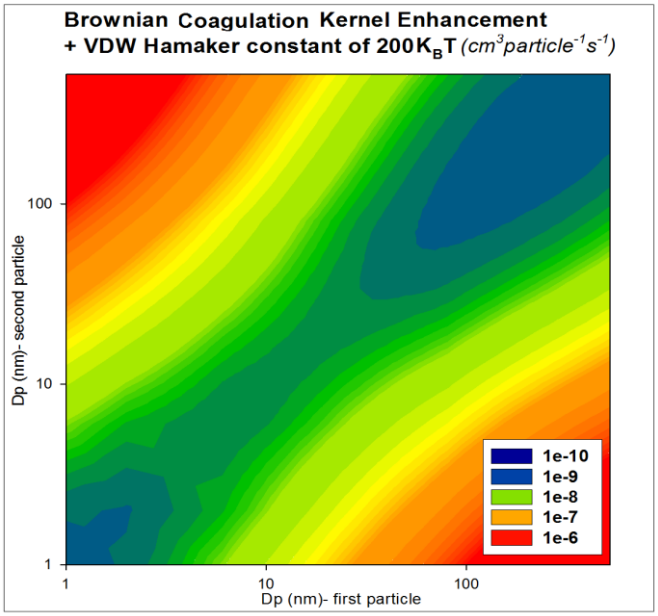

Figure 4.2: Coagulation kernel ($cm^3particle^{-1}s^{-1}$) with consideration of Brownian motion and its convection effects and the van der Waals/viscous force with the Hamaker constant of $200K_BT$.

Coalescence efficiencies

For small particles (D_p <1 μm), the coalescence efficiency is approximately unity (Jacobson and Seinfeld., 2004). Jacobson and Seinfeld (2004) recommend that for two small particles

coalescence is probably enhanced by the van der Waals forces, therefore the van der Waals/viscous forces can be referred to either in terms of a collision kernel, or in terms of a coalescence efficiency.

4.3. Result and Discussion

4.3.1. Indoor/outdoor (I/O) ratios

4.3.1.1. Diurnal patterns of I/O ratios

Figure 4.3 shows the I/O ratios of submicron particles for two sampling campaigns at different times (00:00-06:00; 06:00-12:00; 12:00-18:00; 18:00-24:00). In general, the I/O ratios of a particle greatly depend upon its size. A small particle has a lower I/O ratio than a large one due to its higher loss rate by deposition and coagulation. The I/O ratios for ultrafine particles ranged between 0.2 and 0.8, while those of accumulation mode particles ranged from 0.4 to 0.8.

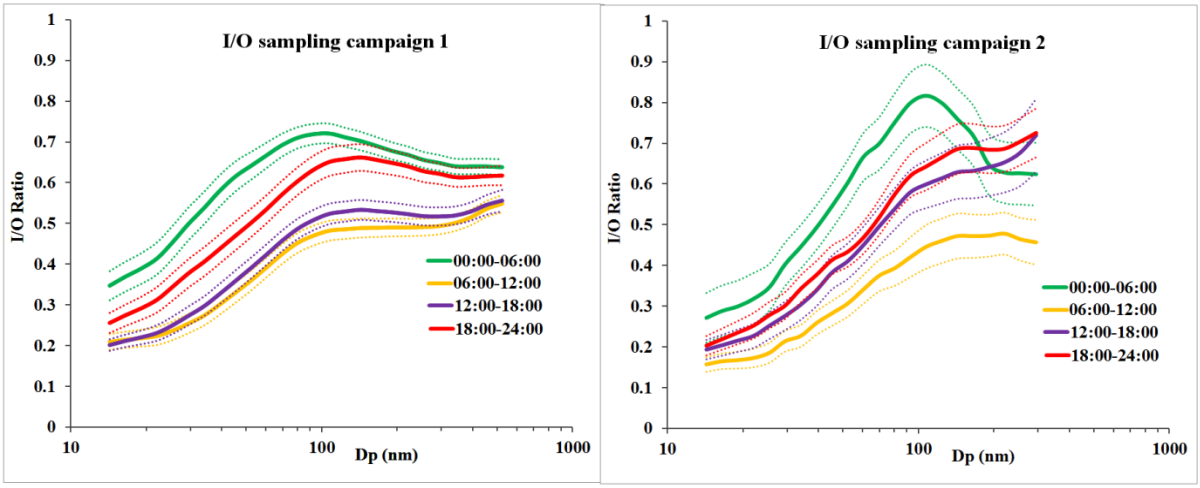

Figure 4.3: I/O ratio as a function of particle diameter at different times (00:00-06:00; 06:00-12:00; 12:00-18:00, and 18:00-24:00). *The upper and lower dashed lines show the confidence level at 95%.*

As shown in Figure 4.3, the I/O ratios at different times presented similar trends, but they were found to be lower in the daytime, particularly during traffic rush hours (6:30-9:30 am),

than at night time (00:00-06:00). In addition, the I/O ratios were found to be higher at the weekend (Figure 4.4). A higher loss rate of ultrafine particles during the daytime could be explained by the influence of coagulation and evaporation. The concentration of ultrafine particles in both outdoor and indoor environments during the daytime was much higher than those during night time. Because of the increased number concentration during the daytime, the loss rate of indoor particles in this time period was increased due to coagulation process, leading to the lower I/O ratios.

Particle volatility may also explain for the loss of ultrafine particle during the daytime. Kittelson (1998) found that particles below 50 nm from traffic emissions consisted of a significant fraction of volatile components. When these particles enter a house, they can lose their volatile fractions and shrink to under 20 nm Kuhn et al. (2005). Zhu et al. (2005) investigated the penetration of ultrafine particles into an unoccupied house near the 405 Freeway in Los Angeles, US. Their study found that the I/O ratios decrease when ultrafine particle size decreases to around 10-20 nm, but then increase again for particles below 10 nm.

Interesting, the I/O ratios of indoor accumulation mode particles (D_p >~ 80 nm) were also found to be significantly higher at night times (00:00-06:00 am) than those in the daytime (06:00-12:00 pm). Moreover, the coagulation process does not significantly affect these particles like as it does with small particles. This could be explained by the higher loss rate due to higher deposition and evaporation rates (this will be discussed in Section 4.3.3.3). In addition, these accumulation mode particles probably consist of a higher fraction of aggregates generated from traffic emissions during the daytime. These particles have a fractal dimension ranging from 1.5 to 2.5, with a typical value around 1.7 (Wentzel et al., 2003). Note that the particle diameter measured by FMPS in our study is the electrical mobility diameter. Because of soot particles, the equivalent volume diameter of the daytime accumulation particles will be smaller than their mobility diameter. Therefore, the diffusion

coefficient for daytime accumulation particles was higher than those for night time accumulation particles (which may have a smaller fraction of aggregates). The deposition of these particles is mainly controlled by diffusion (Hinds, 1999), hence the indoor daytime accumulation particles should have a higher deposition rate than night time particles.

Similarly, I/O ratios on week days were lower than those on weekend days. Figure 4.4 shows the typical diurnal patterns of I/O ratios on both week and weekend days. The I/O ratios were found to be at their lowest between 7:00 and 9:30 AM, corresponding to the traffic rush hours.

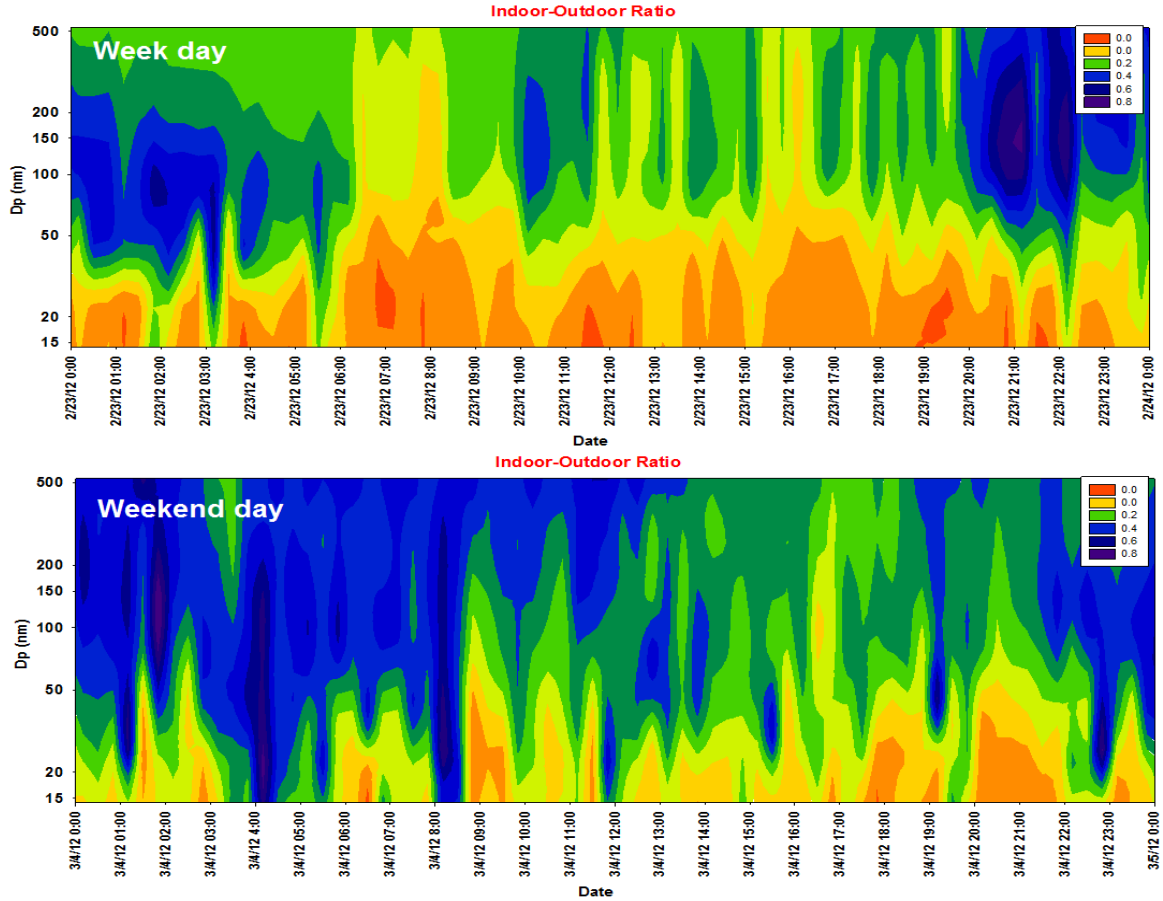

Figure 4.4: Comparison of the diurnal patterns of I/O ratios between a typical week and weekend days.

4.3.1.2. Effects of meteorological parameters on the I/O ratios

Figure 4.5 shows the dependence of I/O ratios on wind speed and direction. I/O ratios, particularly for accumulation particles (D_p >100 nm) increased when the wind speed increased. The effect of wind speed is to dilute the local traffic emissions which would then lead to higher I/O ratios. There was no clear influence of wind direction on the I/O ratios of small particles, but it had a significant effect on the I/O ratios of particles larger than 100 nm. The I/O ratios from SW wind direction were higher as seen in Figure 4.6. This is maybe due to the long range transport of accumulation mode particles in the condition of strong wind at night time (00:00-04:00).

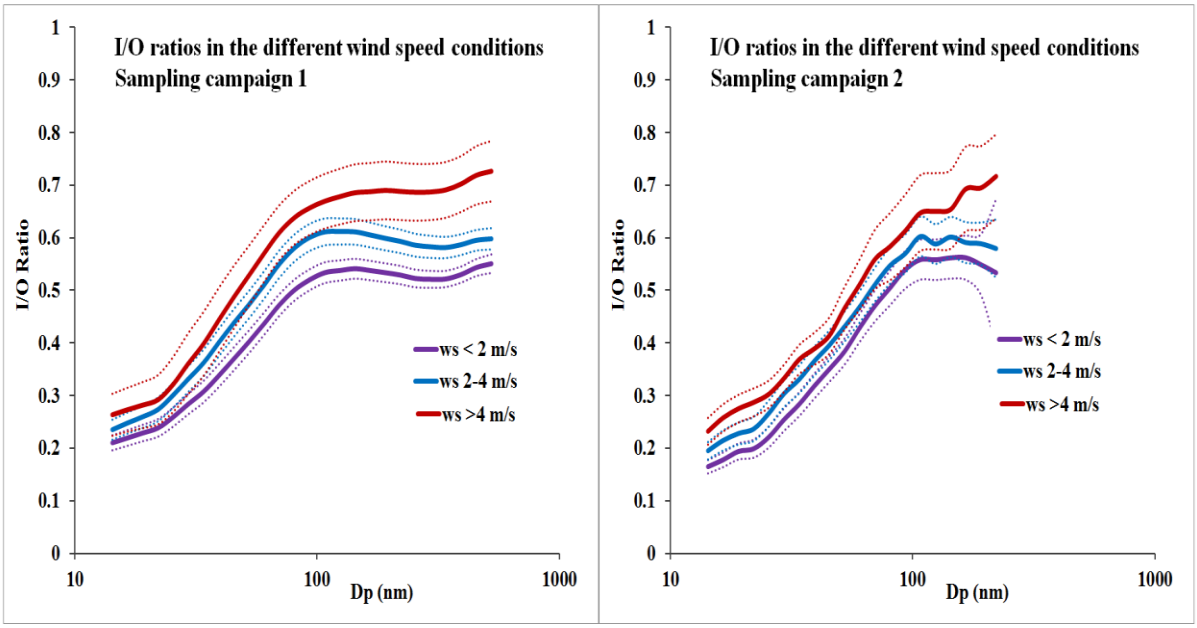

Figure 4.5: I/O ratios in different wind speeds.

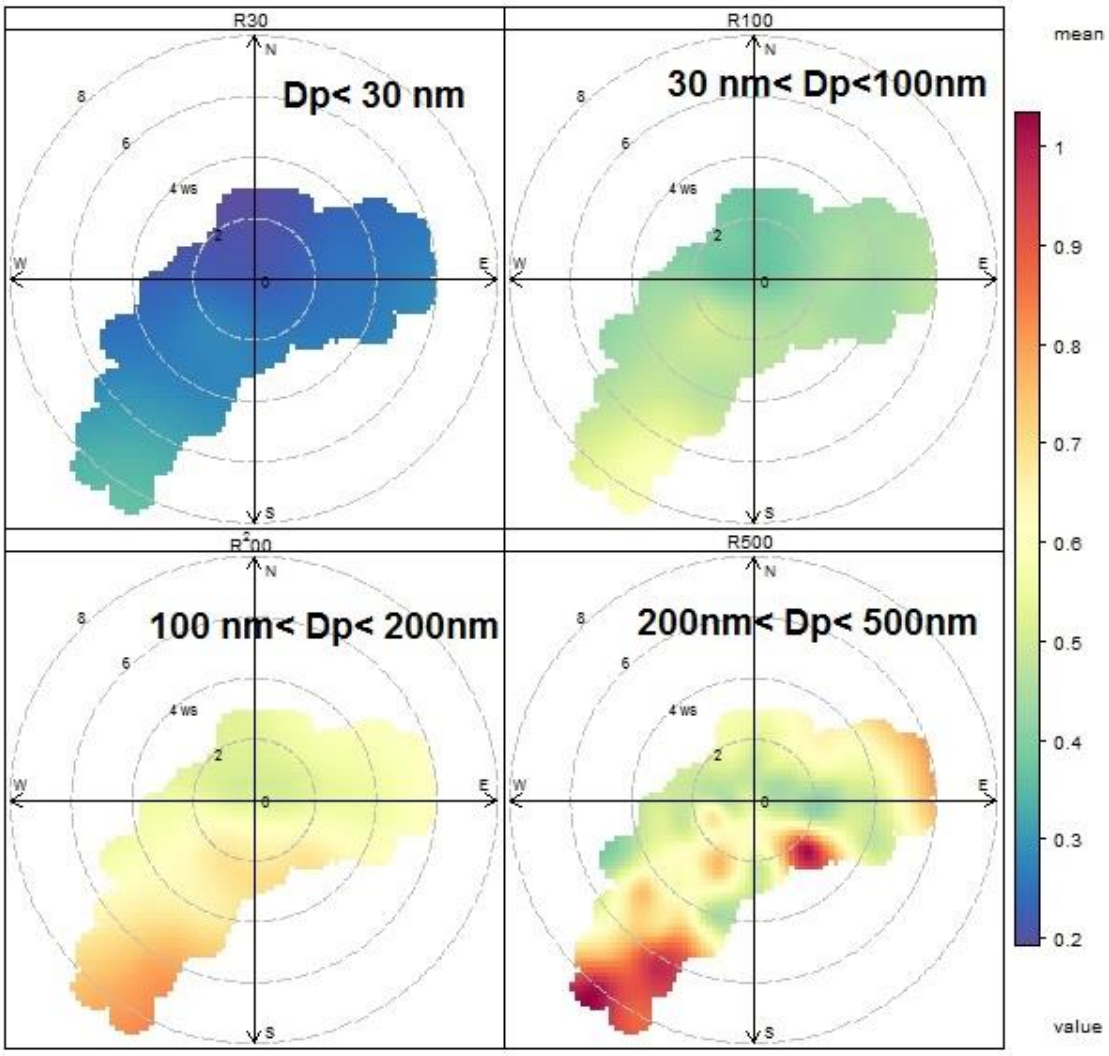

Figure 4.6: I/O ratios in different wind directions

4.3.2. Effect of coagulation on the loss/production of indoor particles

4.3.2.1. Evolution of particle number size distribution due to coagulation only

The coagulation model was run with a time step of 1 s. The simulation time was 20 minutes. The initial particle number size distribution which was extracted from the indoor particle number size distribution data set was measured at 9:10:00 on 22/02/2012 at a house in a busy traffic area. The evolution of particle number size distribution by time due to coagulation only is shown in Figure 4.7.

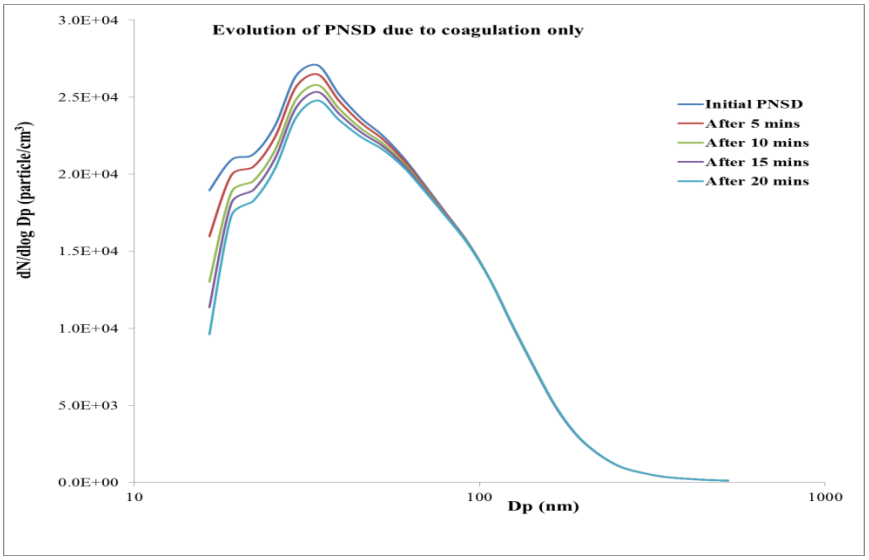

Figure 4.7: The evolution of PNSD due to coagulation only during a 20 minute period.

As shown in Figure 4.7, particles in nucleation and Aitken mode see a large reduction after 20 minutes. For example, particle number concentration at 20 nm, 30 nm and 52 nm was reduced by 14.2%, 10.2% and 4.1%, respectively. In this simulation, all particles are assumed as spherical particles. In contract, the number concentration of larger particles (D_p >150 nm) showed an increase; however, this increase was not significant with a variation lower than 3%. Moreover, the particle number concentration in accumulation mode (90 nm< D_p <150 nm) does not change significantly with a variation of ± 2%.

The first minor peak of 19 nm tends to disappear, while the major peak grows from 34 nm to 60 nm. In summary, the coagulation of particles during a 20 minute period not only has a large effect on particle number, but also on the shape of their size distributions. The loss of particles could increase more due to coagulation, if particles were aggregates (Jacobson and Seinfeld, 2004), therefore we cannot neglect the contribution of coagulation process to loss of indoor particle in the modelling of indoor/outdoor particles in a house in an area with busy traffic.

4.3.2.2. Effects of coagulation on the loss of indoor particles

A coagulation model was applied to the indoor particle size distribution to estimate the loss/ production of particles due to coagulation only during a 20 minute period (a time step in our mass balance model is 20 minutes). The % loss of particle concentration for a particle with a specific size is shown in Figure 4.8. Because the particle size distributions of indoor particles are more stable, the loss or production of indoor particles depends greatly on their concentration.

As shown in Figure 4.8, coagulation has a weaker effect on the loss of indoor particles if the total number concentration of particles is low. In addition, the influence of coagulation on the loss or production of particle increases when the total number concentration increases. For example, particles of 22.1 nm may lose a maximum of 4.3% of their concentrations due to coagulation if the total number concentration is lower than 5000 particles cm^{-3}. When total particle number increases to 1.5×10^4 particles cm^{-3}, more than 15% of those particles could be lost by coagulation. Coagulation has stronger effect on small particles than larger ones. It reduces the particle number concentration of nucleation and Aitken mode particles, but increases the number concentration of accumulation mode particles.

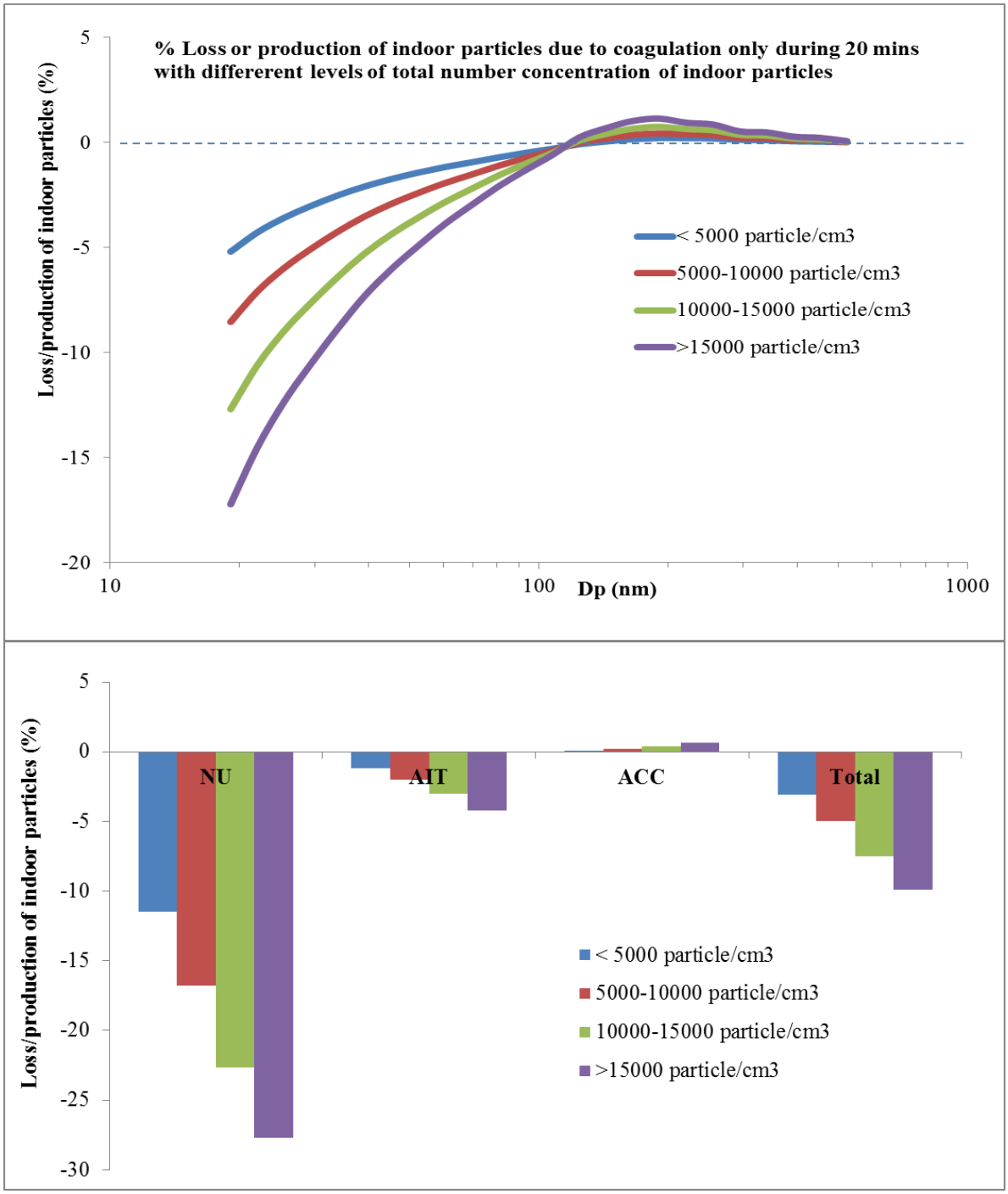

Figure 4.8: Loss or production (%) of indoor particles due to coagulation only during a 20 minute period at different total number concentrations of particles. *Nu: Nucleation mode particles (D_p <30 nm); AIT: Aitken mode particles (30nm< D_p <100 nm); ACC: Accumulation mode particles (100 nm< D_p <620 nm).*

4.3.2.3. Correlations between the loss of indoor particles by coagulation only and their concentrations.

Figure 4.9 shows very high correlations between the loss/production of indoor particles due to coagulation and their concentrations during a 20 minute period. It means the number concentration has a much larger effect on the loss/production of indoor particles due to coagulation than their size distributions.

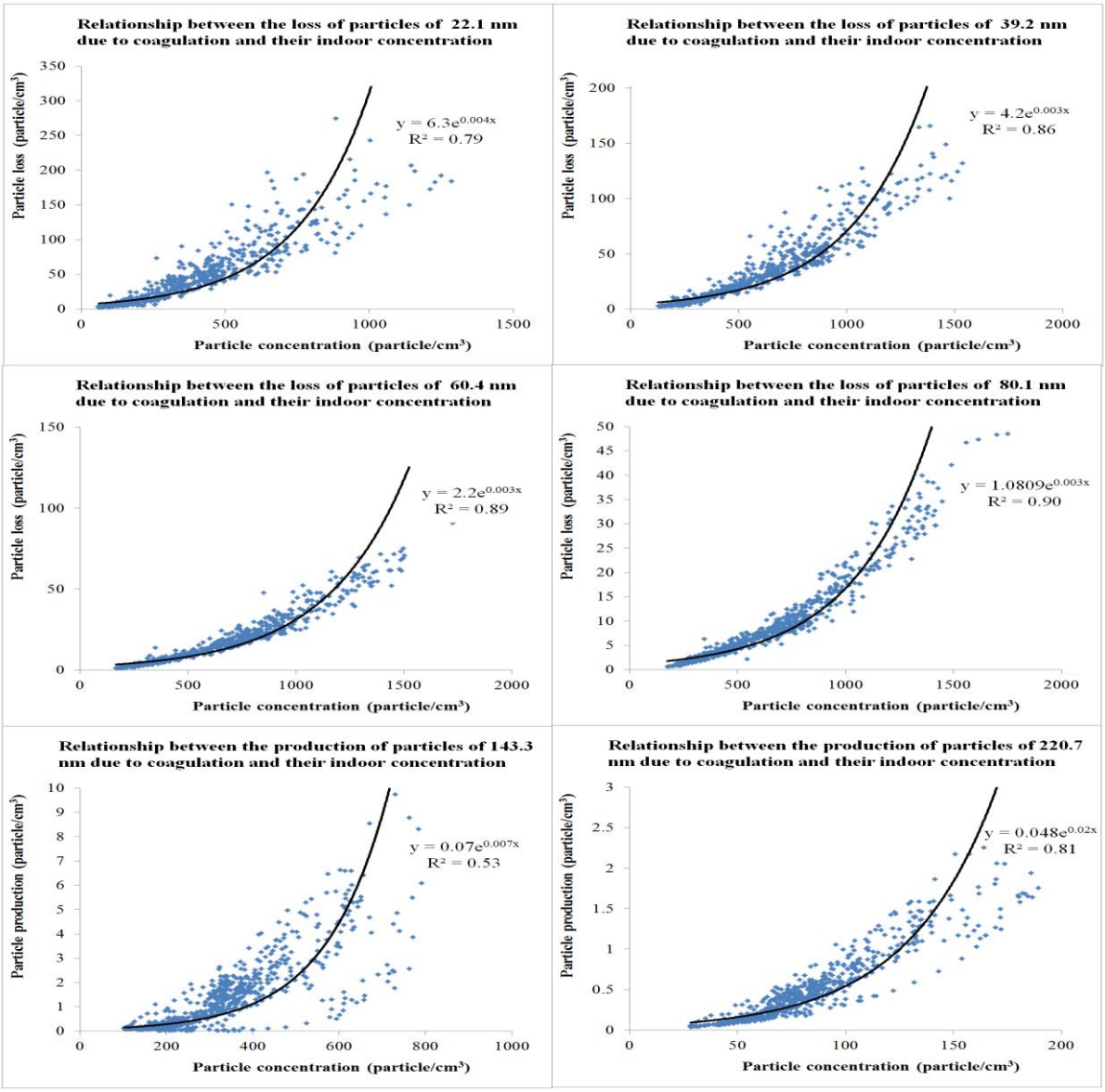

Figure 4.9: Correlation between the loss or production of particles of a specific size and their concentrations during a 20 minute period.

4.3.3. Prediction of the penetration factor, deposition rate, and infiltration factor using a mass balance model

4.3.3.1. Penetration factor (or efficiency)

The penetration factor is defined as the fraction of particles in the infiltration air that enters indoors through the building envelope (Chen and Zhao, 2011). The particle penetration factor through building cracks depends upon particle size, the pressure difference between indoor/outdoor environments, and the characteristics (i.e. surface roughness, geometry) of the cracks. As in the above definition, the penetration efficiency of a particle that passes through a building shell must be lower than unity. Accumulation mode particles (D_p, 0.1-1 μm) have higher penetration efficiencies than ultrafine and coarse particles. It is easier for smaller particles to be lost during the penetration process though the building shell because of their higher diffusion efficiencies, while larger particles are subject to gravitational settling, leading to their lower penetration efficiency (Liu and Nazaroff, 2003).

In this study, the air exchange between indoor and outdoor environments was controlled by a mechanical system which consisted of an external fan connected to an air pipe to force the air to the centre of the room. With this novel experimental design, the penetration factor is close to 1.0 (Sajani et al., 2015). To evaluate the loss of particles through the air exchange system, an additional three-day experiment was performed to measure particle size distribution at the inlet of the fan and the outlet of the pipe using an FMPS system. A switching valve which switched the FMPS inlet every five minutes was deployed to measure outdoor/indoor particle size distributions.

The average number size distribution of upstream and downstream particles and penetration efficiency are shown in Figure 4.10. There was a small loss of particles below 20 nm in the pipe due to their very high diffusion coefficient.

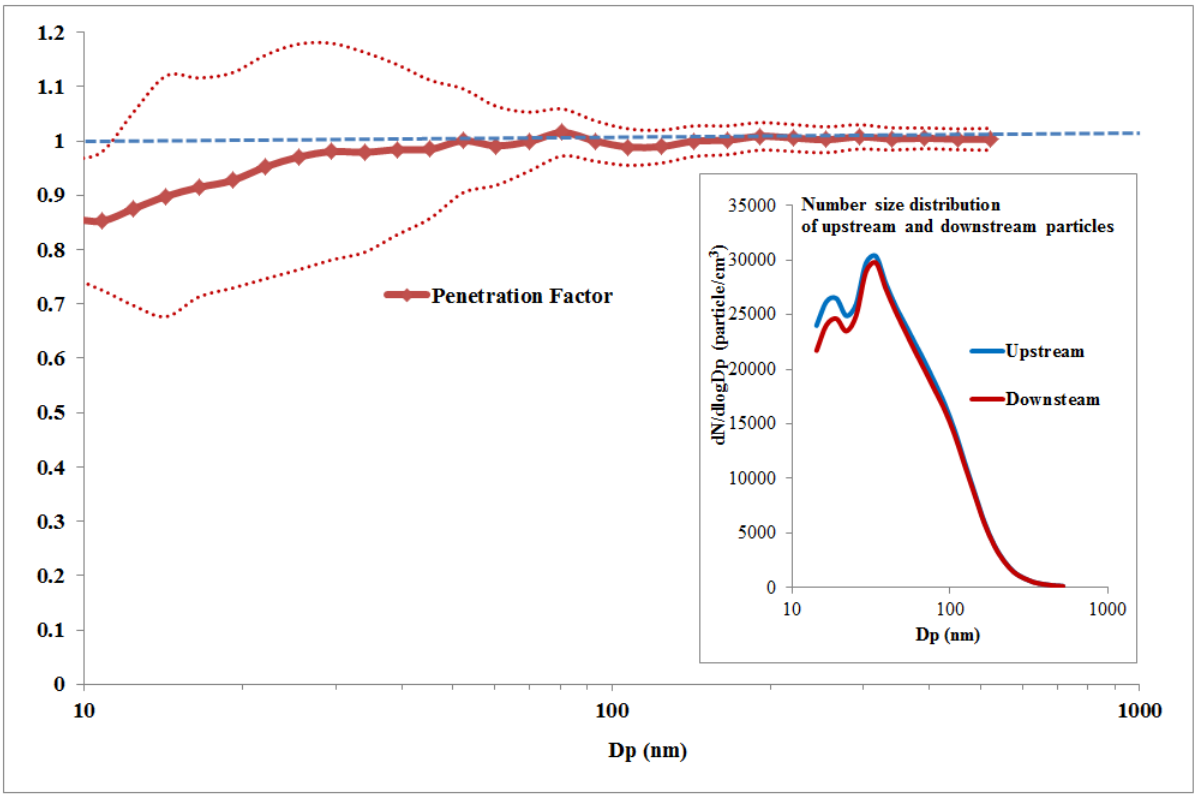

Figure 4.10: Particle penetration factor through the study system.

4.3.3.2. Application of a mass balance model to predict the penetration factor, infiltration factor and deposition rate

A mass balance model was applied to a night-time data set (00:00-06:00 am) which has an averaged indoor number concentration of 5272.6 particles cm^{-3}. As discussed in section 4.3.2.3, the coagulation process could be negligible if total particle concentration is lower than 5000 particles cm^{-3}. Therefore, we assumed that coagulation and evaporation process do not play a significant role in this period. The mass balance model (4.3) will be converted to the following equation:

$$C_{in\,(t+\Delta t)} = \frac{0.5*P*C_{out\,(t+\Delta t)}}{0.5+k_d}\left(1 - e^{-(0.5+k_d)*\Delta t}\right) + C_{in\,(t)}e^{-(0.5+k_d)*\Delta t} \quad (4.12)$$

a. Can we predict simultaneously unknown penetration factor and deposition rate (k_d, h^{-1}) values using a mass balance model?

In equation (4.12), P and k_d (h^{-1}) were allowed to vary independently over the likely ranges of values $0< P \leq 1$ and $k_d > 0$ respectively. In our model, the P values varied with intervals of 0.01 between 0 and 1, and the k_d (h^{-1}) values varied with intervals of 0.01 between 0 and 10. Each pair of P and k_d values result in different values of RMSE and *r*. To obtain the best fit between the modelled and measured indoor concentration, the pair of P and k_d values was selected with a minimum value of RMSE and maximum value of *r*.

As a result, it is impossible to obtain a unique pair of P and k_d values because there are numerous pairs of values for P and k_d that have similar low values of RMSE. For example, Figure 4.10 shows the distribution of RMSE and *r* values for particles at a count diameter of 93.1 nm, depending on different values of P and k_d. The orange curve shown in Figure 4.11 illustrates the area of lowest minimum value of RMSE. This means that there are many pairs of P and k_d values corresponding to a minimum value of RMSE (minimum value of RMSE is 1.45). In this case, P ranged from 0.45 to 1.0 and k_d ranged from 0 to 0.35 h^{-1}. Similarly, as shown in Figure 4.11, there were various pairs of P and k_d that were close to the highest value of *r* (~0.98). This result is in agreement with those of Bennett and Koutrakis (2006), determined the best values for P and k through the minimum value of χ^2 (referred to as the error) using the NLIN procedure in SAS (SAS Inc. Carry, NC).

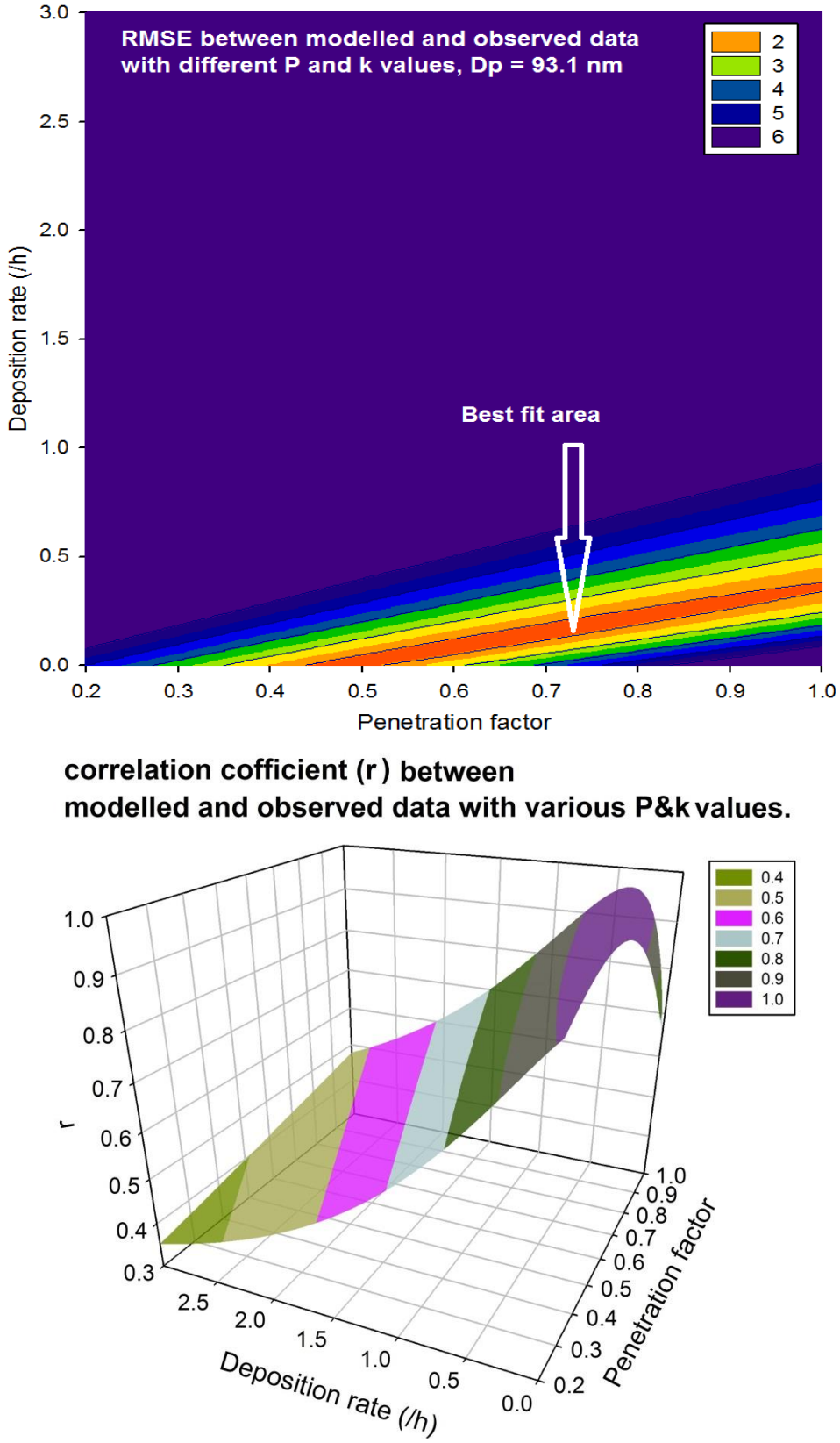

Figure 4.11: Dependence of RMSE and *r* upon penetration factor and deposition rate.

b. Determination of the infiltration factor using a mass balance model

As discussed in section 4.3.3.2, a mass balance model did not successfully yield a unique P and k_p solution, however it did give us various pairs of P and k_d values. As shown in Figure 4.11, there is a linear relationship between these two parameters, suggesting that we may determine the infiltration factor (F_{in}) based on this model.

The infiltration factor (F_{in}) is defined as the equilibrium fraction of outdoor particles that penetrates indoors and remains suspended. Therefore, it is controlled by the penetration factor, exchange rate and deposition rate if we assume that coagulation and evaporation do not have a significant effect. The dynamic infiltration factor is calculated using the following equation:

$$F_{in} = \frac{a_{ER} * P}{a_{ER} + k_d} \tag{4.13}$$

F_{in} represents for the fraction of outdoor particles that enters indoors and remains suspended, hence F_{in} is lower than unity. To combine equations (4.12) and (4.13), the mass balance model will be transferred to the following equation:

$$C_{in\,(t+\Delta t)} = \frac{C_{out\,(t+\Delta t)}}{F_{in}} \left(1 - e^{-\frac{F_{in}}{0.5*P} * \Delta t}\right) + C_{in\,(t)} e^{-\frac{F_{in}}{0.5*P} * \Delta t} \tag{4.14}$$

In this model, F_{in} and P were allowed to vary independently from 0 to 1, leading to different values of RMSE and *r*. As shown in Figure 4.11, the minimum value of RMSE strongly depends upon the value of the infiltration factor. The value of F_{in} was selected if it generated not more than 105% of the minimum of RMSE values. For example, the minimum of an RMSE for particles with a diameter of 93.1 nm is 1.45, therefore the F_{in} value will be considered if it generates an RMSE lower than 1.52. Following this criterion, the F_{in} of these

particles value ranged between 0.45-0.52, as shown in Figure 4.12. In summary, a mass balance model can successfully predict the infiltration factor.

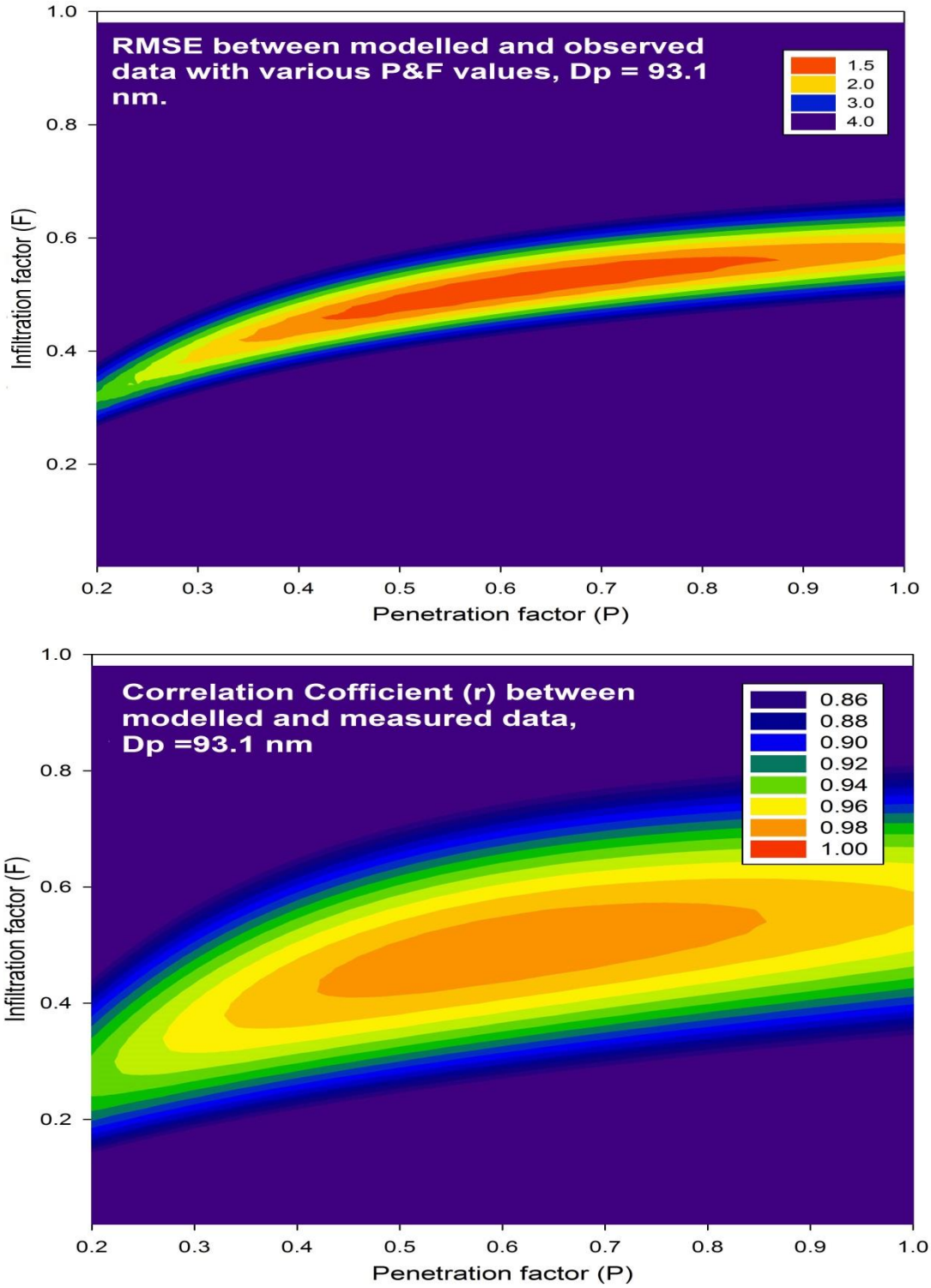

Figure 4.12: RMSE and *r* depend upon penetration and infiltration factors.

c. Determination of the deposition rate (k_d) when the penetration factor is known

The mass balance model fails to predict both unknown P and k_d values, but it gives us the relationship between these values. Therefore, if we know one value of these parameters, it is easy to predict the value of the other. In our novel experimental design, the penetration factor was controlled to be nearly unity, as shown in Figure 4.10; deposition rate was estimated based on the application of a mass balance model to night time data sets. As shown in Figure 4.14, the mass balance model predicts very well indoor particles with a diameter larger than 34 nm (r >0.87), particularly for accumulation particles (r >0.95 for sampling campaign 1), but it is not very good in predictions of nucleation mode particles (r ~0.64-0.81). This is maybe due to the influence of evaporation and the weak effect of coagulation on the small particles.

The estimated particle deposition rates are shown in Figure 4.13. They ranged from 0.3 to 1.97 h^{-1}, closely depending upon particle size. For submicron particles, a smaller particle has a higher deposition rate. The deposition rate of a particle with a diameter of 30 nm is three times higher than that of a particle with a diameter of 100 nm. This finding is consistent with previous studies by Long et al. (2001), Chao et al. (2003) and Hussein et al. (2006). In addition, we compare this deposition rate calculated by a mass balance model with those calculated by Lai and Nazaroff (2000)'s theory models. For particles with a diameter smaller than 150 nm, our estimated deposition rate fits very well with the calculation from models with an assumption of friction velocity (u) ranging from 35 to 40 cm/s. For larger particles, the deposition rate was found to be much higher than a Lai and Nazaroff (2000) deposition rate curve. This is maybe due to their assumption of a perfectly smooth surface, which has a marked effect on the accumulation mode particles.

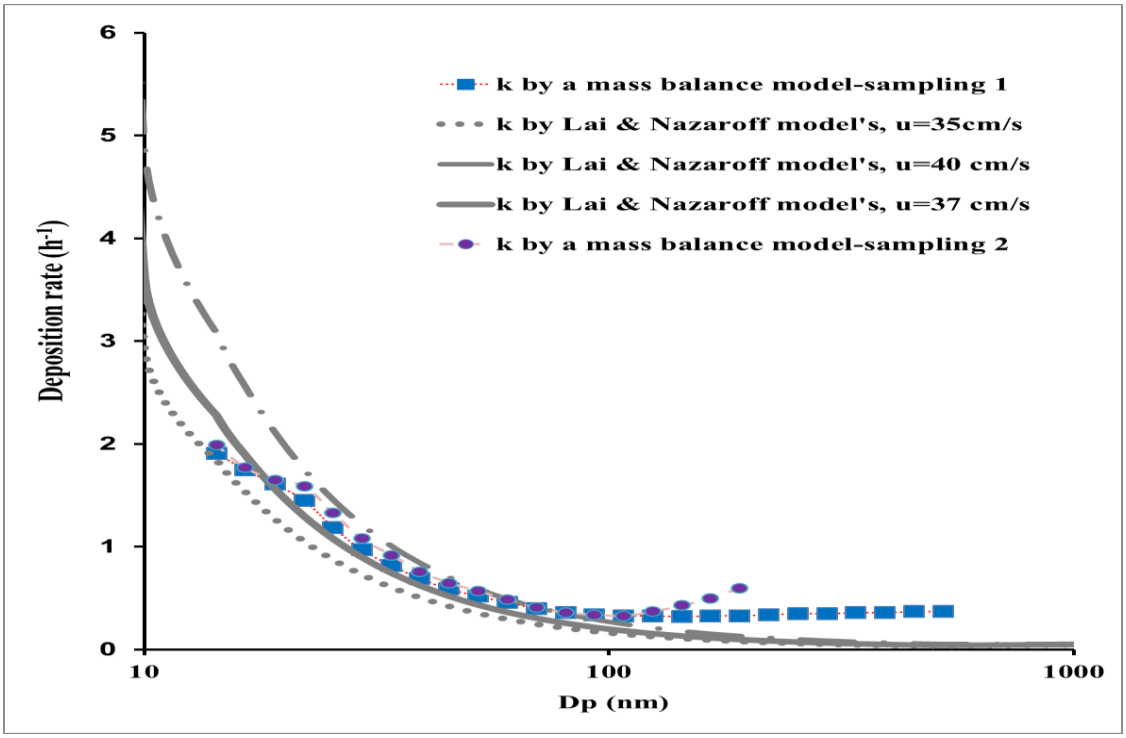

Figure 4.13: Comparison between deposition rates estimated by the mass balance model and Lai&Nazaroff's model.

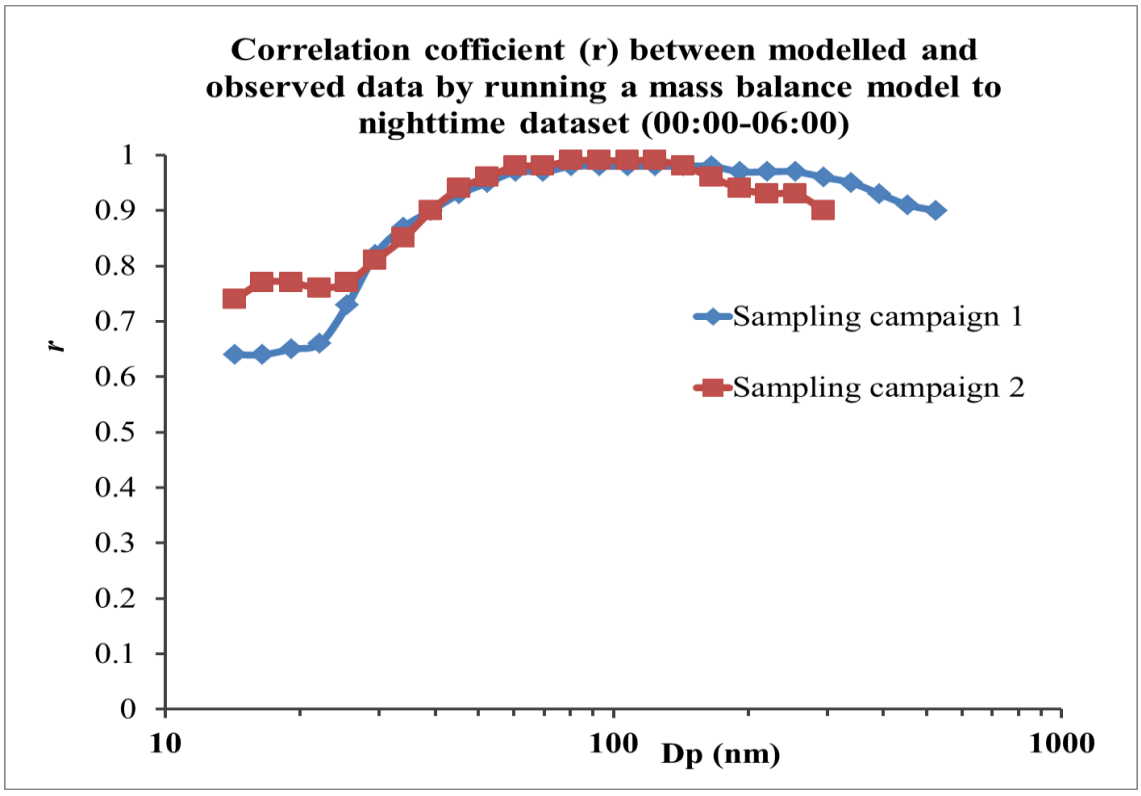

Figure 4.14: Correlation efficient (*r*) between modelled and observed data.

4.3.3.3. Loss rate of particles at different times

In section 4.3.3.2, we found strong correlations between loss/production of particles of a certain diameter due to coagulation and their indoor concentrations. In this section, we assume the loss/production of particles due to evaporation has a strong linear correlation with the number concentration in appropriate time periods like coagulation.

The k_c and k_e are defined as the loss rate of particles due to the coagulation and evaporation processes (h^{-1}). The k_c and k_e can be negative values if these processes produce particles. The mass balance model in equation (4.3) will be transformed to the following equation:

$$\frac{\partial C_{in}}{\partial t} = a_{ER} * P * C_{out} - a_{ER} * C_{in} - k_d * C_{in} - k_c * C_{in} - k_e * C_{in} \quad (4.15)$$

The total loss rate of particles with a certain diameter (k_{loss}) is defined by the sum of the loss rate due to deposition, coagulation and evaporation processes: $k_{loss} = k_d + k_c + k_e$.

Equation (4.15) will be solved in the same way as equation (4.16) for each time step.

$$C_{in\,(t+\Delta t)} = \frac{0.5 * P * C_{out\,(t+\Delta t)}}{0.5 + k_{loss}} \left(1 - e^{-(0.5+k_{loss}) * \Delta t}\right) + C_{in\,(t)} e^{-(0.5+k_{loss}) * \Delta t} \quad (4.16)$$

A mass balance model based on equation (4.16) was applied to the dataset at different times (06:00-12:00; 12:00-18:00; 18:00-24:00) to estimate the loss rate of particles. This total loss rate and the performance of the mass balance model based *r* value are shown in Figure 4.15 and 4.16.

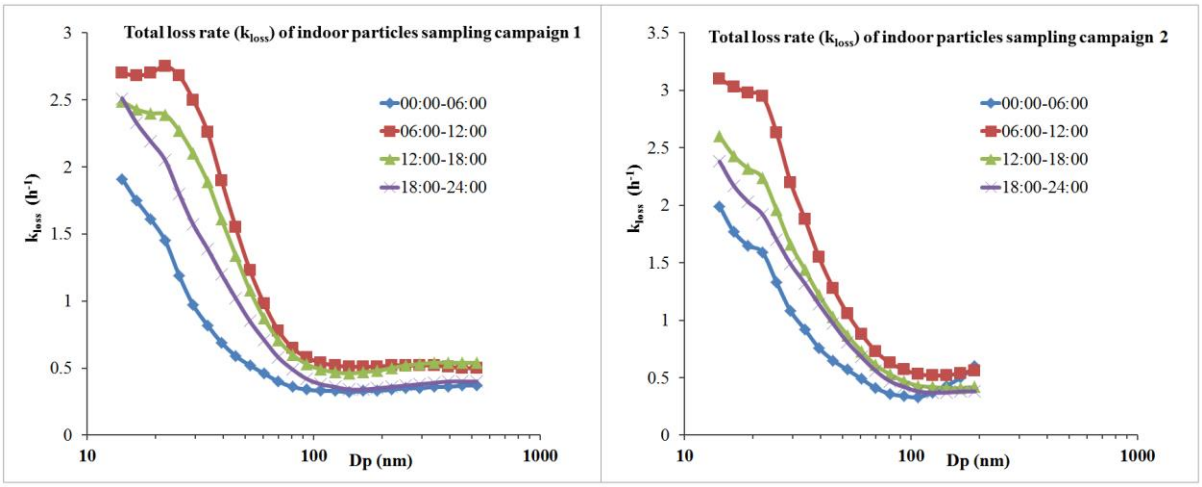

Figure 4.15: Total loss rates (k_{loss}) of indoor particles in different time periods.

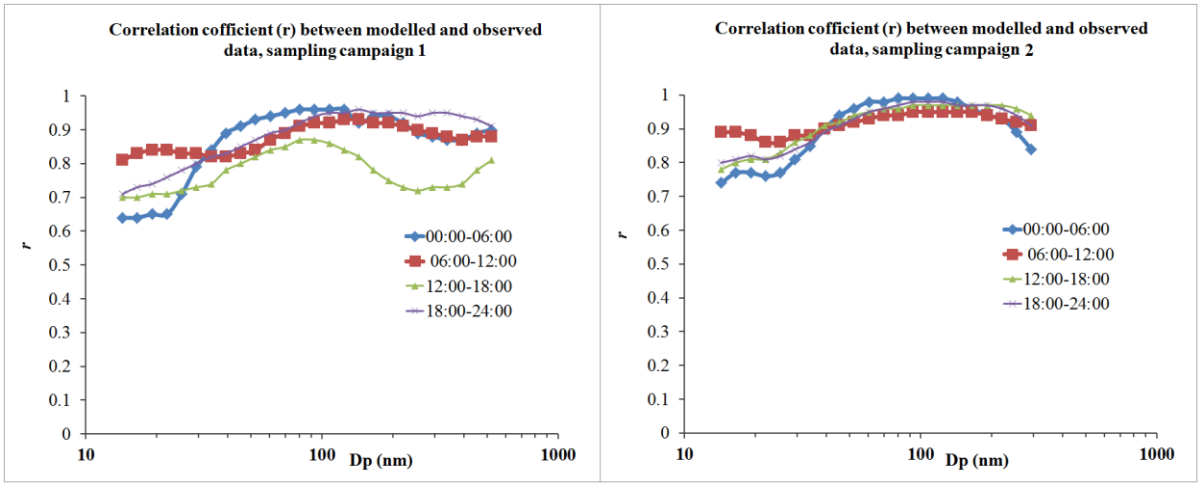

Figure 4.16: Correlation coefficient (r) between modelled and observed data in different time periods.

Interestingly, the mass balance model performs very well in the prediction of nucleation mode particles during the day time. For example, the correlation coefficient (*r*) between the modelled and measured concentration of particles of 14.3 nm for dataset from 6:00-12:00 was very high. It was higher than 0.82 for the first sampling campaign and 0.86 for the second sampling campaign as shown in Figure 4.16. This means that we can use a mass balance model to model the indoor concentration from outdoor in appropriate time periods as well as to predict the total loss rate of particles.

Figure 4.15 shows the total loss rate (k_{loss}) of particles in different time periods. A higher loss rate was found in the period 06:00-12:00 than at night time, suggesting that coagulation and evaporation play very important roles in the loss of particles during the daytime in a house heavily affected by road traffic emissions. As shown in Figure 4.17, the particle number concentration for both outdoor and indoor environments during the daytime was much higher than that during the night time, resulting in a higher particle loss due to the coagulation process.

This result is in agreement with the higher I/O ratio at night time that was discussed in section 4.3.1.1. Like the deposition rate, the loss rate for a particle strongly depends upon its size. The total loss rate of a particle increases exponentially when its size decrease from 100 nm to 22.5 nm. This is due to the greater increase in coagulation and evaporation effects on small particles (the Aitken mode particles) than large particles (accumulation mode particles).

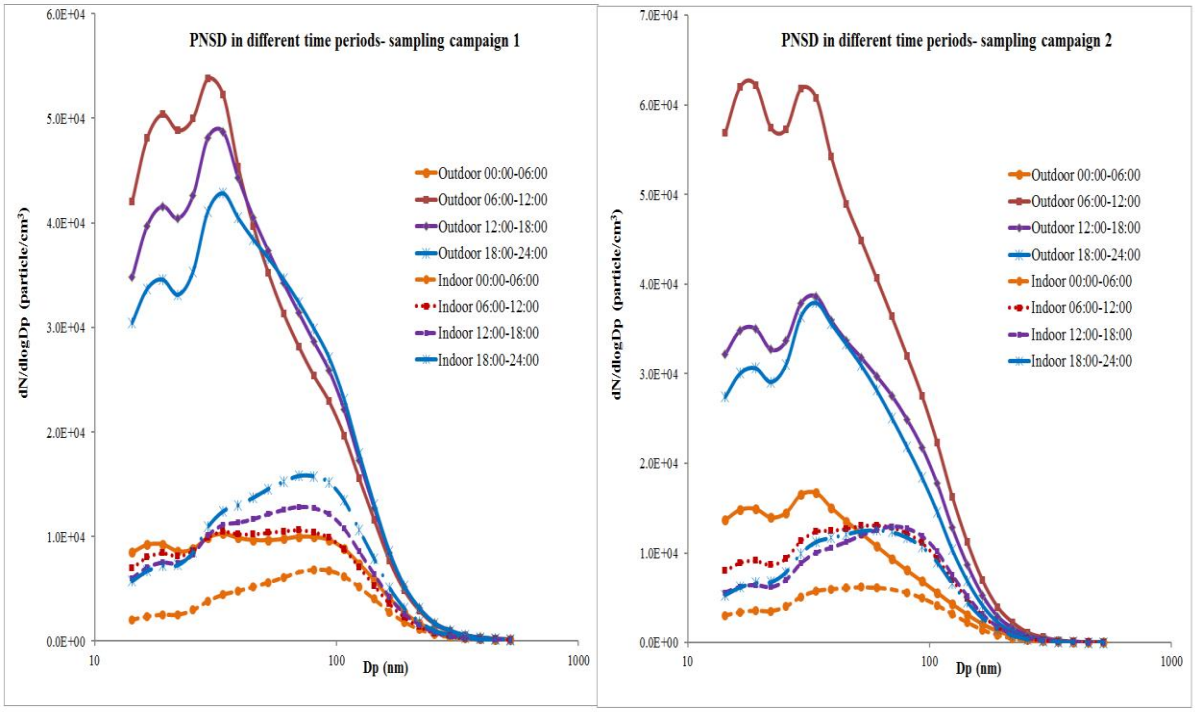

Figure 4.17: Outdoor/indoor particle number size distribution (PNSD) in different time periods.

The total loss rate of particles increased slightly or was unchanged when their sizes decreased to lower than 22.5 nm. Evaporation is probably a main reason for this. Kuhn et al. (2005) found that some particles in the size range 20-40 nm consist of many volatile components. They may become particles of 20 nm or less due to the evaporation of volatile components. Therefore, the loss of particles of 20 nm or less did not increase due to the production of these particles by the evaporation of larger ones.

In summary, the mass balance model can successfully predict indoor particles as well as their loss rate in different time periods. The total loss rate of particles during the daytime was much higher than those during the night time. Coagulation and evaporation play important roles in the loss of indoor particles in a house affected by road traffic emissions.

4.3.4. Modelling the indoor particles at a house affected by traffic emissions based on an application of a mass balance model to the full dataset

In order to model the indoor particles for the full dataset, we performed a mass balance model based on equation (4.16) using two approaches:

(1) Approach 1: We applied a mass balance model to the full dataset without the change in k_{loss} by time. This means that the mass balance model does not consider the change of loss rate due to coagulation and evaporation between daytime and night time.

(2) Approach 2: We applied a mass balance model to full dataset with consideration of the change in k_{loss} in different time periods. In this approach, the k_{loss} will be different corresponding to the four time periods (00:00-06:00; 06:00-12:00; 12:00-18:00; 18:00-24:00).

Figure 4.18 compares the RMSE and *r* values between the two approaches. There was not much difference between the RMSE values in the two approaches, but the indoor data

modelled by the second approach had closer trends to the measured data due to a significantly higher *r* value. The *r* values between the indoor data modelled by the second approach and the measured data were higher than 0.8, suggesting that a mass balance model can predict well the indoor particles using outdoor data.

Figure 4.19, 4.20 & 4.21 show a comparison between indoor concentrations estimated by the models and measured by FMPS.

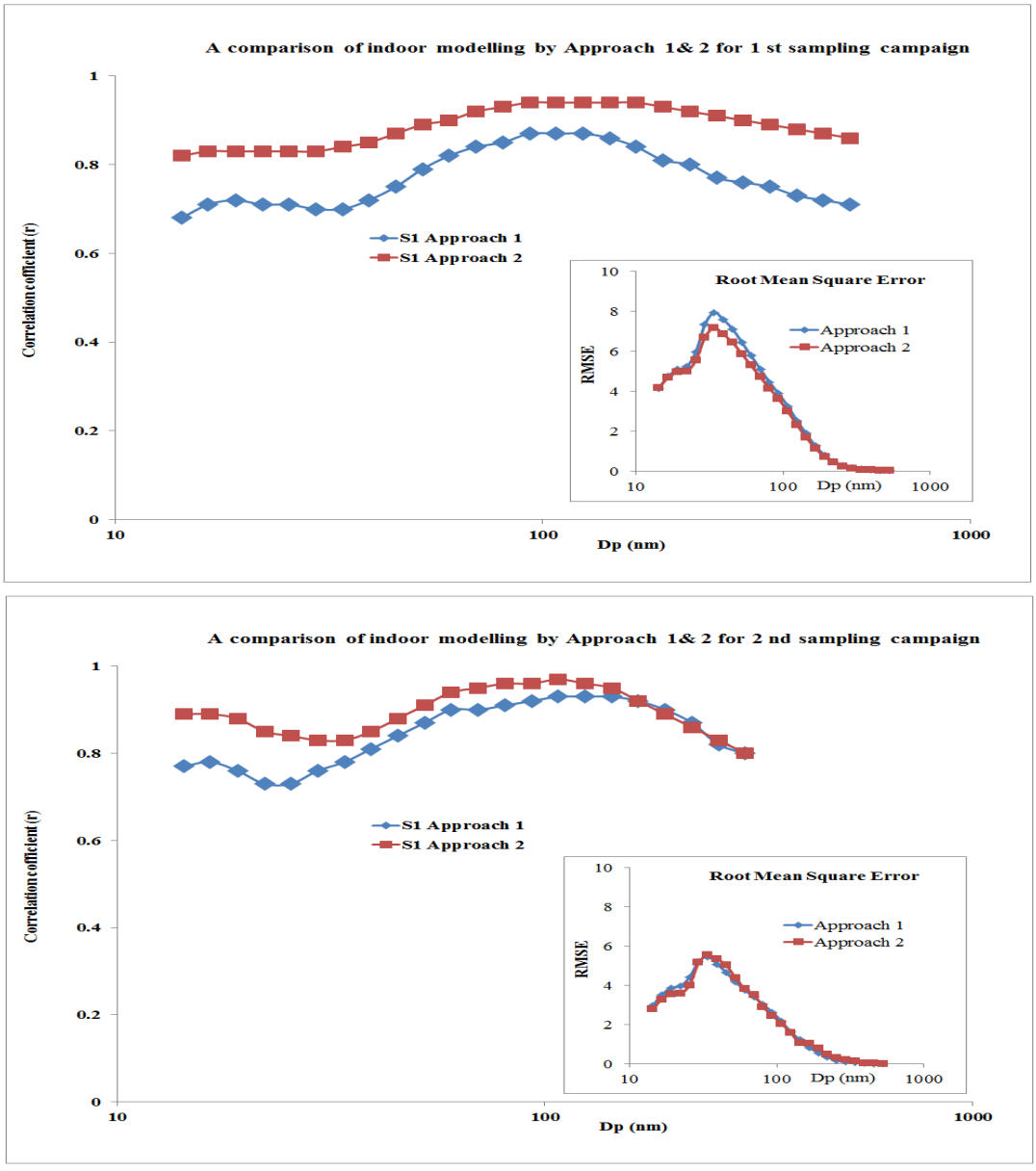

Figure 4.18: Comparison of indoor modelling by two the approaches for 2 sampling campaigns.

4.4. Conclusion

In conclusion, this study had investigated the I/O ratios in different time periods. As a result, these ratios have a strong diurnal pattern and were much lower in the daytime than at night time. In addition, it has evaluated the mass balance model that was applied to predict the indoor concentrations from outdoor concentrations. A mass balance model cannot predict unknown penetration factors and deposition rates separately, but it can predict the infiltration factor. Coagulation and evaporation processes play important roles in the loss or production of particles.

Based on the mass balance model, the loss rate of indoor particles was calculated. This not only depends upon their size, but also the sampling time. A higher loss rate was found for smaller particles and in the daytime. A very high correlation between the modelled and measured indoor data suggests that a mass balance model with a consideration of different loss rates during different time periods can predict very accurately the concentration of indoor particles originating from outdoor particles in a house heavily affected by road traffic emissions.

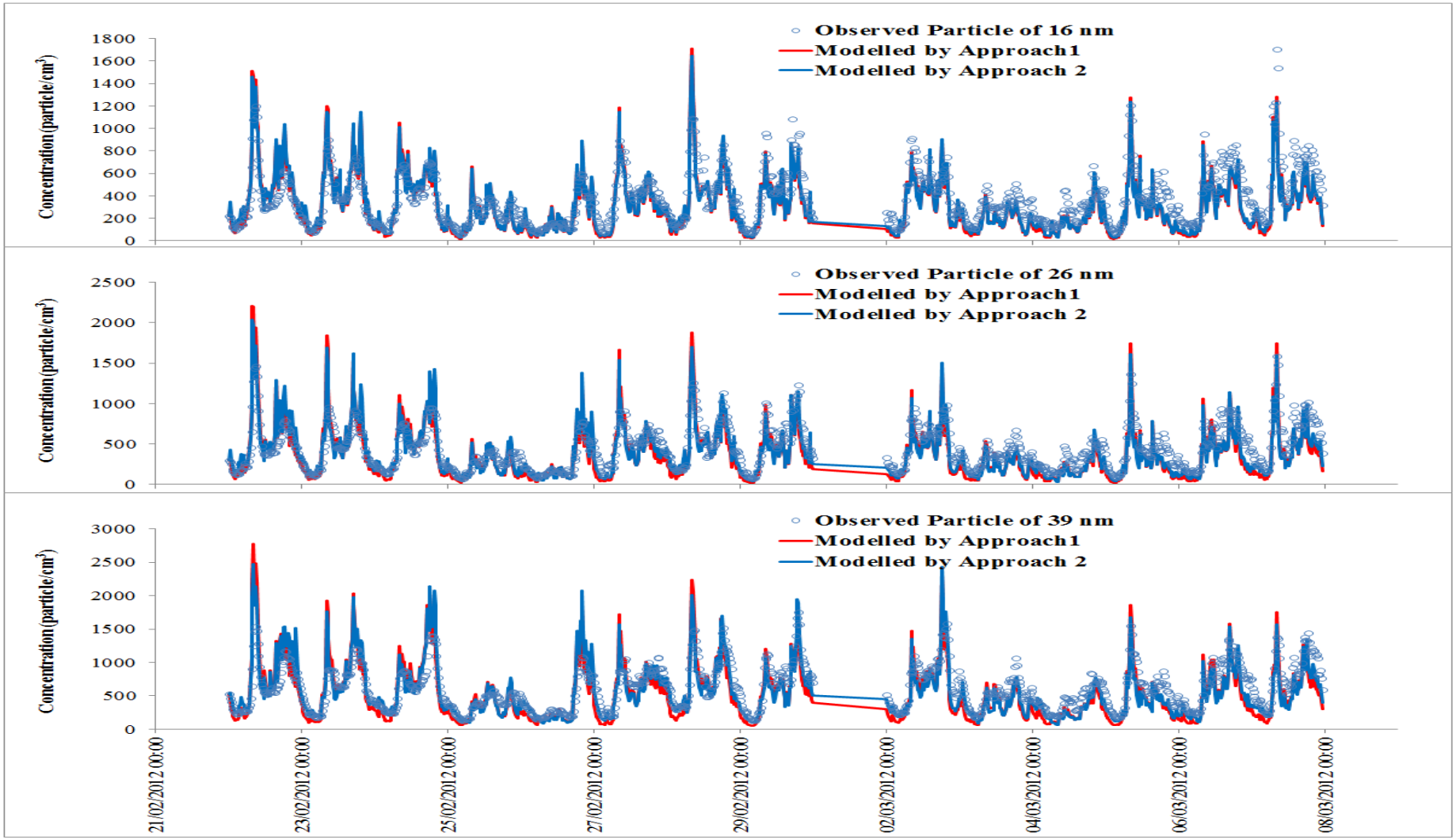

Figure 4.19: Comparison between the indoor concentrations modelled by a mass balance model and measured data for particles with diameters of 16, 26 and 39 nm.

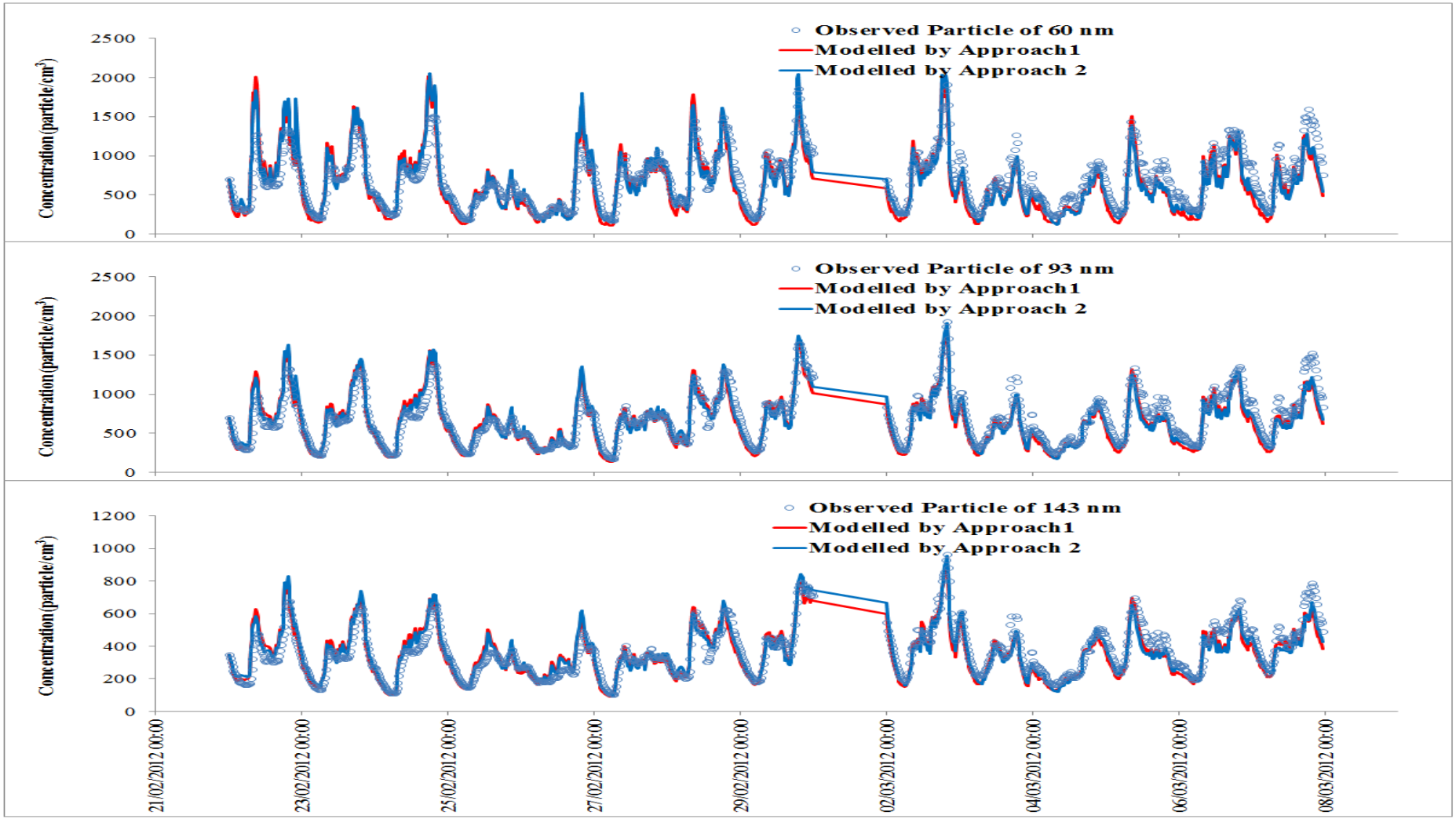

Figure 4.20: Comparison between the indoor concentrations modelled by a mass balance model and measured data for particles with diameters of 60, 93 and 143 nm.

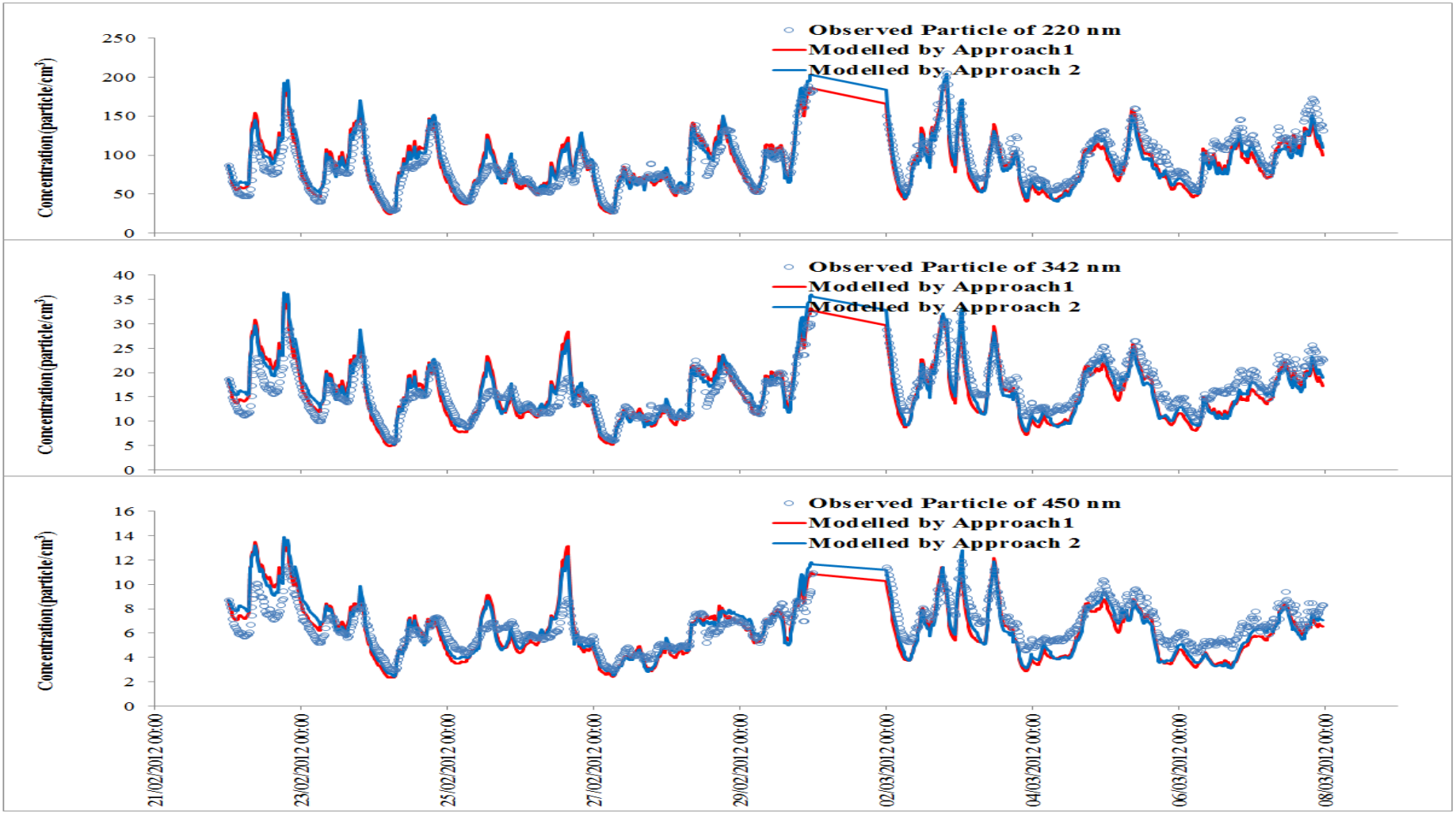

Figure 4.21: Comparison between the indoor concentrations modelled by a mass balance model and measured data for particles with diameters of 220, 242 and 450 nm.

Chapter 5: HYGROSCOPIC PROPERTIES OF PARTICLES AND THEIR IMPLICATIONS FOR THE CALCULATION OF LUNG DEPOSITION FRACTION

This chapter presents the existing knowledge on the hygroscopic growth factor (G_f) of atmospheric submicron particles and their influence on the lung deposition calculation. The chapter first briefly reviews the G_f values of particles emitted from various sources, including nucleation, traffic emissions and biomass burning, and discusses the spatial and temporal variations. It then summarizes the G_f values of submicron particles and the number fraction of each hygroscopic group measured in different ambient environments. These include marine, roadside, urban background and rural environments. Furthermore, the effect of hygroscopicity on the lung deposition fraction of ambient particles has been estimated. The ICRP model seems to predict well the deposition fraction (DF) values for small ambient particles in the extra-thoracic and tracheo-bronchial region, but not the alveolar region, where they are overestimated. Finally, this chapter applies our modified ICRP model to estimate the lung deposition of particles from a street canyon and an urban background site in London and a rural site 80 kilometres to the west of London, UK.

This chapter contains some sections of verbatim text adapted from Vu et al. (2015b) published as part of this PhD. The author's contribution: writing, contribution of ideas and numerical calculations.

5.1. Introduction

Hygroscopic properties are well known to play a vital role in the atmospheric behaviour and health implications of aerosols (Ferron et al., 2005; Hiller, 1991; Tu and Knutson, 1984). Aerosol particles can shrink or grow in size by exchanging water vapour with the surrounding air as relative humidity (RH) changes, thus having a direct effect on the radiation balance of the atmosphere through the change in scattering and absorption of light (Tang et al., 1981). Furthermore, hygroscopicity has a strong influence on the ability of particles to act as cloud condensation nuclei (Hämeri et al., 2001; Petters and Kreidenweis, 2007; Reutter et al., 2009). Consequently, it also indirectly affects the global climate. Particles can also absorb the water vapour in the respiratory tract when they penetrate into the lung, changing in size, and hence affecting their lung deposition fraction (Broday and Georgopoulos, 2001; Chan et al., 2002; Finlay and Stapleton, 1995; Hofmann, 2011).

The hygroscopic growth factor (G_f) is one of most used parameters in determining the hygroscopic properties of particles and their influences. The hygroscopic growth factor (G_f) is defined (Equation 5.1) as the ratio between particle diameter measured at a specific RH (D_w), and dry particle diameter (D_p) measured at a low RH (RH <10%) (Massling et al., 2005; Swietlicki et al., 2008):

$$G_f\,(RH) = \frac{D_w(RH)}{D_p\,(RH<10\%)} \qquad (5.1)$$

The G_f of atmospheric aerosols is determined by several methods, including measurement using particle spectrometers (i.e. the Hygroscopic Tandem Differential Mobility Analyzer H-TDMA) or estimated using models from the growth factors of each particle composition (Meier et al., 2009). G_f values depend upon both the physical and chemical properties of particles, such as particle size and composition. Based on the G_f values, ambient aerosols

have been classified into four hygroscopic groups: nearly hydrophobic particles (G_f =1.0-1.11 for 100 nm particles at RH =90%), less-hygroscopic particles (G_f =1.11-1.33), more-hygroscopic particles (G_f =1.33-1.85) and sea-salt particles (G_f >1.85) (Swietlicki et al., 2008).

Recently, there have been numerous publications which have reported measurements of the hygroscopic growth factors of particles in various environments. Swietlicki et al. (2008) made an excellent review on the hygroscopic properties of submicron atmospheric particles measured with H-TDMA instruments. Swietlicki et al. (2008)'s work describes the G_f measurement methods, the variation in measured G_f between different atmospheres as well as the influence of chemical and physical properties on G_f. In addition, the implications of G_f in predicting particle critical supersaturation have been considered (Rissler et al., 2010; Swietlicki et al., 2008). However, the temporal variation or influence of sources upon G_f has not yet been fully investigated. Therefore, this work aims to summarize the measured G_f values from different sources and the chemical and physical processes which cause the change in G_f values during ageing processes. In addition, we have estimated the influence of hygroscopic properties on the lung deposition of ambient particles. Furthermore, we applied our modified ICRP curves to estimate the regional lung deposition fraction of ambient particles in three sites in southern England with strongly contrasting traffic volumes.

5.2. Hygroscopic properties of aerosols emitted from different source

5.2.1. Traffic Emissions

Traffic emissions are recognised as a main source of particles in urban environments (Morawska et al., 2008), and hence the hygroscopic properties of traffic particles are of much interest. One of the earliest G_f measurements of traffic particles was conducted by

Weingartner et al. (1993). Aerosols were generated by a four-stroke spark ignition engine using unleaded gasoline and then analysed by a Humidity Tandem Differential Mobility Analyzer (HTDMA) system. Measured growth factors of particles with original diameters of 29, 42, 77 and 111 nm at sub-and-super saturations showed very low values (~0.98-1.15), and therefore they were considered to be hydrophobic. The study found that particles of different sizes showed different hygroscopic behaviours. For example, primary particles with diameters of 29 and 42 nm were observed to grow faster than aggregates with a diameter of 77 and 111 nm.

In addition, Weingartner et al. (1995) noted that particles with a diameter of 51.5 nm kept their initial size, whilst larger ones (108 nm), typically non-spherical fractal-like structure aggregates, shrank to around 99% of their initial size at RH ≤95%. This could be explained by the capillary forces of water condensed in the angle cavities of aggregates, which caused any asymmetric part of the aggregates to collapse. When exposed to RH ≥95%, both primary particles and aggregates started to grow, but this growth was not appreciable. Similarly, Weingartner et al. (1997) conducted an experiment on soot particles from a diesel engine and found that these particles were also nearly hydrophobic with growth factors roughly 1.01 for 50-110 nm particles. This result was confirmed by Dua et al. (1999) who measured the hygroscopicity of particles emitted from two different diesel-powered vehicles. The diesel particles were found to be slightly soluble, and did not show a significant growth at a RH greater than 99%.

The hygroscopicity of traffic particles depends upon the type of fuels, fuel additives and pre-treatment devices. Weingartner et al. (1997) found that the growth factors of gasoline particles were smaller than those of diesel particles measured under loads representing a lean air/fuel ratio. In addition, a higher sulphur level in fuel was reported to lead to a higher growth factor of particles. Moreover, soot particles become more hygroscopic once they are

subjected to pre-treatment with O_3 and UV radiation (Weingartner et al., 1997), which can be explained by the oxidation or photolysis of hydrocarbons such as PAHs on the particle surface, which produce more soluble compounds.

In a further study on the effect of fuel on hygroscopic properties of diesel particles, Happonen et al. (2013) studied the effect of adding oxygen into the fuel using hydro-treated vegetable oils (HVO) and with HVO + fuel-oxygenate (di-n-pentyl ether) blend. They found an increased hygroscopicity of exhaust particles after the addition of the oxygen rich blend. Oxygen atoms, which were emitted in larger quantities with oxygenated fuel, may increase the oxygen to carbon ratio of an hypothetical superficial thin layer of organic material on the exhaust particles (Happonen et al. (2013)), resulting in more polar compounds by oxidation, and thus increasing the hygroscopic growth of the emitted particles. This is consistent with the findings of Jimenez et al. (2009), who reported that an increase of the oxygen to carbon-ratio resulted in an in increased hygroscopicity of the organic aerosol.

During the ageing process, the hygroscopic properties of such particles could be changed leading to a higher growth factor. Weingartner et al. (1995) measured the hygroscopicity of aged aerosols in a dark bag filled with exhaust gases from an engine. Their investigation found that particles became more hygroscopic when the residence time increased in the bag. After six hours of the aging process, the G_f values of traffic particles increased from 1.0 to 1.04. Weingartner et al. (1997) suggested four possible mechanisms, to understand the changes in the hygroscopicity of the soot particles during the aging process. These were coagulation, gas-to-particle conversion, cloud processing and photochemical degradation.

Kotzick and Niessner (1999) studied the aging process of ultrafine carbon aerosols in order to clarify which chemical and physical processes were responsible for these changes. They suggested that coagulation of ultrafine carbonaceous aerosols with soluble particles such as

sodium chloride, sulphuric acid aerosols and oxidised hydrophilic species produced by reaction with ozone could transform carbonaceous particles, making then more hydrophilic and allowing them to act as cloud condensation nuclei in the atmospheric condensation process. This is in agreement with Decesari et al. (2002) who suggested that water-soluble organic compounds produced from the oxidation of soot particles make soot particles become more hydrophilic.

In a recent study on the change in hygroscopicity during ageing of diesel soot, the increase in the hygroscopic growth factor of soot particles was linked with the condensation of secondary organic aerosols formed by the photo-oxidation of volatile organic compounds emitted with exhaust gases (Tritscher et al., 2011).

5.2.2. Biomass Burning

Biomass burning is an important source of particulate matter in the atmosphere. The hygroscopicity of particles emitted from biomass burning is known to change the light scattering and cloud nucleation properties, thereby having a strong impact on the earth's radiative balance, as well as the climate. Hence, the hygroscopicity of biomass burning related particles is of much concern.

Freshly emitted biomass burning particles are known to be hydrophobic or less-hygroscopic. Rose et al. (2008) showed a low growth factor with G_f values varying between 1.04 and 1.10 at RH 85%. This low hygroscopic growth factor is due to the chemical properties of particles generated from biomass burning, which mainly consist of organic materials and black carbon, both known to be hydrophobic or less-hygroscopic (Martin et al., 2013). Dusek et al. (2011) suggested that the hygroscopicity of wood burning particles was predominantly influenced by organic compounds. The growth factors of freshly generated biomass burning particles are small and equivalent to particles consisting of 5-20% ammonium sulphate along with

insoluble materials. Investigating the hygroscopic properties of five major organic products (levoglucosan, D-glucose, and vanillic, syringic and 4-hydroxybenozoic acids) from the pyrolysis of wood, Mochida and Kawamura (2004) found that levoglucosan and D-glucose show a significant hygroscopic growth (G_f ~1.37-1.38 at 90% RH) while the remainder do not show any hygroscopic growth even up to 95% RH.

Like traffic-related particles, particles emitted from biomass burning are expected to show an increase in hygroscopic growth factors during ageing in the atmosphere. Kotchenruther and Hobbs (1998) reported that the growth factors for light scattering for aged smoke (1.3-1.5) were higher than those for fresh smoke (1.1-1.3). A recent study by Martin et al. (2013) who conducted different wood burning experiments in a smog chamber found that the hygroscopicity of such particles increased with time during the aging process, except in the smouldering phase experiment. Secondary formation of soluble components such as sulphate and polar organic compounds was responsible for the increase in the hygroscopicity of smoke particles during ageing (Hallquist et al., 2009; Kotchenruther and Hobbs, 1998; Rogers et al., 1991). Furthermore, Decesari et al. (2002) reported that macromolecular humic-like substances can be formed by the atmospheric oxidation of soot; thereby increasing the water uptake properties of aerosol particles. To conclude, the oxidation of organic soot is also known as the main ageing process which makes particles become more hydrophilic (Martin et al., 2013).

5.2.3. Nucleation

New particles formed by nucleation account for a significant fraction of the total number of particles in the atmospheric environment. Ogulei et al. (2007) reported that nucleation related with traffic emissions represented between 15% to 21% of the total number of particles in

Rochester, United States. Similarly, another study conducted by Kasumba et al. (2009) found that nucleation represented between 15.4 to 20.7% of total particle number.

The hygroscopic properties of nucleation mode particles (4-20 nm) have been measured in various environments such as in urban/suburban areas (Petäjä et al., 2007; Sakurai et al., 2005; Väkevä et al., 2002b), in boreal forests (Hämeri et al., 2001; Park et al., 2009) and in coastal regions (Buzorius et al., 2004; Väkevä et al., 2002a). Sakurai et al. (2005) measured G_f in an urban background of Atlanta and reported that the 10 nm nucleation particles were more hygroscopic; showing a growth factor value of ~1.4, which was equivalent to 10 nm ammonium sulphate particles. This finding is in agreement with the hypothesis that new particles in Atlanta consisted of ammonium and sulphate alone (Jung et al., 2006). Similarly, Petäjä et al. (2007) found higher growth factors (G_f maximum ~ 1.6) of nucleation mode particles during nucleation event days, compared to those (G_f maximum ~1.3) on non-event days in Marseille (France). However, this study also found that the condensational growth of nucleation mode particles does not only depend upon sulphuric acid concentration, but is also controlled by other water insoluble components. By dividing the nucleation event days into groups based on the anthropogenic influence, Petäjä et al. (2007) concluded that the G_f values varied between the different properties of condensing vapours. Particularly, during clean events with less anthropogenic influence, the growth of nucleation particles was due to insoluble materials rather than the condensation of water soluble components, whilst during the polluted events, the growth of particles was mainly contributed by water soluble components.

More evidence of the contribution of other insoluble materials to the growth of nucleation particles has been provided by other observations of the lower growth factor values of nucleation particles (Hämeri et al., 2001; Väkevä et al., 2002a; Väkevä et al., 2002b). Väkevä et al. (2002a) reported that the nucleation mode particles (8-10 nm) sampled during

nucleation events on the coast of Ireland were less hygroscopic (G_f ~1.1). This was attributed to new particles formed in coastal areas as a result of the nucleation of iodine oxides (Carpenter et al., 1999; O'Dowd et al., 2002a; O'Dowd et al., 2002b), resulting in a much lower growth factor. In addition, Hämeri et al. (2001) investigated the hygroscopic growth of nucleation particles at a boreal forest site in Southern Finland. This study concluded that the sulphuric acid concentrations could not explain the growth of nucleation particles by themselves in the boreal forest, suggesting that the growth process may be related to organic compounds. To conclude, the hygroscopic growth factor of nucleation mode particles varied between environments, depending upon the air masses as well as the nucleation and growth mechanism in different atmospheres.

5.3. Hygroscopic behaviour of ambient aerosols

5.3.1. Spatial Variation

Urban environments

The growth factors of urban particles in most previous studies have been classified in three groups: near-hydrophobic, less-hygroscopic and more-hygroscopic (Swietlicki et al., 2008). The dominant hydrophobic and less-hygroscopic particles in the urban environments could be explained by the sources of particles at these sites, where traffic-related emissions were found as to be main source of urban ultrafine particles (Morawska et al., 2008). Near-hydrophobic particles can be assumed to originate from fresh traffic emissions that contain black carbon, while less-hygroscopic particles may have originated from transformed oil combustion particles (Swietlicki et al., 2008). In addition, other combustion processes such as wood combustion in some cases contribute significantly to the number fraction of near-hydrophobic and less-hygroscopic particles (Baltensperger et al., 2002; Dusek et al., 2011).

Hygroscopic properties were measured at both urban background and kerbside sites in previous studies. Ferron et al. (2005) reported that the growth factors of particles within a certain size from different sampling sites do not vary significantly, but the hydrophobic/hygroscopic particle fraction is strongly influenced by the type of site. At the kerbside site, the number fraction of the nearly-hydrophobic group accounted for more than 80% of total particles with a size of 50 nm, while this number was 30-40% at the background site. When particle size increases (>100 nm) the fraction of near-hydrophobic particles decreases while the fractions of less hydrophobic and hygroscopic particles increases. For example, nearly-hydrophobic particles measured at an urban background in Neuherberg, Germany accounted for 42% of total particles with size of 50 nm while they only represented 25% of particles with a size of 200 nm (Tschiersch et al., 1997). This is consistent with the decrease in traffic particles of larger sizes. Particle number size distributions of particles emitted from vehicles show peaks at below 50 nm (Charron and Harrison, 2003). Hygroscopic particles, which are known to come from regional background transportation, were found to be dominant in the accumulation mode.

Rural environments

Aerosol particles in rural environments can derive from anthropogenic sources such as traffic or industrial emissions by advection and from local emissions such as biomass burning, as discussed below. They also originate from atmospheric processes such as nucleation. Since rural sites may be exposed to aerosols from multiple sources, the observed G_f show a large variation. Similar to urban environments, the growth factors in rural areas have been classified into three groups: near-hydrophobic (G_f ~1.01-1.14), less-hygroscopic (G_f ~1.14-1.32) and more-hygroscopic (1.34~1.63). The number fractions of the three classes show differences between urban and rural areas. The less- and more-hygroscopic particles are major contributors to the total number of particles. Swietlicki et al. (1999) reported that the

number fraction of more-hygroscopic particles accounted for 64% of total particle number concentrations with a size of 35 nm, while this number increased to 81% of the total particle number with a size of 265 nm. However, during biomass burning events, the contribution of more-hygroscopic groups was limited and the number fraction of less-hygroscopic particles was dominant (Rissler et al., 2006). The large fraction of organic compounds and black carbon emitted from biomass burning were the reason for the abundance of less-hygroscopic particles.

Marine environments

More-hygroscopic particles are ubiquitous in marine environments. Zhou et al. (2001) reported that the frequency of occurrence of more-hygroscopic particles was above 81% and when these were present it represented a number fraction larger than 0.93. A mixture of ammonium sulphate and non-neutralized sulphate, which originate from oceanic biota, are the main components of this group, leading to very high growth factors. For example, the observed G_f of more-hygroscopic particles with a diameter of 50 nm in coastal environments ranges from 1.40 to 1.9 at 90% RH (Zhou et al., 2001). These are much higher than the G_f in rural (G_f ~1.32-1.61) and urban environments (G_f ~1.36-1.49).

The growth factors of marine aerosols are found to be even higher during days with high wind speeds, when the marine aerosols include externally mixed sea salt particles. Wind at high speeds brings freshly produced sea-salt particles with high volume fractions of sodium chloride, with a large growth factor G_f >1.85, resulting in higher growth factors for marine aerosols. However, the lifetime of externally mixed sea salt aerosols is short and limited by ageing processes. During ageing periods, sodium chloride reacts with sulphuric acid or with ammonium and sulphate compounds producing sodium sulphate, which has a lower growth factor (G_f ~1.6). The number fraction of less-hygroscopic and near-hydrophobic particles was

often lower than 0.1 with the occurrence frequency around 20%. These particles could have arrived from continental air masses or local emission from ships.

5.3.2. Temporal Variation

It is clear that the temporal pattern of the number fraction of hydrophobic/hygroscopic particles depends strongly upon the pattern of local sources, as well as the meteorological conditions such as temperature variation, precipitation or the origin of the air mass. Massling et al. (2005) reported that the number fraction of nearly-hydrophobic particles measured in an urban background area showed a distinct diurnal pattern, with peaks corresponding to daily rush hours. Nearly-hydrophobic particles, which are found to be dominant during the daytime in urban areas, can be attributed to soot and organic compounds emitted directly from vehicles or the particles formed by nucleation in the dilution and cooling of fresh vehicular emissions, leading to a lower averaged growth factor during the daytime. In contrast, another study in a boreal forest by Hämeri et al. (2001) showed the opposite behaviour.

The growth factors of particles in nucleation and Aiken modes were found to be at their highest during the early afternoon and lowest during the late evening and early morning. This trend was consistent with other studies (Boy et al., 2004; Ehn et al., 2007; Fors et al., 2011; Petäjä et al., 2007). Fors et al. (2011) suggested that an increase in the planetary boundary layer depth which entrains more hygroscopic particles with height when the sun rises could be an explanation for the increase in hygroscopic particles in boreal forests. Another reason could be from the different atmospheric conditions between day and night (Ehn et al., 2007). For example, the evaporation of semi-volatile organics with low hygroscopicity during the daytime alters more hygroscopic particles (Fors et al., 2011). It could also be associated with daytime oxidative processes which produce more functionalised organic compounds that have higher hygrocopicity (Wong et al., 2011).

There are a few studies on long-term measurements of particle hygroscopicity. The growth factors of each group seem to be stable, while fraction numbers exhibit a seasonal variation (Ferron et al., 2005). A two-year study in southern Sweden reported that the number fraction of less-hygroscopic particles was higher in winter (Fors et al., 2011). This trend concurs with a recent study in Paris (Kamilli et al., 2014).

5.4. Effect of aerosol hygroscopic properties on calculation of lung deposition

5.4.1. Lung Deposition Calculation for Ambient Submicron Aerosols

The International Commission on Radiological Protection (ICRP) model and the Multiple Path Particle Dosimetry model (MPPD) are those most widely used to estimate the regional lung deposition of particles (Hussein et al., 2013). However, when these current mathematical models are utilized to calculate the regional lung dose of ambient particles, the result may not be accurate (Asgharian, 2004). Montoya et al. (2004) compared the total deposition fraction of fine and ultrafine ambient aerosols measured in a group of six healthy adults and the estimated total deposition fraction by the ICRP model. They reported that the ICRP model is likely to predicts the total deposition fraction well for ambient particles smaller than 400 nm, but underestimates the deposition of particles larger than 676 nm, which is in agreement with other studies (e.g., Daigle et al. (2003), Löndahl et al. (2009)). The main reason is that the theoretical models do not account for particle growth due to the hygroscopic properties of ambient particles when they penetrate into the respiratory system (Löndahl et al., 2009; Montoya et al., 2004).

The aim of this section is to investigate and compare the effects of the hygroscopicity of particles from different ambient environments on their lung deposition fraction using a modified ICRP model for hygroscopic particles. This chapter uses 13 published data sets from previous studies for hygroscopic growth factors and their number fraction in rural,

urban background and roadside environments (Roadside: Bavaria (Ferron et al., 2005), Copenhagen (Löndahl et al., 2009), Bresso (Baltensperger et al., 2002); Urban background: Neuherberg (Tschiersch et al., 1997), Leipzig (Massling et al., 2005), Taipei (Chen et al., 2003), Beijing (Massling et al., 2009), Guangzhou (Tan et al., 2013), Shanghai (Ye et al., 2013); Rural: Bologna (Svenningsson et al., 1992), Berlin (Busch et al., 2002), Hohenspeissenberg (Ferron et al., 2005), Great Dun Fell (Swietlicki et al., 1999) as shown in Table 5.1.

Table 5.1: Hygroscopic growth factors and number fractions of three hygroscopic particle groups in the atmosphere *(NH: Nearly-hygroscopic, LH: Less-hygroscopic, MH: More-hygroscopic).*

Locations	Dp	RH	G_f (Number fraction)			Type of environments	References
			NH	LH	MH		
Bavaria, Germany	50	85	1.01(0.83)	-	1.30 (0.17)	Roadside	Ferron et al. (2005)
	100		1.01 (0.84)	-	1.33 (0.16)		
	150		1.01 (0.78)	-	1.39 (0.22)		
	250		1.04 (0.68)	-	1.47 (0.32)		
Copenhagen, Denmark	30	91	1.03 (0.89)	-	1.47 (0.11)	Roadside	Löndahl et al. (2009)
	40		1.03 (0.82)	-	1.39 (0.18)		
	80		1.02 (0.77)	-	1.46 (0.23)		
	160		1.03 (0.72)	-	1.62 (0.28)		
Bresso, Italy	20	90	1.02 (-)	-	-	Roadside (100 m highway)	Baltensperger et al. (2002)
	50		1.03 (0.51)	1.21 (0.49)	-		
	100		1.02 (0.48)	1.25 (0.62)	-		
	200		1.02 (0.28)	1.28 (0.72)	-		
Leipzig, Germany	50	92	1.06 (0.31)	1.25 (0.31)	1.44 (0.39)	Urban background	Massling et al. (2005)
	150		1.09 (0.22)	1.33 (0.15)	1.65 (0.65)		
Neuherberg, Germany	50	90	1.05 (0.42)	-	1.36 (0.58)	Urban	Tschiersch et al. (1997)
	75		1.02 (0.40)	-	1.23 (0.60)		
	110		1.02 (0.40)	-	1.25 (0.60)		
	165		1.03 (0.35)	-	1.29 (0.65)		
	300		1.02 (0.25)	-	1.34 (0.75)		
Taipei, Taiwan	53	90	1.11 (0.78)	-	1.43 (0.22)	Urban	Chen et al. (2003)
	82		1.11 (0.74)	-	1.49 (0.26)		
	95		1.11 (0.61)	-	1.54 (0.39)		

	202		1.11 (0.59)	-	1.66 (0.41)		
Beijing, China	30	90	0.99 (0.17)	1.07 (0.41)	1.26 (0.42)	Urban background	Massling et al. (2009)
	50		1.04 (0.22)	1.21 (0.34)	1.40 (0.45)		
	150		1.06 (0.21)	1.27 (0.25)	1.53 (0.54)		
	250		1.06 (0.24)	1.28 (0.25)	1.58 (0.54)		
	350		1.06 (0.28)	1.30 (0.27)	1.60 (0.46)		
Guangzhou, China	40	90	-	1.16 (0.41)	1.46 (0.59)	Urban background	Tan et al. (2013)
	80		-	1.14 (0.38)	1.48 (0.62)		
	110		-	1.13 (0.33)	1.49 (0.67)		
	150		-	1.12 (0.30)	1.51 (0.70)		
	200		-	1.11 (0.26)	1.55 (0.73)		
Shanghai, China	30	91	1.09 (0.35)	-	1.40 (0.65)	Urban (background)	Ye et al. (2013)
	50		1.08 (0.24)	-	1.49 (0.76)		
	80		1.06 (0.18)	1.31 (0.06)	1.58 (0.76)		
	100		1.05 (0.20)	1.31 (0.04)	1.60 (0.76)		
	130		1.04 (0.21)	1.35 (0.04)	1.63 (0.74)		
	150		1.04 (0.22)	1.36 (0.03)	1.65 (0.74)		
	180		1.03 (0.22)	1.36 (0.02)	1.67 (0.75)		
	200		1.03 (0.21)	1.34 (0.02)	1.68 (0.76)		
Bologna, Italy	30	90	-	1.12 (0.61)	1.59 (0.39)	Rural	Svenningsson et al. (1992)
	50		-	1.13 (0.63)	1.61 (0.37)		
	100		-	1.15 (0.59)	1.58 (0.41)		
	150		-	1.10 (0.53)	1.55 (0.47)		
	200		-	1.12 (0.57)	1.57 (0.43)		
Berlin, Germany	50	90	-	1.12 (0.08)	1.43 (0.92)	Rural (80 km south east of Berlin)	Busch et al. (2002)
	100		-	1.11 (0.12)	1.49 (0.88)		
	150		-	1.08 (0.05)	1.56 (0.95)		
	250		-	1.08 (0.02)	1.63 (0.98)		
Hohenspeissenberg, Germany	50	90	1.07 (0.52)	-	1.29 (0.48)	Rural	Ferron et al. (2005)
	100		1.03 (0.44)	-	1.35 (0.56)		
	150		1.03 (0.38)	-	1.41 (0.62)		
	250		1.04 (0.30)	-	1.48 (0.70)		
Great Dun Fell, UK	35	90	-	1.10 (0.36)	1.38 (0.64)	Rural	Swietlicki et al. (1999)
	50		-	1.12 (0.37)	1.44 (0.63)		
	75		-	1.11 (0.39)	1.52 (0.61)		
	110		-	1.12 (0.31)	1.58 (0.69)		
	165		-	1.14 (0.24)	1.64 (0.76)		
	265		-	1.15 (0.20)	1.69 (0.81)		

5.4.2. A modified ICRP model for ambient particles

The origin ICRP curves for hydrophobic particles are generated for monodisperse spheres of standard density in standard conditions. A modified ICRP model for hygroscopic particles is

based on the previous work of Löndahl et al. (2009), Kristensson et al. (2013) and Hussein et al. (2013). Ambient particles are divided into three groups: near-hydrophobic, less-hygroscopic and more-hygroscopic. Subsequently, the ICRP model is applied separately for each type of particles, with a consideration of their growth when they penetrate into the respiratory tract. The final deposition fraction, which is defined as the fraction of particle can deposit in the lung in each environment was calculated by the mean value of deposition fraction for these three groups weighted by their number fractions for each group as shown in equation (2) and assuming a relative humidity equilibrium in the airways of 99.5%.It is assumed that the submicron particles which have increased to their equilibrium size by their growth in the respiratory tract have the same behaviour as insoluble particles with a similar size in the respiratory system (Asgharian, 2004). For example, hygroscopic particles with an initial size of 50 nm and a G_f value of 2 (at 99.5% RH) are assumed to have an equivalent deposition fraction to hydrophobic particles ($G_f = 1$) with a diameter of 100 nm (Löndahl et al., 2009). However, when a particle penetrates into the lung, its growth is not only controlled by its hygroscopic properties but also due to its residence time.

The submicron particles can growth rapidly while larger particles may not reach their equilibrium size during the inhalation cycle. Hence, the above assumption by Londahl et al. (2009) is limited to small particles which can grow and reach their equilibrium size rapidly. Ferron (1977) found that particles smaller than 0.2 μm can reach their equilibrium size within 0.1 sec in the human respiratory tract. To correct the size growth for particles larger 0.2 μm when they penetrate into the regional lung due to their residence time, our study used an approach which described the correlation between particle growth and residence time, provided by Ferron (1977). Particle growth can be approximated by the following equation (Ferron, 1977; ICRP, 1994):

$$F(t) = \frac{Dp\,(t) - Dp(0)}{Dp(e) - Dp(0)} = \frac{Dp(0) * [\exp\left(-\frac{10t^{0.55}}{Dp(0)}\right)^{0.6} - 1]}{Dp(e) - Dp(0)} \quad (5.2)$$

where, F(t) is the fraction of equilibrium size, D_p (t) is the particle size in aerodynamic diameter at t (s); D_p (0) is the initial dry particle (µm), D_p (e): Equilibrium particle size (µm), and t is the residence time is the lung (s). In our estimation, atmospheric particles are assumed to be spherical particles with unity density, therefore D_p is considered to be equal to the particle volume equivalent (thermodynamic) diameter.

The variation in the hygroscopic growth fraction as a function of time calculated from different initial sizes of dry particles is shown in Figure 5.1.

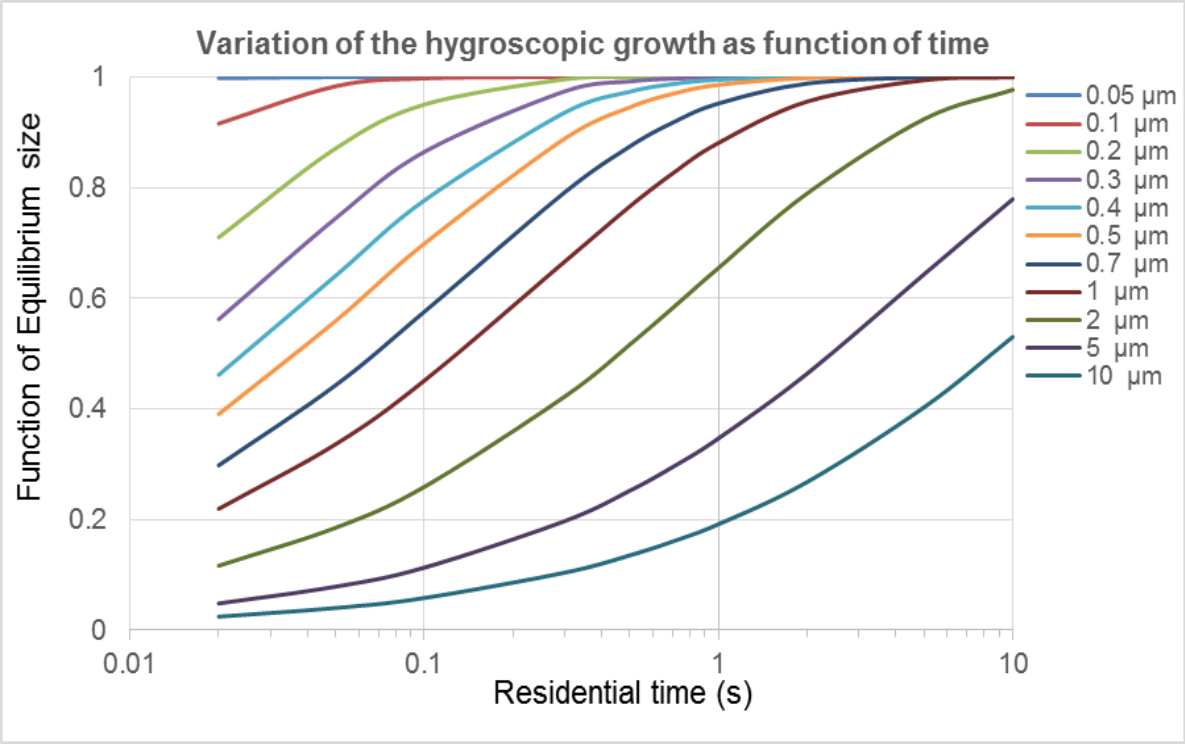

Figure 5.1: Variation in hygroscopic growth as a function of time and size.

To estimate the growth factor in each lung region, we assumed the residence time of particles in the ET, TB, AL regions to be 0.116, 0.308, 1.32 s during inspiration and 1.56, 0.356 and

1.56 during expiration, with a pause time of 0.2 s (Ferron, 1977). The particle growth factor is each region will be calculated by:

$$Averaged\ Gf\ in\ each\ lung\ region = \frac{\int_{t1}^{t2} Gf'(t)*dt}{t_2 - t_1} \quad (5.3)$$

where, t_1 and t_2 are the time when particle come in and out of the regional lung; for example, t_1=0 and t_2 =0.116s for particles coming in and out of the ET region during inspiration.

If we define $G'_{f(t)}$ as the growth factor of particle at t (s) ($G'_{f(t)} = \frac{Dp(t)}{Dp(0)}$), and $G_{f(max)}$ as the maximum growth factor of particles (when particles can reach their equilibrium size) (($G_{f(max)} = \frac{Dp(e)}{Dp(0)}$), from the equation (5.3) we have:

$$G'_{f(t)} = G_{f(max)} + F(t)*(G_{f(max)} - 1) \quad (5.4)$$

In the distal airways, the lumen air is likely to have reached equilibrium. However, in the proximal airways and the extra-thoracic region of the respiratory tract, the relative humidity in the airways may depart substantially from 99.5% equilibrium due to interactions between the ambient air temperature and humidity and the temperature and water activity of the mucus layer. Morrow (1986) showed that supersaturations as large as 130% could occur in the trachea under certain ambient temperature and humidity conditions. Calculations presented in this paper have been made considering a relative humidity of 99.5% and a temperature of 37 ^{o}C consistent throughout the respiratory tract.

$$DF_{ambient} = \alpha.\ DF_{nearly\text{-}hydrophobic} + \beta.DF_{less\text{-}hygroscopic} + \chi.DF_{more\text{-}hygroscopic} \quad (5.5)$$

where, $DF_{ambient}$, $DF_{near\text{-}hydrophobic}$, $DF_{less\text{-}hygroscopic}$, $DF_{more\text{-}hygroscopic}$ are deposition fractions of ambient particles, nearly-hydrophobic particles, less-hygroscopic particles and more-hygroscopic particles, respectively. α, β, χ are the number fraction of nearly-hydrophobic, less-hygroscopic and more-hygroscopic particles ($\alpha + \beta + \chi = 1$).

Calculation of the hygroscopic growth factor of particles at 99.5% RH.

Almost all published data for the growth factor of ambient particles were measured at around 90% RH (Swietlicki et al., 2008), whilst the RH in the respiratory tract is approximately 99.5% (Hussein et al., 2013). To estimate the growth factor of particles at the relative humidity found in the lungs (99.5%), we used Rissler's model (Kristensson et al., 2013; Rissler et al., 2006) which was introduced in previous studies by Swietlicki et al. (1999), Löndahl et al. (2009) and Kristensson et al. (2013).

$$G_f = \sqrt[3]{1 + K_R \frac{M_w}{\rho_W}\left(\frac{a_w}{1-a_w}\right)} \quad (5.6)$$

where, K_R is a hygroscopic parameter which presents the effective number of moles of soluble molecules or ions per dry particle volume unit; M_w, ρ_w are the molecular weight and density of water; and a_w is water activity.

According to the Köhler equation:

$$a_w = \frac{RH}{100.C_k} \quad (5.7)$$

where, C_k is the Kelvin curvature correction factor:

$$C_k = \exp\left(\frac{4M_W\sigma_s}{RT.\rho_w D_p}\right) \quad (5.8)$$

σ_s is the surface tension of the solution; R and T are the ideal gas constant and temperature respectively, and D_p is the particle diameter.

From equation (5.6), we have:

$$G_f^3 = 1 + K_R\frac{M_w}{\rho_w}\frac{a_w}{1-a_w} \quad (5.9)$$

Combined with the Kohler equation (5.7), equation (5.9) will be:

$$G_f^3 = 1 + K_R\frac{M_w}{\rho_w}\frac{RH}{100C_k-RH}$$

$$\Rightarrow \quad K_R = \frac{(G_f^3 - 1)\rho_w(100C_k - RH)}{M_w RH} \tag{5.10}$$

The HTDMA typically measures the G_f at relative humidity a%, which is lower than 99.5 % (normally the relative humidity inside the second DMA of a HTDMA system is around 80-90%). From equation 5.10, we can calculate the hygroscopic parameter at known relative humidity a% measured by HTDMA.

$$K_{R\text{-}a\%} = \frac{(G_{f-a\%}^3 - 1)\rho_w(100C_{k-a\%} - a)}{M_w a} \tag{5.11}$$

$K_{R\text{-}a\%}$: Hygroscopic parameter at relative humidity a %

$C_{k\text{-}a\%}$: Kelvin curvature correction factor at relative humidity a %

From equation (5.8), we have:

$$C_{k\text{-}a\%} = e^{\frac{4M_w\sigma_S}{RT\rho_w D_{p-a\%}}} \tag{5.12}$$

$D_{p\text{-}a\%}$: Particle diameter at relative humidity a %, therefore $D_{p\text{-}a\%} = D_p.G_{f\text{-}a}$, in which D_p: Dry particle diameter and $G_{f\text{-}a}$: growth factor at relative a %.

Similarly, the hygroscopic parameter at relative humidity 99.5% is

$$K_{R\text{-}99.5\%} = \frac{(G_{f-99.5\%}^3 - 1)\rho_w(100C_{k-99.5\%} - 99.5)}{M_w.99.5} \tag{5.13}$$

In Rissler's model, the hygroscopic parameter is assumed as a constant parameter over the relative humidity change, therefore K_R is the same value for a % and 99.5%. From equation (5.11) and (5.13), we have:

$$\frac{(G_{f-99.5\%}^3 - 1)\rho_w(100C_{k-99.5\%} - 99.5)}{M_w.99.5} = \frac{(G_{f-a\%}^3 - 1)\rho_w(100C_{k-a\%} - a)}{M_w a} \tag{5.14}$$

The G_f at 99.5% RH is estimated from the following equation:

$$G_{f-99.5\%}^{3} = 1 + \frac{\left(G_{f-a\%}^{3}-1\right).99.5.(100C_{k-a\%}-a)}{a\,(100C_{k-99.5\%}-99.5)}$$

$$\Rightarrow \quad G_{f\text{-}99.5\%} = \sqrt[3]{1 + \left(G_{f-a}^{3} - 1\right).\frac{99.5}{a}.\frac{(100e^{\frac{2.09}{Dp.Gf-a}}-a)}{(100e^{\frac{2.09}{Dp.Gf-99.5}}-99.5)}} \qquad (5.15)$$

where, $G_{f\text{-}99.5\%}$ is the growth factor at 99.5% RH, $G_{f\text{-}RH}$ is the growth factor at a% RH and D_p is the particle diameter measured at low RH (<10%).

This model assumes that the number of soluble molecules is constant over the relative humidity and the droplet solution is ideal (Rissler et al., 2010), therefore K_R is assumed to be a constant value as relative humidity changes from a% to 99.5%. The value of 2.09 was calculated assuming a surface tension of 0.072 J m^{-2}. (M_{water}=18 g mol^{-1}; R: 8.314 J mol^{-1} K^{-1}; T=298 K) according to Petters and Kreidenweis (2007).

Different surface tensions could cause some bias for growth factors calculation at 99.5%. Most particles in the atmosphere are composed of a substantial amount of organic material, which is functionalized from atmospheric processing and is likely to act as a surfactant and substantially decrease the particle surface tension. However, the error associated with different surface tensions can be acceptable, as proved by a comparison between different models by Rissler et al. (2010).

The H-TDMA system has been used to determine hygroscopic growth factors and their number fractions for particles with selected diameters, typically from 30 nm to 350 nm. To estimate the hygroscopic growth factors and number fractions for a full size range (10-1000 nm), it is assumed that the hygroscopic parameter K_r and number fraction of particles at a diameter of 30 nm, is suitable for those smaller than 30 nm, while those of particles with a diameter of 350 nm are suitable for those larger than 350 nm (Hussein et al., 2013). Growth

factors of the three hygroscopic groups at 99.5% RH were estimated according to equation (5.15), as shown in Figure 5.2 using growth factors reported in the literature.

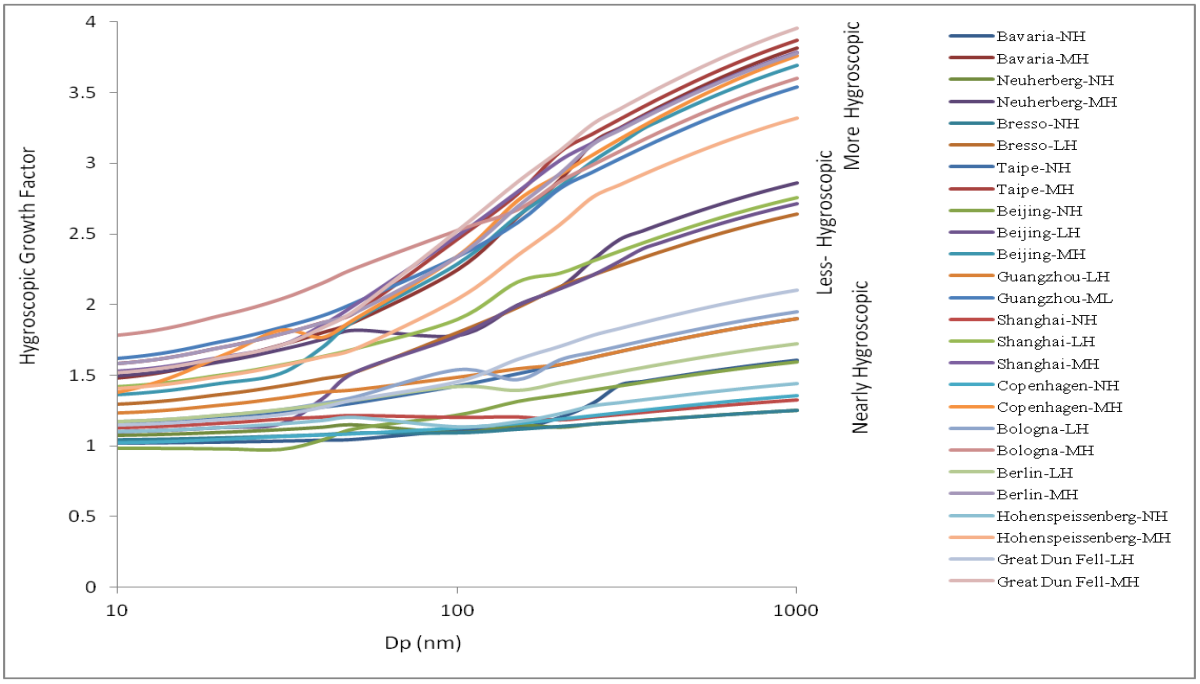

Figure 5.2: Estimated hygroscopic growth factors of nearly, less and more hygroscopic particles at 99.5% RH from different environments. *Calculations according to equation 5.12.*

Effects of Hygroscopic Properties of Particles on Lung Deposition in Different Environments

ICRP model curves were modified using the particle hygroscopic growth factors reported in the literature in each group and then equation (5.2) was used to estimate the average value for the ambient particles. The total average deposition fraction (DF) of particles measured from different environments is shown in Figure 5.3.

As seen in Figure 5.3, the hygroscopic properties of particles have a marked effect on the total lung deposition fraction (DF) of particles. Due to particle hygroscopicity, the deposition fraction curve shifts its minimum from 400 nm for hydrophobic particles to 120-150 nm for rural and urban background particles and to 140-200 nm for roadside particles (dry diameter).

This is consistent with the experimental and modelled deposition of airborne particles at a kerbside site conducted by Löndahl et al. (2009) who report that in kerbside areas, the lung deposition fraction has a minimum value of around 200 nm. The shifts in deposition curves to the left or right could be explained by the decrease in Brownian diffusion and the increase in sedimentation and impaction (ICRP, 1994).

In roadside environments, the ICRP model seems to predict well the deposition fraction of particles smaller than 200 nm. This could be explained by the fact that small particles at traffic sites are freshly emitted from traffic exhaust, and therefore mostly comprise hydrophobic particles.

At rural and urban background sites, the ICRP model seems to overestimate the lung deposition fraction for particles smaller than 150 nm. For example, the deposition fraction of hydrophobic particles with a diameter of 100 nm is found to be 40% higher than those of particles with the same diameter size at rural sites. In contrast, the ICRP model seems to underestimate the total deposition fraction for particles larger than 200 nm.

The DF values for ambient particles with a diameter of 1μm are more than two times higher than those predicted by the ICRP model (Figure 5.3). This means that there is a huge error if the ICRP model is used to predict the lung deposition fraction of ambient particles larger than 200 nm without considering their growth factors. The error of not including the hygroscopicity factor of particles in the lung deposition calculation is of similar magnitude to the individual variability in the deposition fraction for particles in the low deposition fraction range associated with factors such as different lung geometries, breathing patterns, or lung disease.

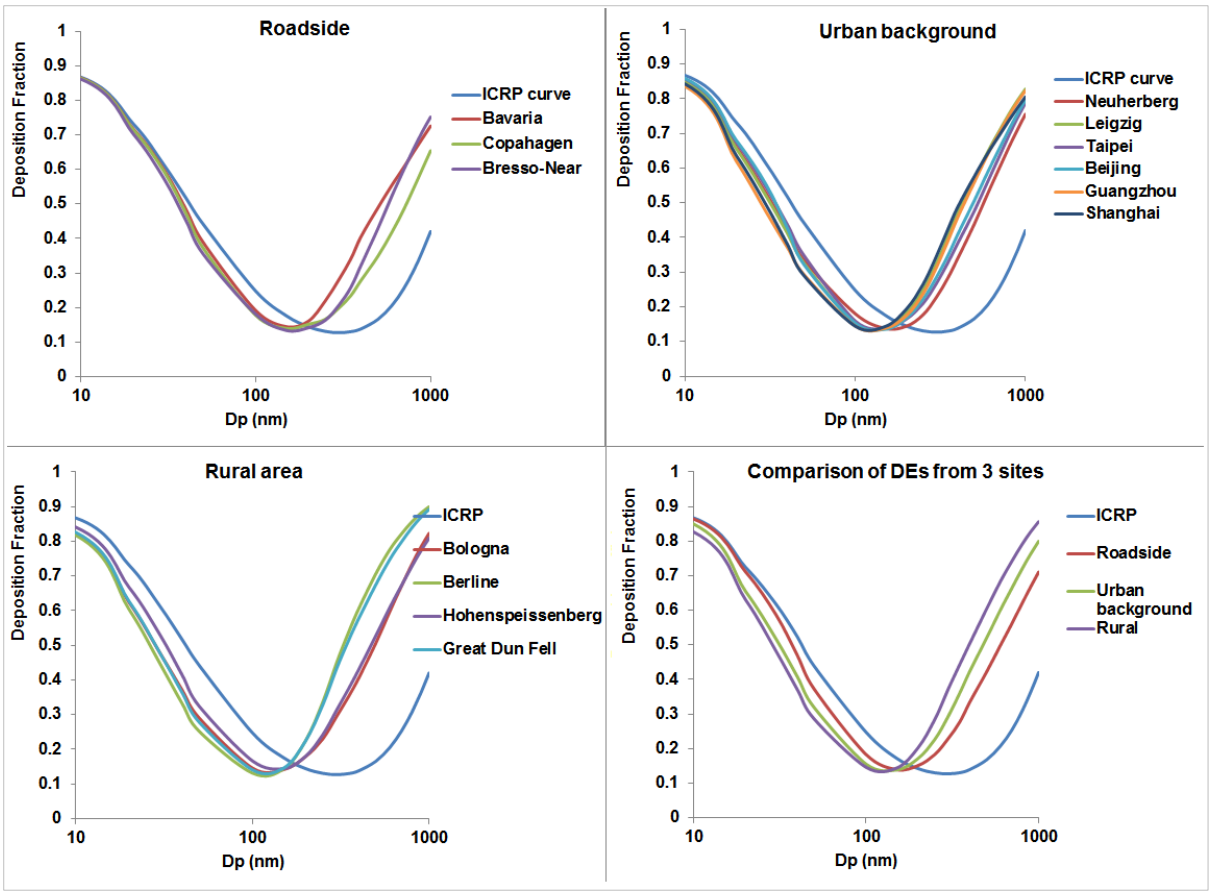

Figure 5.3: Calculations of the deposition fraction in the whole lung of ambient particles in various environments.

There is little difference between the deposition fractions calculated for different sampling sites within each type of environment, suggesting that similar deposition fraction curves are applicable for each type of environment. The maximum variations between deposition fractions for particles smaller than 200 nm calculated for different sampling sites are 6.3%, 15.9% and 13.3% (Figure 5.3) within roadside, urban background and rural environments, respectively.

Figure 5.3 also shows that values of DF for particles in urban background areas seem to be similar to those in rural areas. On the contrary, the DF of a particle in the ultrafine size range in roadside areas is found to be 1.2 to 1.6 times higher than those in urban background and rural areas.

The hygroscopic properties of particles also have a strong influence on the regional lung deposition fraction, as shown in Figure 5.4. In the extra-thoracic region, the hygroscopic properties seem to have little effect on the DF of ultrafine particles (Dp<100 nm), whilst the DF increases considerably according to their hygroscopic growth properties for particles larger than 200 nm (Figure 5.4A). The DF in the tracheo-bronchial region is that the least affected by the growth factor (Figure 5.4B). In the alveolar region, the DF for ambient particles smaller than 200 nm is much lower than for hydrophobic particles, whilst the DF increases for particles larger than 200 nm, according to their hygroscopicity (Figure 5.4C).

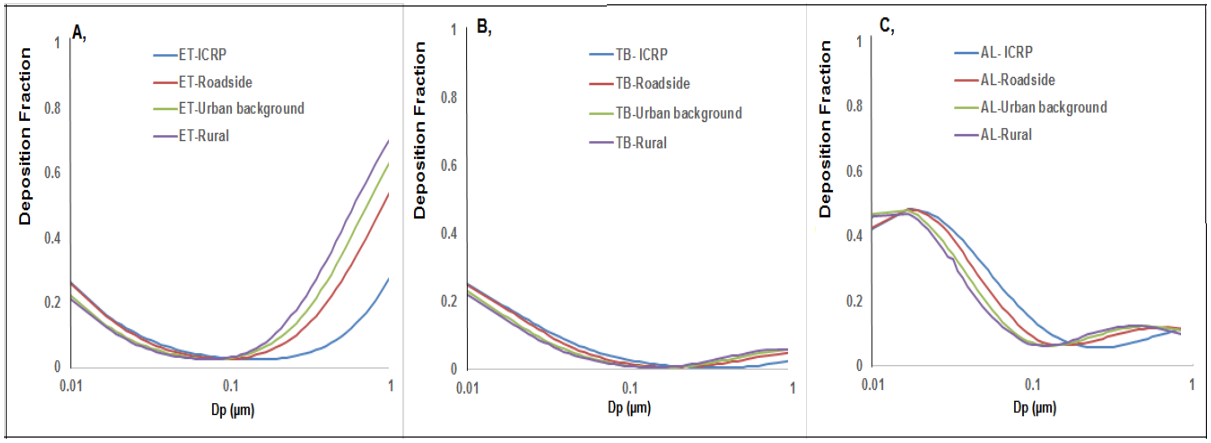

Figure 5.4: Calculations of the deposition fraction in the regional lung of ambient particles in various environments. *A: In the extra-thoracic region (ET); B: in the tracheo-bronchial region (TB) and C: in the alveolar region (AL).*

5.5. Application of a modified ICRP model to calculate the lung deposition fraction of ambient aerosols

5.5.1. Particle size distribution from traffic, urban background and rural areas in London, UK

Particle number size distributions were measured by a Scanning Mobility Particle Sizer (SMPS) covering the size range 16.5-604 nm operated by the Department for Environment,

Food and Rural Affairs (DEFRA). The SMPS system included an Electrostatic Classifier (EC, TSI model 3080) and a Condensation Particle Counter (CPC, TSI model 3775). In this study, a year of data observed at a traffic (Marylebone Road), urban background (North Kensington) and rural (Harwell) monitoring site during 2008 were extracted from the DEFRA website (see http://uk-air.defra.gov.uk/ for more detailed information).

Sampling sites information

Marylebone Road: This monitoring station is classified as a kerbside site by the London Air Quality Network. A SMPS system was located in an air conditioned cabin on Marylebone Road within a street canyon. Marylebone Road comprises six-lane highway and is frequently busy with around 80,000 vehicles per day.

North Kensington: This monitoring station is located in the grounds of Sion Manning School, where is representative of a typical urban background area of London.

Harwell: This monitoring station is within the grounds of the Harwell Science Centre in southern England. This site is representative of a rural background area.

Particle size distributions

Figure 5.5 shows the particle size (number, surface area and mass) distributions from the traffic, urban background and rural areas. In all sampling sites, the majority of particles by number was found in the Aitken mode while particle surface area and mass were mainly distributed in the accumulation mode. The CMD (count median diameter), SMD (surface area median diameter), and MMD (mass median diameter) of submicron particles at the traffic site were 46.2, 150.0 and 217.7 nm, respectively. Higher values than these were found in the urban background and rural areas. The CMD, SMD and MMD of submicron particles in the

urban background area were 52.9, 157.7 and 237.0 nm while the values of submicron particles in the rural area were 56.9, 176.1 and 255.0 nm.

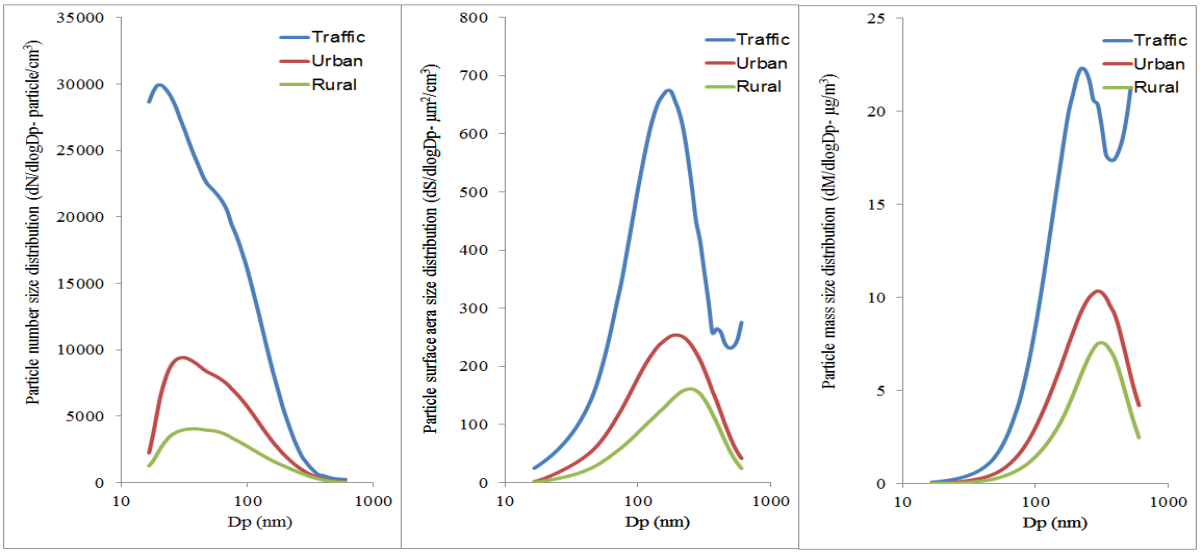

Figure 5.5: Size distribution by number, surface area and mass of submicron particle at traffic (Marylebone Road), urban background (North Kensington) and rural (Harwell) sampling sites. *Assuming particles are spheres and effective density is 1 g cm^{-3}.*

5.5.2. Deposition fraction of particles in traffic, urban background and rural areas

The deposition fractions of particles in traffic, urban background and rural areas were calculated by the application of an original ICRP curve for hydrophobic particles and a modified ICRP curve for hygroscopic particles. Figure 5.6 shows a comparison of the deposition fraction of particles calculated by original and modified ICRP curves. The total DF for submicron particles by number, surface area and mass was 0.49, 0.20 and 0.15 at the traffic site while it was 0.44, 0.19 and 0.15 at the urban background site and 0.42, 0.17 and 0.14 at the rural site using original ICRP curves for hydrophobic particles. Based on the modified ICRP curves for ambient particles, the DF by number decreased whereas those by surface area and mass increased. The total DF for submicron particles by number, surface area and mass calculated by a modified ICRP model was 0.44, 0.23 and 0.22 at the traffic site

while it was 0.34, 0.23 and 0.28 at the urban background site and 0.31, 0.27 and 0.35 at the rural site.

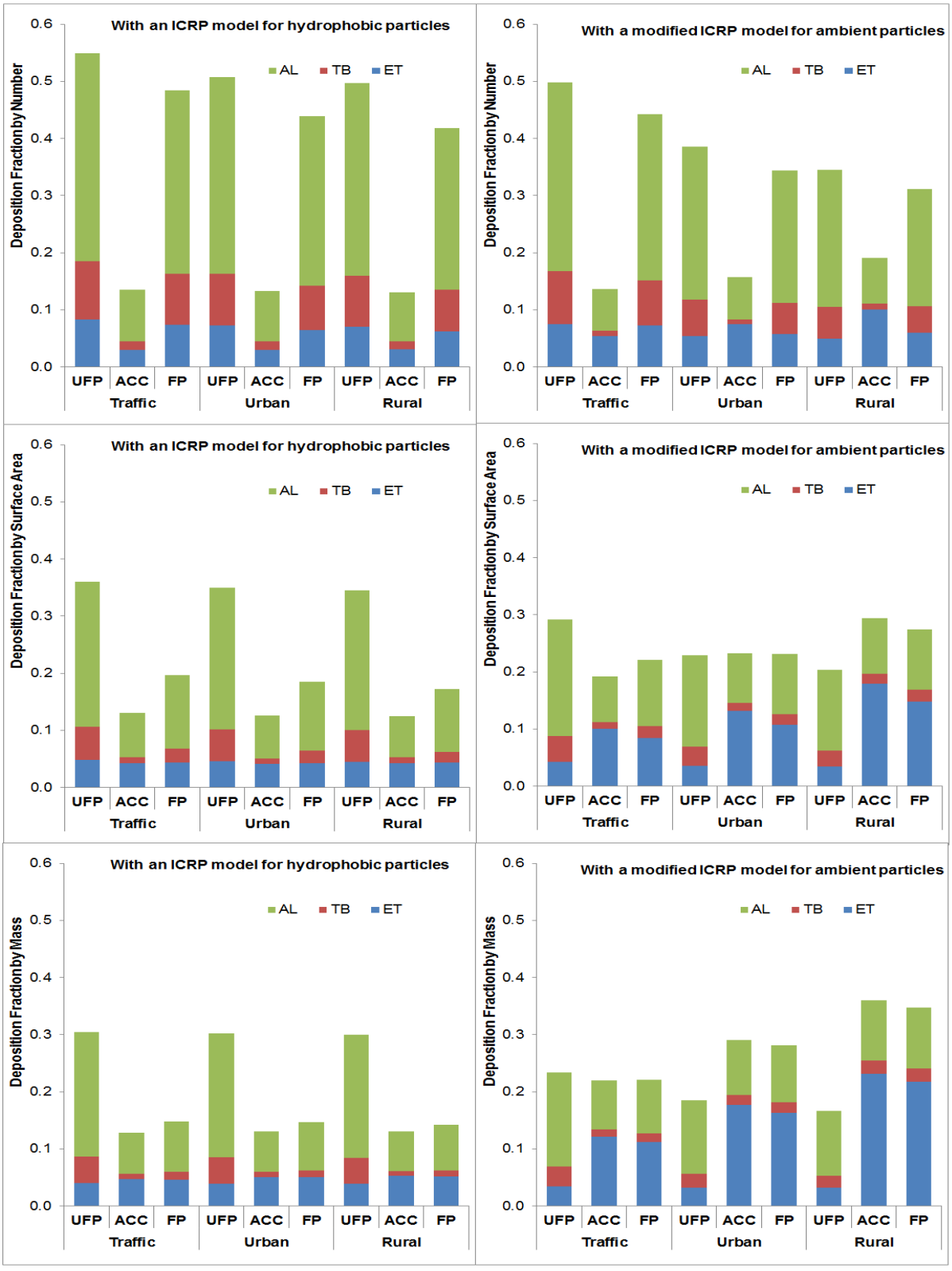

Figure 5.6: Regional fractions of particles from different ambient environments.

At all sites, ultrafine particles (16.4 nm< D_p <100 nm) were found to be deposited mainly in the alveolar region whereas the highest DFs of accumulation mode particles (100nm< D_p <604 nm) for both sites were found in the extra-thoracic region. For example, the DF of ultrafine particles at the traffic site for number, surface area and volume in the alveolar region was 0.33, 0.20 and 0.17, which was much higher than those in both extra-thoracic (0.08, 0.04 and 0.03) and trachea-bronchial regions (0.09, 0.05 and 0.03). Meanwhile, this value of accumulation mode particles was mostly found be highest in the extra-thoracic (0.05, 0.10 and 0.12 for number, surface area and mass, respectively), followed by the alveolar region (0.07, 0.08 and 0.09) and the trachea-bronchial region (0.01, 0.01 and 0.01).

Comparing the DFs of the roadside, urban background and rural sites, the average DFs of total particles by number in the roadside were higher than those in the urban background and rural areas. However, in terms of surface and volume, the highest DFs were found in the rural area.

The total DFs of submicron particles (16.5-604 nm) by number in this study is consistent with a previous experimental study by Morawska et al. (2005), who reported that the DF of 16-625 nm particles by number in the whole lung was 0.30 ± 0.09 for diesel smoke and 0.41 ± 0.08 for petrol smoke. Based on the ICRP model, Kurth et al. (2014) reported the DFs at non-mining areas ranged from 0.3 to 0.5, depending upon seasonal variation. However, our DF values are lower than those of the 12-580 nm particles (0.60, 0.29 and 0.23 for number, surface and mass) from the kerbside of a busy street in Copenhagen from an experiment conducted by Löndahl et al. (2009). In addition, Kristensson et al. (2013) found that the average number, surface and volume DF of 3.2-930 nm traffic particles was 0.59. 0.31 and 0.32, respectively.

The variable DFs from different studies could be explained by the different size range of particles and size distribution variation between studies. Moreover, DFs not only depend upon the measured particle size range, but also on experimental or model conditions such as subjects, activity levels which have been reported differently in previous studies. More studies are clearly needed on the depositions of particles in the human respiratory tract.

Uncertainty

In our above calculation in this chapter, we assumed the effective density of ambient particles is unity while the effective density of ambient particles typically ranged from 1.0 to 2.0 g cm^{-3} (Löndahl et al., 2014). The effective density has no significant effect on the DF of particles with mobility diameters (D_m) lower than 300 nm (Löndahl et al., 2014), but for a larger particle (D_m> 300 nm) the DF of such particles with higher effective densities will increase slightly due to the increase in their aerodynamic deposition.

However, this error is not significant for the calculations of DF of large ambient particles based on our modified ICRP curves, because when an ambient particle larger than 300 nm penetrates the human lung, its effective density tends to be close to unity due to its intake of water vapour. For example, if we assume the effective density of particles with a diameter of 300 nm from urban backgrounds is 2 g cm^{-3}, their averaged growth factor at 99.5 RH% is approximately 2.5 as calculated in Figure 5.2 and Table 1. Based on equation (1.10) (in Chapter 1), the effective densities of those particles in the lung will decrease to 1.05.

5.6. Conclusion

In summary, the typical hygroscopicity of particles varies widely between different environments, depending upon the local sources and air masses, and shows clear diurnal and seasonal trends, with higher values found in the daytime and summer. Hygroscopic particles

emitted from different sources were investigated. Freshly emitted traffic particles and biomass burning particles are hydrophobic or less-hygroscopic, whilst growth factors are found to increase during ageing. Finally, the hygroscopic properties of particles have marked effects, not only on total lung deposition but also on the regional lung deposition of particles, causing a variation in DFs between sampling environments. For ultrafine particles (D_p <100 nm), the DF of these in kerbside areas was 1.2-1.6 times higher than those in urban background and rural areas.

The ICRP model seems to predict well DF values for small ambient particles in the extra-thoracic and tracheo-bronchial regions, but not the alveolar region, where they are overestimated. However for larger particles (D_p >200 nm) the ICRP model underestimates the DF values, with the extra-thoracic region the most affected of the three. As a consequence, the DF values of ambient particles larger than 200 nm in the total lung were much higher than the hydrophobic particles due to their hygroscopic growth, while total lung DF was lower than predicted by the ICRP model for smaller particles in rural and urban background areas, but not in roadside areas.

Based on the modified ICRP model, the deposition fractions of particles in traffic, urban background and rural areas were calculated. The average number DFs of particles in the roadside site were higher than those in the urban background and rural areas, whereas in terms of surface and volume the highest DFs were in the rural area. The DF values not only depend upon the particle size, but also on its hygroscopic properties.

Chapter 6: SOURCE APPORTIONMENT OF THE LUNG DOSE OF AMBIENT SUBMICROMETRE PARTICULATE MATTER

This chapter aims to apportion the sources of submicron particles measured at an urban background area in London and identify which source is most responsible for particles deposited in the human lung. Particle number size distributions (PNSD) measured by a Scanning Mobility Particle Sizer (TSI, USA), covering the size range of 16.5-604 nm at the London North Kensington background sampling site during 2012 were used in a Positive Matrix Factorization (PMF) model to apportion to six dominant sources of particles. These included local traffic emissions (26.6% by number), aged traffic emissions (29.9%), urban accumulation mode (28.3%), nucleation (6.5 %), inorganic secondary aerosols (1.7%) and mixed secondary aerosols (6.9%). Based on the ICRP model, the total deposition fractions of submicron particles for the aforementioned sources in the human respiratory tract were 0.57, 0.41, 0.24, 0.62, 0.24 and 0.24, respectively. In terms of source apportionment of particles deposited in the lung, traffic emissions represent the main source of particles deposited by number in both the regional and total lung, accounting for 59 to 71% of total deposited particles, followed by regional accumulation mode (17%) and nucleation (10%) particles. Secondary aerosols only account for 5.1 % of the total deposited particles by number, but they represent the main source of particles deposited in the lung expressed as surface area (44.6%) and volume (72.3%) of total deposition.

This chapter contains some sections of verbatim text adapted from Vu et al. (2016) published as part of this PhD. The author's contribution: writing, contribution of ideas and numerical calculations.

6.1. Introduction

Particles in urban ambient air are released from various anthropogenic activities, such as the combustion of fuels and from natural sources such as atmospheric nucleation (Ogulei et al., 2007). Exposure to ambient aerosols is consistently associated in numerous scientific studies with adverse health effects (Pope and Dockery, 2006). Very small particles such as ultrafine particles (D_p <100 nm) are able to penetrate deep into the respiratory tract (e.g. reaching the pulmonary epithelium), causing serious health problems such as respiratory morbidity and mortality (Donaldson et al., 1998). Moreover, different types of sources generate particles with different size distributions, chemical compositions and concentration characteristics (Lighty et al., 2000). This results in particles from different sources behaving differently during the process of inhalation, showing different penetration through the respiratory tract and depositing with different fractions in different regions of the lungs. For example, Löndahl et al. (2009) estimated the total lung deposition fraction of particles by number emitted from traffic exhaust was 0.68, which was three times higher than those of particles released from biomass burning (0.22). Therefore a detailed identification of the most relevant sources of atmospheric particles and the association between a particle source and lung deposition could play a vital role not only for risk assessment of air pollution in epidemiological studies, but also for policymakers to introduce optimal legislation for air quality control.

In order to identify and apportion the most relevant sources of ambient particles, applying Positive Matrix Factorization (PMF) to particle number size distributions (PNSD) has become a widely used tool in recent years (Viana et al., 2008). PMF considers each size bin in the PNSD dataset as an input variable. Additional variables such as ion species, heavy metals, gaseous pollutants, meteorological parameters and traffic data can be very valuable to separate and identify the sources of particles as demonstrated in previous studies (Harrison et al., 2011; Ogulei et al., 2006b; Thimmaiah et al., 2009).

The advantage of this method is that it can identify specific sources of very small particles, such as nucleation. It can also separate sources of particles such as brake- and tyre-wear, which are generally difficult to separate using PMF on particle composition data only. In addition to source identification and apportionment of concentrations measured in ambient air, and considering the different deposition fractions of particles generated from different sources, there is still the need for evaluation of which sources are most responsible for particles deposited in the human respiratory tract.

This study aims to estimate the lung deposition of particles generated from specific sources contributing to particle size distribution in North Kensington, an urban background area of London, United Kingdom. In order to do so, we first apportioned the sources of submicron particles in the area using PMF. Subsequently, we estimated the lung deposition fraction of particles generated from each specific source by applying the ICRP model on the PMF factor profiles. Finally, we investigated which source may be most relevant to health outcomes by comparing the results of the source apportionment of particle deposited in the human respiratory tract.

6.2. Materials and Methods

6.2.1. Site Description and Data Measurement

Particle number size distributions and concentrations of other air pollutants were measured in North Kensington, London, UK. This monitoring station, which is located in the grounds of Sion Manning School, is representative of the typical urban background area of London. The site location and pollution climate have been described by Bigi and Harrison (2010).

Particle number size distributions (PNSDs) were measured during 2012 by a Scanning Mobility Particle Sizer (SMPS) operated by the Department for Environment, Food and Rural Affairs (DEFRA) as part of the UK national network. This SMPS system comprised an

Electrostatic Classifier (EC, TSI model 3080) and a Condensation Particle Counter (CPC, TSI model 3775) and was set up at a 15 minute time resolution with six scans of 2.5 minutes covering the size range 16.6-604 nm.

Air pollutants (CO, NO, NO_2 , SO_2, BC, O_3, $PM_{2.5}$ and PM_{10}), aerosol chemical composition data (Na^+, Mg^{2+}, NH_4^+, Ca^{2+}, Cl^-, PO_4^{2-} and SO_4^{2-}) and meteorological data (wind speed and direction) were extracted from the DEFRA website (see http://uk-air.defra.gov.uk/ for more detailed information).

6.2.2. Data Handling, PMF and ICRP Models

6.2.2.1. Data handling

Data statistical analysis, polar plots and concentration weighted trajectories were performed in the R program (Version 3.1.5) using the "Open-air" package developed by Carslaw and Ropkins (2012). Missing data was linearly interpolated between the values from the nearest size bins. Air pollutant concentrations, SMPS data and meteorological data were averaged on an hourly basis.

6.2.2.2. PMF models

In this study, a profile of 6,098 hourly PNSDs comprising 51 size bins ranging from 16.6 to 604 nm were input into the PMF US EPA model version 3. Each size bin in the PNSD was considered as an input variable. Since uncertainties were not provided by the experimental instruments, these were estimated based on an empirical method introduced by Ogulei et al. (2006; 2007).

The method for determining the correct number of factors in the PMF analysis has been described by Lee et al. (1999) and Yakovleva et al. (1999). PMF factors were interpreted based on (1) modal structure of number and volume size distributions, (2) the diurnal patterns

of factor contribution, (3) the contribution of each factor to total number and volume, (4) the relationship with auxiliary information such as gaseous and chemical composition data and (5) source directionality by local wind trajectories and polar plots (Ogulei et al., 2007).

6.2.2.3. ICRP model

The ICRP model was developed to predict the deposition of particles with a wide size range from 1nm to 100 μm in the respiratory system consisting of three main regions: extra-thoracic (ET), trachea-bronchial (TB) and pulmonary/alveolar (AL) (ICRP, 1994). In our calculations, we applied the ICRP model with Hind's parameterization of the grand average particle deposition to estimate the total and regional deposition fraction (DF) due to inhalation by males and females at three exercise levels (Hinds, 1999).

The DFs calculated by the ICRP are for spherical hydrophobic particles. However, hygroscopic particles are typically dominant in the ambient environment (Asgharian, 2004; Löndahl et al., 2009; Montoya et al., 2004). To address this problem, we adjusted the ICRP curve for both hydrophobic and hygroscopic particles based on an assumption that particles generated from combustion sources (i.e. traffic emission or biomass burning) are nearly hydrophobic and inorganic/organic secondary aerosols are a mixture of less hygroscopic and more hygroscopic particles (Cruz and Pandis, 2000; Löndahl et al., 2009; Massling et al., 2005; Tritscher et al., 2011; Väkevä et al., 2002b; Varutbangkul et al., 2006; Weingartner et al., 1997). The details of this method are given in Chapter 5 or Vu et al. (2015a). The regional and total lung deposition fractions of particles from different sources identified by PMF were estimated based on an application of the ICRP model to each source's particle size distribution as adjusted by its expected hygroscopicity.

6.3. Results

6.3.1. Overview of Data

The average total number concentration was 5.6 ± 3.3 x 10^3 particles/cm^3, of which 1.2 ± 0.9 x 10^3, 3.3 ± 2.1 x 10^3 and 1.0 ± 0.9 x 10^3 particles/cm^3 was accounted for by the nucleation mode, Aitken mode, and accumulation mode, respectively. The majority of particles by number were in the ultrafine region (Dp ≤ 100 nm), which represented 81.4 % of total number concentration, whereas accumulation mode particle only accounted for 18.6 % of the total particle number, but represented 90.5% of the total particle volume.

As shown in Figure 6.1a, the particle number size distribution shows a peak number mode at 36.6 nm and a peak volume mode at 294.3 nm. The diurnal pattern (Figure 6.1b) shows two distinct peaks coinciding with the traffic rush hours, and the lowest concentration was found during the early morning.

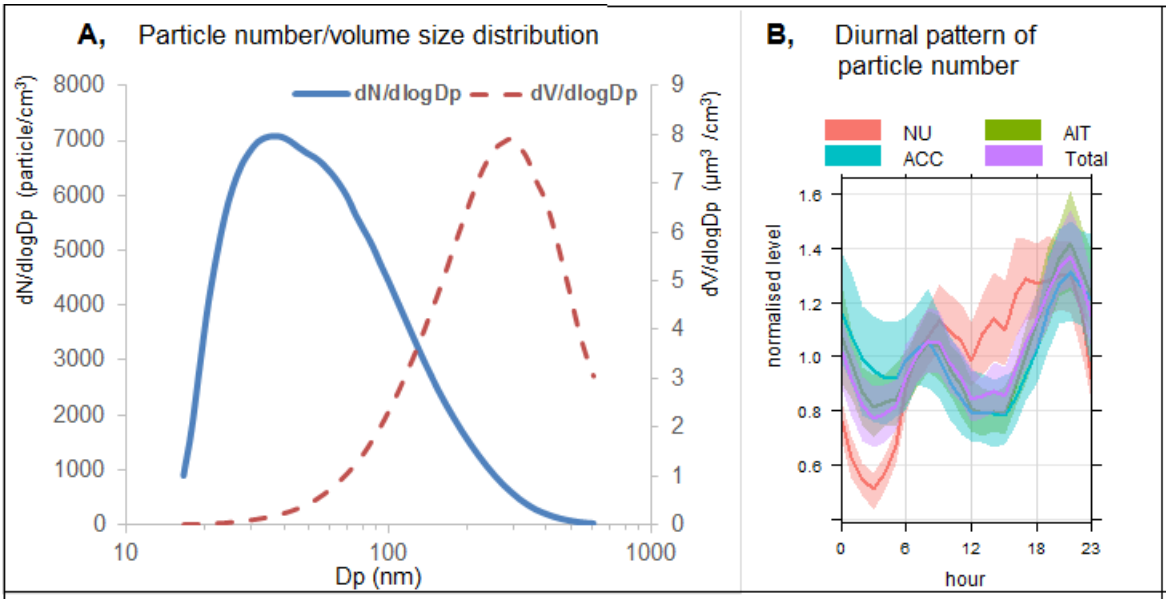

Figure 6.1: Particle number/volume size distribution (A) and diurnal pattern of particles (B) by number in North Kensington, UK during 2012. *Nu: Nucleation mode particles; AIK: Aitken mode particles, ACC: accumulation mode particles, and Total: total particles.*

6.3.2. PMF Results

The PMF method (US EPA PMF version 3.0.), which is described by Ogulei et al. (2006b), was used to apply to particle number size distributions. In this study, α =0.01 and C3 =0.105 were selected to estimate uncertainties. The method of determining the correct number of factors has been described by Lee et al. (1999) and Yakovleva et al. (1999). As shown in Figure 6.2, the number of factors can be from 4 to 10. The value of Q becomes stable when we increase this number.

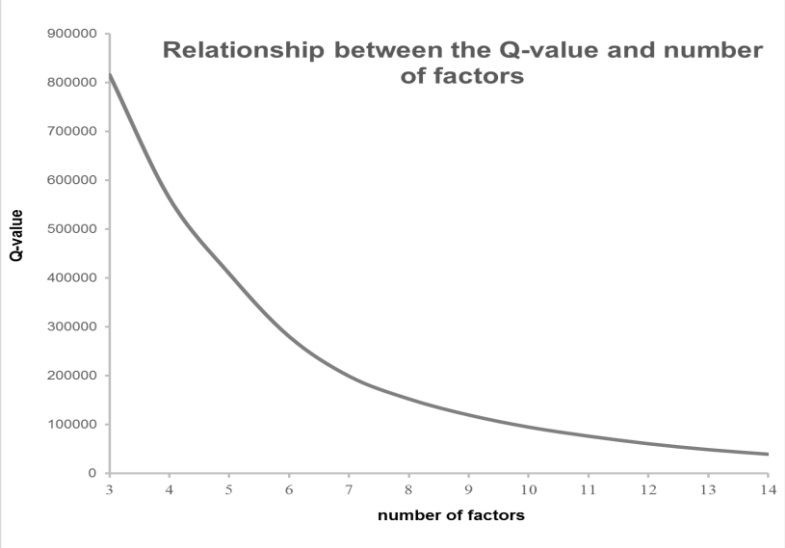

Figure 6.2: Q-value with different number of factors.

The profile of six resolved factors obtained by PMF is shown in Table 6.1 and Figure 6.3. The first factor has a peak by number at a diameter of approximately 29 nm (Figure 6.3). This factor represents 26.6% of the number concentration (Table 6.1), but makes only a small contribution to the volume concentration (3%). The modality of this factor (Figure 6.3) is similar to the shape of the nucleation mode of the particle number size distribution from road traffic emissions (Vogt et al., 2003; Zhang et al., 2004).

These particles could be emitted directly from gasoline cars or from the growth of nucleation particles released from diesel cars (Ristovski et al., 2006; Wehner et al., 2009). This factor has a weak correlation with NO_2 (r^2 =0.43), as shown in Table 6.2. In addition, the strong diurnal pattern shows two dominant peaks corresponding to morning and evening rush hours, suggesting that this factor represents the exhaust nucleation particle mode (Harrison et al., 2011). The polar plot shows no dominant direction, and therefore this factor can be attributed to local traffic emissions.

Table 6.1: Statistics of the particle number and volume concentrations for six factors.

	%N	%V	N-peak	V-peak	%N-NU	%N-AIT	%N-ACC	% V-NU	% V-AIT	% V-ACC
F1	26.6	3.2	29 nm	48 nm; 191 nm	47.1	50.6	2.4	3.9	25.6	70.5
F2	29.9	8.6	52 nm	80 nm; 294 nm	8.0	88.9	3.1	0.3	39.0	60.7
F3	6.5	1.0	20 nm	237 nm	87.2	9.3	3.5	3.8	6.9	89.3
F4	1.7	23.4	86 nm; 216 nm	392 nm	2.2	42.8	55.0	0.0	0.9	99.0
F5	6.9	34.0	27 nm; 205 nm	274 nm	12.6	14.6	72.8	0.0	0.5	99.4
F6	28.3	29.7	93 nm	165 nm	1.4	60.0	38.6	0.0	15.6	84.4

Note, % N: percentage of particles by number; % V: percentage of particles by volume; N-peak: peak number mode; V-peak: peak volume mode; NU: nucleation mode (D_p <30 nm); AIT: Aitken mode (30 nm< Dp <100 nm); ACC: accumulation mode (100 nm< D_p<600 nm).

Table 6.2: Correlations between contributions of six factors with other chemical species.

	Factor 1	**Factor 2**	**Factor 3**	**Factor 4**	**Factor 5**	**Factor 6**
Wind speed	-.146**	-.381**	.069**	-.400**	-.388**	-.419**
CO	.252**	.531**	-.124**	.519**	.556**	.688**
O_3	-.251**	-.436**	.124**	-.392**	-.215**	-.355**
SO_2	.155**	.316**	.102**	.251**	.249**	.330**
NO	.224**	.505**	-.104**	.501**	.476**	.684**
NO_2	.428**	.643**	-.129**	.494**	.496**	.693**
NO_x	.320**	.603**	-.123**	.545**	.528**	.751**
BC	.290**	.638**	-.056**	.563**	.581**	.819**
OC	.035**	.363**	.110**	.488**	.628**	.770**
$PM_{2.5}$	-.005	.384**	-.142**	.861**	.788**	.664**
PM_{10}	.087**	.418**	-.190**	.853**	.747**	.677**
Ca^{2+}	.175**	.114**	-.053**	.250**	.175**	.211**
Cl^-	-.021	-.037*	-.198**	.024	-.015	.037*
PO_4^{3-}	-.009	.183**	-.100**	.386**	.347**	.410**
Mg^{2+}	-.011	-.026	-.181**	-.025	-.065**	.033
Na^+	.126**	-.046**	-.277**	.004	-.105**	.015
NH_4^+	-.044*	.244**	-.234**	.801**	.631**	.466**
SO_4^{2-}	-.111**	.146**	-.014	.619**	.508**	.272**
NO_3^-	.011**	.131**	.100**	.757**	.549**	.280**

*Note: ** Correlation is significant at the p value <0.01; * Correlation is significant at the p value < 0.0.*

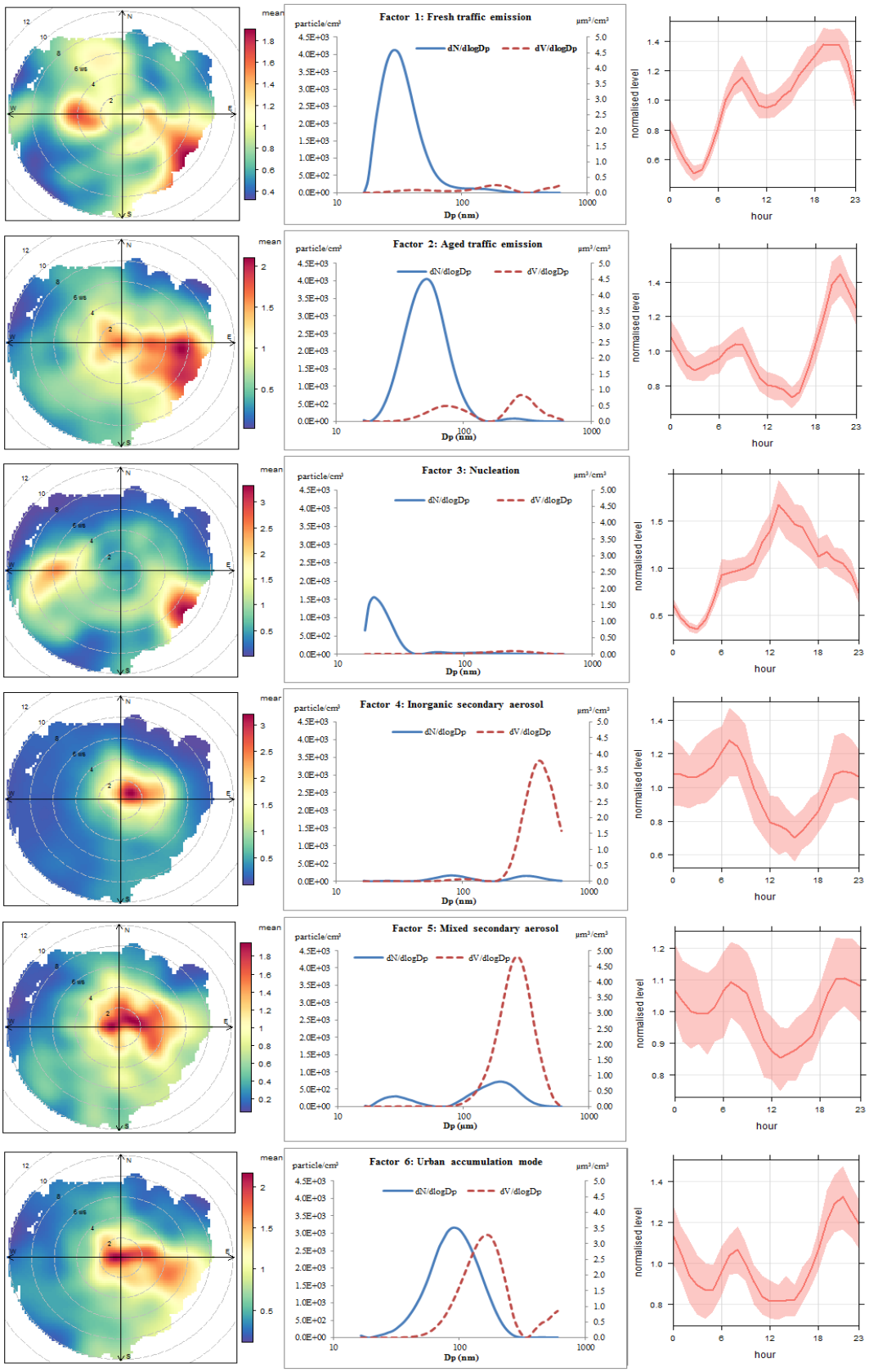

Figure 6.3: Polar plot, particle size distribution and diurnal patterns of six resolved PMF factors.

The second factor shows the main particle number distribution in the size range between 20 nm and 100 nm, with the peak diameter around 52 nm, corresponding to solid carbonaceous particles from diesel exhaust (Shi et al., 2000). This factor contributes 29.9% of the total number concentration and only 8.6% of total volume concentration. The diurnal variation shows obvious morning and evening peaks. In addition, this factor contribution has strong correlations with other air pollutants (CO, NO, NO_2 and BC) and a moderate correlation with PM_{10} (see Table 6.2). Hence, this factor mainly comprises traffic emission sources, but unlike factor 1, the polar plot shows that this source dominantly comes from easterly and south-easterly directions. Therefore, it could be aged traffic emissions (Zhou et al., 2004), transported from central London. There was an increase in the factor contribution in the winter and on weekend days, and therefore this factor may also contain domestic combustion sources, such as biomass burning or cooking.

The particle number size distribution of factor 3 is dominated by nucleation size range particles, with 87% of the total number concentration being within this range (see footnote to Table 6.1 for definitions of size ranges). This factor possesses small particle number concentrations (6.5%) and small volume concentration (1%). The diurnal pattern shows a major peak around noon, which is attributed to regional photochemical nucleation events. The seasonal variation shows that this factor is mostly found from June to September, and the polar plot shows marked directionality from the western sector as shown in Figure 6.3. This could suggest that factor 3 is aged nucleation particles with an origin in the westerly sector. This is supported by a study on new particle formation at a rural site in southeast England which found that nucleation events occur predominantly with westerly maritime air masses, high wind speed, and low $PM_{2.5}$ and NO_x concentrations (Charron et al., 2007; Charron et al.,

2008). There is a smaller contribution of factor 3 from the south-easterly sector, which is less easily explained.

The fourth factor accounts for only around 2% of total particle number, but accounts for nearly 25% of total particle volume. The size distribution of this factor shows a bimodal distribution with two peaks at 86 nm and 216 nm, and more than 95% of total particle number in the Aitken and accumulation ranges, while 99% of total particle volume is within the accumulation mode. Factor 4 is strongly correlated with $PM_{2.5}$ (r^2 =0.86), PM_{10} (r^2 =0.85), NH_4^+ (r^2 =0.80), NO_3^- (r^2 =0.76) and SO_4^{2-} (r^2 =0.62), and has an inverse correlation with ozone. The obvious directionality shows that this factor originates from the east and northeast sectors, and the diurnal variation shows a significant decrease in the afternoon. This behaviour suggests that this factor represents regional inorganic secondary aerosols. This is consistent with results from cluster analysis conducted by Beddows et al. (2009), who associated regional air pollutant transport with clusters of concentrations showing a correlation with PM_{10}, an inverse correlation with ozone and a decreasing concentration in the afternoon.

Factor 5 shows a main accumulation mode at 205 nm and a smaller peak at 27 nm. This factor has a similar diurnal pattern to factor 4. The main directionality is from the northeastly, southeastly and easterly sectors. This factor also has high and moderate correlations with other air pollutants ($PM_{2.5}$ (r^2 =0.79), PM_{10} (r^2 =0.75), NH_4^+ (r^2 =0.63), NO_3^- (r^2 =0.55) and SO_4^{2-} (r^2 =0.51), although weaker correlations than those of factor 4. In addition, this factor shows a moderate correlation with total organic carbon (r^2 =0.63). Therefore, it also suggests an association with secondary aerosol, but to a mixture of inorganic and organic aerosols.

The "Concentration Weighted Trajectory Approach analysis" was performed using the "Open-air" package as shown in Figure 6.4 and 6.5. This approach is useful for viewing the long-range transport of secondary aerosols because the accumulation mode particles (from secondary aerosols) have a long lifetime in the atmosphere. Figure 6.4 shows the major directionality of factor 4 and factor 5 with $PM_{2.5}$, PM_{10}, NH_4 and SO_4, suggesting that secondary aerosol could originated from mainland Europe due to long-range transport. This is consistent with a study of receptor modelling of secondary particulate matter at UK sites (Charron et al., 2013).

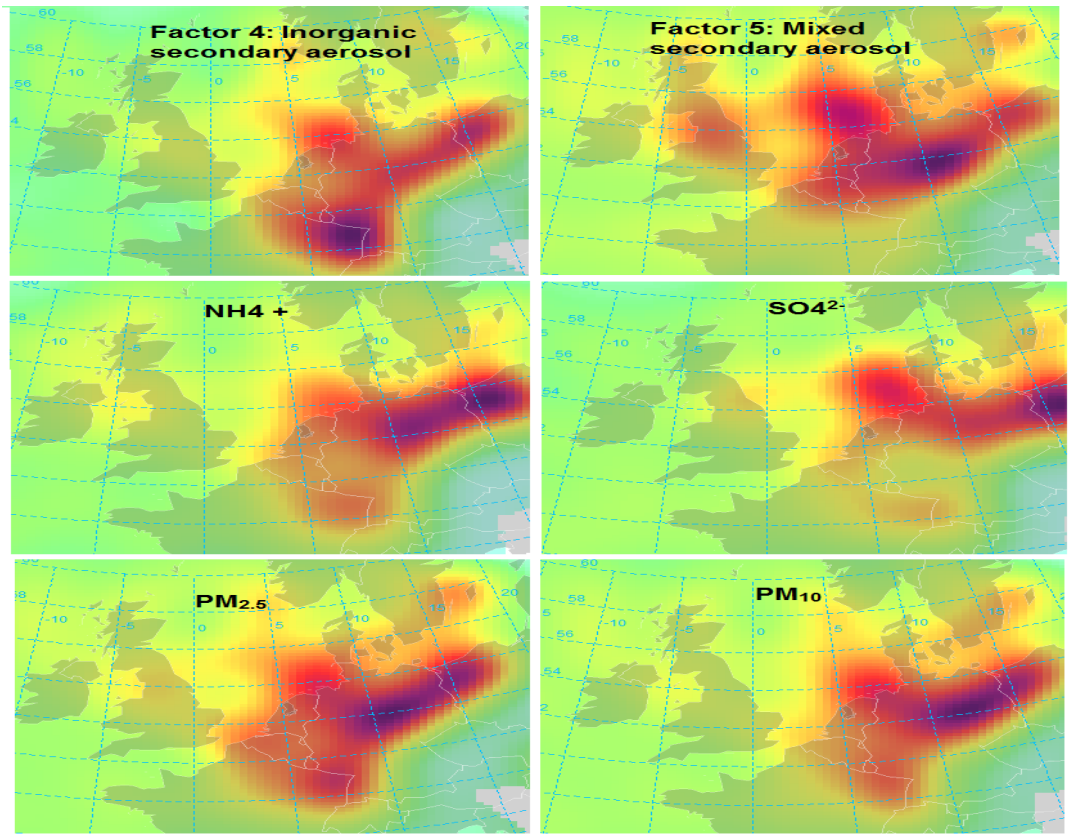

Figure 6.4: Gridded and smoothed back trajectory concentrations showing mean factor 4, factor 5, NH_4^+, SO_4^{2-}, $PM_{2.5}$ and PM_{10} concentrations using the Concentration Weighted Trajectory approach.

The last factor (Factor 6) shows uni-modal number/volume size distribution with a peak around 93 nm by number and 165 nm by volume. This particle size distribution was attributed to combustion sources which mainly contain carbonaceous particles (Hildemann et al., 1991; Venkataraman et al., 1994). In addition, this factor accounts for 28.3% of the total number concentration and 29.7% of the total volume concentration. The diurnal pattern shows a peak in the morning rush hours and a peak later in the evening rush hours. This factor correlates with the second factor which has been identified as traffic emissions (r^2 =0.6). Moreover, this factor has strong correlations with NO, NO_2, NO_x, and CO (Table 6.2), suggesting that it could also represent the solid particle mode from traffic emissions (Dall'Osto et al., 2012; Harrison et al., 2011). However, an increase in the contribution of this factor on weekend days and in the cold season, and its strong correlations with both black and organic carbon, shows that this factor could also be emitted by other combustion sources such as power stations or biomass burning, which also show a peak around 100 nm (Janhäll et al., 2010; Wang et al., 2013).

The polar plot shows the main directionality of this factor to be in the east and southeast sectors. Hence, this factor could be the regional background accumulation mode. By using cluster analysis, Beddows et al. (2009) also found a large accumulation mode at 100 nm at the British Telecom Tower, which is also classified as being in an urban background area of London. A recent study by Beddows et al. (2015) found that there were four sources of particle number, namely traffic emissions, urban background, nucleation and secondary aerosols, based on application of PMF to a two-year data set of particle number size distribution in North Kensington.

In this study, we selected six factors because we found that the urban background factor consisted mainly of aged traffic emissions and wood burning emissions and the secondary aerosols contained inorganic secondary aerosols and mixed secondary aerosols, therefore

these two factors (urban background and secondary) could split into four. This separation increased the best fit between modelled and measured data by reducing the total residual; however, we noted that this separation was not totally clean since the traffic emissions and other combustion such as wood burning could share a common size distribution profile.

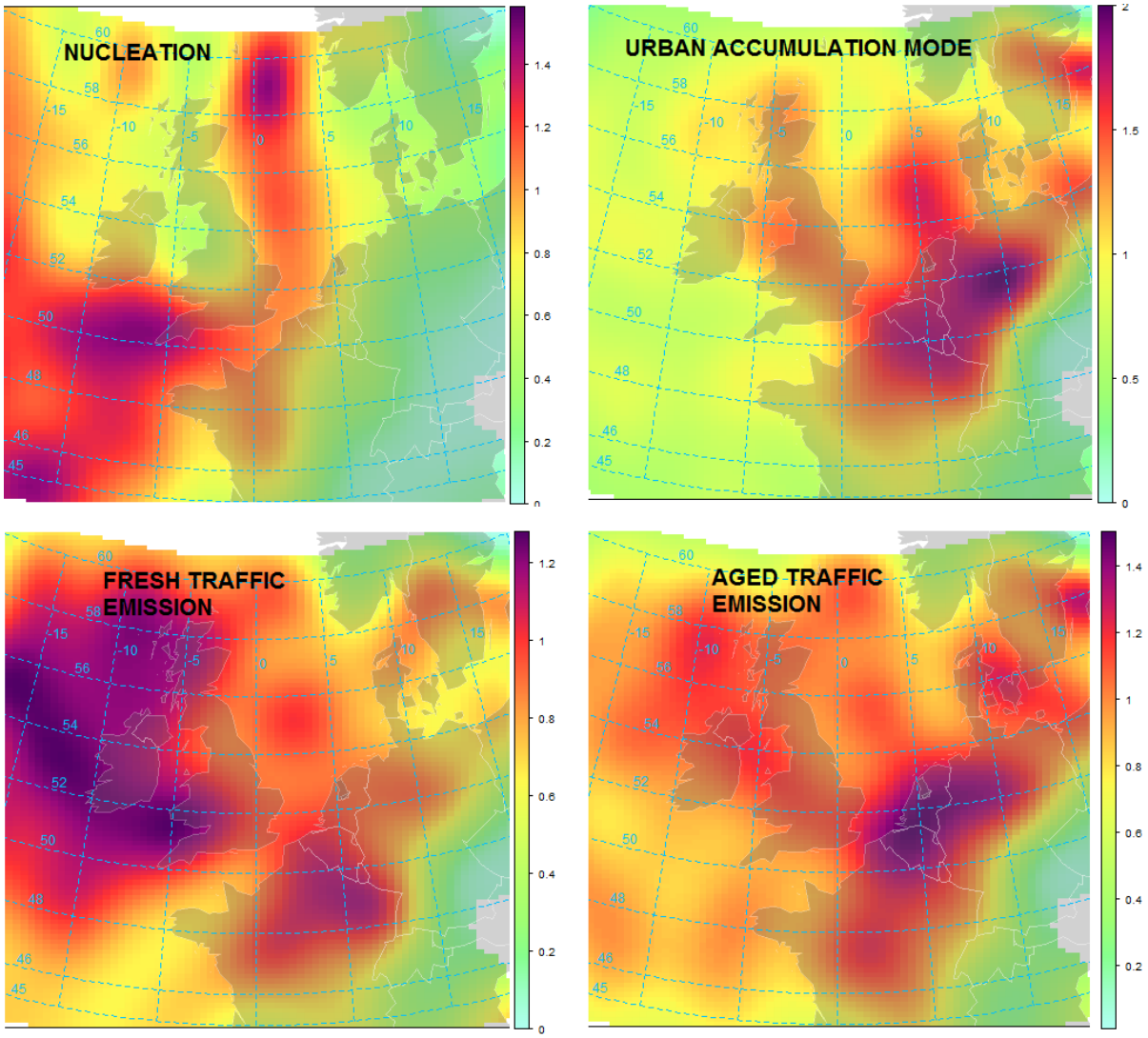

Figure 6.5: Gridded and smoothed back trajectory concentrations showing mean 4 factor contributions using the CWT approach.

To conclude, the dominant source contribution of particles by number in the London urban background area was attributed to traffic emissions (56.6 %). This was followed by the urban accumulation mode (28.3%), which could mainly originate from combustion sources such as

wood burning. The highest contribution of traffic emissions to total particle number in urban areas was also found in the previous studies by Ogulei et al. (2007), Pey et al. (2009), Gu et al. (2011) and Wang et al. (2013). Gu et al. (2011) reported that traffic and combustion emissions represented 65.2 and 26.1% of total particles number in Augsburg, Germany. Particles from combustion- related sources (aged traffic and urban accumulation mode) have strong correlations with black and organic carbon, suggesting that these sources mainly comprise carbonaceous particles. Secondary aerosols accounted for a small fraction of the particles number (8.6%), but they were the main contribution source of submicron particles by volume (57.4%). These particles were considered to contain mainly ammonium nitrate and sulfate, and organic aerosols. The urban accumulation mode accounted for 29.7% of particles by volume, while those of traffic emissions and nucleation were 11.8 and 1.0%, respectively. In terms of particle surface area, the urban accumulation mode was the most domination fraction (39.2 %), following by mixed secondary aerosol (26.9%), aged traffic emission (14.2%), inorganic secondary aerosol (13.2%), fresh traffic emission (6%) and nucleation (1.3%).

Differences between the PMF results of this study and the PMF results from Beddows et al. (2015)

Beddows et al. (2015) applied PMF model to two-year PNSD data sets collected at North Kensington and found that there were four main sources of particles: traffic emissions (44.8% by number), urban background (43.0%), nucleation (7.8%) and secondary aerosols (4.4 %). The differences between the PMF results of this study and from Beddows et al. (2015) are due to the following reasons:

- In this study, the PMF analysis used a one-year particle number size distribution while Beddows et al. (2015) ran PMF on a combined 2011 and 2012 data sets. The PNSD from

2012 looks very interesting and different to the previous year because an increase in particle number was found on the weekend days.

- If the number of factors selected is 4, the result seems to be similar to Beddows' findings (as shown in Figure 6.6), with the same profile for each factor.

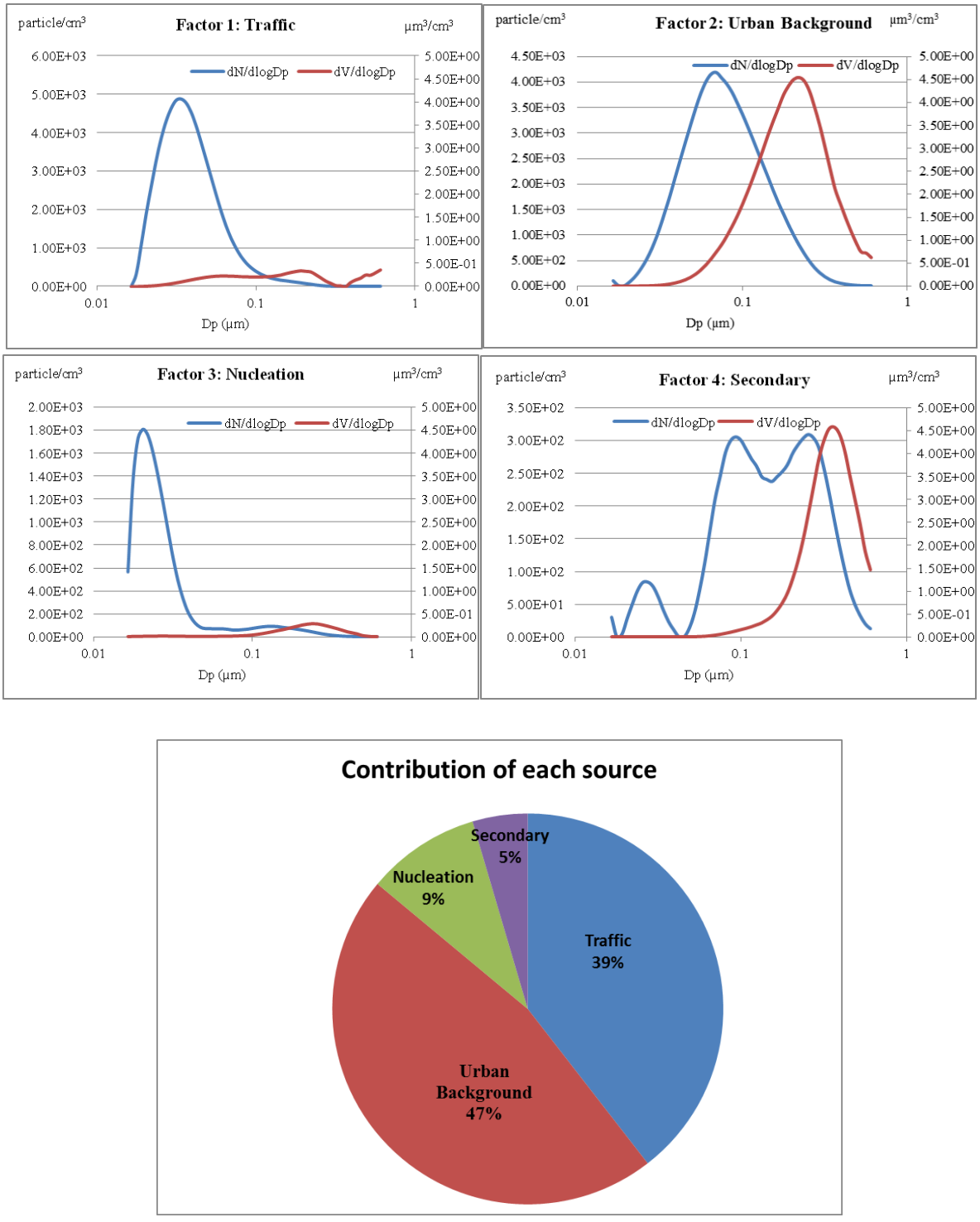

Figure 6.6: Profiles and contribution of each factor from PMF with four factor solution.

Using the four factor solution, the traffic emission factor only includes sizes in the range of 30-40 nm; however, several studies have found that the traffic emissions also shows a distribution in the accumulation mode (around 70-100 nm). Therefore, the urban background may mostly reflect soot traffic emissions. The increase in the urban background factor on weekend days may be explained by wood burning or cooking. It is preferable to separate the traffic emissions and the wood burning, since traffic emissions typically show a number size distribution of around 70-100 nm, and wood burning above 100 nm (Janhäll et al., 2010; Reid et al., 2005; Reid and Hobbs, 1998).

By increasing the number of factors to six, the nucleation and traffic emission factors keep their profiles, but the secondary aerosol factor splits into two factors, inorganic secondary aerosols and mixed (organic and inorganic) secondary aerosols, and the urban background factor also splits into two factors (aged traffic and urban accumulation mode) (as shown in Figure 6.7).

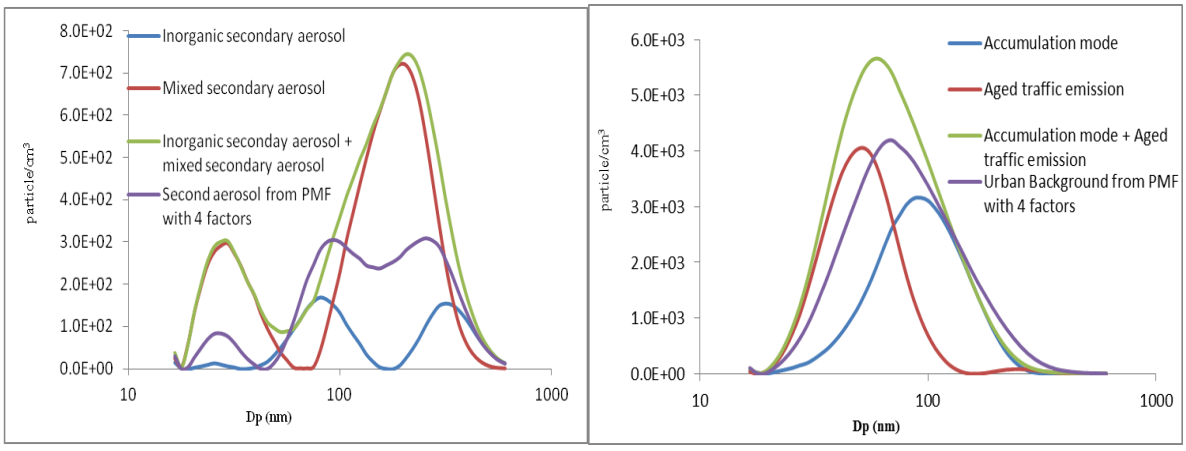

Figure 6.7: Comparison of the secondary and urban background aerosols between the PMF solutions of four and six factors.

From the seasonal polar plots for factor 4 (mixed inorganic and organic secondary aerosol) and factor 6, a strong effect of local sources (probably wood burning) in the winter is seen (see Figure 6.8).

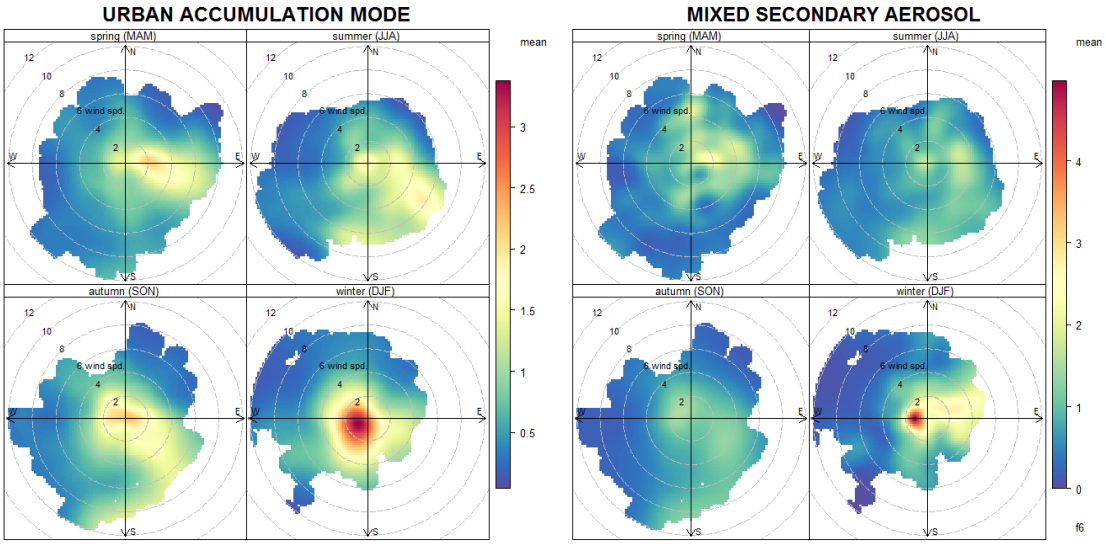

Figure 6.8: Seasonal polar plot of urban accumulation mode and mixed secondary aerosols.

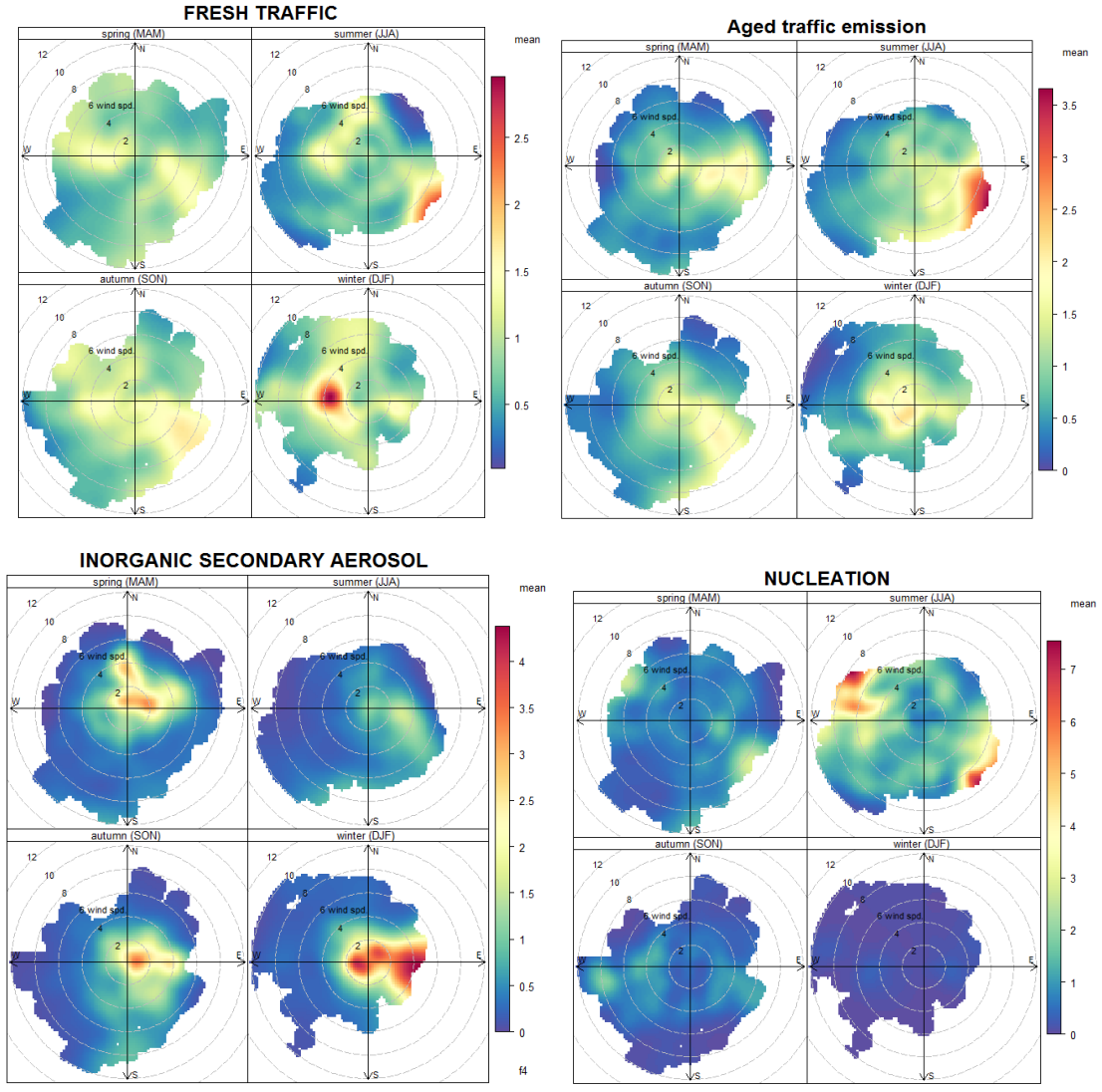

Figure 6.9: Seasonal polar plot of local traffic, aged emission, inorganic secondary aerosols, and nucleation.

In addition, the accumulation mode had a very high correlation with the wood smoke indicator (CWOD) (r^2 =0.84) during the winter period (Figure 6.10). The mixed secondary aerosol factor has a stronger correlation (r^2 =0.63) with OC than the inorganic aerosol factor (r^2 =0.49), but weaker one (r^2 =0.63) with NH_4 than the inorganic aerosol factor (r^2 =0.81). This suggests that wood burning could release accumulation mode particles from organic secondary aerosols.

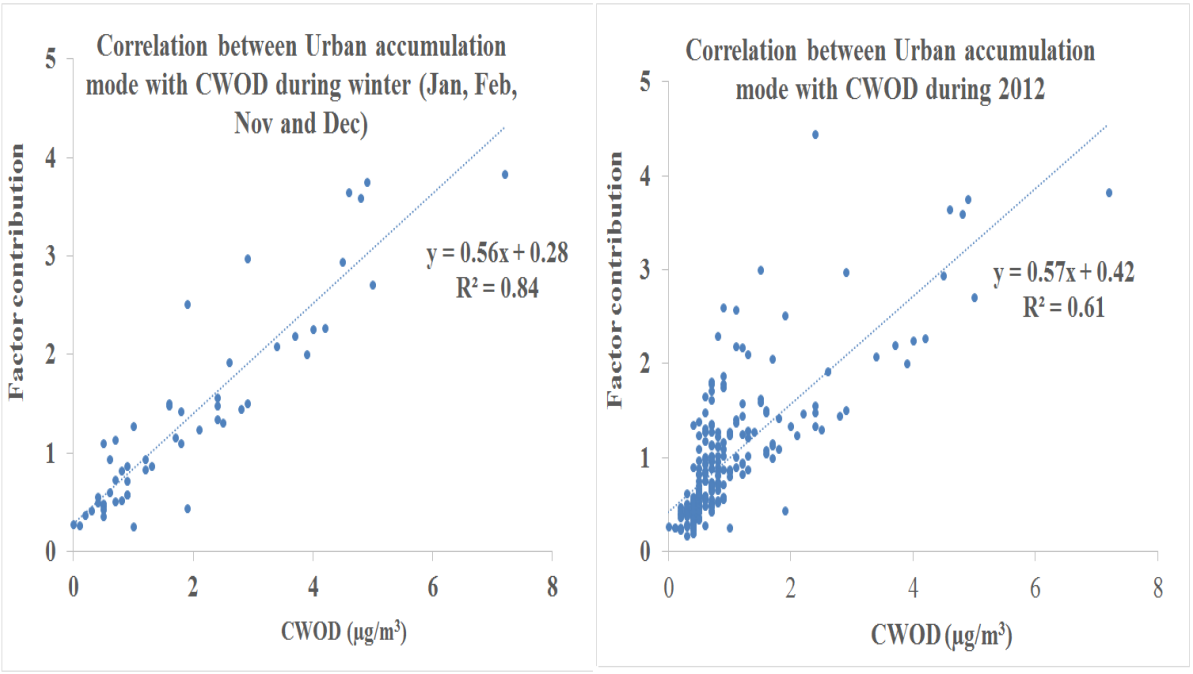

Figure 6.10: Correlation between the urban accumulation mode factors and CWOD.

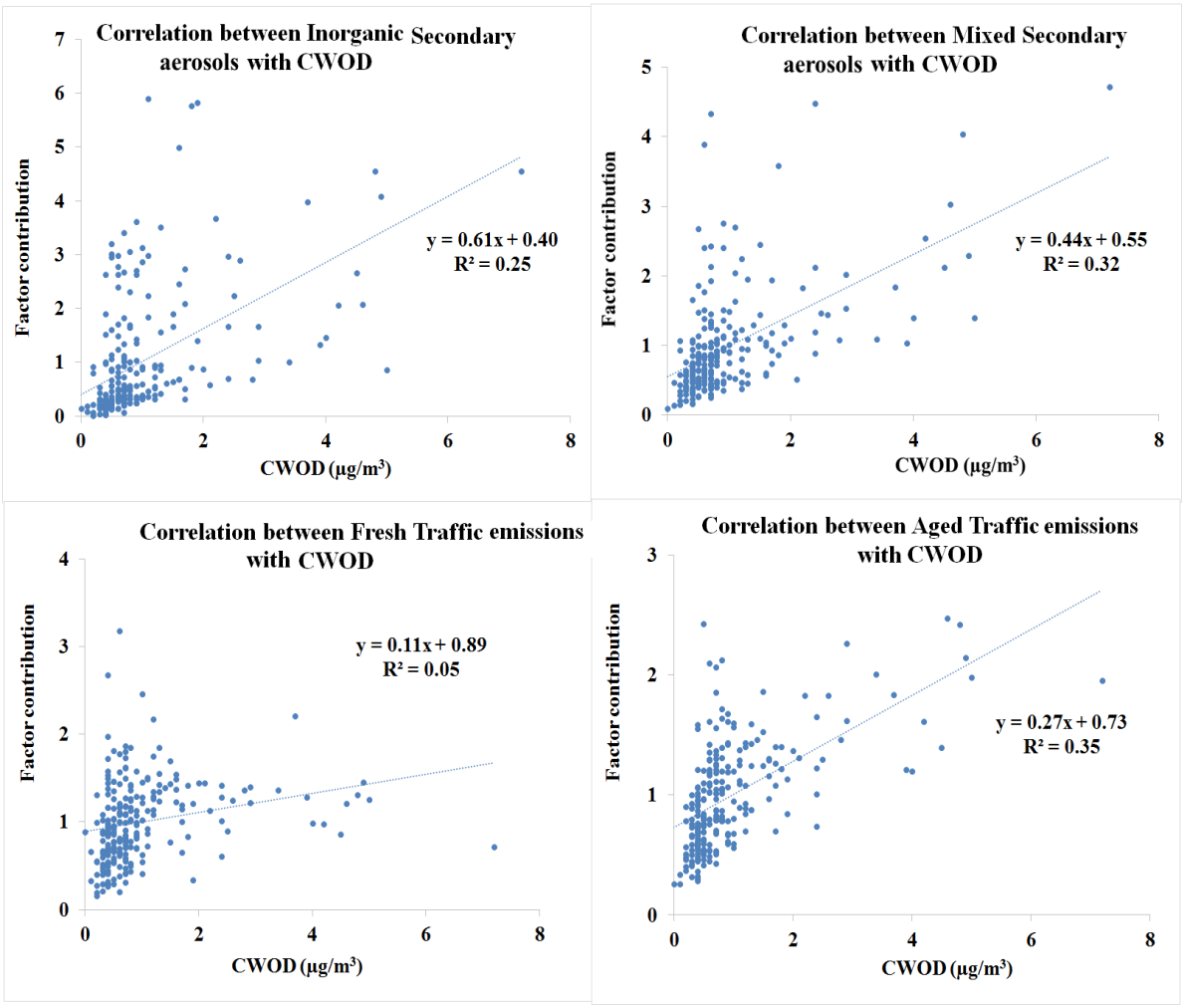

Figure 6.11: Correlation between other factors and CWOD.

In conclusion, the PMF results with six factors can explain more about the secondary aerosol and urban background sources and the contribution of wood burning to those sources. Moreover, the residual between modelled and measured concentrations decreases by increasing the number of factors from four to size. However, there is a disadvantage with this solution:

- The urban accumulation mode (mostly due to wood burning) and traffic emissions is not totally cleanly split (as seen in Figure 6.12), due to the similar size distribution profiles of these two sources. Wardoyo et al. (2006) note that wood burning could have a CMD of 30-70 nm during fast burning of wood in laboratory-scale experiments. Therefore, the urban accumulation background can contain traffic particles, and on the other hand the aged traffic

emissions also can contain particles emitted from wood burning or cooking emissions. The highest correlations of these factors are shown in Figure 6.12:

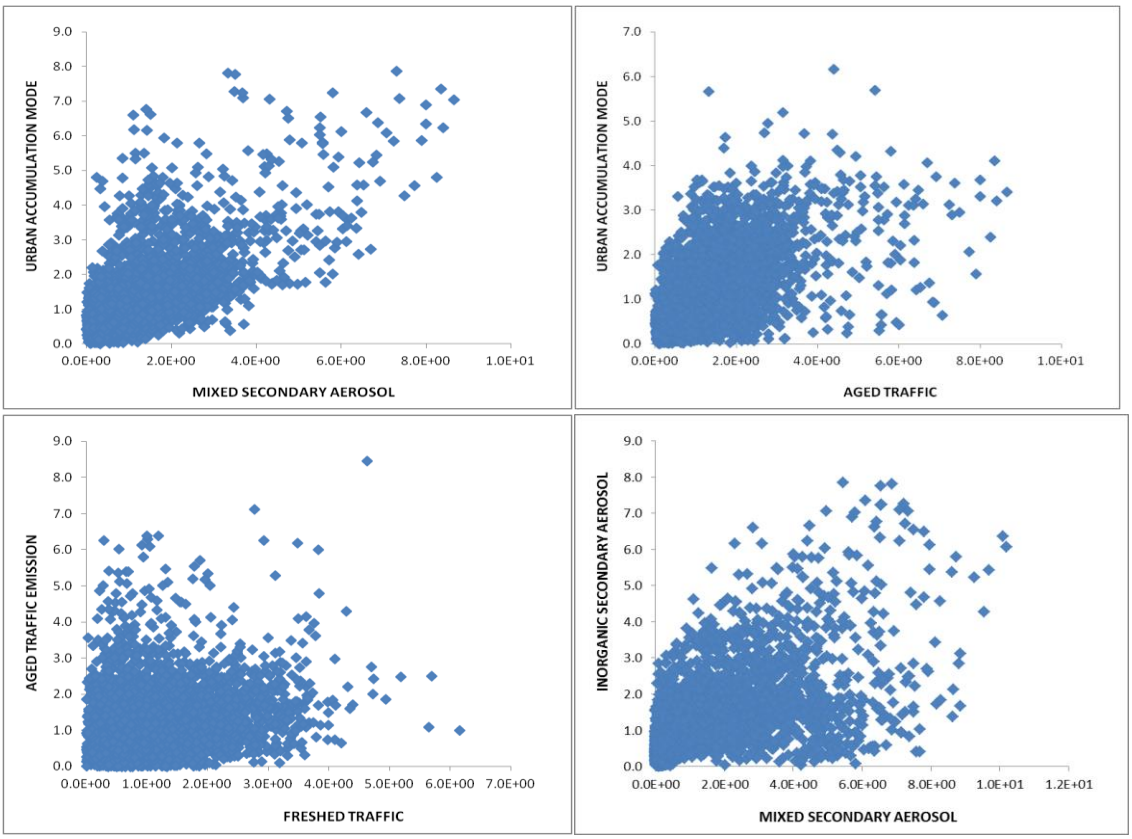

Figure 6.12: Correlation between each factor.

6.3.3. Which Source is Most Responsible for Particles Deposited in the Human Respiratory Tract?

6.3.3.1. Total and regional lung deposition fractions (DFs)

Table 6.3 shows the regional lung deposition fractions (DF) of particles from different sources. These were estimated by applying a modified ICRP model (Vu et al., 2015a) to the PMF factor profiles. In terms of particle number, particles released from nucleation (F3) and local traffic emission sources (F1) were found to have the highest deposition fractions in the total lung, with DFs of 0.62 and 0.57, respectively, followed by aged traffic particles (F2, DF =0.41). In contrast, the volume deposition fraction of nucleation particles (F3) is only 0.17,

while the volume deposition fraction for secondary aerosol was found to be the highest, ranging between 0.25 (F5) and 0.41 (F4). By surface area, 22-37% of total secondary aerosol surface concentration can be deposited into the lung, while the surface area deposition fraction for accumulation mode particles (F6) is only 16%. The total surface area deposition fraction for local (F1), aged traffic emission (F2) and nucleation (F3) is 0.37, 0.28 and 0.27, respectively.

Table 6.3: Total and regional lung deposition fraction (DF) of each source.

	Number				**Surface Area**				**Volume**			
	ET	TB	AL	Total	ET	TB	AL	Total	ET	TB	AL	Total
F1: Local traffic	0.06	0.11	0.4	0.57	0.04	0.06	0.26	0.37	0.05	0.03	0.15	0.22
F2: Aged traffic	0.04	0.07	0.3	0.41	0.03	0.04	0.21	0.28	0.04	0.02	0.13	0.20
F3: Nucleation	0.07	0.13	0.42	0.62	0.05	0.04	0.18	0.27	0.06	0.01	0.09	0.17
F4: Inorganic Sec.	0.11	0.02	0.11	0.24	0.23	0.02	0.11	0.37	0.26	0.03	0.12	0.41
F5: Mixed Sec.	0.08	0.03	0.14	0.24	0.12	0.01	0.09	0.22	0.14	0.01	0.09	0.25
F6: Urban Acc.	0.03	0.04	0.18	0.24	0.03	0.02	0.12	0.16	0.03	0.02	0.10	0.14

Note: Sec.: secondary aerosol, Acc. : accumulation mode; $DF_{total}=DF_{ET} + DF_{TB}+ DF_{AL}$

In terms of regional lung deposition, traffic and regional nucleation particles have higher deposition fractions in the alveolar (AL) region rather than in the extra-thoracic (ET) or tracheo-brochial (TB) regions in all three number, surface area and volume metrics. For example, the deposition fraction of local traffic particles (F1) by number is 0.40, 0.11 and 0.06 for AL, TB and ET regions. But for secondary aerosols, the highest deposition fraction values are found in the ET region by volume and surface area. The regional and total lung deposition fractions of particles generated from different sources are mainly controlled by their size distribution. Smaller particles such as nucleation or local traffic emission are found to penetrate deeper into the respiratory tract. Table 6.4 shows a compilation of deposition fractions reported in previous studies.

Table 6.4: Deposition Fractions of particles in the whole lung in previous studies.

Sources	Size (nm)	Number	Surface	Volume or mass	References
Diesel particles	10-500	0.47-0.65	0.39-0.32	0.27-0.28	Rissler et al. (2012)
ETS	15-670	0.36	-	-	Morawska et al. (2005)
Diesel	15-670	0.3	-	-	
Petrol smoke	15-670	0.41	-	-	
Hydrophobic	12-100	0.26-0.46	-	-	Löndahl et al. (2007)
Traffic particles	3.2-930	0.69	0.31	0.32	Kristensson et al. (2013)
Wood particles	3.2-930	0.38	0.22	0.22	
Traffic exhaust	12-580	0.68	0.35	0.28	Löndahl et al. (2009)
Biomass burning	12-580	0.22	0.23	0.24	

6.3.3.2. Which sources are most responsible for particles deposited in different regions of the lung?

The contribution of each source to deposited submicron particles by number, surface area and volume in the extra-thoracic (ET), trachea-bronchial (TB), and alveolar (AL) regions and total lung are shown in Table 6.5.

Table 6.5: Source apportionment of submicron particles deposited in the regional lung (%)

	Number				Surface Area				Volume			
	ET	TB	AL	total	ET	TB	AL	total	ET	TB	AL	total
F1: Local traffic	34.2	41.2	37.0	37.4	3.3	15.3	11.9	9.4	1.1	5.0	4.4	2.8
F2: Aged traffic	24.8	29.6	31.5	30.4	6.2	24.8	22.4	17.2	2.4	11.2	11.0	6.9
F3: Nucleation	9.9	11.6	9.7	10.0	0.9	2.3	1.8	1.6	0.4	0.8	0.9	0.7
F4: Inorganic Sec.	4.0	0.5	0.7	1.0	36.0	11.8	10.6	19.3	43.9	33.7	26.0	38.4
F5: Mixed Sec.	11.4	2.5	3.3	4.1	40.9	12.2	18.3	25.3	38.7	23.4	30.2	33.9
F6: Urban Acc.	15.7	14.6	17.7	16.9	12.7	33.6	35.0	27.3	7.4	25.9	27.5	17.3

Note: Sec.: secondary aerosol, Acc.: accumulation mode

6.3.3.3. By number

The majority of particles by number deposited in the total and regional lung are found to be related to combustion sources, in which traffic emissions were found to be the main contributor. Local and aged traffic particles are responsible for 67.8% of particle number deposited in the total lung. In terms of lung regions, traffic emissions are dominant and account for 68.5% of particle deposition in the AL region and up to 70.8% in the TB region. Regional accumulation mode and nucleation particles account for approximately 17% and 10% of particle number deposited in the total lung while secondary aerosols only account for around 5.1%. The dominant contribution to particles deposited in the total lung is traffic emissions because they are the main source of particles by number in an urban area. In addition, traffic particle size distributions were found predominantly in the ultrafine size range (<100 nm), with high deposition fractions. Therefore, traffic emission particles can easily penetrate and to be deposited in the human respiratory tract.

6.3.3.4. By surface area

Both combustion and secondary aerosols account for the majority of particles by surface area deposited in the lung. Secondary aerosols contribute nearly half of the particle surface area deposited in the total lung (44.6%), while regional accumulation mode particles and traffic particles account for 27.3% and 26.6%, respectively. In the AL and TB regions, regional accumulation mode particles, traffic emissions and secondary aerosols share around one third of total deposited particles. However, in the ET region secondary aerosols account for more than 76% of the total particle surface area, while accumulation mode particles and traffic emissions account for 12.7 and 9.5%. Only 1.6% of the particle surface area deposited in the total lung is attributed to nucleation particles.

6.3.3.5. By volume

Secondary aerosols are identified as the main source of submicron particles by volume deposited in the total and regional lung. They represent approximately 71.4% of particle volume deposited in the total lung and up to 82.6% in the ET regional. This can be explained by the major contribution of secondary aerosols to particle volume. In addition, due to their more hygroscopic properties, their lung deposition fractions are much higher than those from hydrophobic particles with the same initial dry diameter (Vu et al., 2015a). Accumulation mode particles account for 7.4%, 25.9%, 27.5% and 17.3% of total particle volume deposited in the ET, TB, AL and total lung, respectively. Traffic emissions only represent around 10% of the particle volume deposited in the total lung. Traffic emission particles mainly penetrate and are deposited into the TB and AL regions, where they account for around 15-16%, while they only contribute to 3.5% of particle volume deposited in the ET region. Nucleation particles do not make a significant contribution to total submicron particle deposition by volume in the lung (<1%).

Some studies suggest that ultrafine particles that are most commonly measured in terms of their number concentrations could have higher toxicity compared to corresponding masses of fine particles due to their large surface area, oxidative capacity and radical species formation, which can lead to cellular DNA damage or induce inflammatory effects (Atkinson et al., 2010; Kreyling et al., 2004). In addition, Harrison et al. (2010) indicate that relating health outcomes to measured particle concentrations is likely to underestimate the public health impacts and emphasizes that the regional dose, not pollutant exposure, probably drives health outcomes. Therefore, our findings of the various source contributions of particles in the different regional lung and particle metrics can be useful in addressing part of the question of what the most important metric linked to health effects in epidemiology studies is. It also helps policy makers to make decisions on controlling particulate matter. For example, if we plan to reduce particles by number in urban areas, we should first consider traffic emissions

because of their greatest contribution (59.0-70.8%) in both the whole and regional lung. But if the target is to reduce submicron particles by mass, we need to first consider the secondary aerosols and urban accumulation mode (mostly urban combustion).

6.4. Conclusions

This study found that traffic emissions were the most relevant ambient source of submicron particles deposited by number into the human respiratory tract, accounting for 67.8% of particles deposited in the total lung by number at the North Kensington site. This can be explained by considering local and aged traffic sources as major sources of submicron particles by number (56.5%) in this urban background area in conjunction with their high lung deposition fraction (0.41-0.57). Moreover, traffic particles can penetrate deeper into the lung with deposition fractions of 0.3-0.4 in the AL region and 0.07-0.11 in the TB region. Considering the high concentrations by number attributed to traffic emissions in the PMF analysis, local and aged traffic emissions represent 68.5% and 70.8% of the total particle number deposited in the TB and AL regions, respectively. Urban accumulation mode particles and regional nucleation particles were also found to contribute significantly to the increased number of particles deposited in the lung (16.9% and 10% respectively). Secondary aerosols contribute only approximately 5.1% of submicron particles deposited in the total lung by number, but they represent a major source of particles deposited in the regions and total lung by volume (56.2-82.6%), followed by urban accumulation mode (7.4-27.5%), traffic emissions (3.5-16.2%) and nucleation (0.4-0.9%). In terms of deposited particles by surface area, secondary aerosols were found to be most dominant in the ET region (76.9%), while the main contribution in the TB region was from traffic emissions (40.1%) and urban accumulation mode (33.6%). In the AL region, urban accumulation mode was the highest contributor of particle surface area (35.0%), followed by traffic emissions (34.3%), secondary aerosols (28.9%) and nucleation (1.8%).

Chapter 7: PHYSICAL PROPERTIES AND LUNG DEPOSITION OF PARTICLES EMITTED FROM FIVE MAJOR INDOOR SOURCES

This chapter studies the physical properties of indoor particles were measured with an SMPS system an APS and an H-TDMA in a flat located in an urban background site in Prague (Czech Republic) from 15th August to 8th September, 2014. Particles emitted from cleaning activities showed unimodal number size distributions, with the majority of particles (>98.2%) in the ultrafine size range (D_p <100 nm) and modes at a diameter of 19.8 nm for vacuum cleaning and 30.6 nm for soap/W5 cleaning. Smoking and incense burning predominantly generated particles in the accumulation mode with a count median diameter around 90-150 nm while cooking emissions showed a bimodal structure with a main mode at 47.8 nm. Particles from vacuum cleaning, incense burning, smoking and cooking emissions were found to be "nearly hydrophobic" with averaged growth factor (Gf) around 1.01-1.10, while particles emitted from desk cleaning using organic compounds were found to be "less-hygroscopic" (Gf ~1.12-1.16). Based on an adjusted MPPD model with a consideration of the hygroscopic properties of particles, the total lung deposition efficiencies of these particles by number when they penetrate into the human lung were 0.73 ± 0.02, 0.62 ± 0.03, 0.37 ± 0.03, 0.32 ± 0.03 and 0.49 ± 0.02 for vacuum cleaning, desk cleaning, smoking, incense burning and cooking, respectively.

This chapter contains some sections of verbatim text adapted from a manuscript of "Physical properties and lung deposition of particles emitted from five major indoor sources" which has accepted on the Air Quality, Atmosphere & Health journal. The author's contribution: writing, contribution of ideas and numerical calculations.

7.1. Introduction

People in developed countries spend the majority of their time (approximately 90%) in indoor environments (Delgado-Saborit et al., 2011), and as consequence they may be exposed to a range of pollutants of an indoor origin, particularly ultrafine particles which may cause cardiovascular, respiratory, and neurological hazards to human health (Diffey, 2011; Donaldson et al., 1998). Morawska et al. (2013) reported that 19-76% of the integrated daily residential exposure to ultrafine particles originated from indoor generated ones. Furthermore, their study found that particles emitted from indoor sources could represent up to 30% of the total burden of disease caused by aerosol exposure.

In recent years, many studies have been performed to characterize a range of indoor generated particles from various microenvironments, such as home, office, school or work place. For example, He et al. (2004) measured the contribution from 21 different types of indoor activities to particle number and mass concentration in 15 residential houses. Their study found that the indoor particle number concentrations showed an increase of 1.5 to over 27 times during indoor activities, while the $PM_{2.5}$ concentration was also estimated to increase during smoking, grilling and frying activities from 3 to 90 times above the background level. Similarly, Bhangar et al. (2011) investigated ultrafine particle concentration in seven residences in northern California and indicated that cooking was the most important indoor activity contributing to the indoor ultrafine particle level.

Different types of indoor activities release particles with different physical properties including their size distribution. The majority of particles generated from indoor combustion sources including, cooking, wood burning, candle burning, and fireplace or kerosene heating, were found in the submicron size range (Hussein et al., 2006). On the other hand, particles originating from resuspension from indoor surfaces due to building occupant movement are

predominantly distributed in the coarse mode, with a diameter lager than 1 μm (Thatcher and Layton, 1995). Characterization of the particle size distribution of indoor sources is not only useful in determining the regional lung deposition of particles, but also in source apportionment of indoor aerosols based on receptor modelling methods (Vu et al., 2015b). Ogulei et al. (2006a) ran a positive matrix factorization (PMF) analysis on indoor particle size distributions in an occupied townhouse in Reston (Washington DC, USA) to identify the contribution of indoor sources to indoor aerosols.

Although the number of studies focusing on indoor aerosols has increased in recent years, the physical characterization database of indoor sources, particularly the hygroscopicity of indoor particles, which is known to be an important determinant of lung deposition fraction of particles in the human respiratory tract is still limited (Vu et al., 2015a). The aim of this study was to investigate physical properties including size distribution, density and the hygroscopicity of particles, originating from five typical indoor sources. The regional lung deposition fraction of indoor particles was calculated based on a modified Multiple-Path Particle Dosimetry Model (MPPD). Finally, the minute regional lung dose of indoor generated particles was estimated and compared.

7.2. Materials and Methods

7.2.1. Site Description and Data Measurement

The experimental campaign was conducted from 15th August to 8th September 2014 in an apartment located in the suburban background of Prague, Czech Republic. The apartment was unoccupied during the sampling period. It is located on the ground floor of a two floor building and has a living room, a small bathroom next to the kitchen and two bedrooms, one of them containing the instruments. The apartment (as shown in Figure 7.1) and sampling site have been described in detail by Hussein et al. (2006).

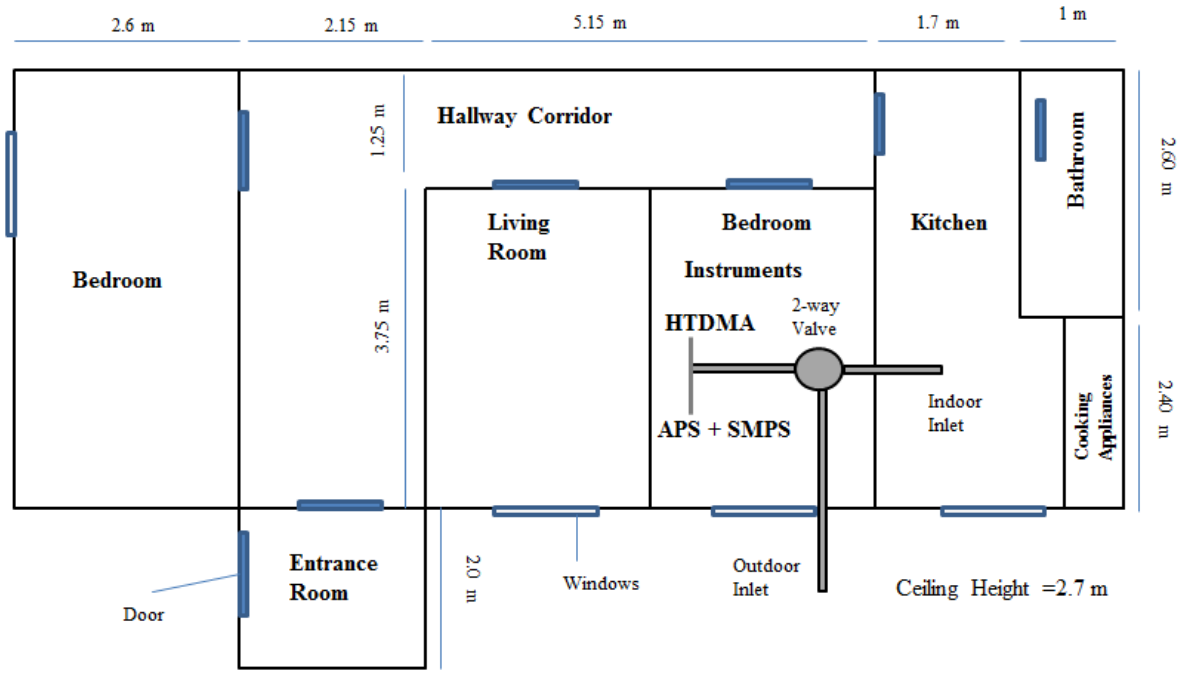

Figure 7.1: Plan view of the apartment.

The particle number size distribution (14.6-850 nm) was measured by a Scanning Mobility Particle Sizer system (SMPS 3696, TSI Inc., USA), comprising a TSI 3080 electrostatic classifier, a TSI 3081 differential mobility analyzer (long DMA) and a TSI 3775 condensation particle counter (CPC). Larger particles and their number size distribution (0.54-18 µm) were measured by an Aerodynamic Particle Sizer (APS 3321, TSI Inc., USA). The SMPS system was operated at a low aerosol flow rate of 0.3 L min^{-1} and the APS flow rate was 5 L min^{-1}, with a 5 minute time resolution. A Hygroscopic Tandem Differential Mobility Analyzer (HTDMA) developed by the Laboratory of Aerosol Chemistry and Physics, Institute of Chemical Process Fundamentals of the ASCR, (ICPF, Czech Republic) was installed to measure the hygroscopic growth factors at 90% relative humidity for particles with three selected initial dry sizes with diameters of 50, 100 and 200 nm.

Indoor particles were generated in a closed kitchen, except cooking activity with opened door. The cleaning, smoking, incense burning and cooking activities were conducted during a period of approximately 10, 5, 60 and 20 minutes. There are two persons smoked with two

cigarettes inside the kitchen during smoking experiments. Cooking experiments were conducted by frying sausages with sunflower oil, and toasting breads. Sampling inlet was put in breathable zone. All SMPS/APS datasets were corrected for particle loss inside the tube (the length of the tube ~ 1.2 m) before analysis.

7.2.2. Data Handling

Merging SMPS/APS data

Two types of data sets (aerodynamic and mobility) collected from the APS and SMPS instruments were merged into one particle size spectrum matrix (mobility diameter from 14.9-10000 nm) using an enhanced algorithm which was developed in CRAN R by Beddows et al. (2010). The effective density of the particles was estimated based on the best fit between two instrument (APS/SMPS) datasets for number, surface area and volume spectra. The final diameter type obtained by this enhanced merging algorithm was mobility diameter, and it can be converted to aerodynamic diameter models using the following equations:

$$D_a = x.D_m.\sqrt{\frac{C(D_m)}{C(D_a)}} \tag{7.1}$$

$$x = \sqrt{\frac{\rho_e}{\rho_0}} \tag{7.2}$$

where, D_a and, D_m are aerodynamic and mobility diameters (nm), respectively; C is the Cunningham slip correction factor and $x$is known as the free parameter that is determined by giving the best fit between the APS/SMPS spectra. ρ_0 is unit density and ρ_e is the estimated transition-regime effective density (g cm^{-3}). Particles were assumed to be spherical, therefore mobility diameter equals to equivalent volume diameter. PM mass concentrations were estimated from the merged size distribution and effective density.

7.2.3. Estimation of hygroscopic growth factors in regions of the lung

To analyse the growth factors from the HTDMA, a TDMAinv conversion approach provided by the Laboratory of Atmospheric Chemistry, Paul Scherrer Institute (PSI, Switzerland), was applied (Gysel et al., 2009). The TDMAinv toolkit was run on the Igor Wave Metric software version 6.1. This algorithm retrieved the actual growth factor probability density function (GF-PDF) as a piecewise linear function from the measurement distribution function of the HTDMA. The GF-PDF is defined as the growth factor probability density function, c(g,D) for particles with dry diameter $D=D_0$ to present a growth factor (GF) is g, and the total probability of the presented GF is unity: $\int_0^\infty c(g, D_0)dg = 1$ (Gysel et al., 2009). In this study, the HTDMA measured the mean growth factor at 90% RH: $GF_{mean} = \int_0^\infty gc(g, D_0)dg$.

To calculate the growth factors at 99.5% RH, which is assumed as the RH in the respiratory tract, from the observed growth factor at 90% RH from our TDMA measurements, we applied an approach provided by Rissler et al. (2010) using the following calculation:

$$G_{f\text{-}99.5\%} = \sqrt[3]{1 + \frac{99.5}{90}\left(G_{f-90\%}^3 - 1\right)\frac{(C_{k\ at\ 90\ \%\ RH} - 0.90)}{(C_{k\ at\ 99.5\ \%\ RH} - 0.95)}} \quad (7.3)$$

where, C_k is the Kelvin curvature correction factor

$$C_{k\ at\ a\%\ RH} = \exp\left(\frac{4M_W\sigma_s}{RT.\rho_W D_{p-at\ a\%\ RH}}\right) \quad (7.4)$$

M_w (18 g mol^{-1}) and, ρ_w(1 g cm^{-3}) are the molecular weight and density of water; σ_s is the surface tension of the solution (assuming a surface tension of 0.072 J m^{-2}); R (8.314 J mol^{-1}) and T (298 K) are the ideal gas constant and temperature respectively, and D_p is the particle diameter (nm).

In this study, the HTMA only measured particles at three selected dry sizes of 50, 100 and 200 nm at 90% RH. For particles of below 50 nm and over 200 nm, this study assumed that the soluble volume fraction of particles at a diameter of 50 nm is also descriptive of those smaller than 50 nm, while that of particles with a diameter of 200 nm also describes those larger than 200 nm. In our measurements, particle size distributions were collected using SMPS/APS instruments without a dryer. It is therefore necessary to calculate the effects of ambient humidity on the size distribution measured by the SMPS/APS before using the data for the lung dose calculation.

The dry diameter of a particle can be estimated by the ratio of particle size measured by SMPS and the growth factor of that dry particle in the ambient relative humidity (RH). The RH for the indoor environment during vacuum cleaning, soap cleaning, smoking, incense burning and cooking was 47.9, 57.2, 47.3, 66.2 and 72.8%, respectively. According to our calculation, the effect of ambient relative humidity on the measured size distributions is not significant since the growth factors of particles were approximately unity under these low RH conditions. When a particle penetrates into the lung, its growth not only depends on particle size but also upon its residence time. To address the particle growth dependence upon time, we used an approach provided by Ferron (1977) as equation (5.2) and (5.3) as introduced in Chapter 5.

7.2.4. Modelling Particle Deposition in the Human Respiratory System.

Many mathematical models have been developed in recent decades to estimate the total and regional lung deposition of particles; for example, the ICRP model (International Commission on Radiological Protection), the NCRP model (National Council on Radiation Protection and Measurement), the IDEAL model (Inhalation, Deposition and Exhalation of Aerosols in/from the Lung) or the MPPD model (Multiple-Path Particle Dosimetry)

(Asgharian et al., 2001; ICRP, 1994; Protection and Measurements, 1997). This study utilized the MPPD model to calculate the total and regional lung deposition of particles emitted from each source.

The MPPD model was developed by Asgharian et al. (2001). The software (MPPD software version 2.11) was downloaded via http://www.ara.com/products/mppd.htm. In this study, we used the MPPD model to calculate the deposition fraction of particles by number in three regions of the lung, the extra-thoracic (ET), tracheo-bronchial (TB) and alveolar (AL) regions and the entire lung for adults. This study used the reference respiratory values for light exercise for Caucasian people during cooking and cleaning activities and for resting (sitting) during smoking and incense burning based on the reference data recommended by ICRP (1994). The input data for the MPPD model are shown in Table 7.1.

Table 7.1: Input data to the MPPD model based on the reference respiratory values from ICRP (1994).

MPPD model input data		Cooking, cleaning		Smoking, incense burning	
		Man	Woman	Man	Woman
	Model	Yeh/ Schum 5-Lobe			
	Functional Residual Capacity (mL)	3301	2681	3301	2681
	Upper Respiratory Tract Volume (mL)	50	50	50	50
Particle Properties	Density (g cm^{-3})	0.88 -1.56			
	Nanoparticle Model	YES (for particles smaller than 100 nm)			
	Inhalability Adjustment	YES (for particles larger than 1 μm)			
	Geometric Standard Deviation	1			
Exposure scenario	Acceleration of gravity (cm s^{-2})	981	981	981	981
	Body orientation	Upright			
	Breathing Frequency (min^{-1})	20	21	12	14
	Tidal Volume (mL)	1250	992	750	464
	Inspiratory Fraction	0.435			
	Pause Fraction	0.05			
	Breathing Scenario	Nasal	Nasal	Nasal	Nasal

However, the MPPD model may under-estimate the lung deposition of ambient particles if their hygroscopic properties are not taken into account (Vu et al., 2015a). In order to correct for the influence of particle hygroscopicity, the MPPD curves were modified for both indoor and outdoor particles with consideration of their hygroscopicity according to an approach introduced by previous studies (Kristensson et al., 2013; Löndahl et al., 2009; Vu et al., 2015a).

In this approach, submicron particles which have increased to their equilibrium size by their growth in the regional lung have the same deposition fraction in the respiratory system as hydrophobic particles with an identical size. Because no information was available for the hygroscopic growth factor for coarse particles, this study only calculated the deposition fraction of submicron particles (Dp <1 μm) by number. However, the deposition fraction of submicron particles by number is not significantly different to that of total particles since the submicron particles accounted for more than 99% of total particles by number.

7.3. Results and discussion

7.3.1. Particle Size Distributions

7.3.1.1. Outdoor/indoor background levels

The total number concentration for outdoor and indoor levels (with no indoor sources) was $4.2 \pm 2.1 \times 10^3$ and $3.3 \pm 1.3 \times 10^3$ particles cm^{-3}, respectively. As shown in Figure 7.2, the particle number size distribution of both outdoor and indoor particles appears to be the sum of log-normal size modes. The number mode for outdoor and indoor particle size distributions was 22.9 and 28.4 nm, respectively. The majority of particles by number (84.0% and 80.2% of total outdoor and indoor particles respectively) was found in the ultrafine size range (Dp <100 nm).

7.3.1.2. Vacuum cleaning

The peak particle number concentration was 9.4×10^4 particles cm^{-3}, which decreased to 7.08×10^4 particles cm^{-3} by the fifteenth minute after cleaning stopped. The particle number size distribution shows a unimodal distribution with the mode at 19.8 nm. This mode increased to 22.9 nm and 26.5 nm at 15 and 30 minutes after the activity stopped. More than 98% of total particles by number were found in the ultrafine particle size range (Dp <100 nm) during vacuum cleaning. This high number of ultrafine particles emitted from the vacuum cleaner is consistent with previous studies (Géhin et al., 2008; Knibbs et al., 2011; Wu et al., 2011). Knibbs et al. (2011) investigated particle emissions from 21 vacuum cleaners in a flow tunnel and found that the median emission rate of ultrafine particles was 9.92×10^9 particles min^{-1}, with a median value of CMD (count median diameter) of 25.5 nm.

In terms of mass concentration, vacuum cleaning also generated a large fraction of coarse particles. The peak $PM_{1.0}$, $PM_{2.5}$ and PM_{10} mass concentrations were 1.5, 22.7 and 75.4 µg m^{-3}. Szymczak et al. (2007) suggest that particles are in part generated by mechanical abrasion of the graphite brushes and copper commutator. However, the major source of ultrafine particles may be due to the spark discharging that occurs at voltages above 100V between two carbon electrodes within the vacuum cleaner motor (Helsper et al., 1993; Szymczak et al., 2007). Knibbs et al. (2011) reported lower ultrafine particle emissions with two battery-driven vacuum cleaners at lower voltages (14 and 22 V).

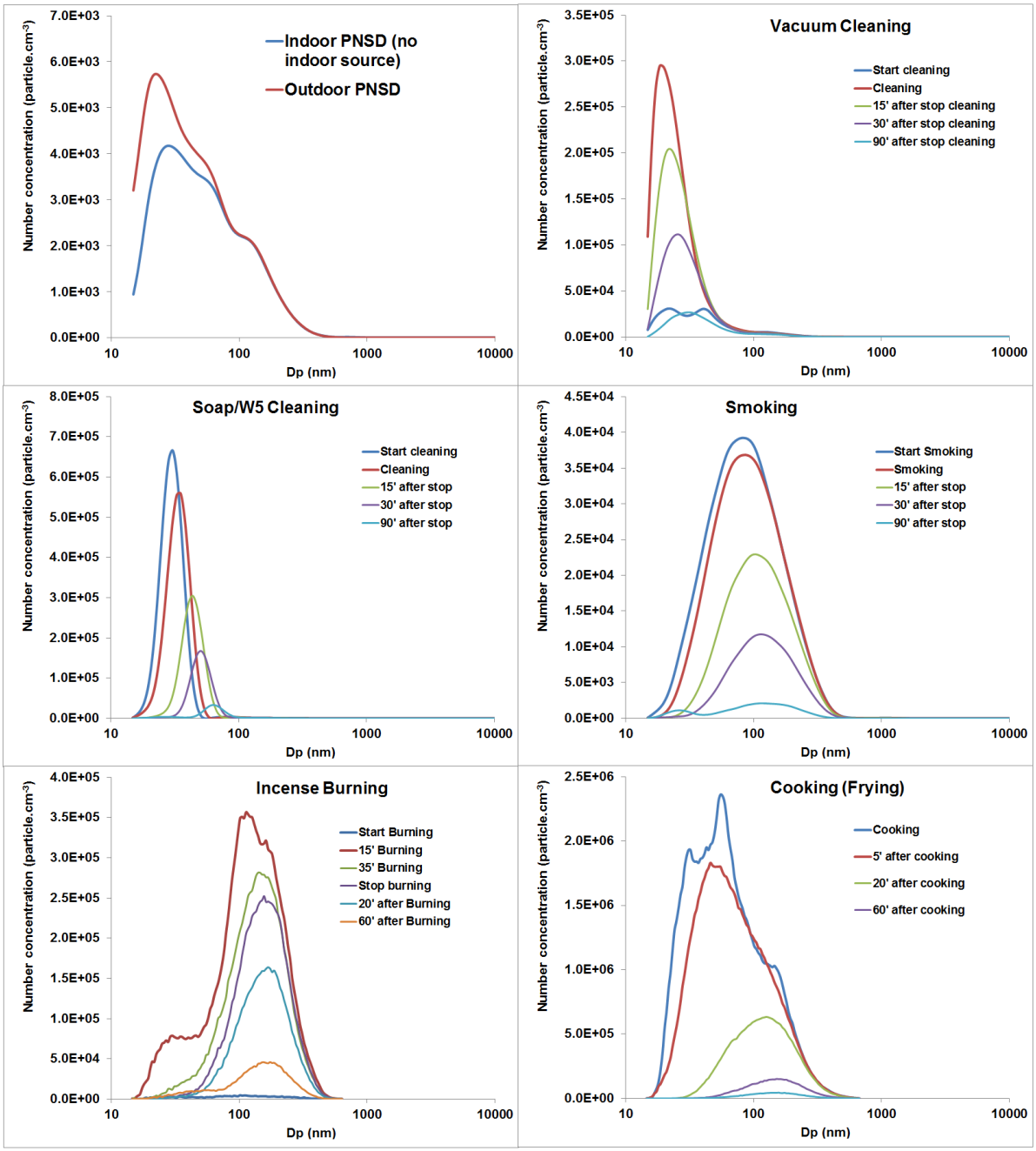

Figure 7.2: Particle number size distribution from indoor (without indoor sources) and outdoor environments and five major indoor sources.

There are few studies on the chemical properties and morphology of particles emitted from vacuum cleaners. Szymczak et al. (2007) used a MOUDI to collect particles in the size range of 0.057-18.0 μm and suggested that ultrafine particles comprise mainly copper, which may be generated from abrasion of the copper commutator inside the motor. Lioy et al. (1999) reported that particles larger than 0.01 μm in diameter mainly consist of chemical binders,

copper and carbon (elemental and organic) which were induced by rubbing and arcing between carbon rods and the copper commutator. In this study, the effective density of vacuum cleaner generated particles obtained by the APS/SMPS merging algorithm was 1.16 g cm^{-3} which was much lower than the material density of carbon (~2 g cm^{-3}) and copper (8 g cm^{-3}). This finding suggests that particles released from the vacuum cleaner motor were possibly carbon internal void aggregates (DeCarlo et al., 2004; Helsper et al., 1993; Lioy et al., 1999) which have a lower effective density.

7.3.1.3. Kitchen cleaning by soap/W5 spray cleaner

As seen in Figure 7.2, kitchen top cleaning using organic compounds (brand name:W5 cleaner) generated predominantly ultrafine particles with a maximum concentration of 1.25 × 10^5 particle cm^{-3} and a peak number mode of 30.6 nm. As with the vacuum cleaning, the count median diameter CMD increased and particle number concentration decreased rapidly due to coagulation and deposition processes after the cleaning activity finished.

Cleaning using chemical cleaners also generated both ultrafine and coarse particles. Average $PM_{1.0}$, $PM_{2.5}$ and PM_{10} mass concentrations during cleaning activity were 2.5, 10.4 and 22.0 µg m^{-3}, respectively. On the other hand, nano/ultrafine particles were probably produced by the oxidation and condensation of volatile organic compounds (VOCs) released from the cleaning agent during the cleaning activity (Nazaroff and Weschler, 2004; Rohr, 2013; Singer et al., 2006a; Zhu et al., 2001). Singer et al. (2006b) reported that a large amount of VOCs were found using pine-oil cleaner. They reported a concentration measured overone hour of 10–1300 µg m^{-3} for individual terpenoids, including α-terpinene (90–120µg m^{-3}), d-limonene (1000–1100 µg m^{-3}), terpinolene (900–1300 µg m^{-3}), and α-terpineol (260–700 µg m^{-3}). In addition, Sarwar et al. (2004) found that terpenes from cleaning products can react with ozone, resulting in secondary organic aerosol production in an indoor environment.

This study used W5 orange cleaner, which contains some surface active components (not specified in the details on the product label), soap and limonene. In general, limonene has been identified to play an important role in the formation of indoor nanoparticles (Langer et al., 2008; Wainman et al., 2000; Wang et al., 2007b; Waring et al., 2011). Langer et al. (2008) showed that the nucleation and growth of particles from the reaction of O_3 and limonene could occur even at a low concentration of reactants. The effective density obtained by the APS/SMPS merging process was 0.88 g cm^{-3}, indicating that the majority of particles generated by use of cleaning products were predominantly organic.

7.3.1.4. Tobacco smoking

The particle number size distribution from cigarette smoking showed a unimodal structure with a mode at 90 nm and peak number concentration of 2.89×10^4 particles cm^{-3} (note that two cigarettes were simultaneously smoked by regular smokers in this experiment). During the ageing process, the CMD increased to 120 nm, as shown in Figure 7.2. These results are consistent with previous studies (Hussein et al., 2006; Wu et al., 2011). Wu et al. (2011) measured the submicron particle number size distribution emitted from five brands of cigarettes and found that the number mode ranged from 102.9 to 116.7 nm with the maximum number concentration of 1.38×10^6 particles cm^{-3}. The number concentration of particles is not only dependent on the emission rate of the source, but also the volume of the chamber or the indoor environment where the smoking takes place, and the ventilation.

Fine particles (D_p< 2.5 μm) emitted from cigarette smoking were found to make a dominant contribution to mass concentration, with an averaged fraction of more than 82% of total PM_{10} mass. Averaged $PM_{1.0}$, $PM_{2.5}$ and PM_{10} concentrations were 3.2, 133.6 and 149.6 μg m^{-3}, respectively. In a review of indoor particles, Wallace (1996) indicated that the most important indoor source of fine and coarse particles in the US was tobacco smoking, with an estimated

increase of up to 45 μg m^{-3} in homes with smokers. The effective density of cigarette smoke particles was 1.56 g cm^{-3} based on APS/SMPS merging results. This value was slightly lower than the material density of black carbon (~2g cm^{-3}) and similar to the effective density of humic acids and humic-like substances (1.54-1.77 g cm^{-3}) from wood burning (Dinar et al., 2006).

7.3.1.5. Incense burning and cooking

Incense burning generated the majority of particles in the accumulation mode, with a CMD of around 110-150 nm. The total number concentration was up to 2.25×10^5 particles cm^{-3}. In the first scan of incense burning, it showed a distinct mode at 30.5 nm, suggesting that some nanoparticles were formed in the first few minutes of burning.

The number size distribution of particles released during incense burning was in agreement with previous studies. Wu et al. (2011) measured particle number size distributions from five types of incense stick and found that four of them had a CMD ranging from 124.1 to 148.9 nm and the other had a CMD of 75.5 nm. A similar study conducted by Ji et al. (2010) reported that the peak number mode of incense smoke was 136 nm, which was found to have a larger size distribution in comparison to other combustion processes such as diesel, wood or biomass burning. Unfortunately, the APS sampler had a problem with its inlet during measurement of particle size for incense burning and cooking, hence this study could not measure the coarse size for incense burning and cooking emissions. In this study, we adopted an effective density of 1.1 and 1.0 g cm^{-3} to convert the mobility to aerodynamic diameter for incense burning and cooking particles respectively based upon (Buonanno et al., 2009; Ji et al., 2010).

Cooking emissions showed a tri-modal distribution, with a peak mode at 47.8 nm. After cooking, the peak mode quickly increased to 135.8 nm. The reason is probably related to the

ventilation (open door when people leave the kitchen after cooking activity). During the cooking, a large number of particles was generated, with a peak number concentration of 1.57 $\times 10^6$ particles cm^{-3}. In a review of cooking emission, Abdullahi et al. (2013) reported a large fraction of ultrafine particles released during cooking activity with the peak number mode around 20-100 nm.

7.3.2. Hygroscopic Growth Factor of Particles

7.3.2.1. Hygroscopic growth factor of outdoor and indoor particles when no indoor source was present

The hygroscopic growth factors (Gf) of outdoor and indoor particles at an initial dry diameter of 50, 100 and 200 nm were measured during periods when no indoor source was present, from 15 to 21 August 2014. The growth factor probability density function (GF-PDF) of each particle size from the outdoor and indoor environments is shown in Figure 7.3. For particle sizes of 50 nm and 100 nm, two fractions of nearly-hydrophobic (Gf ~1.01-1.11) and less-hygroscopic particles (Gf ~1.11-1.33) were found dominant in both indoor and outdoor environments. For the particle size of 200 nm, the main fractions of particles were less-hygroscopic and more-hygroscopic (Gf ~1.11-1.85).

Mean growth factors for outdoor particles were 1.15 ± 0.07, 1.17 ± 0.09 and 1.23 ± 0.10 for the particle sizes of 50, 100 and 200 nm respectively. The mean growth factors for indoor particles were slightly higher than those of outdoor particles with values of 1.16 ± 0.07 and 1.18 ± 0.09 for particles with diameters of 50 and 100 nm, respectively. The loss of semi-volatile organic constituents due to volatilization or uptake on the indoor wall surface during penetration from the outdoor to indoor environment could explain the small decrease in the fraction of nearly hydrophobic particles in the indoor environment when no indoor source was present. On the other hand, the mean growth factor for indoor particles with a diameter

of 200 nm was 1.22 ± 0.07, which was practically the same as the growth factor for outdoor particles (1.23 ± 0.10).

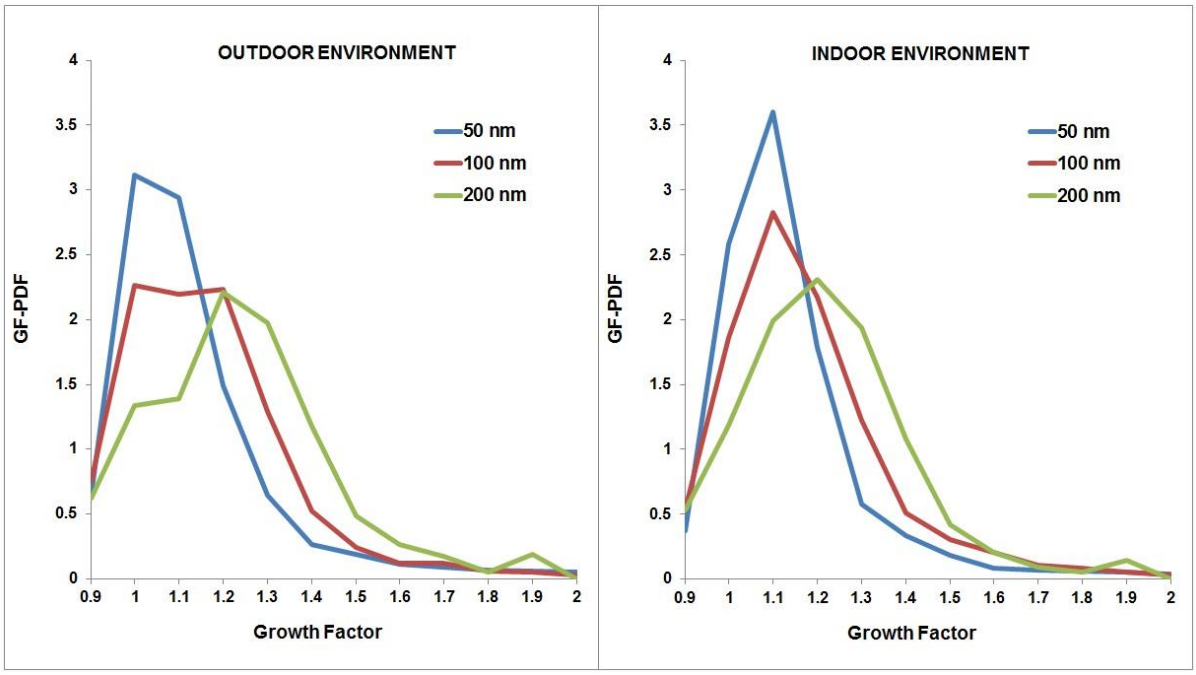

Figure 7.3: Hygroscopic growth factor probability density function (GF-PDF) for outdoor (left) and indoor (right) particles.

7.3.2.2. Hygroscopic growth factor of particles generated from indoor sources

Figure 7.4 shows the hygroscopic growth factor of particles emitted from five indoor sources at three particle sizes of 50, 100 and 200 nm. Particles generated from vacuum cleaning were found to be "nearly-hydrophobic" with an average growth factor (Gf) of around 0.98-1.10 for particle sizes of 50 and 100 nm. This finding is in agreement with the discussed hypothesis that particles emitted from vacuum cleaners mainly comprise carbon and copper. The growth factor of particles of 200 nm was 1.16, which is higher than those for smaller particles due to the mix of particles generated from the vacuum cleaner motor and background.

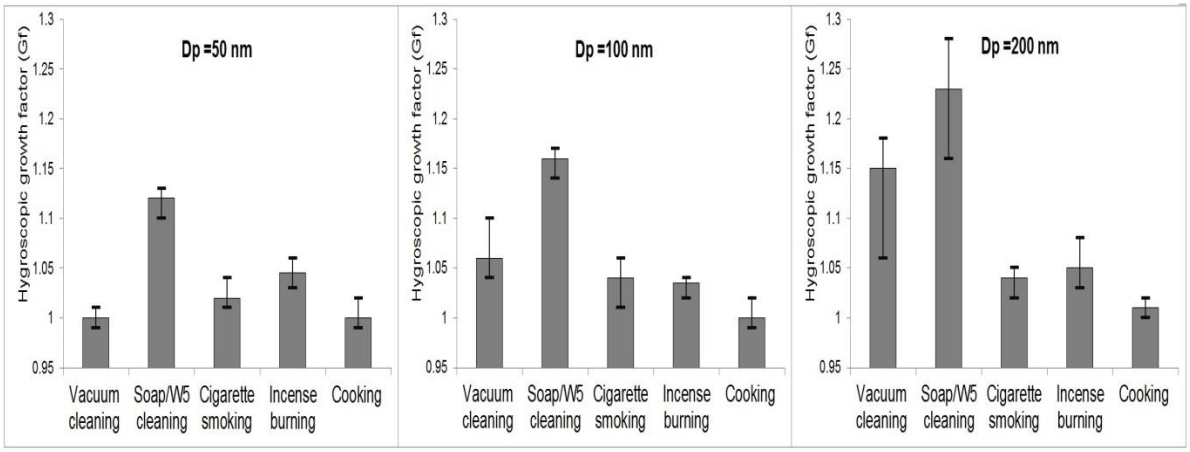

Figure 7.4: Hygroscopic growth factor of particles generated from different indoor sources.

Particles emitted from soap/W5 cleaner were found to be "less-hygroscopic" (Gf ~1.12-1.15 for particles at 50 and 100 nm). This finding is consistent with the above suggestion that the ultrafine particles generated by cleaning activities using soap/W5 cleaner predominantly consist of organic compounds such as the products of oxidation of limonene. Virkkula et al. (1999)conducted a measurement of the hygroscopic properties of aerosol formed by oxidation of limonene, α-pinene, and β-pinene, and found that the hygroscopic growth factor was approximately 1.10 at 84% RH, consistent with our results. The hygroscopic growth factor of particles of 200 nm was 1.22. This high growth factor could also be explained by the mix of particles generated from cleaning activities and background in the large size range, while the majority of particles during this activity were found in the ultrafine size range.

The average hygroscopic growth factors of particles emitted from cigarette smoking were approximately 1.01- 1.04 for all sizes of 50, 100 and 200 nm. This hygroscopic growth factor is found slightly to be higher than diesel combustion (Gf ~1.01), but lower than biomass burning (Gf ~1.04-1.10). This low hygroscopic growth factor is probably due to the chemical properties of particles generated from combustion, which mainly comprise black carbon and organic compounds. Morawska et al. (2005) found a similar count median diameter for both inhaled and exhaled submicron particles, suggesting that the change in particle size after its

travel into the lung is not significant. However, the lack of growth of particles cannot be concluded with certainty due to different temperature and humidity regimes between the chamber and the lung. Li and Hopke (1993) found the hygroscopic growth factor of cigarette mainstream and sidestream smoke particles at 200 nm was approximately 1.40-1.42 at RH 99.5%, which was slightly higher than the estimated growth factor value in our study (Gf ~1.3 for Dp =200 nm at 99.5% humidity calculated from Gf ~1.04 at 90% measured by HTDMA).

Similarly, particles emitted from incense burning were found to be nearly hydrophobic with the hygroscopic growth factors ranging from 1.01 to 1.05 for all particle sizes of 50, 100 and 200 nm. A dominance of carbonaceous particles released from incense burning can explain those low hygroscopic growth factors. Wang et al. (2007a) measured the characteristics of air pollutants from incense burning in two temples in Hong Kong and found that the organic and elemental carbon accounted for around 60% of $PM_{2.5}$ mass, while inorganic ion species only accounted for 12% of $PM_{2.5}$ mass. Li and Hopke (1993) predicted that the hygroscopic growth factor of particles at 99.5% RH from the burning of incense was around 1.45 and 1.7 for particle sizes of 100 and 200 nm, while the values in our estimation were much lower (Gf ~1.16 and 1.31 for particles of 100 and 200 nm at 99.5% RH). Li and Hopke (1993) indicated that 8% errors were found in their estimation of the hygroscopic growth ratio mainly due to the humidity uncertainty in their HTDMA system. Furthermore, variations in particle composition and influences of the local environment may account for differences when measuring the hygroscopic growth factor of combustion aerosols.

Particles generated from cooking activity were found to be nearly-hydrophobic (Gf ~1.0-1.02 for all particle sizes of 50, 100 and 200 nm). In our study, we performed the cooking experiments by frying sausages with sunflower oil and toasting bread. This result is

consistent with Dua and Hopke (1996), who observed that there was no growth of particles emitted from cooking oils and sweet Italian sausages.

7.3.2.3. Growth factors of particles in the lung

The mean growth factors for particles from outdoors, indoors without indoor sources, and five major indoor sources in their maximum growth at 99.5% and different regions of the lung are shown in Figure 7.5.

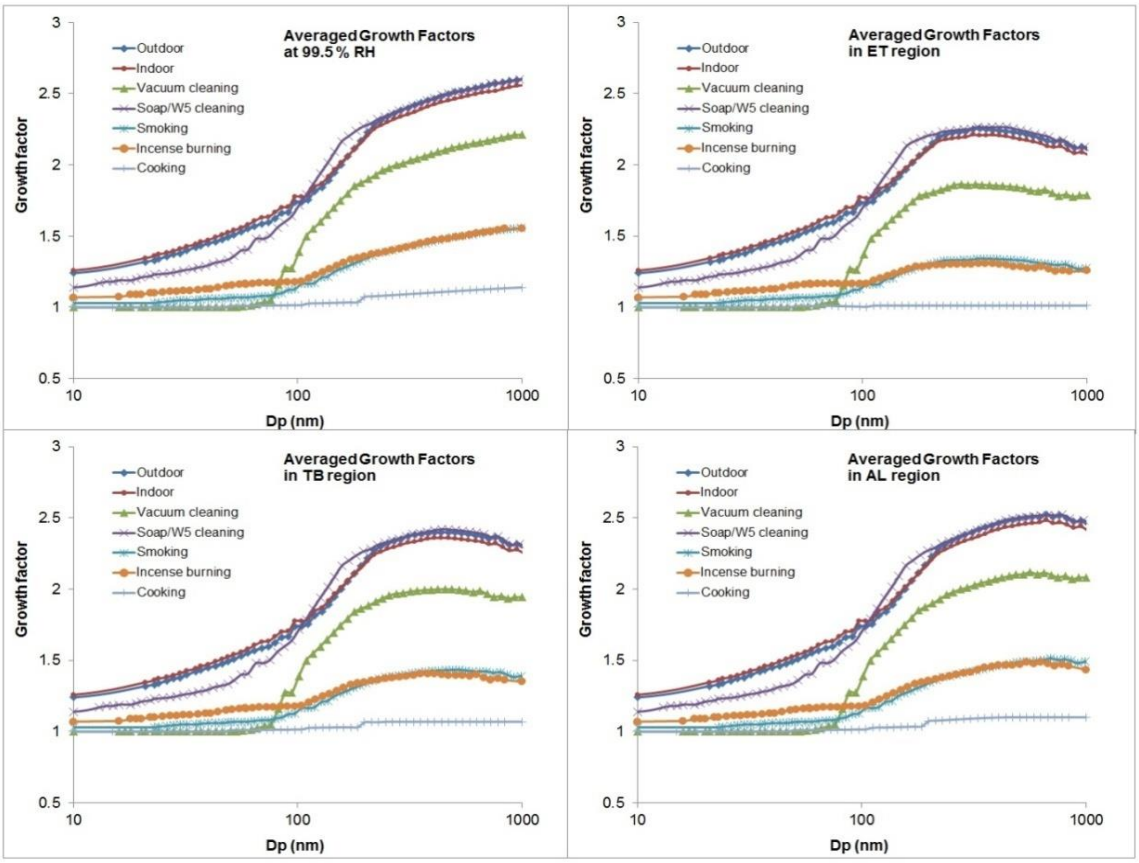

Figure 7.5: Hygroscopic growth factors at 99.5% RH and in the human respiratory tract.

As discussed above, the hygroscopic properties of particles arising from different indoor activities show different characteristics. Particles generated from soap/W5 cleaning products show a more hygroscopic tendency than particles from indoor combustion sources. Particles emitted from cooking activities show no significant growth in all sizes. When particles penetrate into the respiratory tract, those with a diameter below 200 nm can quickly reach

their equilibrium size in all lung regions. For particles larger than 400 nm, growth factors in the ET region can be more than 10% lower than those in the AL region.

7.3.3. Effects of Particles from Indoor Sources on the Lung Dose of Particles

7.3.3.1. MPPD models for different genders and activities

Based on the MPPD model, the deposition fraction curves of hydrophobic particles for men and women in light exercise and resting are shown in Figure 7.6. The total deposition fraction was found to be slightly greater for men than for women when resting. Specifically, the deposition fraction of ultrafine particles in the AL regions was found to be greater by up to 1.35 times greater for men compared to women. On the other hand, there was no significant difference between the lung deposition fraction for men and women during light exercise.

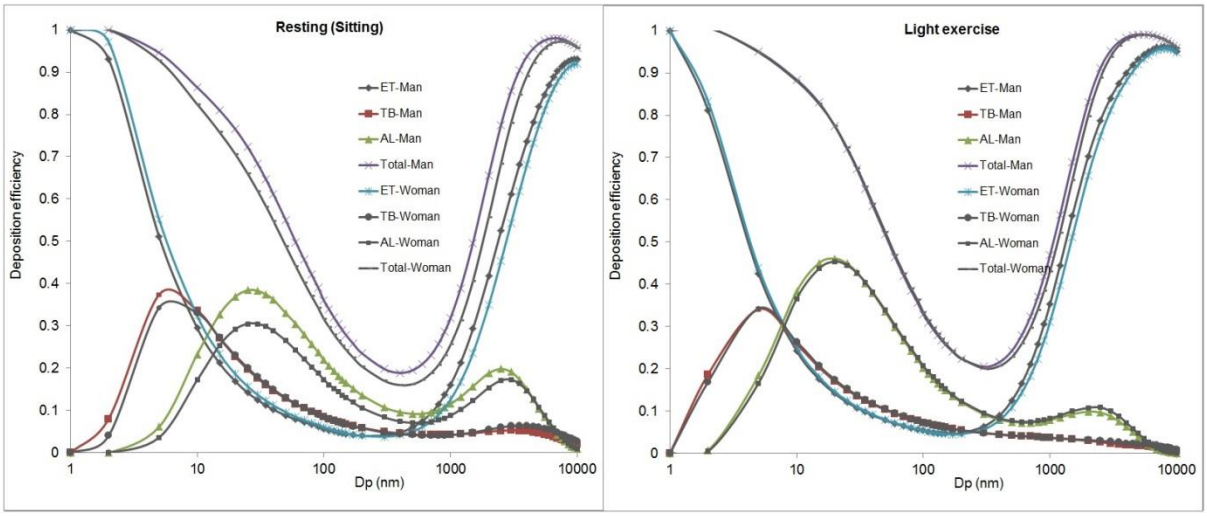

Figure 7.6: Deposition fraction curve from the MPPD model for man and woman in resting and in light exercise.

7.3.3.2. Regional lung deposition of particles emitted from each source

The total and regional lung deposition efficiencies of outdoor and indoor particles (with and without indoor source particles) for adults (males and females) by number are shown in Figure 7.7. The fractional total lung deposition fraction for outdoor particles and indoor

particles (without indoor sources) was 0.49 and 0.45. The slightly lower total deposition of particles from the indoor environment compared to the outdoor one was due to the shift in the outdoor particle number size distribution to a larger size range when they penetrated to indoor environments from outdoors. For both environments, a dominant fraction of particles was deposited in the AL region (57.6%), followed by the TB region (25.5%). Only 16.6% of particles by number were deposited in the ET region.

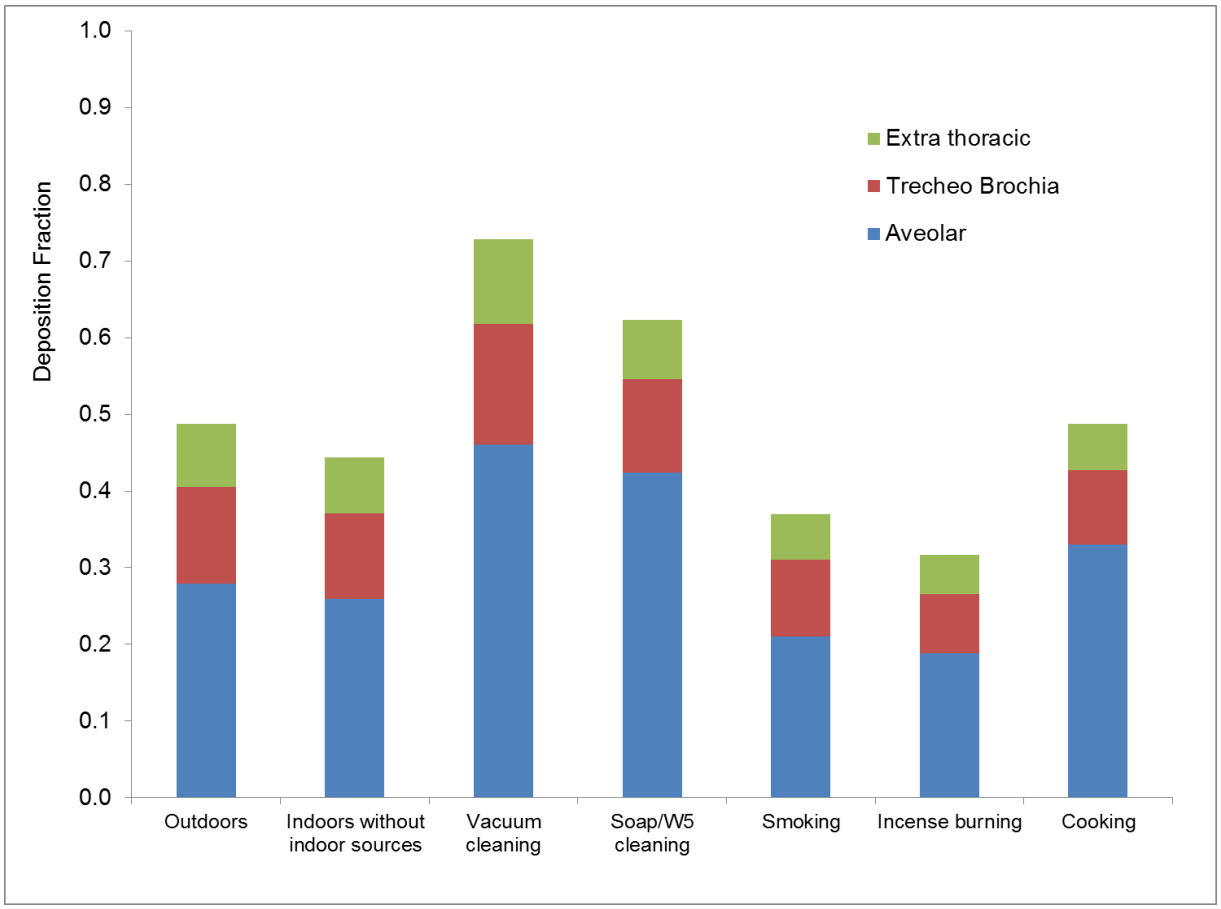

Figure 7.7: Deposition fraction of particle number in regions of the lung for adults.

For the indoor sources, alteration in the lung deposition of particles is mainly due to the change in size distribution. Up to 62 and 73% of total particles were deposited in the lung during soap/W5 cleaning and vacuum cleaning. This can be explained by the majority of particles released during cleaning activities being present as nanoparticles, which easily penetrate into the deeper regions of the lung. In contrast, the lung deposition fraction of

particles emitted from indoor combustion sources such as cooking, incense burning or smoking was lower because the main fraction of particles by number was found in the larger size range, particularly in the Aitken range, for cooking and the accumulation mode for incense burning or cigarette smoking. The total lung deposition fractions were 0.49, 0.32 and 0.37 for indoor particles generated during cooking, incense burning and smoking. For these particles, a predominance of deposited particles by number was found in the AL region (56.7-68.1%), followed by the TB region (19.5-27.0%). Only 12.2-16.2% of total deposited particles by number were found in the ET region.

7.3.3.3. Discussion of the contribution of indoor sources to the lung dose of aerosols

In order to determine and compare the effects of indoor sources upon human exposure, this study has compared the lung dose rate of particles by number in the indoor environment with and without indoor activities. The lung dose of particle number in different regions of the lung (i) within a specific particle size range was calculated based on the following equation (Hussein et al., 2013):

$$Dose_{i,} = V_E * DF_i * C_N * \Delta t \quad (7.7)$$

where, V_E is the minute ventilation (m^3/min); DF_i is the deposited fraction of particles in the different regions of the human respiratory tract; C_N is the total number concentration (particle cm^{-3}); and Δt is the exposure time period (minutes). The respiratory tract deposition particle dose rate, which is defined as the total particle number deposited in the respiratory system during a specific time period (in this study, Δt was set up to 1 minute), can be estimated from:

$$\text{Minute dose rate}_{i,} = V_E * DF_i * C_N \quad (7.8)$$

V_E was set at 7.75×10^{-3} for sitting and 2.29×10^{-2} m^3 $minute^{-1}$ for light exercise, calculated by averaging the respective VE values for men and women at two exercise levels (sitting and light exercise) (ICRP, 1994).

Table 7.2: Lung deposition of particles from outdoor and indoor environments (without and with indoor sources) for adults (averaged deposition fraction for both men and women).

	Deposition fraction				V_E (m^3 min^{-1})	**Dose (10^6 particles min^{-1})**			
	AL	TB	ET	Total		AL	TB	TB	Total
Outdoors	0.28	0.13	0.08	0.49	$7.75*10^{-3}$	9.0	4.0	2.6	16.1
Indoors*	0.26	0.11	0.07	0.45	$7.75*10^{-3}$	6.6	2.9	1.9	11.4
Vacuum cleaning	0.46	0.16	0.11	0.73	$2.29*10^{-2}$	992.5	338.2	238.0	1568.3
Soap/W5 cleaning	0.42	0.12	0.08	0.62	$2.29*10^{-2}$	1419.3	406.9	258.4	2084.5
Smoking	0.21	0.10	0.06	0.37	$7.75*10^{-3}$	47.1	21.5	13.7	82.9
Incense burning	0.19	0.08	0.05	0.32	$7.75*10^{-3}$	328.7	128.3	86.6	549.5
Cooking	0.33	0.10	0.06	0.49	$2.29*10^{-2}$	11874.5	3413.3	2159.0	17630.0

**: Indoor environment with no indoor sources; V_E: Ventilation rate (minute ventilation.*

Table 7.2 shows the minute dose rate of particles by number for adults in the outdoor and indoor environment (with and without indoor sources). During indoor activities, humans can be exposed to a huge number of particles. For example, a person when cooking could have an exposure of more than 1.76×10^{10} particles every minute, which is a thousand times higher than the exposure value for outdoor particles (16.1×10^6 particles). The one minute dose of cooking particles by number at the light exercise level is equivalent to 18.3 and 6.2 hours exposure to outdoor particles at the resting and exercise respiration rate respectively. Similarly, the total minute lung dose of particles from vacuum cleaning, soap/W5 cleaning, smoking and incense burning could be up to 1.6×10^9, 2.1×10^9, 8.3×10^7, 5.5×10^8 particles $minute^{-1}$. Based on equation (7.7), it is clear that the minute lung dose rate of particles strongly depends upon V_E, DF_i and C_N. While the total DF_i for particles from the

different indoor sources had a range of 0.32 (for incense burning) to 0.73 (for vacuum cleaning) and the minute ventilation rate for a male adult can range by nearly 6.7 times from 7.5×10^{-3} to 5×10^{-2} m^3 min^{-1} (ICRP, 1994), the concentration of particles by number was found to show the largest variation from 3.3×10^3 (for indoor environment with no source) to 1.57×10^6 (for cooking emissions) particles cm^{-3}. This suggests that the concentration level is the main factor controlling the lung dose.

Indoor particles not only contribute a large fraction of human exposure to aerosols during indoor activities, but also after indoor activities. Figure 7.8 shows the evolution of minute lung dose rate, concentration and lung deposition fraction of indoor particles after finishing indoor activities under low ventilation conditions (closed windows and door after indoor generation). It was found that the total concentration and minute lung dose decrease dramatically after stopping indoor particle generation, but the minute lung dose was still very high after 30 minutes, especially for cleaning activities. Because of deposition, coagulation and the mixing with outdoor particles due to air exchange, the size was also changed, altering the lung deposition fraction. For cleaning activities, the lung deposition fraction decreased to that of average indoor particles without indoor sources. For incense burning and passive smoking, the lung deposition fraction first decreased within the first 30 minutes after finishing indoor activities, but then increased to the background level. This can be explained by the deposition of particles on kitchen surfaces in the first 20-30 minutes which shifts the particle size distributions to a larger size. Subsequently, the mixing with outdoor particles which have a smaller size than incense burning and smoking aerosols, moves the particle number size distribution to the smaller size range, consequently affecting deposition fraction.

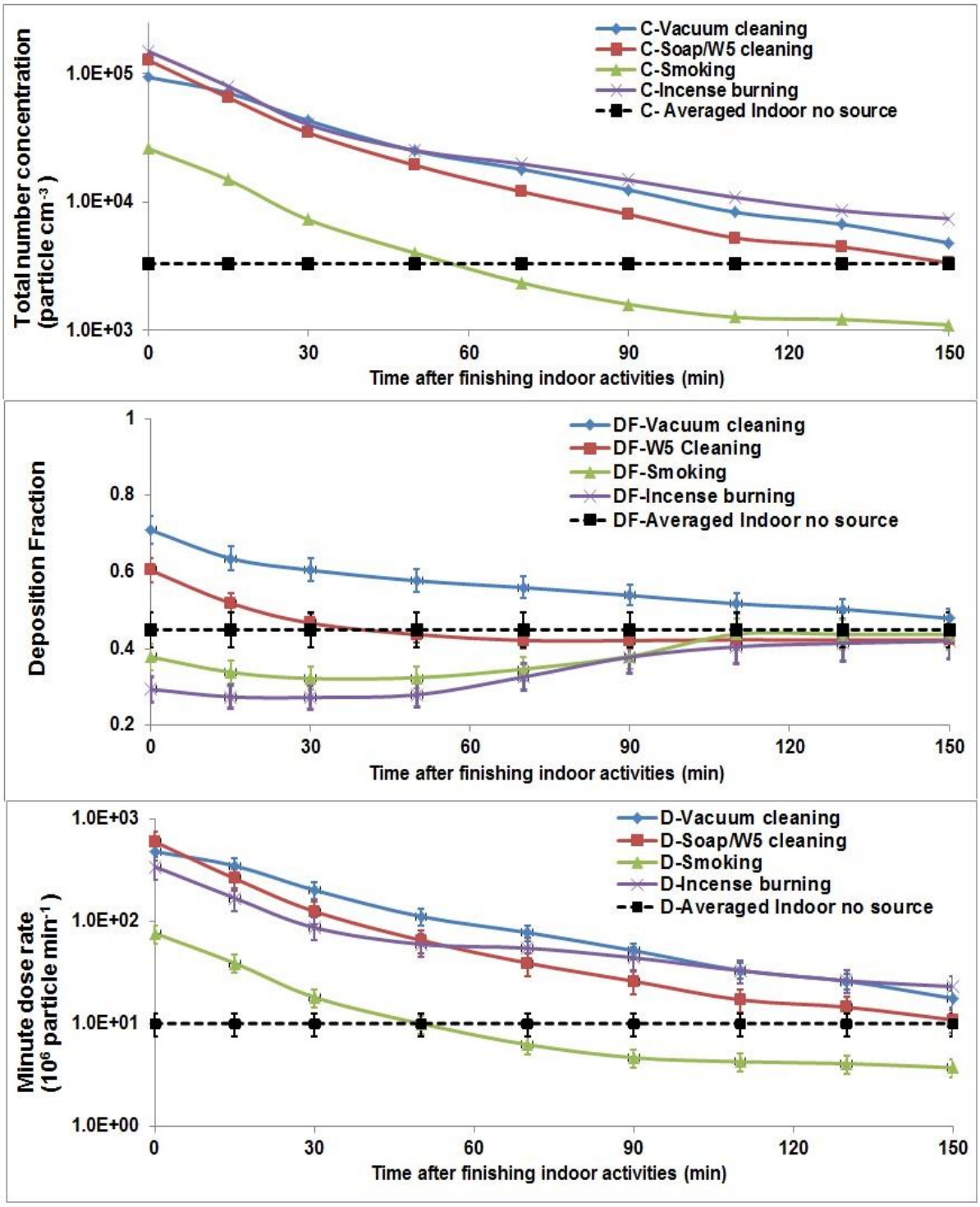

Figure 7.8: Minute lung dose rates, concentrations and lung deposition fractions of particles after different indoor activities.

Uncertainty for minute dose rate calculation

As shown in equation (8), the uncertainty for minute dose rate calculation depends upon the variation of minute ventilation (V_E), deposition fraction (DF), and particle number concentration (C_N). In this study, the minute ventilation is assumed as a constant value for each activity. Therefore, the uncertainty in the minute dose rate calculation can be estimated from the uncertainties in the lung deposition fraction and particle number concentration. The relative standard error of lung deposition fractions of particles generated from each indoor source mainly depends on the variation of input size distribution, and subject difference such as gender, and lung structure. Since the MPPD model does not provide estimates of uncertainty, this study could only estimate the errors caused by the variation of particle number size distribution and gender. The estimated relative standard deviations of total lung deposition fraction calculated for vacuum cleaning, soap/W5 cleaning, smoking, incense burning and cooking particles were 2.7, 4.8, 8.1, 9.4 and 4.1%, respectively.

The uncertainty in particle number concentrations measured for each source depends on the variation of particle number concentrations obtained by each SMPS measurement scan during the period of indoor source generation. The cleaning, smoking, incense burning and cooking experiments were performed during a period of approximately 10, 5, 60 and 20 minutes respectively. Each SMPS measurement combined two SMPS scans during 5 minutes. The relative standard deviation was estimated by dividing the standard deviation by the average number concentration of particles measured during each activity. The estimated relative standard deviation for particle number concentration measurement was 17.4, 9.4, 7.1, 22.3, 14.4% for vacuum cleaning, soap/W5 cleaning, smoking, incense burning and cooking measurements. By combination of the relative standard deviation for lung deposition fractions and particle number concentrations, the uncertainty in the minute lung dose rate was

estimated as 17.6%, 10.6%, 10.8%, 24.2% and 15.0% respectively. Clearly, the uncertainty in minute lung dose rate depends mainly upon the variation of particle number concentration.

7.3.4. Estimation of daily regional deposited dose: A case study

This section aims to estimate the daily regional deposited dose of submicron particles for inhabitants in the suburbs of Prague (Czech Republic) in the case of absent indoor sources. It then estimated the relative contribution of indoor sources to the total daily lung dose. The daily regional dose of particles was calculated following equation (1.3) which is introduced in the Chapter 1. The daily lung dose depends on the particle concentration, minute ventilation, deposition fraction and exposure time in the different exposure scenarios.

7.3.4.1. Daily time activity patterns

Daily time activity patterns data in this work is based on Novák and Sýkora (2007) and Schweizer et al. (2007). This was carried out using the time microenvironment activity diary for suburban inhabitants in Prague during working days. As a result, people spend nearly 94% their time indoor environments. The average time per day at home, work indoors and other indoors was 13.9, 6.5 and 1.7 h day^{-1}, respectively. Novák and Sýkora (2007) found that people spend 6.5 h day^{-1} on sleeping from 23:00 pm to 07:00 am, 1.8 h day^{-1} on eating and personal hygiene, 3 h day^{-1} on leisure and entertainment, 1.5 h day^{-1} on homework and care for children, 0.5 h day^{-1} at neighbourhood house during working days. Suburban inhabitants spend approximately 2 hours day^{-1} on transportation during 7:00-9:00 am and 17:00-20:00, corresponding to traffic hours. 70% of them used their passenger cars for commuting to work. According this information, this study assumed the daily time activity patterns and minute ventilation for each activity in the below table 7.3:

Table 7.3: Assumption of time-activity and location for employments living in new suburbs of Prague according to Novak and Sykora (2007) and Scheizer et al. (2007).

Activity	Time spend (h)	Time periods	Location
Sleeping	6.6	23:00-7:00	Home
Eating and personal hygiene	1.8	7:00-8:00; 12:00-13:00; 18:00-20:00	Home
Work and study	8.8	08:00-19:00	Office
Leisure-at home	1.8	17:00-23:00	Home
Leisure- outdoor	1.2	16:00-22:00	Outdoor
Homework and child care	1.5	17:00-22:00	Home
Transportation	2	7:00-9:00; 17:00-20:00	Car
Shopping and service	0.3	15:00-19:00	Shop

7.3.4.2. Relative contribution of indoor sources to the daily lung dose

In terms of particle number size distributions in each microenvironment, we assumed the particle levels at homes, offices and shops are similar to those indoor levels measured in the unoccupied kitchen during the sampling campaign. We assume particles in a car cabin was described by lognormal distributions with a CMD of 53.4 nm (σ =1.35) from previous work by Joodatnia et al. (2013) and Apte et al. (2011). In terms of minute ventilations, this study was adopted from parameters recommended by ICRP (1994). This study assumes that minute ventilations during eating and personal hygiene, leisure at home, and transportation are similar to those at rest or sitting activity (0.54 m^3 h^{-1} for men and 0.39 m^3 h^{-1} for women). The minute ventilations for outdoor activities (leisure at outdoors) are similar to those for light exercise levels (1.5 m^3 h^{-1} for males and 1.25 m^3 h^{-1} for females), while minute ventilations for work and study, and homework and childcare are assumed as an average of those from resting and light exercise levels. Particle number concentrations and ventilations for men and women in different exposure scenarios are shown in Table 7.4.

Table 7.4: Assumed particle number concentrations, CMD and minute ventilations for males and females in the different exposure scenarios.

Activities	Number (10^3 particles cm^{-3})	CMD (nm)	V_E (m^{-3} h^{-1}) (for a man)	V_E (m^{-3} h^{-1}) (for a woman)
Sleeping	3.2	71.4	0.45	0.32
Eating and personal hygiene	3.5	65.4	0.54	0.39
Work and study	3.1	66.7	1.02	0.82
Leisure at home	3.8	60.9	0.54	0.39
Leisure outdoors	4.9	53.4	1.5	1.25
Homework and child care	3.8	60.7	1.02	0.82
Transportation	39	42.5	0.54	0.39
Shopping and service	3.4	60.4	1.02	0.82

Deposition fractions (DFs) of particles in the human respiratory tract for adults in the different exposure scenarios were estimated by a MPPD model as shown in Figure 7.9. The DF values in total lung ranged from 0.38 to 0.57. Deposited particles were mainly found in the AL region (54.3-65.4%), followed by the TB region (21.2-27.2%) and the ET region (13.3-18.5%).

By combination of regional lung deposition fraction as shown in Figure 7.9 with daily time activity patterns in table 7.4, the daily regional lung dose of particles by number for a man and a woman in case of no indoor sources were estimated as shown in Figure 7.10. Daily dose of particles by number in the whole lung was 51.8×10^9 and 47.8×10^9 particles day^{-1} for a man and a woman, respectively. The majority of deposited particles were found in the AL region (61.1%), while only 24.4% and 15.3% of deposited particles were found in the TB and ET regions. These findings are in agreement with previous results by Hussein et al. (2013) who reported that the total deposited dose of fine particles on workdays was around 57×10^9 and 40×10^9 particles day^{-1} in adult males and females.

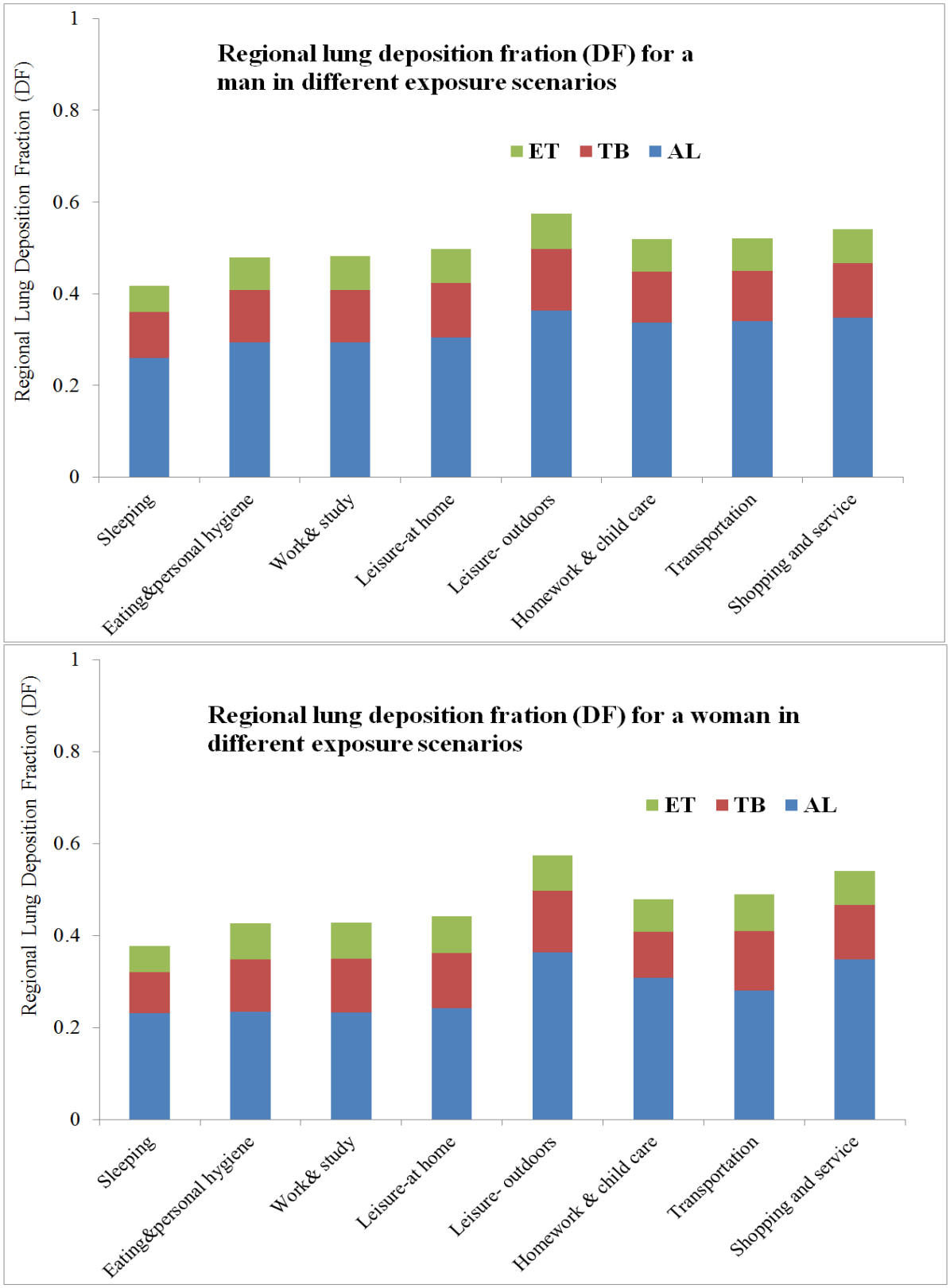

Figure 7.9: Deposition fractions of particles in lung regions for a man and a woman in the different exposure scenarios.

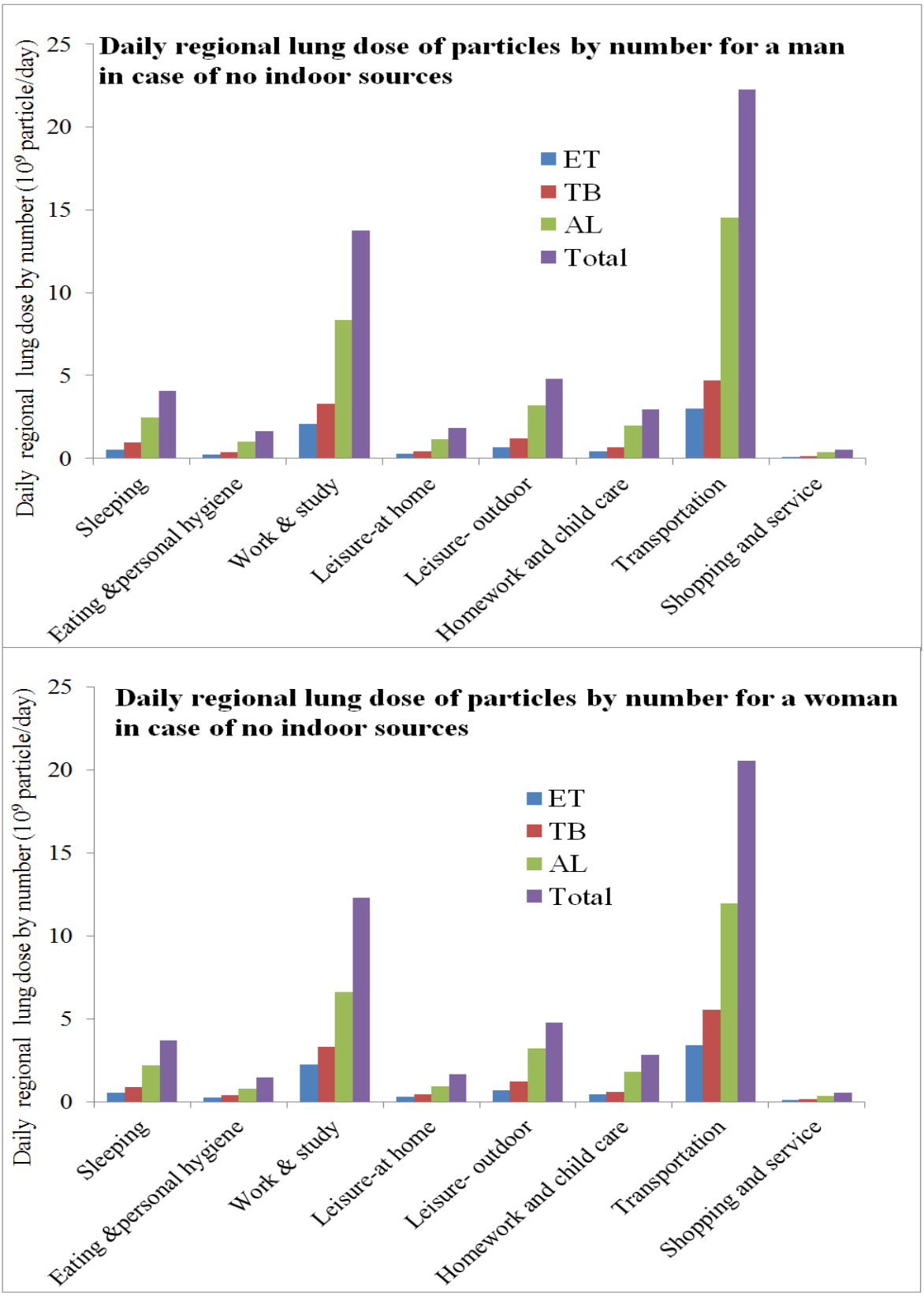

Figure 7.10: Daily regional lung dose of particles by number for a man and a woman in case of no indoor sources.

By considering exposure to particles released by indoors, we assumed time exposure to particles emitted from each indoor sources is about 10 minutes. The daily regional lung dose of particles associated with 10 minutes exposure to each indoor source were estimated and shown in Figure 7.11. Indoor sources have marked effects on both total and regional lung dose. For example, by adding expose to cooking emissions for 10 minutes, daily total deposited dose by number for adults will increase by 4.5 times.

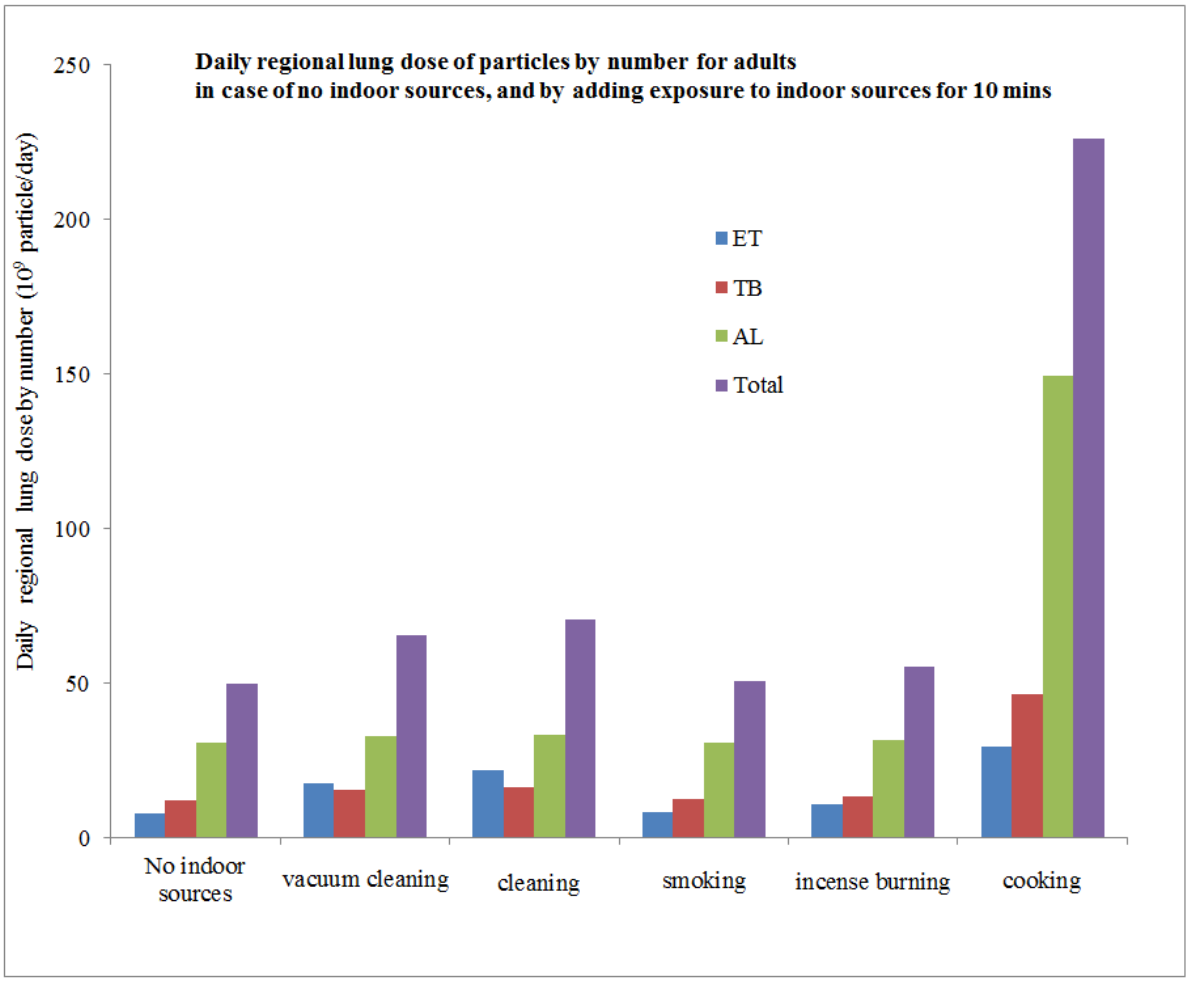

Figure 7.11: A comparison of averaged daily regional lung dose for adults between no indoor source and with exposure to each indoor source for 10 minutes.

7.4. Conclusion

Particles released from indoor activities have many physical properties such as concentration, particle size, particle density and hygroscopicity which are relevant to determining lung deposition. Particles generated from vacuum cleaning and soap/W5 cleaning activities are mainly distributed in the nano size range while those from incense burning and cigarette smoking were found predominantly in the accumulation mode, and those from cooking activity were found in the Aitken mode. Most of the particles released from indoor sources were nearly-hydrophobic, except the particles from soap/W5 cleaning, which were less-hygroscopic. Particles from cleaning activities showed very high total lung deposition fraction by number. This was up to 0.73 and 0.66 for vacuum cleaner and soap/W5 cleaning particles, respectively.

Particles are predicted to deposit by number mainly in the AL region, followed by the TB region. This study found that people could be exposed to high aerosol concentrations due to indoor sources. The minute lung dose of particles during indoor source episodes was found to be much greater than the indoor background level without an indoor source. The total minute lung dose rate of particles from vacuum cleaning, soap/W5 cleaning, smoking and incense burning could be up to 1.6×10^9, 2.2×10^9, 7.2×10^7, 5.4×10^8 particles minute^{-1} respectively, while those for average outdoor and indoor background levels were 1.4×10^7 and 1.0×10^7 particles minute^{-1}. This suggests that indoor sources may make the main contribution to the total lung dose of indoor particles expressed by number.

CHAPTER 8: CONCLUSION

8.1. Summary

In summary, this study has investigated the physical properties (particle number size distribution, hygroscopicity and effective density) of particles measured in different microenvironments, including both outdoor and indoor sources. These properties play very important roles in determining the dose of particles in the human respiratory system. In addition, this study successfully utilized particle number size distributions to apportion the sources of particles using a PMF model. The dynamic processes of particles between outdoor and indoor environments were addressed.

Particle number size distributions were measured at ambient sites (traffic, urban background, and rural areas), microenvironments (a house and, a flat) and a chamber (brake rig test). Atmospheric particle size distributions generated from multiple sources can be described as a sum of log-normal distributions. Each source displays a characteristic modal structure such as peak mode or count median diameter. After emission from the source, particles are subject to various dynamic processes, such as nucleation, coagulation, deposition, condensation or evaporation, which alter their sizes. By number, ultrafine particles, the main contributors to particle number concentration in urban areas, accounted for the majority of particles emitted from combustion sources. Formation of nanoparticles (Dp< 30 nm) has been found from both outdoor sources (i.e. brake emissions) and indoor sources (i.e. cleaning activities). In addition, a mass balance model was used to predict indoor particle size distributions from outdoor PNSD data sets. It was found that a mass balance model can not only accurately predict indoor PNSDs, but can also help us estimate the loss rates of particles. These loss rates depend greatly on both particle size and concentrations. Smaller particles have higher

loss rates. Deposition, coagulation and evaporation play important roles in the determination of indoor PNSDs in a house heavily affected by road traffic emissions.

The typical hygroscopicity of particles shows a wide variation of growth factors among different environments, depending upon local sources and air masses. In urban environments, hydrophobic and less-hygroscopic particles were dominant whereas more-hygroscopic particles were ubiquitous in marine environments. The dominant hydrophobic and less-hygroscopic particles in the urban environments could be explained by the sources of particles at these sites, where traffic-related emissions were found to be the main source of urban ultrafine particles. Freshly emitted traffic particles and biomass burning particles were hydrophobic or less-hygroscopic, whilst growth factors were found to increase during ageing.

This study investigated the hygroscopic properties of particles measured in both outdoor and indoor environments in Prague, Czech Republic. The hygroscopic factor of a particle was found to be a function of its size. Large particles, which normally consist of more-hygroscopic particles, had higher growth factors than small ones. For particles with diameters of 50 nm and 100 nm, two fractions of nearly-hydrophobic (Gf ~1.01-1.11) and less-hygroscopic particles (Gf ~1.11-1.33) were found to be dominant in both indoor and outdoor environments. For particles with diameter of 200 nm, the main fractions of particles were less-hygroscopic and more-hygroscopic particles (Gf ~1.11-1.85). The hygroscopic properties of particles generated from five major indoor sources, including cleaning activities, tobacco smoking, incense burning and cooking, were studied. Most of the particles released from those sources were nearly-hydrophobic, apart from those from soap/W5 cleaning, which were less-hygroscopic. Based on the merger of SMPS and APS data sets, the effective densities of particles from outdoor and indoor environments, and five indoor sources were also investigated. Effective density has no significant effects on the regional lung dose of ultrafine particles because the main deposition mechanism of these particles is diffusion.

This study developed an approach to calculating the dose of particles by considering particle growth in the human respiratory tract due to its hygroscopic properties. It was found that the hygroscopic properties of particles have marked effects, not only on total lung deposition but also on the regional lung deposition of particles, leading to a variation in DFs between the sampling environments. This study estimated the lung deposition fractions of submicron particles emitted from different environments and sources. By number, the lung deposition fractions of particles released from cleaning activities were much higher than those of particles from combustion sources (cooking, incense burning or tobacco smoking). Indoor sources were major contributors to the total daily lung dose of particles by number.

Furthermore, the study combined the PMF and ICRP models to apportion the sources of the lung dose of ambient submicron particles in the human respiratory system (Figure 8.1). It was found that traffic emissions were the most common ambient source of submicron particles deposited by number into the human respiratory tract. They accounted for 67.8% of particles deposited in the total lung by number at the North Kensington site. In terms of regional lung dose, they represented 59%, 68.5% and 70.8% of the total particle number deposited in the ET, TB and AL regions, respectively. Secondary aerosols contributed only approximately 5.1% of submicron particles deposited in the total lung by number, but they represented a major source of particles deposited in the regions and total lung by volume. In terms of deposited particles by surface area, secondary aerosols were found most dominant in the ET region, while the main contributors in the TB, and AL regions were traffic emissions and urban accumulation mode.

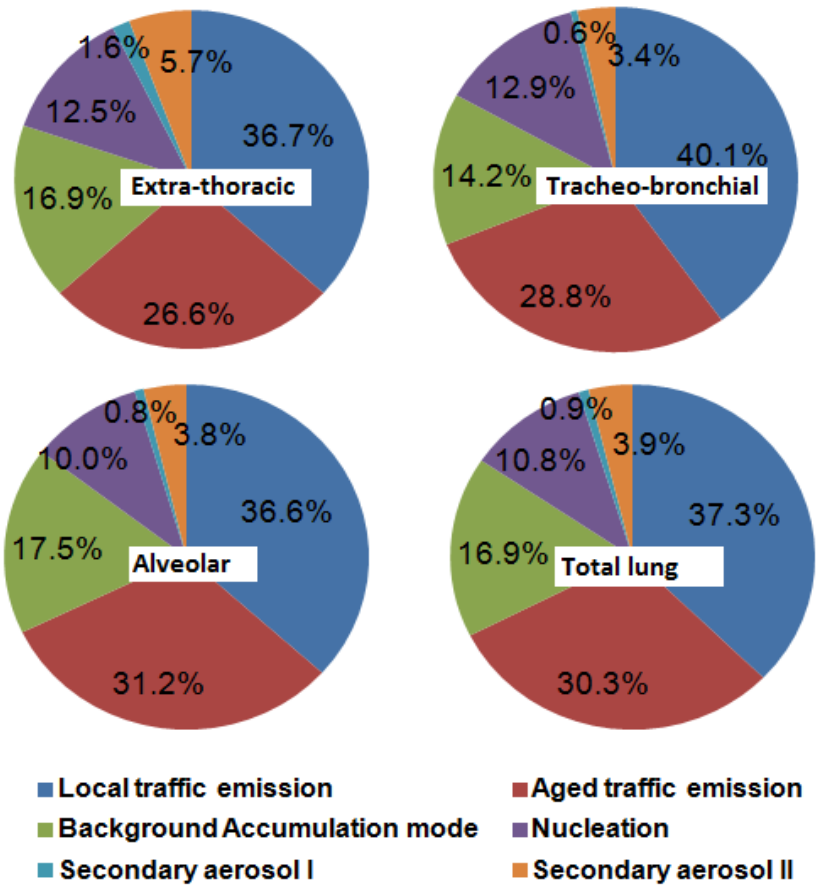

Figure 8.1: Source apportionment of particles deposited in the human respiratory tract.

8.2. Conclusion

This thesis presents a comprehensive data set on physical properties of particles (particle number size distribution, particle density and hygroscopic growth factor) and their implications for human lung dose calculation and source apportionment studies. The key findings obtained from this thesis are given as follows:

- Particle size distributions measured from different micro-environments display different characteristic modal structure such as peak mode or count median diameter. Ultrafine particles are accounted for the majority of particles by number emitted from combustion sources.

- Hygroscopic properties of particles plays an important role for the calculation of the human regional lung dose of particles, particularly for larger particles (Dp >200 nm). Most of the particles released from major indoor sources (vacuum cleaning, smoking, incense burning and cooking) were nearly-hydrophobic, apart from those from soap/W5 cleaning, which were less-hygroscopic.
- The sources of ambient particles deposited in the human respiratory system were successfully estimated by application of both PMF and ICRP models on the PNSD data set. It concludes that traffic emissions were the most common ambient source of submicron particles deposited by number into the human respiratory tract at urban background area.
- Indoor sources have marked effects on daily lung dose of particles in the human respiratory system. For example, daily total deposited dose by number for adults will increase by 4.5 times by adding exposure to cooking emissions for only 10 minutes.

8.3. Implications

This work has made an extensive study of the physical properties of particles. These properties not only provide us with information on atmospheric processes, but they also play vital roles in source apportionment and human exposure studies.

In terms of the source apportionment studies of particles, it has been shown that the sources of particles can be identified by running a PMF model on their number size distributions. In addition, we can apportion the sources of particles in the human respiratory tract based on an application of lung dose models to the PMF results. These findings are useful in identifying which sources are most relevant for deposited particles in the human respiratory tract by different metrics (number, surface area and volume). This therefore helps policy makers to

make decisions on the control of particulate matter. For instance, we should consider traffic emissions first in order to reduce ambient particles by number due their predominant contribution (59.0 - 70.8 %) in both the total and regional lung, whereas we need to consider secondary aerosols and urban accumulation mode mostly urban combustion, if the reduction target is submicron particles by mass.

In terms of human exposure studies, it has been shown that the deposition fraction of particles depends greatly on their size and hygroscopic properties. As a result, particles emitted from different sources shows different deposition fractions in the human respiratory system due to their different size distribution and hygroscopic properties. Estimating the total and regional lung dose of particles can help people control the risk of aerosols. Moreover, this work can be utilized in the toxicology of aerosols.

8.4. Limitations and Future directions

In the study, we have estimated the regional lung dose of particles from ambient environments and indoor sources using the ICRP and MPPD models with consideration of their hygroscopic properties and densities. However, one limitation of the work is that the analysis of size distributions is limited to those within the range of the SMPS. In addition, the H-TDMA system can measure the hygroscopic properties of submicron particles only and therefore particle dose (especially for volume/mass) due to the larger size fractions is not considered. In future studies, the lung dose of large particles should be estimated. (Harrison et al., 2010) suggest that lung dose, not mass metrics ($PM_{2.5}$ and PM_{10}), is the key metric to determine the health outcomes of particle exposure. Hence, this could be usefully linked to epidemiological studies in order to evaluate the consequences of the doses estimated.

Another limitation of this work is that the effects of morphology and the composition of particles on their deposition fraction in the human respiratory tract have not fully considered.

In future studies, a new deposition approach with consideration of particle shape and chemical composition, is needed to estimate the regional lung dose of non-spherical aerosols. In the brake rig test experiments, this study used a closed chamber. However, the PNSD of brake ware particles could be changed due to the dilution with different air ventilation by wind in the real scenarios. And the temperature of pad should be higher in the real scenarios than the lab experiments by the heat transfer from car engine through the shaft. Therefore, in the next experiments PNSD of brake ware particles should be measured in an open chamber with well control of air ventilation and temperature. In addition, more particle number size distributions in other microenvironments such as offices, schools or other working places should be collected in order to estimate the daily lung dose. The lung dose calculation of chemical species associated with aerosols, which can maybe help us understand the toxicity of aerosols, should be addressed in future work.

LIST OF RESEARCH PAPERS AND PRESENTATIONS

❖ **Peer-reviewed Articles**

[1] **Vu, T.V**., J., Ondráček, V., Ždímal, Delgado-Saborit, J.M., Harrison, R. M. (2016). Physical properties and lung deposition of particles emitted from five major indoor sources. Air Quality, Atmosphere & Health journal (accepted).

[2] **Vu, T. V.**, Beddows, D.C.S, Delgado-Saborit, J. M., Harrison, R. M. (2016). Source apportionment of the lung dose of ambient submicrometre particulate matter. Aerosol and Air Quality Research, *DOI: 10.4209/aaqr.2015.09.0553*.

[3] Masiol, M., **Vu, T.V.,** Beddows, D.C.S, Harrison, R.M. (2016). Source apportionment of wide range particle size spectra and black carbon collected at the airport of Venice (Italy). Atmospheric Environment (accepted).

[4] **Vu, T. V.**, Delgado-Saborit, J. M., Harrison, R. M. (2015). A review of hygroscopic growth factors of submicron aerosols from different sources and its implication for calculation of lung deposition efficiency of ambient aerosols. Air Quality, Atmosphere & Health, 8 (5), 429 - 440.

[5] **Vu, T. V.**, Delgado-Saborit, J. M., Harrison, R. M. (2015). A review of particle number size distributions from seven major sources and implications for source apportionment studies. Atmospheric Environment, 122, 114-132.

❖ **Peer-Reviewed Journal Articles in Progress**

[6] **Vu, T.V**., Zauli-Sajani, S., Delgado-Saborit, J.M., Harrison, R. M. Loss processes affecting submicrometre particles in a house heavily affected by road traffic emissions (In manuscript preparation).

❖ **Conferences Presentation**

[1] Vu, T.V., Delgado-Saborit, J.M., Sajani, S.Z, Harrison, R. M. Evaluation of a mass balance model for predicting the penetration, deposition and infiltration rate of submicron particles to the indoor environment. The 4th UK & Ireland Exposure Science Conference, Buxton, UK.

[2] Fonseca, A.S., Talbot, N., Schwarz, J., Ondráček, J., Ždímal, V., Kozáková, J., Viana M., Karanasiou, A., Querol, X., Alastuey, A., **Vu, T.V**., Delgado-Saborit, J.M., Harrison, R. M. (2016). Intercomparison of four different cascade impactors for fine and ultrafine particle sampling in two European locations. European Aerosol Conference (EAC), Milan, Italy

[3] **Vu, T.V.,** Beddows, D.C.S., Sanderson, P., Delgado-Saborit, J.M., Olatunbosun, O., Crooks M.,Harrison, R.M (2015). An investigation into the particle size distribution collected from an automotive brake caliper test rig. European Aerosol Conference (EAC), Milan, Italy.

[4] Masiol, M., Harrison, R.M., **Vu, T.V.**, Squizzato, S., Visin, F (2015) Source apportionment of chemically resolved PM2.5 and particle size spectra collected downwind of London Heathrow (UK): Preliminary results. European Aerosol Conference (EAC), Milan, Italy.

[5] Masiol, M., **Vu, T.V.**, Harrison, R.M (2015) Black carbon and particle number size distributions collected at an international airport located in an area affected by a complex emission scenario. European Aerosol Conference (EAC), Milan, Italy.

[6] **Vu, T. V.,**Ondracek, J., Zdimal, V., Delgado-Saborit, J. M. and Harrison, R. M. Physical properties and lung deposition of particles emitted from five major indoor sources (2015). UK Review Meeting on Outdoor and Indoor Air Pollution Research, Solihull, UK.

[7] **Vu, T.V.,** Masiol, M., Harrison, R.M (2014). Traffic and marine-influenced submicron particle number size distribution in the Venice mainland, Italy. Aerosol Society Annual Conference, Birmingham, UK.

[8] **Vu, T.V.,** Delgado-Saborit J.M., Harrison, R.M (2014). Regional lung dose of submicron aerosol particles in urban background, roadside and rural atmospheres. International Aerosol Conference, Busan, Korea.

[9**] Vu, T.V.,** Beddows D.C.S., Harrison, R.M (2014). Source apportionment of submicron particles deposited in the human respiratory system measured at an urban background site in London. Annual Review Meeting: Outdoor and Indoor Air Pollution Research, Solihull, UK.

REFERENCES

Abbasi, S., Jansson, A., Olander, L., Olofsson, U., Sellgren, U., 2012a. A pin-on-disc study of the rate of airborne wear particle emissions from railway braking materials. Wear 284, 18-29.

Abbasi, S., Olander, L., Larsson, C., Olofsson, U., Jansson, A., Sellgren, U., 2012b. A field test study of airborne wear particles from a running regional train. Proceedings of the Institution of Mechanical Engineers, Part F: Journal of Rail and Rapid Transit 226, 95-109.

Abdullahi, K.L., Delgado-Saborit, J.M., Harrison, R.M., 2013. Emissions and indoor concentrations of particulate matter and its specific chemical components from cooking: A review. Atmospheric Environment 71, 260-294.

Alam, M.K., 1987. The effect of van der Waals and viscous forces on aerosol coagulation. Aerosol Science and Technology 6, 41-52.

Aleksandropoulou, V., Lazaridis, M., 2013. Development and application of a model (ExDoM) for calculating the respiratory tract dose and retention of particles under variable exposure conditions. Air Quality, Atmosphere & Health 6, 13-26.

Anderson, P., Wilson, J., Hiller, F., 1990. Respiratory tract deposition of ultrafine particles in subjects with obstructive or restrictive lung disease. CHEST Journal 97, 1115-1120.

Apte, J.S., Kirchstetter, T.W., Reich, A.H., Deshpande, S.J., Kaushik, G., Chel, A., Marshall, J.D., Nazaroff, W.W., 2011. Concentrations of fine, ultrafine, and black carbon particles in auto-rickshaws in New Delhi, India. Atmospheric Environment 45, 4470-4480.

Asgharian, B., 2004. A model of deposition of hygroscopic particles in the human lung. Aerosol Science and Technology 38, 938-947.

Asgharian, B., Hofmann, W., Bergmann, R., 2001. Particle deposition in a multiple-path model of the human lung. Aerosol Science and Technology 34, 332-339.

Atkinson, R.W., Fuller, G.W., Anderson, H.R., Harrison, R.M., Armstrong, B., 2010. Urban ambient particle metrics and health: a time-series analysis. Epidemiology 21, 501-511.

Baltensperger, U., Streit, N., Weingartner, E., Nyeki, S., Prévôt, A., Van Dingenen, R., Virkkula, A., Putaud, J.P., Even, A., Ten Brink, H., 2002. Urban and rural aerosol characterization of summer smog events during the PIPAPO field campaign in Milan, Italy. Journal of Geophysical Research: Atmospheres (1984–2012) 107, LOP 6-1-LOP 6-14.

Beddows, D., Harrison, R., Green, D., Fuller, G., 2015. Receptor modelling of both particle composition and size distribution from a background site in London, UK. Atmospheric Chemistry and Physics Discussions 15, 10123-10162.

Beddows, D.C., Dall'Osto, M., Harrison, R.M., 2009. Cluster analysis of rural, urban, and curbside atmospheric particle size data. Environmental science & technology 43, 4694-4700.

Beddows, D.C.S., Dall'osto, M., Harrison, R.M., 2010. An Enhanced Procedure for the Merging of Atmospheric Particle Size Distribution Data Measured Using Electrical Mobility and Time-of-Flight Analysers. Aerosol Science and Technology 44, 930-938.

Bennett, D., Koutrakis, P., 2006. Determining the infiltration of outdoor particles in the indoor environment using a dynamic model. Journal of Aerosol Science 37, 766-785.

Bennett, W.D., Zeman, K.L., Kim, C., 1996. Variability of fine particle deposition in healthy adults: effect of age and gender. American journal of respiratory and critical care medicine 153, 1641-1647.

Bhangar, S., Mullen, N., Hering, S., Kreisberg, N., Nazaroff, W., 2011. Ultrafine particle concentrations and exposures in seven residences in northern California. Indoor Air 21, 132-144.

Bigi, A., Harrison, R.M., 2010. Analysis of the air pollution climate at a central urban background site. Atmospheric Environment 44, 2004-2012.

Boy, M., Petäjä, T., Maso, M.D., Rannik, Ü., Rinne, J., Aalto, P., Laaksonen, A., Vaattovaara, P., Joutsensaari, J., Hoffmann, T., 2004. Overview of the field measurement campaign in Hyytiälä, August 2001 in the framework of the EU project OSOA. Atmospheric Chemistry and Physics 4, 657-678.

Broday, D.M., Georgopoulos, P.G., 2001. Growth and deposition of hygroscopic particulate matter in the human lungs. Aerosol Science and Technology 34, 144-159.

Brown, J.S., Zeman, K.L., Bennett, W.D., 2002. Ultrafine particle deposition and clearance in the healthy and obstructed lung. American Journal of Respiratory and Critical Care Medicine 166, 1240-1247.

Buonanno, G., Giovinco, G., Morawska, L., Stabile, L., 2011. Tracheobronchial and alveolar dose of submicrometer particles for different population age groups in Italy. Atmospheric Environment 45, 6216-6224.

Buonanno, G., Morawska, L., Stabile, L., 2009. Particle emission factors during cooking activities. Atmospheric Environment 43, 3235-3242.

Busch, B., Kandler, K., Schütz, L., Neusüß, C., 2002. Hygroscopic properties and water-soluble volume fraction of atmospheric particles in the diameter range from 50 nm to 3.8 μm during LACE 98. Journal of Geophysical Research: Atmospheres (1984–2012) 107, LAC 2-1-LAC 2-11.

Buzorius, G., McNaughton, C., Clarke, A., Covert, D., Blomquist, B., Nielsen, K., Brechtel, F., 2004. Secondary aerosol formation in continental outflow conditions during ACE-Asia. Journal of Geophysical Research: Atmospheres (1984–2012) 109.

Carpenter, L., Sturges, W., Penkett, S., Liss, P., Alicke, B., Hebestreit, K., Platt, U., 1999. Short-lived alkyl iodides and bromides at Mace Head, Ireland: Links to biogenic sources and halogen oxide production. Journal of Geophysical Research: Atmospheres (1984–2012) 104, 1679-1689.

Carslaw, D.C., Ropkins, K., 2012. Openair—an R package for air quality data analysis. Environmental Modelling & Software 27, 52-61.

Chalupa, D.C., Morrow, P.E., Oberdörster, G., Utell, M.J., Frampton, M.W., 2004. Ultrafine particle deposition in subjects with asthma. Environmental Health Perspectives 112, 879.

Chan, H.-K., Eberl, S., Daviskas, E., Constable, C., Young, I., 2002. Changes in lung deposition of aerosols due to hygroscopic growth: a fast SPECT study. Journal of Aerosol Medicine 15, 307-311.

Chao, C.Y., Wan, M., Cheng, E.C., 2003. Penetration coefficient and deposition rate as a function of particle size in non-smoking naturally ventilated residences. Atmospheric Environment 37, 4233-4241.

Charron, A., Birmili, W., Harrison, R.M., 2007. Factors influencing new particle formation at the rural site, Harwell, United Kingdom. Journal of Geophysical Research: Atmospheres (1984–2012) 112.

Charron, A., Birmili, W., Harrison, R.M., 2008. Fingerprinting particle origins according to their size distribution at a UK rural site. Journal of Geophysical Research: Atmospheres (1984–2012) 113.

Charron, A., Degrendele, C., Laongsri, B., Harrison, R.M., 2013. Receptor modelling of secondary and carbonaceous particulate matter at a southern UK site. Atmospheric Chemistry and Physics 13, 1879-1894.

Charron, A., Harrison, R.M., 2003. Primary particle formation from vehicle emissions during exhaust dilution in the roadside atmosphere. Atmospheric Environment 37, 4109-4119.

Chen, C., Zhao, B., 2011. Review of relationship between indoor and outdoor particles: I/O ratio, infiltration factor and penetration factor. Atmospheric Environment 45, 275-288.

Chen, L.-Y., Jeng, F.-T., Chen, C.-C., Hsiao, T.-C., 2003. Hygroscopic behavior of atmospheric aerosol in Taipei. Atmospheric Environment 37, 2069-2075.

Cruz, C.N., Pandis, S.N., 2000. Deliquescence and hygroscopic growth of mixed inorganic-organic atmospheric aerosol. Environmental Science and Technology 34, 4313-4319.

Daigle, C.C., Chalupa, D.C., Gibb, F.R., Morrow, P.E., Oberdörster, G., Utell, M.J., Frampton, M.W., 2003. Ultrafine particle deposition in humans during rest and exercise. Inhalation Toxicology 15, 539-552.

Dall'Osto, M., Beddows, D., Pey, J., Rodriguez, S., Alastuey, A., Harrison, R.M., Querol, X., 2012. Urban aerosol size distributions over the Mediterranean city of Barcelona, NE Spain. Atmospheric Chemistry and Physics 12, 10693-10707.

DeCarlo, P.F., Slowik, J.G., Worsnop, D.R., Davidovits, P., Jimenez, J.L., 2004. Particle morphology and density characterization by combined mobility and aerodynamic diameter measurements. Part 1: Theory. Aerosol Science and Technology 38, 1185-1205.

Decesari, S., Facchini, M., Matta, E., Mircea, M., Fuzzi, S., Chughtai, A., Smith, D., 2002. Water soluble organic compounds formed by oxidation of soot. Atmospheric Environment 36, 1827-1832.

Delgado-Saborit, J.M., Aquilina, N.J., Meddings, C., Baker, S., Harrison, R.M., 2011. Relationship of personal exposure to volatile organic compounds to home, work and fixed site outdoor concentrations. Science of the Total Environment 409, 478-488.

Diffey, B.L., 2011. An overview analysis of the time people spend outdoors. British Journal of Dermatology 164, 848-854.

Dinar, E., Mentel, T.F., Rudich, Y., 2006. The density of humic acids and humic like substances (HULIS) from fresh and aged wood burning and pollution aerosol particles. Atmospheric Chemistry and Physics 6, 5213-5224.

Donaldson, K., Li, X., MacNee, W., 1998. Ultrafine (nanometre) particle mediated lung injury. Journal of Aerosol Science 29, 553-560.

Donaldson, K., Stone, V., Seaton, A., MacNee, W., 2001. Ambient particle inhalation and the cardiovascular system: potential mechanisms. Environmental Health Perspect 109 Suppl 4, 523-527.

Dua, S., Hopke, P., 1996. Hygroscopic growth of assorted indoor aerosols. Aerosol Science and Technology 24, 151-160.

Dua, S., Hopke, P., Raunemaa, T., 1999. Hygroscopicity of diesel aerosols. Water, Air, and Soil Pollution 112, 247-257.

Dusek, U., Frank, G., Massling, A., Zeromskiene, K., Iinuma, Y., Schmid, O., Helas, G., Hennig, T., Wiedensohler, A., Andreae, M., 2011. Water uptake by biomass burning aerosol at sub-and supersaturated conditions: closure studies and implications for the role of organics. Atmospheric Chemistry and Physics 11, 9519-9532.

Ehn, M., Petäjä, T., Aufmhoff, H., Aalto, P., Hämeri, K., Arnold, F., Laaksonen, A., Kulmala, M., 2007. Hygroscopic properties of ultrafine aerosol particles in the boreal forest: diurnal variation, solubility and the influence of sulfuric acid. Atmospheric Chemistry and Physics 7, 211-222.

Elihn, K., Berg, P., Lidén, G., 2011. Correlation between airborne particle concentrations in seven industrial plants and estimated respiratory tract deposition by number, mass and elemental composition. Journal of Aerosol Science 42, 127-141.

EPA, U.S. Environmental Protection Agency, 2009. Metabolically derived human ventilation rates: A revised approach based upon oxygen consumption rates. National Center for Environmental Assessment, Office of Research and Development (2009) EPA/600/R-06/129F

Ferron, G., 1977. The size of soluble aerosol particles as a function of the humidity of the air. Application to the human respiratory tract. Journal of Aerosol Science 8, 251-267.

Ferron, G., Karg, E., Busch, B., Heyder, J., 2005. Ambient particles at an urban, semi-urban and rural site in Central Europe: hygroscopic properties. Atmospheric Environment 39, 343-352.

Ferron, G., Kreyling, W., Haider, B., 1988. Inhalation of salt aerosol particles—II. Growth and deposition in the human respiratory tract. Journal of Aerosol Science 19, 611-631.

Finlay, W., Stapleton, K., 1995. The effect on regional lung deposition of coupled heat and mass transfer between hygroscopic droplets and their surrounding phase. Journal of Aerosol Science 26, 655-670.

Fors, E., Swietlicki, E., Svenningsson, B., Kristensson, A., Frank, G., Sporre, M., 2011. Hygroscopic properties of the ambient aerosol in southern Sweden–a two year study. Atmospheric Chemistry and Physics 11, 8343-8361.

Garg, B.D., Cadle, S.H., Mulawa, P.A., Groblicki, P.J., Laroo, C., Parr, G.A., 2000. Brake wear particulate matter emissions. Environmental science & technology 34, 4463-4469.

Géhin, E., Ramalho, O., Kirchner, S., 2008. Size distribution and emission rate measurement of fine and ultrafine particle from indoor human activities. Atmospheric Environment 42, 8341-8352.

Grigoratos, T., Martini, G., 2015. Brake wear particle emissions: a review. Environmental Science and Pollution Research 22, 2491-2504.

Gu, J., Pitz, M., Schnelle-Kreis, J., Diemer, J., Reller, A., Zimmermann, R., Soentgen, J., Stoelzel, M., Wichmann, H.E., Peters, A., Cyrys, J., 2011. Source apportionment of ambient particles: Comparison of positive matrix factorization analysis applied to particle size distribution and chemical composition data. Atmospheric Environment 45, 1849-1857.

Gysel, M., McFiggans, G., Coe, H., 2009. Inversion of tandem differential mobility analyser (TDMA) measurements. Journal of Aerosol Science 40, 134-151.

Hallquist, M., Wenger, J., Baltensperger, U., Rudich, Y., Simpson, D., Claeys, M., Dommen, J., Donahue, N., George, C., Goldstein, A., 2009. The formation, properties and impact of secondary organic aerosol: current and emerging issues. Atmospheric Chemistry and Physics 9, 5155-5236.

Hämeri, K., Väkevä, M., Aalto, P., Kulmala, M., Swietlicki, E., Zhou, J., Seidl, W., Becker, E., O'dowd, C., 2001. Hygroscopic and CCN properties of aerosol particles in boreal forests. Tellus B 53, 359-379.

Happonen, M., Heikkilä, J., Aakko-Saksa, P., Murtonen, T., Lehto, K., Rostedt, A., Sarjovaara, T., Larmi, M., Keskinen, J., Virtanen, A., 2013. Diesel exhaust emissions and particle hygroscopicity with HVO fuel-oxygenate blend. Fuel 103, 380-386.

Harrison, R.M., Beddows, D.C., Dall'Osto, M., 2011. PMF analysis of wide-range particle size spectra collected on a major highway. Environmental Science and Technology 45, 5522-5528.

Harrison, R.M., Delgado-Saborit, J.M., Baker, S.J., Aquilina, N., Meddings, C., Harrad, S., Matthews, I., Vardoulakis, S., Anderson, H., 2009. Measurement and modeling of exposure to selected air toxics for health effects studies and verification by biomarkers. Research report (Health Effects Institute), 3-96; discussion 97-100.

Harrison, R.M., Giorio, C., Beddows, D.C., Dall'Osto, M., 2010. Size distribution of airborne particles controls outcome of epidemiological studies. Science of the Total Environment 409, 289-293.

He, C., Morawska, L., Hitchins, J., Gilbert, D., 2004. Contribution from indoor sources to particle number and mass concentrations in residential houses. Atmospheric Environment 38, 3405-3415.

Held, A., Zerrath, A., McKeon, U., Fehrenbach, T., Niessner, R., Plass-Dülmer, C., Kaminski, U., Berresheim, H., Pöschl, U., 2008. Aerosol size distributions measured in urban, rural and high-alpine air with an electrical low pressure impactor (ELPI). Atmospheric Environment 42, 8502-8512.

Helsper, C., Mölter, W., Löffler, F., Wadenpohl, C., Kaufmann, S., Wenninger, G., 1993. Investigations of a new aerosol generator for the production of carbon aggregate particles. Atmospheric Environment. Part A. General Topics 27, 1271-1275.

Hildemann, L.M., Markowski, G.R., Cass, G.R., 1991. Chemical composition of emissions from urban sources of fine organic aerosol. Environmental Science and Technology 25, 744-759.

Hiller, F.C., 1991. Health implications of hygroscopic particle growth in the human respiratory tract. Journal of Aerosol Medicine 4, 1-23.

Hinds, W.C., 1999. Aerosol Technology: Properties. Behavior, and Measurement of airborne Particles (2^{nd}). Wiley Interscience.

Hofmann, W., 2011. Modelling inhaled particle deposition in the human lung—a review. Journal of Aerosol Science 42, 693-724.

Hofmann, W., Martonen, T., Graham, R., 1989. Predicted deposition of nonhygroscopic aerosols in the human lung as a function of subject age. Journal of Aerosol Medicine 2, 49-68.

Hussein, T., Glytsos, T., Ondráček, J., Dohányosová, P., Ždímal, V., Hämeri, K., Lazaridis, M., Smolík, J., Kulmala, M., 2006. Particle size characterization and emission rates during indoor activities in a house. Atmospheric Environment 40, 4285-4307.

Hussein, T., Londahl, J., Paasonen, P., Koivisto, A.J., Petaja, T., Hameri, K., Kulmala, M., 2013. Modeling regional deposited dose of submicron aerosol particles. Science of the Total Environment 458-460, 140-149.

Hussein, T., Wierzbicka, A., Löndahl, J., Lazaridis, M., Hänninen, O., 2015. Indoor aerosol modeling for assessment of exposure and respiratory tract deposited dose. Atmospheric Environment 106, 402-411.

ICRP, 1994. ICRP Publication 66: Human Respiratory Tract Model for Radiological Protection. Elsevier Health Sciences.

Iijima, A., Sato, K., Yano, K., Tago, H., Kato, M., Kimura, H., Furuta, N., 2007. Particle size and composition distribution analysis of automotive brake abrasion dusts for the evaluation of antimony sources of airborne particulate matter. Atmospheric Environment 41, 4908-4919.

Ingham, D., 1975. Diffusion of aerosols from a stream flowing through a cylindrical tube. Journal of Aerosol Science 6, 125-132.

Jacobson, M.Z., 1994. Developing, Coupling, and Applying a Gas, Aerosol, Transport, and Radiation Model to Study Urban and Regional Air Pollution. PhD thesis. Univesity of California, Los Angeles.

Jacobson, M.Z., 2005. Fundamentals of atmospheric modeling. Cambridge University Press.

Jacobson, M.Z., Seinfeld, J.H., 2004. Evolution of nanoparticle size and mixing state near the point of emission. Atmospheric Environment 38, 1839-1850.

Janhäll, S., Andreae, M.O., Pöschl, U., 2010. Biomass burning aerosol emissions from vegetation fires: particle number and mass emission factors and size distributions. Atmospheric Chemistry and Physics 10, 1427-1439.

Jeong, C.-H., Evans, G.J., 2009. Inter-comparison of a fast mobility particle sizer and a scanning mobility particle sizer incorporating an ultrafine water-based condensation particle counter. Aerosol Science and Technology 43, 364-373.

Ji, X., Le Bihan, O., Ramalho, O., Mandin, C., D'Anna, B., Martinon, L., Nicolas, M., Bard, D., Pairon, J.C., 2010. Characterization of particles emitted by incense burning in an experimental house. Indoor Air 20, 147-158.

Jimenez, J., Canagaratna, M., Donahue, N., Prevot, A., Zhang, Q., Kroll, J., DeCarlo, P., Allan, J., Coe, H., Ng, N., 2009. Evolution of organic aerosols in the atmosphere. Science 326, 1525-1529.

Joodatnia, P., Kumar, P., Robins, A., 2013. Fast response sequential measurements and modelling of nanoparticles inside and outside a car cabin. Atmospheric Environment 71, 364-375.

Jung, J., Adams, P.J., Pandis, S.N., 2006. Simulating the size distribution and chemical composition of ultrafine particles during nucleation events. Atmospheric Environment 40, 2248-2259.

Kamilli, K., Poulain, L., Held, A., Nowak, A., Birmili, W., Wiedensohler, A., 2014. Hygroscopic properties of the Paris urban aerosol in relation to its chemical composition. Atmospheric Chemistry and Physics 14, 737-749.

Kaminski, H., Kuhlbusch, T.A., Rath, S., Götz, U., Sprenger, M., Wels, D., Polloczek, J., Bachmann, V., Dziurowitz, N., Kiesling, H.-J., 2013. Comparability of mobility particle sizers and diffusion chargers. Journal of Aerosol Science 57, 156-178.

Kasumba, J., Hopke, P.K., Chalupa, D.C., Utell, M.J., 2009. Comparison of sources of submicron particle number concentrations measured at two sites in Rochester, NY. Science of the Total Environment 407, 5071-5084.

Kim, C.S., Kang, T.C., 1997. Comparative measurement of lung deposition of inhaled fine particles in normal subjects and patients with obstructive airway disease. American Journal of Respiratory and Critical Care Medicine 155, 899-905.

Kim, E., Hopke, P.K., Larson, T.V., Covert, D.S., 2003. Analysis of ambient particle size distributions using unmix and positive matrix factorization. Environmental Science and Technology 38, 202-209.

Kittelson, D.B., 1998. Engines and nanoparticles: a review. Journal of Aerosol Science 29, 575-588.

Knibbs, L.D., He, C., Duchaine, C., Morawska, L., 2011. Vacuum cleaner emissions as a source of indoor exposure to airborne particles and bacteria. Environmental Science and Technology 46, 534-542.

Koblinger, L., Hofmann, W., 1990. Monte Carlo modeling of aerosol deposition in human lungs. Part I: Simulation of particle transport in a stochastic lung structure. Journal of Aerosol Science 21, 661-674.

Kotchenruther, R.A., Hobbs, P.V., 1998. Humidification factors of aerosols from biomass burning in Brazil. Journal of Geophysical Research: Atmospheres (1984–2012) 103, 32081-32089.

Kotzick, R., Niessner, R., 1999. The effects of aging processes on critical supersaturation ratios of ultrafine carbon aerosols. Atmospheric Environment 33, 2669-2677.

Kreyling, W.G., Semmler, M., Möller, W., 2004. Dosimetry and toxicology of ultrafine particles. Journal of Aerosol Medicine 17, 140-152.

Kristensson, A., Rissler, J., Löndahl, J., Johansson, C., Swietlicki, E., 2013. Size-resolved respiratory tract deposition of sub-micrometer aerosol particles in a residential area with wintertime wood combustion. Aerosol and Air Quality Research 13, 24-35.

Kuhn, T., Krudysz, M., Zhu, Y., Fine, P.M., Hinds, W.C., Froines, J., Sioutas, C., 2005. Volatility of indoor and outdoor ultrafine particulate matter near a freeway. Journal of Aerosol Science 36, 291-302.

Kukutschová, J., Moravec, P., Tomášek, V., Matějka, V., Smolík, J., Schwarz, J., Seidlerová, J., Šafářová, K., Filip, P., 2011. On airborne nano/micro-sized wear particles released from low-metallic automotive brakes. Environmental Pollution 159, 998-1006.

Kumar, P., Morawska, L., Birmili, W., Paasonen, P., Hu, M., Kulmala, M., Harrison, R.M., Norford, L., Britter, R., 2014. Ultrafine particles in cities. Environment International 66, 1-10.

Kumar, P., Morawska, L., Harrison, R.M., 2013. Nanoparticles in European cities and associated health impacts, Urban Air Quality in Europe. Springer, pp. 339-365.

Kumar, P., Robins, A., Vardoulakis, S., Britter, R., 2010. A review of the characteristics of nanoparticles in the urban atmosphere and the prospects for developing regulatory controls. Atmospheric Environment 44, 5035-5052.

Kurth, L.M., McCawley, M., Hendryx, M., Lusk, S., 2014. Atmospheric particulate matter size distribution and concentration in West Virginia coal mining and non-mining areas. Journal of Exposure Science and Environmental Epidemiology 24, 405-411.

Kwak, J., Lee, S., Lee, S., 2014. On-road and laboratory investigations on non-exhaust ultrafine particles from the interaction between the tire and road pavement under braking conditions. Atmospheric Environment 97, 195-205.

Lai, A.C., Nazaroff, W.W., 2000. Modeling indoor particle deposition from turbulent flow onto smooth surfaces. Journal of Aerosol Science 31, 463-476.

Langer, S., Moldanová, J., Arrhenius, K., Ljungström, E., Ekberg, L., 2008. Ultrafine particles produced by ozone/limonene reactions in indoor air under low/closed ventilation conditions. Atmospheric Environment 42, 4149-4159.

Lee, E., Chan, C.K., Paatero, P., 1999. Application of positive matrix factorization in source apportionment of particulate pollutants in Hong Kong. Atmospheric Environment 33, 3201-3212.

Lelieveld, J., Evans, J., Fnais, M., Giannadaki, D., Pozzer, A., 2015. The contribution of outdoor air pollution sources to premature mortality on a global scale. Nature 525, 367-371.

Li, W., Hopke, P., 1993. Initial size distributions and hygroscopicity of indoor combustion aerosol particles. Aerosol Science and Technology 19, 305-316.

Lighty, J.S., Veranth, J.M., Sarofim, A.F., 2000. Combustion aerosols: factors governing their size and composition and implications to human health. Journal of the Air & Waste Management Association 50, 1565-1618.

Lioy, P.J., Wainman, T., Zhang, J., Goldsmith, S., 1999. Typical household vacuum cleaners: the collection efficiency and emissions characteristics for fine particles. Journal of the Air & Waste Management Association 49, 200-206.

Liu, D.-L., Nazaroff, W.W., 2003. Particle penetration through building cracks. Aerosol Science and Technology 37, 565-573.

Löndahl, J., Massling, A., Pagels, J., Swietlicki, E., Vaclavik, E., Loft, S., 2007. Size-resolved respiratory-tract deposition of fine and ultrafine hydrophobic and hygroscopic aerosol particles during rest and exercise. Inhalation Toxicology 19, 109-116.

Löndahl, J., Massling, A., Swietlicki, E., Bräuner, E.V., Ketzel, M., Pagels, J., Loft, S., 2009. Experimentally determined human respiratory tract deposition of airborne particles at a busy street. Environmental science & technology 43, 4659-4664.

Löndahl, J., Möller, W., Pagels, J.H., Kreyling, W.G., Swietlicki, E., Schmid, O., 2014. Measurement techniques for respiratory tract deposition of airborne nanoparticles: A critical review. Journal of Aerosol Medicine and Pulmonary Drug Delivery 27, 229-254.

Londahl, J., Swietlicki, E., Rissler, J., Bengtsson, A., Boman, C., Blomberg, A., Sandstrom, T., 2012. Experimental determination of the respiratory tract deposition of diesel combustion particles in patients with chronic obstructive pulmonary disease. Part Fibre Toxicol 9, 23.

Long, C.M., Suh, H.H., Catalano, P.J., Koutrakis, P., 2001. Using time-and size-resolved particulate data to quantify indoor penetration and deposition behavior. Environmental Science and Technology 35, 2089-2099.

Martin, M., Tritscher, T., Juranyi, Z., Heringa, M.F., Sierau, B., Weingartner, E., Chirico, R., Gysel, M., Prévôt, A.S., Baltensperger, U., 2013. Hygroscopic properties of fresh and aged wood burning particles. Journal of Aerosol Science 56, 15-29.

Martonen, T., Rosati, J., Isaacs, K., 2005. Modeling deposition of inhaled particles. Aerosols Handbook. Measurement, Dosimetry and Health Effects. CRC Press, Boca Raton, 113-155.

Massling, A., Stock, M., Wehner, B., Wu, Z., Hu, M., Brüggemann, E., Gnauk, T., Herrmann, H., Wiedensohler, A., 2009. Size segregated water uptake of the urban submicrometer aerosol in Beijing. Atmospheric Environment 43, 1578-1589.

Massling, A., Stock, M., Wiedensohler, A., 2005. Diurnal, weekly, and seasonal variation of hygroscopic properties of submicrometer urban aerosol particles. Atmospheric Environment 39, 3911-3922.

Mathissen, M., Scheer, V., Vogt, R., Benter, T., 2011. Investigation on the potential generation of ultrafine particles from the tire–road interface. Atmospheric Environment 45, 6172-6179.

Meier, J., Wehner, B., Massling, A., Birmili, W., Nowak, A., Gnauk, T., Brüggemann, E., Herrmann, H., Min, H., Wiedensohler, A., 2009. Hygroscopic growth of urban aerosol particles in Beijing (China) during wintertime: a comparison of three experimental methods. Atmospheric Chemistry and Physics 9, 6865-6880.

Mochida, M., Kawamura, K., 2004. Hygroscopic properties of levoglucosan and related organic compounds characteristic to biomass burning aerosol particles. Journal of Geophysical Research: Atmospheres (1984–2012) 109.

Montoya, L., Lawrence, J., Murthy, G.K., Sarnat, J., Godleski, J., Koutrakis, P., 2004. Continuous measurements of ambient particle deposition in human subjects. Aerosol Science and Technology 38, 980-990.

Morawska, L., Afshari, A., Bae, G., Buonanno, G., Chao, C., Hänninen, O., Hofmann, W., Isaxon, C., Jayaratne, E., Pasanen, P., 2013. Indoor aerosols: from personal exposure to risk assessment. Indoor Air 23, 462-487.

Morawska, L., Hofmann, W., Hitchins-Loveday, J., Swanson, C., Mengersen, K., 2005. Experimental study of the deposition of combustion aerosols in the human respiratory tract. Journal of Aerosol Science 36, 939-957.

Morawska, L., Ristovski, Z., Jayaratne, E., Keogh, D.U., Ling, X., 2008. Ambient nano and ultrafine particles from motor vehicle emissions: Characteristics, ambient processing and implications on human exposure. Atmospheric Environment 42, 8113-8138.

Morrow, P.E., 1986. Factors determining hygroscopic aerosol deposition in airways. Physiol. Rev 66, 330-376.

Mortensen, J., Stout, L., Bagley, B., Burkart, J., Schaap, R., Crapo, J., Smolko, E., Miller, F., Graham, J., Hayes, A., 1989. Age related morphometric analysis of human lung casts. Extrapolation of Dosimetric Relationships for Inhaled Particles and Gases, 59-68.

Mortensen, J., Young, J.D., Stout, L., Stout, A., Bagley, B., Schaap, R.N., 1983. A numerical identification syterm for airways in the lung. The Anatomical Record 206, 103-114.

Mosleh, M., Blau, P.J., Dumitrescu, D., 2004. Characteristics and morphology of wear particles from laboratory testing of disk brake materials. Wear 256, 1128-1134.

Müller, H., 1928. Zur allgemeinen Theorie ser raschen Koagulation. Fortschrittsberichte über Kolloide und Polymere 27, 223-250.

Nazaroff, W.W., Weschler, C.J., 2004. Cleaning products and air fresheners: exposure to primary and secondary air pollutants. Atmospheric Environment 38, 2841-2865.

Novák, J., Sýkora, L., 2007. A city in Motion: Time-space activity and mobility patterns of suberban inhabitants and the structration of the spatial organization of the Prague metropolitan area. Geografiska Annaler: Series B, Human Geography 89, 147-168.

O'Dowd, C.D., Hämeri, K., Mäkelä, J.M., Pirjola, L., Kulmala, M., Jennings, S.G., Berresheim, H., Hansson, H.C., de Leeuw, G., Kunz, G.J., 2002a. A dedicated study of New Particle Formation and Fate in the Coastal Environment (PARFORCE): Overview of

objectives and achievements. Journal of Geophysical Research: Atmospheres (1984–2012) 107, PAR 1-1-PAR 1-16.

O'Dowd, C.D., Jimenez, J.L., Bahreini, R., Flagan, R.C., Seinfeld, J.H., Hämeri, K., Pirjola, L., Kulmala, M., Jennings, S.G., Hoffmann, T., 2002b. Marine aerosol formation from biogenic iodine emissions. Nature 417, 632-636.

Olofsson, U., 2011. A study of airborne wear particles generated from the train traffic—Block braking simulation in a pin-on-disc machine. Wear 271, 86-91.

Ogulei, D., Hopke, P., Wallace, L., 2006a. Analysis of indoor particle size distributions in an occupied townhouse using positive matrix factorization. Indoor Air 16, 204-215.

Ogulei, D., Hopke, P.K., Chalupa, D.C., Utell, M.J., 2007. Modeling source contributions to submicron particle number concentrations measured in Rochester, New York. Aerosol Science and Technology 41, 179-201.

Ogulei, D., Hopke, P.K., Zhou, L., Pancras, J.P., Nair, N., Ondov, J.M., 2006b. Source apportionment of Baltimore aerosol from combined size distribution and chemical composition data. Atmospheric Environment 40, 396-410.

Park, K., Kim, J.-S., Park, S.H., 2009. Measurements of hygroscopicity and volatility of atmospheric ultrafine particles during ultrafine particle formation events at urban, industrial, and coastal sites. Environmental science & technology 43, 6710-6716.

Petäjä, T., Kerminen, V.-M., Maso, M.D., Junninen, H., Koponen, I., Hussein, T., Aalto, P., Andronopoulos, S., Robin, D., Hämeri, K., 2007. Sub-micron atmospheric aerosols in the surroundings of Marseille and Athens: physical characterization and new particle formation. Atmospheric Chemistry and Physics 7, 2705-2720.

Peters, A., Wichmann, H.E., Tuch, T., Heinrich, J., Heyder, J., 1997. Respiratory effects are associated with the number of ultrafine particles. American Journal of Respiratory and Critical Care Medicine 155, 1376-1383.

Petters, M., Kreidenweis, S., 2007. A single parameter representation of hygroscopic growth and cloud condensation nucleus activity. Atmospheric Chemistry and Physics 7, 1961-1971.

Pey, J., Querol, X., Alastuey, A., Rodríguez, S., Putaud, J.P., Van Dingenen, R., 2009. Source apportionment of urban fine and ultra-fine particle number concentration in a Western Mediterranean city. Atmospheric Environment 43, 4407-4415.

Pope, C.A., Dockery, D.W., 2006. Health Effects of Fine Particulate Air Pollution: Lines that Connect. Journal of the Air & Waste Management Association 56, 709-742.

Protection, N.C.o.R., Measurements, 1997. Deposition, Retention, and Dosimetry of Inhaled Radioactive Substances: Recommendations of the National Council on Radiation Protection and Measurements. National Council on Radiation Protection and Measurements.

Reid, J., Koppmann, R., Eck, T., Eleuterio, D., 2005. A review of biomass burning emissions part II: intensive physical properties of biomass burning particles. Atmospheric Chemistry and Physics 5, 799-825.

Reid, J.S., Hobbs, P.V., 1998. Physical and optical properties of young smoke from individual biomass fires in Brazil. Journal of Geophysical Research: Atmospheres (1984–2012) 103, 32013-32030.

Reutter, P., Su, H., Trentmann, J., Simmel, M., Rose, D., Gunthe, S., Wernli, H., Andreae, M., Pöschl, U., 2009. Aerosol-and updraft-limited regimes of cloud droplet formation: influence of particle number, size and hygroscopicity on the activation of cloud condensation nuclei (CCN). Atmospheric Chemistry and Physics 9, 7067-7080.

Rissler, J., Svenningsson, B., Fors, E.O., Bilde, M., Swietlicki, E., 2010. An evaluation and comparison of cloud condensation nucleus activity models: Predicting particle critical saturation from growth at subsaturation. Journal of Geophysical Research: Atmospheres (1984–2012) 115.

Rissler, J., Swietlicki, E., Bengtsson, A., Boman, C., Pagels, J., Sandström, T., Blomberg, A., Löndahl, J., 2012. Experimental determination of deposition of diesel exhaust particles in the human respiratory tract. Journal of Aerosol Science 48, 18-33.

Rissler, J., Vestin, A., Swietlicki, E., Fisch, G., Zhou, J., Artaxo, P., Andreae, M., 2006. Size distribution and hygroscopic properties of aerosol particles from dry-season biomass burning in Amazonia. Atmospheric Chemistry and Physics 6, 471-491.

Ristovski, Z., Jayaratne, E., Lim, M., Ayoko, G.A., Morawska, L., 2006. Influence of diesel fuel sulfur on nanoparticle emissions from city buses. Environmental science & technology 40, 1314-1320.

Rogers, C., Hudson, J., Zielinska, B., Tanner, R., Hallett, J., Watson, J., 1991. Cloud condensation nuclei from biomass burning, Global biomass burning. Atmospheric, Climatic, and Biospheric Implications.

Rohr, A.C., 2013. The health significance of gas- and particle-phase terpene oxidation products: A review. Environment International 60, 145-162.

Rose, D., Nowak, A., Achtert, P., Wiedensohler, A., Hu, M., Shao, M., Zhang, Y., Andreae, M., Pöschl, U., 2008. Cloud condensation nuclei in polluted air and biomass burning smoke near the mega-city Guangzhou, China–Part 1: Size-resolved measurements and implications for the modeling of aerosol particle hygroscopicity and CCN activity. Atmospheric Chemistry and Physics Discussions 8, 17343-17392.

Rudolf, G., Köbrich, R., Stahlhofen, W., 1990. Modelling and algebraic formulation of regional aerosol deposition in man. Journal of Aerosol Science 21, S403-S406.

Ruzer, L.S., Harley, N.H., 2012. Aerosols handbook: measurement, dosimetry, and health effects. CRC press.

Sajani, S.Z., Ricciardelli, I., Trentini, A., Bacco, D., Maccone, C., Castellazzi, S., Lauriola, P., Poluzzi, V., Harrison, R.M., 2015. Spatial and indoor/outdoor gradients in urban concentrations of ultrafine particles and PM 2.5 mass and chemical components. Atmospheric Environment 103, 307-320.

Sakurai, H., Fink, M.A., McMurry, P.H., Mauldin, L., Moore, K.F., Smith, J.N., Eisele, F.L., 2005. Hygroscopicity and volatility of 4–10 nm particles during summertime atmospheric nucleation events in urban Atlanta. Journal of Geophysical Research: Atmospheres (1984–2012) 110.

Sanders, P.G., Xu, N., Dalka, T.M., Maricq, M.M., 2003. Airborne brake wear debris: size distributions, composition, and a comparison of dynamometer and vehicle tests. Environmental Science and Technology 37, 4060-4069.

Sarwar, G., Olson, D.A., Corsi, R.L., Weschler, C.J., 2004. Indoor Fine Particles: The Role of Terpene Emissions from Consumer Products. Journal of the Air & Waste Management Association 54, 367-377.

Sceats, M.G., 1989. Brownian coagulation in aerosols—the role of long range forces. Journal of Colloid and Interface Science 129, 105-112.

Schiller-Scotland, C.F., Hlawa, R., Gebhart, J., 1994. Experimental data for total deposition in the respiratory tract of children. Toxicology Letters 72, 137-144.

Schweizer, C., Edwards, R.D., Bayer-Oglesby, L., Gauderman, W.J., Ilacqua, V., Jantunen, M.J., Lai, H.K., Nieuwenhuijsen, M., Künzli, N., 2007. Indoor time–microenvironment–activity patterns in seven regions of Europe. Journal of Exposure Science and Environmental Epidemiology 17, 170-181.

Seinfeld, J.H., Pandis, S.N., 2012. Atmospheric chemistry and physics: from air pollution to climate change. John Wiley & Sons.

Shi, J.P., Mark, D., Harrison, R.M., 2000. Characterization of particles from a current technology heavy-duty diesel engine. Environmental Science and Technology 34, 748-755.

Singer, B.C., Coleman, B.K., Destaillats, H., Hodgson, A.T., Lunden, M.M., Weschler, C.J., Nazaroff, W.W., 2006a. Indoor secondary pollutants from cleaning product and air freshener use in the presence of ozone. Atmospheric Environment 40, 6696-6710.

Singer, B.C., Destaillats, H., Hodgson, A.T., Nazaroff, W.W., 2006b. Cleaning products and air fresheners: emissions and resulting concentrations of glycol ethers and terpenoids. Indoor Air 16, 179-191.

Stanier, C.O., Khlystov, A.Y., Pandis, S.N., 2004. Ambient aerosol size distributions and number concentrations measured during the Pittsburgh Air Quality Study (PAQS). Atmospheric Environment 38, 3275-3284.

Svenningsson, I., Hansson, H.C., Wiedensohler, A., Ogren, J., Noone, K., Hallberg, A., 1992. Hygroscopic growth of aerosol particles in the Po Valley. Tellus B 44, 556-569.

Swietlicki, E., Hansson, H.C., Hämeri, K., Svenningsson, B., Massling, A., McFiggans, G., McMurry, P., Petäjä, T., Tunved, P., Gysel, M., 2008. Hygroscopic properties of

submicrometer atmospheric aerosol particles measured with H-TDMA instruments in various environments—A review. Tellus B 60, 432-469.

Swietlicki, E., Zhou, J., Berg, O.H., Martinsson, B.G., Frank, G., Cederfelt, S.-I., Dusek, U., Berner, A., Birmili, W., Wiedensohler, A., 1999. A closure study of sub-micrometer aerosol particle hygroscopic behaviour. Atmospheric Research 50, 205-240.

Szymczak, W., Menzel, N., Keck, L., 2007. Emission of ultrafine copper particles by universal motors controlled by phase angle modulation. Journal of Aerosol Science 38, 520-531.

Tan, H., Yin, Y., Gu, X., Li, F., Chan, P., Xu, H., Deng, X., Wan, Q., 2013. An observational study of the hygroscopic properties of aerosols over the Pearl River Delta region. Atmospheric Environment 77, 817-826.

Tang, I., Wong, W., Munkelwitz, H., 1981. The relative importance of atmospheric sulfates and nitrates in visibility reduction. Atmospheric Environment (1967) 15, 2463-2471.

Thatcher, T.L., Layton, D.W., 1995. Deposition, resuspension, and penetration of particles within a residence. Atmospheric Environment 29, 1487-1497.

Thimmaiah, D., Hovorka, J., Hopke, P.K., 2009. Source apportionment of winter submicron Prague aerosols from combined particle number size distribution and gaseous composition data. Aerosol and Air Quality Research 9, 209-236.

Thorpe, A., Harrison, R.M., 2008. Sources and properties of non-exhaust particulate matter from road traffic: a review. Science of the Total Environment 400, 270-282.

Tritscher, T., Jurányi, Z., Martin, M., Chirico, R., Gysel, M., Heringa, M.F., DeCarlo, P.F., Sierau, B., Prévôt, A.S., Weingartner, E., 2011. Changes of hygroscopicity and morphology during ageing of diesel soot. Environmental Research Letters 6, 034026.

Tschiersch, J., Busch, B., Fogh, C.L., 1997. Measurements of concentration, size distribution and hygroscopicity of Munich winter aerosol. Journal of Aerosol Science 28, S209-S210.

TSI, 2005. Engine Exhaust Particle Sizer Spectrometer.

TSI, 2006. Aerosol Instrument Manager Software for Aerodynamic Particle Sizer (APS) Spectrometers

TSI, 2007. Condensation Particle Counter Model 3775 Operation and Service Manual.

TSI, 2010. Scanning Mobility Particle Sizer (SMPS) Spectrometer Operation and Service Manual.

Tu, K., Knutson, E., 1984. Total deposition of ultrafine hydrophobic and hygroscopic aerosols in the human respiratory system. Aerosol Science and Technology 3, 453-465.

Väkevä, M., Hämeri, K., Aalto, P., 2002a. Hygroscopic properties of nucleation mode and Aitken mode particles during nucleation bursts and in background air on the west coast of Ireland. Journal of Geophysical Research: Atmospheres (1984–2012) 107, PAR 9-1-PAR 9-11.

Väkevä, M., Kulmala, M., Stratmann, F., Hämeri, K., 2002b. Field measurements of hygroscopic properties and state of mixing of nucleation mode particles. Atmospheric Chemistry and Physics 2, 55-66.

Varutbangkul, V., Brechtel, F., Bahreini, R., Ng, N., Keywood, M., Kroll, J., Flagan, R., Seinfeld, J., Lee, A., Goldstein, A., 2006. Hygroscopicity of secondary organic aerosols formed by oxidation of cycloalkenes, monoterpenes, sesquiterpenes, and related compounds. Atmospheric Chemistry and Physics 6, 2367-2388.

Venkataraman, C., Lyons, J.M., Friedlander, S.K., 1994. Size distributions of polycyclic aromatic hydrocarbons and elemental carbon. 1. Sampling, measurement methods, and source characterization. Environmental Science and Technology 28, 555-562.

Viana, M., Kuhlbusch, T., Querol, X., Alastuey, A., Harrison, R., Hopke, P., Winiwarter, W., Vallius, M., Szidat, S., Prevot, A., 2008. Source apportionment of particulate matter in Europe: a review of methods and results. Journal of Aerosol Science 39, 827-849.

Virkkula, A., Van Dingenen, R., Raes, F., Hjorth, J., 1999. Hygroscopic properties of aerosol formed by oxidation of limonene, α-pinene, and β-pinene. Journal of Geophysical Research: Atmospheres 104, 3569-3579.

Vogt, R., Scheer, V., Casati, R., Benter, T., 2003. On-road measurement of particle emission in the exhaust plume of a diesel passenger car. Environmental Science and Technology 37, 4070-4076.

Von Bismarck-Osten, C., Birmili, W., Ketzel, M., Massling, A., Petäjä, T., Weber, S., 2013. Characterization of parameters influencing the spatio-temporal variability of urban particle number size distributions in four European cities. Atmospheric Environment 77, 415-429.

Vu, T.V., Delgado-Saborit, J.M., Harrison, R.M., 2015a. A review of hygroscopic growth factors of submicron aerosols from different sources and its implication for calculation of lung deposition efficiency of ambient aerosols. Air Quality, Atmosphere & Health, 1-12.

Vu, T.V., Delgado-Saborit, J.M., Harrison, R.M., 2015b. Review: Particle number size distributions from seven major sources and implications for source apportionment studies. Atmospheric Environment 122, 114-132.

Wahlström, J., Olofsson, U., 2014. A field study of airborne particle emissions from automotive disc brakes. Proceedings of the Institution of Mechanical Engineers, Part D: Journal of Automobile Engineering, 0954407014550053.

Wahlström, J., Olander, L., Olofsson, U., 2010a. Size, shape, and elemental composition of airborne wear particles from disc brake materials. Tribology Letters 38, 15-24.

Wahlström, J., Söderberg, A., Olander, L., Jansson, A., Olofsson, U., 2010b. A pin-on-disc simulation of airborne wear particles from disc brakes. Wear 268, 763-769.

Wahlström, J., Söderberg, A., Olander, L., Olofsson, U., 2009. A disc brake test stand for measurement of airborne wear particles. Lubrication Science 21, 241-252.

Wainman, T., Zhang, J., Weschler, C.J., Lioy, P.J., 2000. Ozone and Limonene in Indoor Air: A Source of Submicron Particle Exposure. Environmental Health Perspectives 108, 1139-1145.

Wallace, L., 1996. Indoor particles: a review. Journal of the Air & Waste Management Association 46, 98-126.

Wang, B., Lee, S.C., Ho, K.F., Kang, Y.M., 2007a. Characteristics of emissions of air pollutants from burning of incense in temples, Hong Kong. Science of the Total Environment 377, 52-60.

Wang, C.-S., 1975. Gravitational deposition of particles from laminar flows in inclined channels. Journal of Aerosol Science 6, 191-204.

Wang, S., Ang, H.M., Tade, M.O., 2007b. Volatile organic compounds in indoor environment and photocatalytic oxidation: State of the art. Environment International 33, 694-705.

Wang, Y.-F., Tsai, P.-J., Chen, C.-W., Chen, D.-R., Dai, Y.-T., 2011a. Size distributions and exposure concentrations of nanoparticles associated with the emissions of oil mists from fastener manufacturing processes. Journal of Hazardous Materials 198, 182-187.

Wang, Y.-F., Tsai, P.-J., Chen, C.-W., Chen, D.-R., Hsu, D.-J., 2010. Using a modified electrical aerosol detector to predict nanoparticle exposures to different regions of the respiratory tract for workers in a carbon black manufacturing industry. Environmental Science and Technology 44, 6767-6774.

Wang, Y., Hopke, P.K., Chalupa, D.C., Utell, M.J., 2011b. Long-term study of urban ultrafine particles and other pollutants. Atmospheric Environment 45, 7672-7680.

Wang, Z., Hu, M., Wu, Z., Yue, D., He, L., Huang, X., Liu, X., Wiedensohler, A., 2013. Long-term measurements of particle number size distributions and the relationships with air mass history and source apportionment in the summer of Beijing. Atmospheric Chemistry and Physics 13, 10159-10170.

Wardoyo, A.Y.P., Morawska, L., Ristovski, Z.D., Marsh, J., 2006. Quantification of particle number and mass emission factors from combustion of Queensland trees. Environmental Science and Technology 40, 5696-5703.

Waring, M.S., Wells, J.R., Siegel, J.A., 2011. Secondary organic aerosol formation from ozone reactions with single terpenoids and terpenoid mixtures. Atmospheric Environment 45, 4235-4242.

Wehner, B., Uhrner, U., Von Löwis, S., Zallinger, M., Wiedensohler, A., 2009. Aerosol number size distributions within the exhaust plume of a diesel and a gasoline passenger car under on-road conditions and determination of emission factors. Atmospheric Environment 43, 1235-1245.

Weijers, E., Khlystov, A., Kos, G., Erisman, J., 2004. Variability of particulate matter concentrations along roads and motorways determined by a moving measurement unit. Atmospheric Environment 38, 2993-3002.

Weingartner, E., Baltensperger, U., Burtscher, H., 1995. Growth and structural change of combustion aerosols at high relative humidity. Environmental Science and Technology 29, 2982-2986.

Weingartner, E., Burtscher, H., Baltensperger, U., 1993. Hygroscopic behavior of combustion aerosols. Journal of Aerosol Science 24, S371-S372.

Weingartner, E., Burtscher, H., Baltensperger, U., 1997. Hygroscopic properties of carbon and diesel soot particles. Atmospheric Environment 31, 2311-2327.

Wentzel, M., Gorzawski, H., Naumann, K.-H., Saathoff, H., Weinbruch, S., 2003. Transmission electron microscopical and aerosol dynamical characterization of soot aerosols. Journal of Aerosol Science 34, 1347-1370.

Winkler-Heil, R., Ferron, G., Hofmann, W., 2014. Calculation of hygroscopic particle deposition in the human lung. Inhalation Toxicology 26, 193-206.

Wong, J., Lee, A., Slowik, J., Cziczo, D., Leaitch, W., Macdonald, A., Abbatt, J., 2011. Oxidation of ambient biogenic secondary organic aerosol by hydroxyl radicals: Effects on cloud condensation nuclei activity. Geophysical Research Letters 38.

Wu, C., Chao, C.Y., Sze-To, G., Wan, M., Chan, T., 2011. Ultrafine particle emissions from cigarette smouldering, incense burning, vacuum cleaner motor operation and cooking. Indoor and Built Environment, 1420326X11421356.

Xu, G., Yu, C., 1986. Effects of age on deposition of inhaled aerosols in the human lung. Aerosol Science and Technology 5, 349-357.

Yakovleva, E., Hopke, P.K., Wallace, L., 1999. Receptor modeling assessment of particle total exposure assessment methodology data. Environmental Science and Technology 33, 3645-3652.

Ye, X., Tang, C., Yin, Z., Chen, J., Ma, Z., Kong, L., Yang, X., Gao, W., Geng, F., 2013. Hygroscopic growth of urban aerosol particles during the 2009 Mirage-Shanghai Campaign. Atmospheric Environment 64, 263-269.

Yeh, H.-C., Schum, G., 1980. Models of human lung airways and their application to inhaled particle deposition. Bulletin of Mathematical Biology 42, 461-480.

Yue, D.L., Hu, M., Wang, Z.B., Wen, M.T., Guo, S., Zhong, L.J., Wiedensohler, A., Zhang, Y.H., 2013. Comparison of particle number size distributions and new particle formation between the urban and rural sites in the PRD region, China. Atmospheric Environment 76, 181-188.

Zeman, W.D.B.K.L., 1998. Deposition of fine particles in children spontaneously breathing at rest. Inhalation Toxicology 10, 831-842.

Zhang, K.M., Wexler, A.S., Zhu, Y.F., Hinds, W.C., Sioutas, C., 2004. Evolution of particle number distribution near roadways. Part II: the 'Road-to-Ambient'process. Atmospheric Environment 38, 6655-6665.

Zhang, L., Asgharian, B., Anjilvel, S., 1997. Inertial deposition of particles in the human upper airway bifurcations. Aerosol Science and Technology 26, 97-110.

Zhou, J., Swietlicki, E., Berg, O.H., Aalto, P.P., Hämeri, K., Nilsson, E.D., Leck, C., 2001. Hygroscopic properties of aerosol particles over the central Arctic Ocean during summer. Journal of Geophysical Research: Atmospheres (1984–2012) 106, 32111-32123.

Zhou, L., Kim, E., Hopke, P.K., Stanier, C., Pandis, S.N., 2005. Mining airborne particulate size distribution data by positive matrix factorization. Journal of Geophysical Research: Atmospheres 110, D07S19.

Zhou, L., Kim, E., Hopke, P.K., Stanier, C.O., Pandis, S., 2004. Advanced factor analysis on Pittsburgh particle size-distribution data special issue of aerosol science and technology on findings from the Fine Particulate Matter Supersites Program. Aerosol Science and Technology 38, 118-132.

Zhu, J., Cao, X.-L., Beauchamp, R., 2001. Determination of 2-butoxyethanol emissions from selected consumer products and its application in assessment of inhalation exposure associated with cleaning tasks. Environment International 26, 589-597.

Zhu, Y., Hinds, W.C., Krudysz, M., Kuhn, T., Froines, J., Sioutas, C., 2005. Penetration of freeway ultrafine particles into indoor environments. Journal of Aerosol Science 36, 303-322.